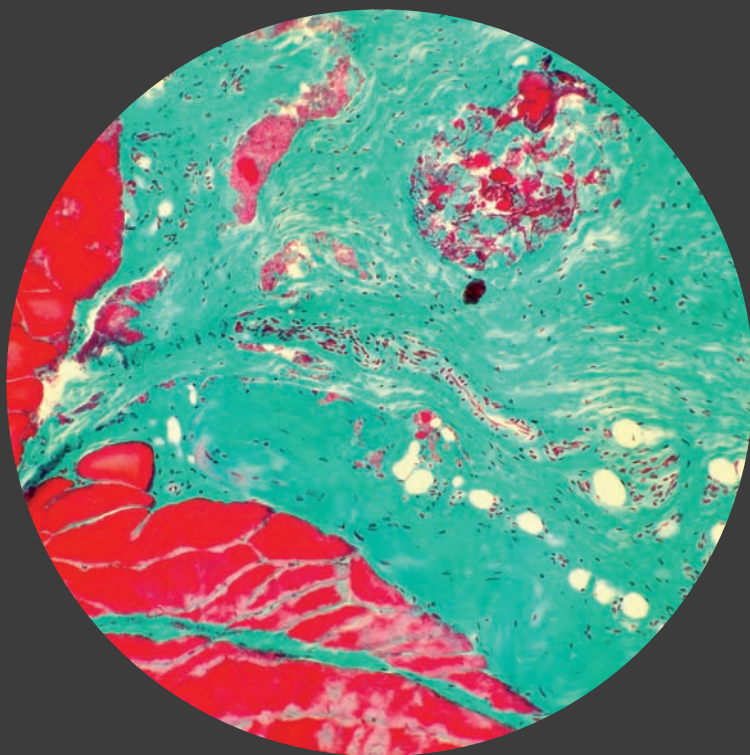


# Towards An injectable system for protein delivery in situ bone tissue engineering

Shorouk Fahmy-Garcia





# **TOWARDS IN SITU BONE TISSUE ENGINEERING**

An injectable system for protein delivery

Shorouk Fahmy-Garcia

## **Colofon**

Copyright © Shorouk Fahmy-Garcia, The Netherlands, 2019

ISBN 978-94-6361-268-5

All rights reserved. No parts of this thesis may be reproduced, distributed, stored in a retrieval system, or transmitted in any form or by any means, without written permission of the author or, when appropriate, the publisher of the publications.

The work presented in this thesis was conducted at the Departments of Orthopaedics and Internal Medicine, Erasmus MC, University Medical Center Rotterdam, the Netherlands.

The research leading to these results was supported by European Commision FP7 Programme Bioinspire under REA grant agreement n° 607051.

Cover design: Shorouk Fahmy-Garcia and Erwin Timmerman

Layout and printing: Optima Grafische Communicatie, Rotterdam, The Netherlands

Printing of this thesis was financially supported by:

Department of Orthopaedics, Erasmus MC, University Medical Center Rotterdam

Erasmus University Rotterdam

Netherlands Society for Biomaterials and Tissue Engineering

PeproTech EC Ltd

PerkinElmer



# TOWARDS IN SITU BONE TISSUE ENGINEERING

An injectable system for protein delivery

Het maken van botweefsel met een injecteerbaar eiwit afgiftesysteem

## **Proefschrift**

ter verkrijging van de graad van doctor aan de  
Erasmus Universiteit Rotterdam  
op de gezag van de rector magnificus

Prof. dr. R.C.M.E Engels

en volgens besluit van het College voor Promoties.  
De openbare verdediging zal plaatsvinden op

Dinsdag 21 mei 2019 om 13:30 uur

door

**Shorouk Fahmy Garcia**  
geboren te Valencia, Spanje

## **PROMOTIECOMMISSIE**

Promotoren      Prof. dr. G.J.V.M. van Osch  
                         Prof. dr. J.P.T.M. van Leeuwen

Overige leden    Prof. dr. I.M.J. Mathijssen  
                         Prof. dr. P. Habibovic  
                         Prof. dr. J. de Boer

Copromotoren   Dr. E. Farrell  
                         Dr. M. van Driel

*"Menos policías y más heladerías"*  
*David Trueba, Tierra de campos.*

*"Y al regresar el mismo decorado pero con un guion totalmente distinto"*  
*Xoel López, Patagonia.*

*"Everything is art. Everything is politics"*  
*Ai Weiwei, Inoculation.*

A mi madre, porque es y siempre será sinónimo de casa.

A mi padre, que nunca me ha dejado soñar pequeño.

A mis hermanos, gracias por ser tan diferentes a mí.

To Jordi, who always double-checks the accuracy of the thermometers



## TABLE OF CONTENTS

<b>Chapter 1</b>	Introduction	9
<b>Chapter 2</b>	Novel <i>in situ</i> gelling hydrogels loaded with recombinant collagen peptide microspheres as a slow-release system induce ectopic bone formation	23
<b>Chapter 3</b>	Injectable BMP-2 delivery system based on collagen derived microspheres and alginate induced bone formation in a time- and dose-dependent manner	53
<b>Chapter 4</b>	Nell-1, HMGB1, and CCN2 enhance migration and vasculogenesis, but not osteogenic differentiation compared to BMP-2	71
<b>Chapter 5</b>	Follistatin effects in migration, vascularization and osteogenesis <i>in vitro</i> and bone repair <i>in vivo</i>	89
<b>Chapter 6</b>	General discussion and conclusions	115
<b>Chapter 7</b>	Summary	127
<b>Chapter 8</b>	References	133
<b>Appendices</b>		155
	Nederlandse Samenvatting	157
	List of publications	161
	Acknowledgements	163
	PhD portfolio	167
	Curriculum Vitae	169



# 1

Introduction





## 1.1 Bone

Bone owes its origin close to half a billion years ago. Bone arose as a primitive mineralized tissue of the exoskeleton of the oldest vertebrate-predecessor organisms to the threat of invertebrate predation, leading to a major evolutionary leap (1, 2). However, having a rigid armor entails some restrictions, such as limited movement and locomotion. Relocation of the bony skeleton from the outside to the inside of animal bodies overcame these restrictions and triggered the development of a strong muscular system, enabling them to populate new habitats (3, 4). The use of calcium phosphate instead of calcium carbonate as mineralization strategy also proved to be a major adaptive advantage. Blocks built of calcium hydroxyapatite are more stable and apatite saturation can be regulated enzymatically. The origin of a phosphate-based endoskeleton is of great importance considering both the necessity of a continually remodeled skeleton and the pH changes that take place due to the high metabolic activity of the vertebrates. Without these major adaptative changes the evolution of the higher vertebrates could never have taken place (3, 5).

Bone is, therefore, a dynamic mineralized connective tissue. It exerts important functions in the body, such as locomotion, protection to vulnerable organs, regulation of calcium and phosphate homeostasis, and sheltering of bone marrow (6, 7). Bone cells make up 10% of the total bone volume, while the other 90% is composed of the extracellular matrix (ECM), consisting of: mineral matrix, organic matrix, lipids and water (8). To preserve the mechanical strength of the bone and the homeostasis of calcium and phosphate, bone is being continuously remodeled due to the coordinated actions of bone cells. A human body consists in 270 bones at birth and by adulthood some bones have fused together decreasing the number of bones in the human skeleton to 206 (9). Therefore, contrary to the traditional view, bone is not a passive lifeless scaffold but a dynamic living tissue.

The osseous tissues in mammals are formed via two different processes during embryogenesis. In the early stages of embryonic development, cartilage and fibrous tissue are the main components that form embryo's skeleton. Around the seventh week, osteogenesis and therefore, bone development, starts. Bone could be considered then a replacement tissue, which means that cartilage is utilized as a precursor for bone formation. This process of bone formation is called endochondral ossification and it is the principal process responsible for forming much of the mammalian skeleton. It is essential for the formation of long bones such as the femur or tibia and parts of the axial skeleton that are weight-bearing, like the vertebrae (10). The other process for bone formation is intramembranous ossification, in which the bone tissue is directly synthesized by mesenchymal stem cells (MSCs) without the involvement of an intermediate cartilage (11). Intramembranous ossification is the process that leads to the formation of flat bones, the ones forming parts of the skull, clavicle and mandible among others. Both modes of bone

formation begin during fetal development and continue remodeling the skeleton until adulthood (12).

### 1.1.1 Bone cells

There are two types of bone cells: the bone-forming cells and the bone resorbing cells. The bone-forming cells, osteoblasts, arise from MSCs committed to the osteoprogenitor lineage, and develop into osteocytes. The bone resorbing cells, osteoclasts, are derived from monocyte/macrophage cells of the hematopoietic lineage (Figure 1.1) (13).

Osteoblasts are responsible of synthesizing and secreting the organic bone matrix. When osteoprogenitor cells become preosteoblasts, they continue to proliferate and produce some of the bone matrix proteins, such as collagen and fibronectin (14). The preosteoblasts differentiate then into mature osteoblasts with increasing levels of alkaline phosphatase activity (ALP), a key enzyme that provides high concentrations of phosphate ions and is responsible of the mineralization of the ECM. At last, matrix mineralization occurs and mature osteoblasts get their characteristic cuboidal shape (15). At this stage, mature osteoblasts can remain quiescent bone lining cells (BLCs), become osteocytes, or undergo apoptosis (Figure 1.1).

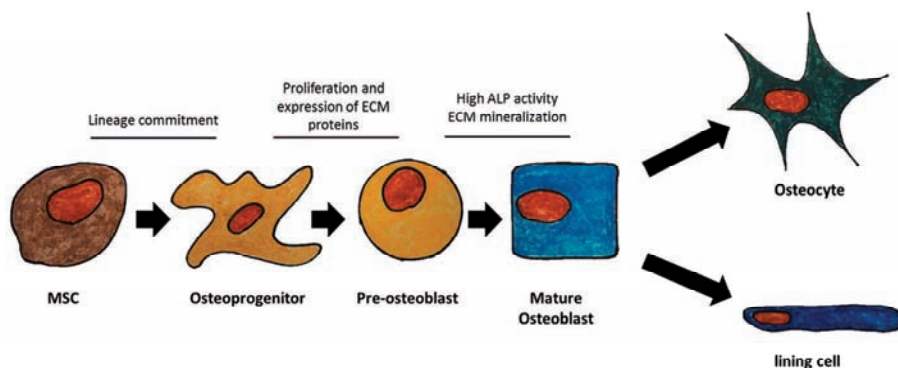


**Figure 1.1. Osteoblast differentiation.** MSC differentiation into osteoblasts is achieved by a complex differentiation program that involves a coordinated interaction between growth factors, hormones and ECM-related proteins among others. When osteoblasts become trapped in the matrix that they secrete, they become osteocytes. Osteocytes are involved in bone maintenance, while bone lining cells cover the bone surface, providing nutritional support to osteocytes and regulating the movement of fluids, calcium and phosphate in and out the bone.

Bone lining cells are quiescent mature osteoblasts extended over non-remodeling bone surfaces (16). Although BLCs together with osteocytes are the largest proportion of cells in mineralized bone, they are poorly understood. However, there is evidence showing that BLCs work as a biological membrane to prevent the direct interaction between osteoclast, tissue fluids and bone. BLCs are also known to be essential bone remodeling, by coupling

bone resorption and bone formation (17, 18). Osteocytes are extremely long-lived mechanosensing cells and are the most abundant cell type in the bone. They are able to survive for decades, residing in lacunae and embedded in the mineralized bone matrix (14). Numerous dendritic cellular processes connect osteocytes to each other and to the vasculature facilitating the intercellular transport of signaling molecules, oxygen and nutrients (6, 13). Osteoclasts are giant multinucleated cells responsible for bone degradation, and therefore, they are pivotal players in bone remodeling (Figure 1.2). As bone-resorptive cells, osteoclasts attach to the bone surface and delimit the area to degrade. Then, they solubilize it via acidification and proteases secretion (7).

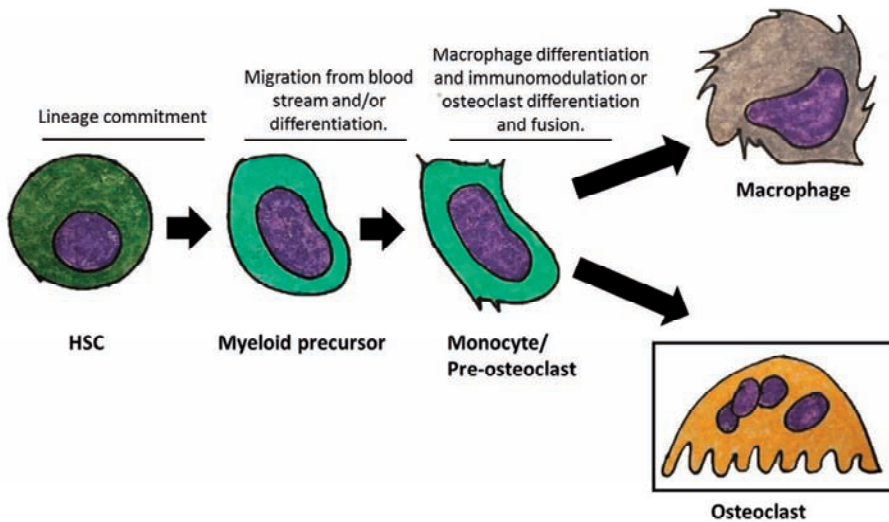


**Figure 1.2. Osteoclast differentiation.** Osteoclasts are multinucleated cells derived from hematopoietic stem cells (HSCs). Monocyte-macrophage precursor cells differentiate into tissue-specific macrophages with fused polykaryons, which are mature osteoclasts. Different factors such as RANKL and M-CSF-1 drive osteoclast precursors towards osteoclastogenesis and activation of mature osteoclasts. Osteoclasts are capable of resorbing mineralized bone and are essential in bone remodeling.

### 1.1.2 Bone remodeling during fracture repair

Fracture repair progresses through consecutive well-orchestrated processes. There are two types of fracture healing: primary and secondary. Primary healing rarely occurs; it is characterized by a minimal fracture gap and requires rigid fixation which suppresses the formation of a callus (19). In this type of bone fracture, bone can heal directly through the process of normal bone remodeling by which osteoclasts remove the mineralized bone followed by the formation of bone matrix through the osteoblasts. Secondary fracture healing is the most common method of bone healing and it usually involves a combination

of both intramembranous and endochondral ossification (20). The main phases that occur during secondary fracture healing are: the inflammatory, renewal and remodeling phase.

### **Inflammatory phase**

When bone fractures, the surrounding tissues and the local vasculature are also disrupted and the blood is usually clotted resulting in a hematoma. Platelets are then activated, coagulation reactions take place, resulting in the formation of an insoluble network of fibrin and trapped platelets. Platelet-derived factors and signaling molecules are meanwhile released. It is during this phase when the influx of inflammatory cells such as neutrophils or macrophages occurs, while the fibrin network acts then as a provisional matrix (21). Macrophages secrete a multitude of pro-inflammatory cytokines, chemokines and growth factors to recruit MSCs, fibroblasts and endothelial cells to the injury site (22). Thus, while macrophages clear the provisional matrix and the necrotic tissues, recruited fibroblasts and endothelial cells support vascular ingrowth and MSCs proliferate and differentiate into osteoprogenitor cells (Figure 1.3). These events necessitate ongoing communication between cells of the monocyte-macrophage-osteoclast lineage, MSCs and endothelial progenitor cells. Therefore, the initial acute inflammatory response and re-vascularization are considered pivotal phases for successful bone repair (22).

### **Renewal phase**

Fractures normally heal by the combination of both intramembranous and endochondral ossification. At the margin areas of the injured site, where better blood supply and mechanical stability can be found, stem cells proliferate and differentiate into osteoblasts and the formation of mineralized osteoid takes place, creating a reparative callus that will enhance mechanical stability of the site (23). At the same time, in the mechanically unstable regions with low oxygen tension, endochondral bone formation starts, bridging the fractured gap. This process ends in the formation of the primary spongiosa consisting of both cartilage and woven bone (24). Woven bone is formed when osteoblasts produce osteoid –unmineralized bone matrix–, it is mechanically weak and it is characterized by a random organization of the collagen fibers of the matrix. Eventually, immature woven bone connects the two fracture ends, and the remodeling process begins. This phase starts within the first days and lasts for several weeks (Figure 1.3) (25).

### **Remodeling phase**

This phase consists in the replacement of the immature woven bone by lamellar bone, which is mechanically stronger and composed of sublayers of aligned mineralized collagen fibrils. The final events represent the normal remodeling activity of bone, in which osteogenic and osteoclastic processes happen together (Figure 1.3). This process can take several months to complete, but ultimately the process restores the normal form and integrity of the bone completing the process of fracture healing (20).

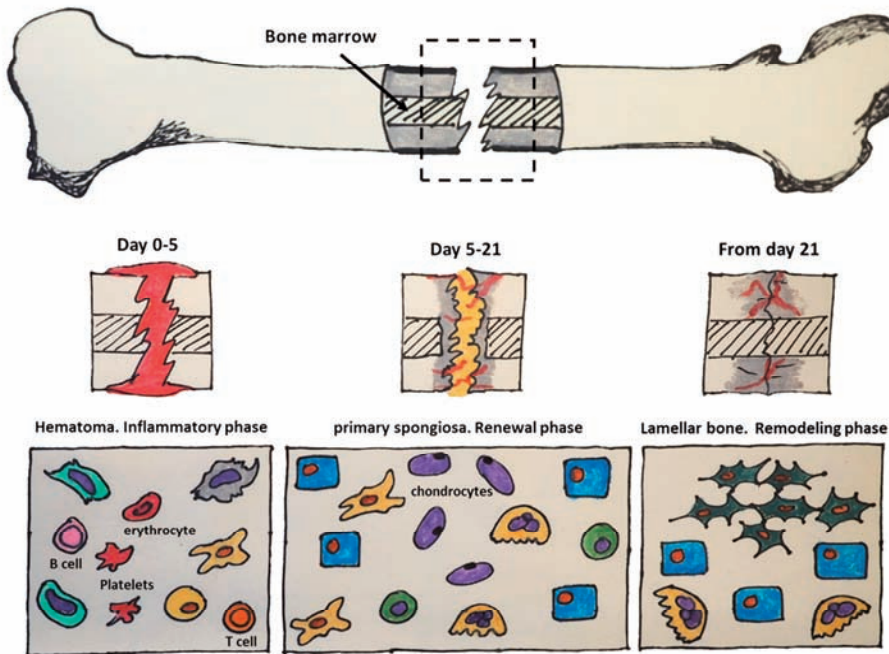


**Figure 1.3. Secondary fracture healing.** The main metabolic processes during fracture repair are divided in three major biological phases: inflammatory, renewal and remodeling phase. The primary cell types that are found at each stage are either denoted or match with the cell types shown in Figures 1.1 and 1.2. The figure shows the approximate time-frame of each stage and the prevalence of the cell types found in each stage are also denoted. Figure adapted from Einhorn et al. (26).

## 1.2 Bone grafting

The treatment of bone defects continues to be very challenging in orthopaedic practice. More than two million bone grafting procedures are performed annually worldwide (27). The main causes are traumatic events such as car accidents and extremity injuries in wars or civil conflicts, and the treatment of pathologies like infections and cancer ablation (28). The use of grafts to treat bone defects is practically as old as humanity itself and it is not a coincidence that from the Greek mythology to the Old Testament references to bone transplants are regularly found (29). Bone grafts are commonly used to treat skeletal fractures, replace and regenerate lost bone or treat delayed unions, among others, as demonstrated by the huge amount of bone grafting procedures performed every year. In fact, after blood transfusion, the second most frequent tissue transplantation carried out around the globe is bone grafting (27).

Bone grafts and bone substitutes must be histocompatible and their regenerative capacity is measured in terms of their osteoconductive, osteoinductive and osteogenic potential. A

bone graft or bone graft substitute has osteoconductive properties if it provides the support needed for the bone tissue regeneration such as vascularization or bone apposition. The osteoinductive potential of a bone graft is defined as its capability to recruit osteoprogenitor cells to stimulate their differentiation towards chondrocytes and osteoblasts to form bone. A bone graft is osteogenic if it houses growth factors and bone-forming cells involved in the synthesis of new bone (30).

### **1.2.1 Bone grafts: allografts and autografts**

The modern age of bone grafting dates back to 1668, when Job van Meekeren, a Dutch surgeon, reported the usage of the first heterologous graft in which a section of dog cranium was successfully implanted to repair the skull of an injured soldier (31). In the late 1800s, the first human allograft, where bone is harvested from a donor and transplanted to the patient, was performed by the Scottish surgeon William Macewen, who reconstructed the humerus of a child by a graft obtained from the tibia of another child with rickets (32). Since then, numerous reports have been published about the matter, leading ultimately to the use of autologous bone for grafting, where bone is harvested from an anatomic site and transplanted to another site in the same patient. By the middle of the 1900s, the clinical application of autografts was widely recognized (33). Autografts are inherently histocompatible, and nowadays they are still considered the gold standard due to their osteoconductive, osteoinductive and osteogenic healing potential. Autografts are typically obtained from non-essential parts of bones such as the iliac crest, but they can also be obtained from many others as the femur, ribs, tibia or radius. Autografts have an excellent success rate (the overall major complication rate related to their use oscillates between 6-9% (34, 35)). Nevertheless, there are many disadvantages associated with their use such as donor site morbidity, limited supply and substantial costs (36). To date allografts from cadavers or living donors are used as an alternative, especially in circumstances where large volumes of bone are required. However, they carry the risk of immune rejection and, although the probability is minimal, the risk for disease transmission is present. Allografts' major benefit over autografts is the elimination of donor site morbidity, but they lack the osteogenic and osteoinductive capacity of autografts and their osteoconductive properties might be affected by the preservation and sterilization techniques used (37).

### **1.2.2 Bone graft substitutes**

The use of bone graft substitutes has been refined by humankind throughout history. It can be said that the first generation of bone graft substitutes was mainly focused on matching the physical properties of the repaired tissue, such as mechanical strength. Therefore, since the Neolithic era, where a frontal defect of a tribal chief was repaired with a hammer-applied gold plate, to the present, metals have been used to repair bone defects (38). The evolution of bone grafts substitutes can be defined by three different technological

generations (Figure 1.4). The first generation of bone graft substitutes involved the so called inert materials of industrial use, which translated during the twentieth century in the use of titanium, stainless steel, ceramics such as zirconia, and synthetic polymers, like silicone or polymethylmethacrylate (39). A major drawback of the usage of these materials is the growth of fibrous tissue on the surface of the biomaterial and the risk of a persisting inflammatory response, which might lead to the graft encapsulation and aseptic loosening. Meanwhile, World War I and World War II gave rise to many unfortunate events but led to great medical advances in the field of bone repair. Bone banks were established to be able to treat bone defects more rapidly; however, they were limited by the storage capacity and the interrupted power supply, which was necessary to cryopreserve allogenic bone grafts (40). Bone research drove then the discovery of demineralized bone matrix (DBM). Although DBM did not offer mechanical support, it was suitable for filling defects, contained osteogenic factors, and revascularised quickly (41). From 1980s onwards, the second generation of bone graft substitutes appeared with the development of bioactive interfaces to coat the previously established substitutes, improving the ability of the grafts to integrate with the surrounding tissue. Many bone graft substitutes were made biodegradable to match their degradation rate with the bone formation process, and different biomolecules and polymers were conjugated to trigger bone repair. Some of the most used materials were bioactive ceramics such as hydroxyapatite or  $\beta$ -tricalcium phosphate and biomaterials or coated metals (39, 42). Common used polymers were hyaluronic acid, chitosan or polyglycolide, among others (43). Third generation of bone graft substitutes aims to get closer to the autograft features and, to do so, tries to induce the cellular and molecular responses needed for successful bone repair using second generation bone graft substitutes and relying on the notion of tissue engineering (TE) (39). In this line, using controlled-release systems to deliver drugs or factors from a scaffold can accelerate the local regenerative process while avoiding potential undesired systemic effects. Factors must meet a minimum threshold to be effective but, due to their short half-lives, it is challenging to achieve a reparative response at the site of injury for an extended period of time without causing unwanted side effects due to the use of supraphysiological doses (44). A good example of this problem is illustrated below, in section 3.1.2. through the use and limitations of one of the most osteogenic proteins discovered so far, bone morphogenetic protein-2 (BMP-2). Consequently, different types of materials are being employed to deliver factors in a controlled manner, without negatively affecting the patient or the physical-chemical properties of the scaffold. Among those materials, hydrogels made from natural polymers, porous materials and the combination of both are being currently investigated as controlled release systems (45). In summary, it is during the last 100 years when greater progress has been made in the art of repairing bone. Bone graft substitutes are made from a wide range of materials and, although they have been widely used, their limitations prompted the search for other alternatives.

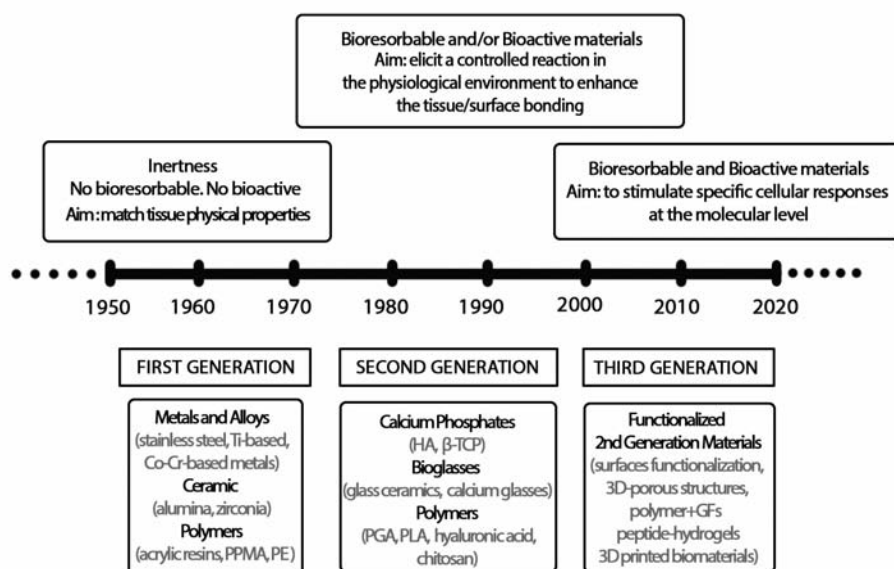


**Figure 1.4. Biomaterials evolution in the field of bone grafting.** Main goals and features of each biomaterials generation are cited at the upper boxes, while some examples of the most representative materials used in each generation are mentioned at the bottom boxes.

### Injectable Biomaterials

Injectable materials are particularly attractive systems for bone regeneration due to their minimally invasive nature and their structural similarity to the ECM. Injectable hydrogels can fill irregular defects, which is especially useful in the maxillofacial region, and can be fabricated from both natural and synthetic materials (46). However, synthetic materials are not very biocompatible and lack biological activity compared to natural biomaterials (47). The most used natural injectable biomaterials in bone repair are listed in Table 1.1. Besides, a number of studies have been recently published about the use of *in situ* forming hydrogels (48-50). Bone has a highly organized and complicated structure. The three-dimensional architecture of the *in situ* gelling hydrogels provides an appropriate microenvironment for growth factor incorporation, and the recruitment and differentiation of the cells involved in bone repair (47).



**Table 1.1. Natural injectable biomaterials used in bone repair.**

TYPE OF INJECTABLE BIOMATERIAL	REFERENCES
Chitosan-based injectable hydrogels	(51-53)
Collagen-based injectable hydrogels	(54-58)
Hyaluronic acid-based	(48, 59, 60)
Fibrin-based	(61-63)
Alginate-based	(64-67)
Heparin-based	(61, 68, 69)
Elastin-based	(70-72)

### 1.3 Bone tissue engineering

Several studies have estimated that 5-10% of all fractures are associated with impaired healing, resulting in delayed union or nonunion (73), and TE represents a promising approach that would likely eliminate many of the pitfalls of current treatments in the future. In the TE research field the principles of engineering and life sciences are combined to create functional substitutes to restore, maintain or improve the tissue functions (74). Bone TE is based on the idea of mimicking as much as possible the natural process of bone repair. To this end, bone-forming cells and biomolecules are incorporated into a scaffold to trigger bone regeneration. In the last 25 years, bone TE has gained notoriety and different approaches have been investigated. Many studies have shown over the years that the presence of cells generally benefits tissue regeneration (75, 76); however, the clinical implementation of this concept may still be limited by numerous problems surrounding the costly stages of cell harvesting and preparation under Good Manufacturing Practice (GMP) conditions associated with cell therapy based approaches (75). Therefore, cell-free engineered constructs immediately available to a wider population should be created. Overcoming the need for the addition of cells to scaffolds is a critical challenge in the field of TE. Ideally, endogenous cells would serve as a target and they would be recruited and guided to regenerate the damaged tissue. To this end, a huge variety of biomolecules and chemical agents that induce and instruct bone defect repair by the cells of the patient are being investigated.

#### 1.3.1 Growth factor delivery for bone tissue engineering

Growth factors are soluble-secreted signalling polypeptides that regulate a broad spectrum of cellular responses. These responses can result in a very wide range of actions such as chemotaxis, cell growth, or differentiation, and can be guided to a specific subset of cells (77). The use of growth factors has increased drastically in the field of bone TE. Bone morphogenetic proteins (BMPs), especially BMP-2, have been the most used proteins in bone repair due to their great potential for bone regeneration.

## **Bone Morphogenetic proteins**

In 1965, Marshall Urist demonstrated that DBM implanted intramuscularly in a rat resulted in bone formation, which himself called the bone induction principle (78). Later, Urist identified the protein responsible of this osteoinductive phenomenon, naming it bone morphogenetic protein. However, it was in the 1980s when isolation of the first BMP occurred and, subsequently, bone morphogenetic proteins 2 and 4 were cloned (79, 80). Currently, more than 20 BMPs have been identified and they constitute the largest subgroup of the transforming growth factor beta (TGF- $\beta$ ) superfamily. BMPs have been implicated in a variety of functions, although they are specially known as the most important growth factors in bone formation (81). The research of BMPs significantly expanded over the years and their use in different animal models and clinical studies demonstrated their therapeutic potential in bone repair, leading to the Food and Drug Administration (FDA) approval of BMP-2 for use in human surgery (82). BMP-2 FDA-approved usage is limited to a specific carrier –an absorbable collagen sponge– and to certain procedures such as spinal fusion, orthopaedic trauma and oral-maxillofacial treatments, although the clinical off-label use of BMP-2 is overwhelming (83-85).

## **The need of alternative proteins**

Despite widespread BMP-2 use, complications such as soft tissue swelling, ectopic bone formation, inflammation and an increased risk of cancer have been reported over the past years (86, 87). Several large-scale studies have confirmed that the clinical use of BMP-2 is relatively often associated with adverse events like inflammatory complications, increased osteolysis or life-threatening cervical spine swelling. Because of all the reported clinical side effects associated with BMP-2-based treatments, the FDA was forced to issue a warning of the potential complications related to its use (88). Several of these complications might be related to how the protein is delivered in the clinical setting. Currently, a collagen sponge soaked with BMP-2 with a burst release is used as the protein carrier, with half of the loaded BMP-2 being released within two days (89). Consequently, supraphysiological doses of the protein are needed to exert its function, resulting in the above-mentioned undesired effects. In order to avoid those complications, new therapeutic concepts are being investigated, including the spatiotemporal dosing of BMP-2 through controlled-release systems and the use of alternative growth factors that are also able to induce the signaling cascades needed for bone repair. Regarding to the latter point, some factors involved in osteogenic, angiogenic and inflammatory processes have been investigated (90) and used in bone TE both single or combined with BMP-2 (91). Among them, angiogenic and chemotactic factors such as platelet-derived growth factor (PDGF) and endothelial growth factor (VEGF) have been widely tested for the treatment of bone defects (92-95). However, when used alone, their effect on bone repair was not as substantial as BMP-2's effect (92, 96). Consequently, to improve bone formation while

avoiding the side effects observed when using BMP-2 alone, the delivery of multiple growth factors with synergistic effects is being extensively investigated (90, 97).

## 1.4 Aims and outline of this thesis

Bone possesses the intrinsic capacity for regeneration as part of the repair process in response to injury. However, in many cases of post-traumatic skeletal conditions fracture healing is impaired and there is a need for bone grafting. Unfortunately, no satisfactory solutions for bone grafts are currently available due to the limited effectiveness of treatment options. Conventionally, bone defect reconstruction is performed by the use of either autografts or allografts. Autografts are considered the gold standard; however, their use can lead to complications such as donor-site morbidity, pain, and infection. The alternative, allografts, lack the osteogenic and osteoinductive capacity of autografts and hold the risk of carrying infectious agents or immune rejection. Because of the urgent need to overcome the limitations associated with conventional treatments, bone TE has offered a promising approach to regenerate bone. However, combining bone-forming growth factors with a scaffold to mimic the bone microenvironment and supporting the formation of new bone is not an easy challenge. Due to their minimally invasive application and the possibility of repairing irregular defects, injectable biomaterials have attracted attention for bone regeneration. These materials also offer the possibility of being chemically modified what, added to their remarkable flexibility, allow them to be used for a wide range of applications. Therefore, the research described in this thesis is performed to identify and evaluate the therapeutic potential of novel injectable biomaterials and promising proteins for bone regeneration.

Currently, supraphysiological doses of bone-forming proteins are needed to successfully heal bone. The major reason for this is the burst-release of the protein from the biomaterial. In **Chapter 2**, we develop three different *in situ* gelling formulations: two alginate based-formulations and one hyaluronan-based. The *in vitro* release of BMP-2-one of the most studied bone-forming proteins- from these formulations is analyzed as well as bone formation *in vivo* after their use. From this study, one of the alginate-based formulations is selected for further investigation. Consequently, the aim of **Chapter 3** is to assess time and dose dependent ectopic bone formation with this injectable slow-release formulation and investigate the kinetics of retention of BMP-2 when loaded in the formulation. The bone regeneration of this system loaded with BMP-2 is investigated in a rat calvarial defect model.

In **Chapter 4**, because of the need to eliminate the risks of BMP-2 use *in vivo*, the ability of three factors to enhance essential processes for bone defect repair is studied *in vitro* and compared to BMP-2. These factors, which are described as bone-forming proteins in the literature, are Nel-like molecule type 1 (Nell-1), high mobility group box 1 (HMGB1), and connective tissue growth factor (CTGF, also called CCN2). Specifically, we investigate

whether these proteins are able to attract osteoprogenitor and endothelial cells from human origin and promote their differentiation. **Chapter 5** focusses on another osteogenic protein, follistatin (FST), and its use in bone TE. For that, the effect of two different FST variants with significantly different cell-surface binding *in vitro* and orthotopically is studied. Bone repair is investigated using the previously developed alginate-based delivery system formulation loaded with the FST variants in a rat calvarial defect. This thesis ends with a general discussion, conclusion and future perspectives of the work presented (**Chapter 6**), followed by a summary in English and Dutch (**Chapter 7**).

# 2

## Novel *in situ* gelling hydrogels loaded with recombinant collagen peptide microspheres as a slow-release system induce ectopic bone formation

Shorouk Fahmy-Garcia<sup>#</sup>, Didem Mumcuoglu<sup>#</sup>, Laura de Miguel, Veerle Dieleman, Janneke Witte-Bouma, Bram C. J. van der Eerden, Marjolein van Driel, David Eglin, Jan A. N. Verhaar, Sebastiaan G. J. M. Kluijtmans, Gerjo J. V. M. van Osch, and Eric Farrell

<sup>#</sup>Authors contributed equally to this work

Adv. Healthcare Mater. 2018, 7, 1800507. doi: 10.1002/adhm.201800507

## 2.1 Abstract

New solutions for large bone defect repair are needed. Here, *in situ* gelling slow-release systems for bone induction are assessed. Collagen-I based Recombinant Peptide (RCP) microspheres (MS) are produced and used as a carrier for bone morphogenetic protein-2 (BMP-2). The RCP-MSs are dispersed in three hydrogels: high mannuronate (SLM) alginate, high guluronate (SLG) alginate, and thermoresponsive hyaluronan derivative (HApN). HApN+RCP-MS forms a gel structure at 32 °C or above, while SLM+RCP-MS and SLG+RCP-MS respond to shear stress displaying thixotropic behavior. Alginate formulations show sustained release of BMP-2, while there is minimal release from HApN. These formulations are injected subcutaneously in rats. SLM+RCP-MS and SLG+RCP-MS loaded with BMP-2 induce ectopic bone formation as revealed by X-ray tomography and histology, whereas HApN+RCP-MS do not. Vascularization occurs within all the formulations studied and is significantly higher in SLG+MS and HApN+RCP-MS than in SLM+RCP-MS. Inflammation (based on macrophage subset staining) decreases over time in both alginate groups, but increases in the HApN+RCP-MS condition. It is shown that a balance between inflammatory cell infiltration, BMP-2 release, and vascularization, achieved in the SLG+RCP-MS alginate condition, is optimal for the induction of *de novo* bone formation.

## 2.2 Introduction

Bone is a tissue with high self-regeneration capacity. However, in cases of trauma or certain diseases bone does not heal properly and therefore surgical intervention using autografts or allografts is necessary. Currently, autografts are the gold standard; however, they are associated with donor site morbidity, increased pain, high cost, and long patient recovery time. The alternative is to use allografts, but they carry the risk of immunogenicity, infectious agents, and lack the osteoinductive capacity of autografts (39). To overcome these limitations there has been a vast effort to develop new biomaterials to aid large bone defect repair. Among these materials, natural biomaterials have been widely studied due to their advantages, such as biodegradability, biocompatibility and the ability to interact with the extracellular matrix and cells (98). Injectable formulations are preferred over implants for the treatment of defects that do not require operational fixation since the application is easier and the patient will not suffer from surgery and consequently, achieve a faster recovery. Moreover, in the case of irregular bone defects, injectable scaffolds might be advantageous because they can adapt to the defect shape better (99). Alginate, hyaluronic acid (HA) and collagen derived materials have been investigated as scaffolds, particles and *in situ* gelling hydrogels (100).

Materials can be combined with bone-forming proteins such as bone morphogenetic protein-2 (BMP-2) to stimulate bone formation. BMP-2 is considered to be one of the most powerful osteoinductive factors and is the only bone morphogenetic protein (loaded in a collagen sponge) approved and currently used as a bone graft substitute (86, 101). However, large doses of BMP-2 are needed to produce a significant osteogenic effect (102). The major reason for this is the burst-release of the protein from the collagen sponge. Half of the BMP-2 was released in the first two days *in vivo* in a rabbit ulna osteotomy model (103). This often results in undesired ectopic bone formation, soft tissue swelling and bone resorption (104). Therefore, a biomaterial that can provide a slower protein release may perform better in clinics, eliminating adverse effects. There are several challenges for developing a suitable protein carrier material (105). It should promote the recruitment of skeletal and endothelial progenitor cells and trigger their differentiation to mature osteoblasts and endothelial cells with a minimum amount of loaded protein.

Recombinant collagen-like peptide (RCP) material and its use for tissue engineering have been investigated by several studies, showing an optimum pore size and porosity for osteoconduction and high cell viability (58, 106, 107). RCP does not only facilitate the cell attachment by its arginylglycylaspartic acid (RGD) rich peptide sequence (106) but can also be expected to decrease the risk of immune reaction due to its animal free origin compared to other collagen-based products. In fact, RCP is produced under good manufacturing process conditions within the facilities of Fujifilm. The use of RGD rich microspheres comprised of RCP (RCP-MS) for the stimulation of cell attachment is very

important when using materials where cell attachment is suboptimal, such as alginates and HA. We have previously investigated the use of recombinant collagen-like peptide microspheres for slow release of BMP-2. In that study, we optimized the water uptake in the RCP-MS for BMP-2-loading. Particle size before and after swelling was also assessed by rheology, showing a similar storage and loss modulus, which indicated that the material was not degraded. Therefore, RCP-MS were intact for 2 weeks in cell culture medium and were only degraded when collagenase treatment was applied (58). In light of these results, here we aim to develop and test 3 *in situ* gelling formulations, based on alginate and hyaluronic acid to retain BMP-2 releasing microspheres, resulting in slow localized growth factor release.

In a search for an injectable hydrogel system to deliver BMP-2 carrying RCP-MS, we have investigated two potential systems: one system that could be crosslinked and form a network in the presence of ions, and another system that could change conformation with a temperature switch. These two systems were alginate and poly(*N*-isopropylacrylamide) (PNIPAM) modified hyaluronic acid (HApN) respectively, both widely used in bone tissue engineering.

Alginate is a polysaccharide composed of  $\beta$ -D-mannuronic acid (M-block) and  $\alpha$ -L-guluronic acid (G-block) monomers. Several studies have demonstrated the potential of this hydrogel for bone tissue engineering (66). Mineralization of alginate has also been characterized by Raman spectroscopy (108). Alginate *in situ* gelling formulations have been developed in combination with particles and *in vitro* experiments showed the potential of the formulations for drug delivery (109). Previously, alginate hydrogel with gelatin microspheres loaded with BMP-2 was used to study osteogenesis *in vivo*. However, the formulations could not induce bone formation probably due to fast degradation of material; and only after addition of biphasic calcium phosphate granules, was the bone formation achieved (110). There are various types of alginate and it is known that the composition (guluronic acid/mannuronic acid ratio), and molecular weight among others are critical factors affecting the physical properties of the resultant hydrogels, such as the degradation behavior (111); however, although it is known that the ratio effect of these two monomers play some role in biocompatibility –alginate with higher guluronate content produced gels has been shown to be less biocompatible– (112), its effect on bone regeneration remains unknown. Therefore, among different types of alginates we have chosen two sterile lyophilized alginates with high mannuronate and high guluronate content (SLM-20 and SLG-20) that have lower molecular weight (MW: 75000 - 220000 g/mol) and lower viscosity than other commercial alginates (i.e. SLM-100 and SLG-100) based on the idea that injectable formulations can be obtained easier with lower viscosity alginates. *In situ* gelling formulations of alginates were developed via calcium complexation. HA is another linear polysaccharide consisting of repeating units of D-glucuronic acid and N-acetyl-D-glucosamine and is an abundant glycosaminoglycan in



extracellular matrices. Therefore, injectable HA hydrogels have been used for bone regeneration in the presence of BMP-2 (113, 114). However, to induce subcutaneous bone formation with HA, a very high dose of BMP-2 (150 µg/mL) is normally used (59, 114). Surprisingly, even when high doses of BMP-2 are supplied, HA has failed to induce bone formation (114). To optimize the performance of gels, those are often functionalized to engineer better delivery systems and that is also the case of HA and its derivations. Investigators have recently shown that HA gels functionalized with fibronectin formed more ectopic bone than its nonfunctionalized counterpart (115). However, functionalizing HA did not always induce more bone formation. For example, heparin functionalization of HA led to less ectopic bone formation than its nonfunctionalized counterpart formation when implanted intramuscularly (116). Another study examined the suitability of acrylated hyaluronic acid for tissue regeneration, concluding that it is as a potential carrier of cells and growth factors (117). These studies showed that HA and alginates have potential for use in bone regeneration. However, choosing the right formulations of engineered materials with a right dose of BMP-2 is challenging. Additionally, a huge demand in bone regeneration field is the development of *in situ* gelling materials that enable slow protein release, support cell attachment, vascularization and thus induction of bone formation. In this study, we have used poly(*N*-isopropylacrylamide) functionalized hyaluronic acid (HApN) that shows thermoresponsive gelling behavior.

We aimed to develop *in situ* gelling formulations with natural polymers (alginate or HA) to retain the RCP-MS which would provide slow BMP-2 release and increase cell attachment. We also wanted to assess how the hydrogel matrices influence the *in vitro* release of BMP-2 from the microspheres and the bone induction *in vivo*. For that purpose, we have developed three different hydrogel-microsphere systems: two different thixotropic alginate formulations and a thermoresponsive (gelling above 32 °C) HApN. The three distinct formulations are different in terms of chemical composition, crosslinking and physical/mechanical properties. Here we aimed to assess them in terms of their ability to support bone formation acting as a growth factor slow-release system. Thus, the function of these gels is to be injectable, *in situ* gelling, provide a sustained release of BMP-2 and ultimately induce *de novo* bone formation. The mechanical properties of these gels and BMP-2 release characteristics *in vitro* were evaluated. The bone formation ability of these materials was studied in an ectopic bone formation model *in vivo*. The volume and morphology of the ectopic bone, vascularization, cellular infiltration and inflammation were evaluated.

## 2.3 Materials and methods

### 2.3.1 Materials

Human collagen type I based recombinant peptide (RCP) is a product of Fujifilm commercially available as Cellnest. It is produced in a fermentation process by genetically modified yeast *Pichia pastoris* as described elsewhere (106, 118). RCP is composed of 571 amino acids; it has an isoelectric point (pI) of 10.02 and a molecular weight of 51.2 kDa. BMP-2 was produced as described previously (119) and it was kindly provided by Dr. Joachim Nickel (Fraunhofer IGB, Germany). Pronova SLM20 (G/M Ratio:  $\leq 1$ , sterile alginate, viscosity: 20-99 mPa\*s, MW: 75-150 kDa,) and Pronova SLG20 (G/M Ratio:  $\geq 1.5$ , sterile alginate, viscosity: 20-99 mPa\*s, MW: 75-150 kDa) were ordered from Novamatrix (Sandvika, Norway). Thermoresponsive HApN (MW: 1.68 MDa) consisting of HA grafted with PNIPAM was prepared as described in D'Este et al. (120).

Hexamethylene diisocyanate (HMDIC), corn oil, sodium chloride, calcium carbonate ( $\text{CaCO}_3$ ), and glucono delta-lactone (GDL) were purchased from Sigma-Aldrich (St. Louis, MO, USA). Ethanol, acetone, and hydrochloric acid were purchased from Millipore (Billerica, MA, USA). ELISA development kit and reagents for BMP-2 determination were ordered from Peprotech (Rocky Hill, NJ, USA). Dulbecco's Modified Eagle's Medium (DMEM), fetal bovine serum (FBS), phosphate-buffered saline (PBS), and penicillin-streptomycin (P/S) were ordered from Thermofisher Scientific (Waltham, MA, USA).

### 2.3.2 RCP microsphere preparation

The types of RCP-MS used in this study were selected based on a previous study in which the adsorption of BMP-2 to the RCP-was described (58), as well as the effect of BMP-2 concentration, RCP-MS size, porosity, and crosslinking of the RCP-MS on BMP-2 release. Based on this study, HMDIC crosslinked RCP-MS with a range of diameter 50-75  $\mu\text{m}$  were selected as a promising candidate in terms of slow-release of BMP-2.

RCP-MS were produced by emulsification using calcium carbonate ( $\text{CaCO}_3$ ). Briefly, a 20% aqueous RCP solution was prepared and mixed with  $\text{CaCO}_3$  fine powder (with a size of  $<1 \mu\text{m}$ ) in a 1:1 (w/w) ratio of RCP to  $\text{CaCO}_3$ . This suspension was emulsified in corn oil at 50 °C. After cooling, the emulsified microspheres were precipitated and washed three times with acetone, and subsequently dried overnight at 60 °C. The microspheres were sieved to 50-75  $\mu\text{m}$  size (Retsch GmbH, Germany). Particles were then crosslinked by HMDIC by mixing 1 g of spheres and 1 mL of HMDIC in 100 mL ethanol for 1 day while stirring. Excess crosslinker was removed by washing several times with ethanol after which the particles were dried at 60 °C. The particles used for the alginate and HApN formulations were prepared in identical way except that, for the HApN formulation,  $\text{CaCO}_3$  was removed after the crosslinking step. For the alginate formulations the  $\text{CaCO}_3$  was left in as the  $\text{Ca}^{2+}$

also serves to crosslink the alginate into a hydrogel. For the HApN formulation  $\text{CaCO}_3$  was removed by suspension of RCP-MS in 0.23 M hydrochloric acid for 30 min, followed by repeated washing with water until a neutral pH was achieved, and the RCP-MS were dried at 60 °C. Complete removal of the calcium was confirmed by energy dispersive X-ray (EDX) mapping (Figure S2.1). The morphology of  $\text{CaCO}_3$  containing and  $\text{CaCO}_3$  free microspheres was analyzed by scanning electron microscope (SEM) (Jeol JSM-6335F Field Emission Scanning Electron Microscope) (Figure S2.2).  $\text{CaCO}_3$  crystals clearly can be observed on the surface of the  $\text{CaCO}_3$  comprising microspheres (Figure S2.1). Particles were gamma sterilized at 25 kGray (Synergy Health, The Netherlands) prior to use *in vitro* and *in vivo*.

### 2.3.3 Preparation of the hydrogel formulations

To prepare the formulations with SLM20 and SLG20 alginates, alginates were dissolved in 0.9% sterile sodium chloride to create 2% w/v solution. 68 mg of calcium comprising microspheres were incubated overnight at 4 °C with 170  $\mu\text{L}$  of 122.5  $\mu\text{g}/\text{mL}$  BMP-2. The following day, the swollen particles were mixed with 1014  $\mu\text{L}$  of SLM or SLG solution. Alginates have the ability to form soft hydrogels in the presence of calcium ions; however, although the calcium carbonate released by the microspheres was enough to crosslink the alginate SLM, it was not enough to crosslink alginate SLG. Table 2.1 shows the composition of the formulations. Calcium ions released in the SLM formulation were below the detection limit of the colorimetric assay. In the final SLG formulation, more calcium ions (3.18  $\mu\text{M}$ ) were released. Therefore, in order to crosslink alginate SLG, GDL was used. GDL has been combined with alginate extensively to obtain an injectable gel with optimal mechanical properties (121-123). GDL is normally used as an acidifier and it was added to alginate SLG formulation in order to release more calcium ions from the  $\text{CaCO}_3$  upon gradual hydrolysis of GDL to gluconic acid and therefore increase the mechanical properties of SLG formulation. Briefly, to the SLG formulation, 106  $\mu\text{L}$  of 0.06 M freshly-prepared GDL solution was added and mixed immediately. GDL was used to dissolve minute amounts of  $\text{CaCO}_3$  so that alginate can be crosslinked and increase the mechanical properties of the formulation. In parallel, 106  $\mu\text{L}$  of 0.9% sodium chloride was added to the SLM formulation for which it was not necessary to add GDL as shown by rheology. The formulations were immediately thoroughly mixed and incubated overnight at 4 °C to equilibrate. One day later, prepared formulations were mixed again prior to injection *in vivo* or to use for *in vitro* experiments. For both *in vivo* and *in vitro* experiments 200  $\mu\text{L}$  of the prepared formulations were used. The final amount of BMP-2 was 3.3  $\mu\text{g}$  in each 200  $\mu\text{L}$  hydrogel+RCP-MS formulation (Table 2.1). Solubilized  $\text{Ca}^{2+}$  ion as shown in  $\mu\text{M}$  and % in Table 2.1 was detected by calcium colorimetric assay following the manufacturer's instructions (Sigma-Aldrich).

The following formulations were used for *in vitro* and *in vivo* experiments. First, a 15% w/w solution of HApN was prepared in PBS. On the same day, 170  $\mu\text{L}$  BMP-2 at 122.5  $\mu\text{g}/\text{mL}$  concentration was added to 34 mg of RCP-MS (without  $\text{CaCO}_3$ ) and particles were incubated at 4  $^{\circ}\text{C}$  overnight. The next day, 850  $\mu\text{L}$  HApN (15% w/w) and 270  $\mu\text{L}$  PBS were added to the swollen particles and the formulation was mixed with a 1 mL syringe and 19 G needle. The composition of the final formulations is shown in Table 2.1. In order to keep the amount of RCP the same in all different formulations, half of the microspheres were used in HApN condition compared to SLM+RCP-MS or SLG+RCP-MS formulations that contained 50%  $\text{CaCO}_3$  and 50% RCP in the microspheres. The prepared formulations were mixed and incubated overnight at 4  $^{\circ}\text{C}$  to equilibrate. All formulations were prepared under sterile conditions. Biomineralization of the hydrogels formulations was not studied, since interactions between RCP-MS and hydrogels were not expected to change the mineralization properties of the formulation (107, 108).

### 2.3.4 Characterization of the formulations

The mechanical properties of prepared hydrogels containing BMP-2 loaded microspheres were measured by a rheometer (Anton Paar MCR301, Austria). A 20 mm diameter parallel plate measuring system was used. After sample addition to the plate, silicon oil was applied to the edges to prevent evaporation. All measurements were performed with a normal force of 0.1 N. As a precharacterization, the storage (or elastic) modulus ( $G'$ ) and loss (or viscous) modulus ( $G''$ ) were measured at different strains to determine the linear viscoelastic region. To determine the linear viscoelastic region in alginate formulations (shown in Table S2.1) four different formulations were prepared. SLG alginate (1.5%, w/v); SLG alginate (1.5%, w/v) with microspheres (8%, w/v); SLG alginate (1.5%, w/v) with microspheres (8%, w/v) and GDL (5 mM); and SLG alginate with  $\text{CaCO}_3$  (4%, w/v) and GDL (5 mM) were prepared. After precharacterization, thermosensitive HApN+RCP-MS formulation was measured at 2% strain, at 1 Hz while heating from 15  $^{\circ}\text{C}$  to 40  $^{\circ}\text{C}$  followed by cooling from 40  $^{\circ}\text{C}$  to 15  $^{\circ}\text{C}$ .

Alginate formulations were measured by a two-step repeating cycle. At the first step of the cycle, storage and loss moduli were measured at 1% strain, at 1 Hz, at 37  $^{\circ}\text{C}$ . At the second step, 500% strain, 1 Hz frequency, 37  $^{\circ}\text{C}$  temperature was applied. The cycle repeated four times to characterize thixotropic behavior. During the measurements, perturbations due to collisions and cantings of the particles were not observed.

The morphology of the formulations was investigated by using SEM. To prepare the samples prior to analysis, RCP-MS loaded hydrogels were immersed into liquid nitrogen and freeze-dried at -50  $^{\circ}\text{C}$ . The cross-section of the formulations was sputter-coated with gold before loading onto the microscope.

### 2.3.5 Release of BMP-2 from hydrogel formulations

The formulations containing hydrogels and BMP-2 loaded microspheres were prepared as described above. 200  $\mu$ L of hydrogel formulations was added to 24 well plate inserts with 0.4  $\mu$ m pore size. 1 mL DMEM with 10% FBS and 1% P/S per well was added to the reservoir plate. The plates were incubated at 37 °C under constant agitation at 300 rpm. When removed from the incubator, the plates were put on a hot plate at 37 °C to prevent the gel-sol transition of HApN hydrogels. At each time point 1 mL medium was collected and changed with fresh medium. The collected release media were analyzed by rhBMP-2 ELISA development kit (Peprotech) according to manufacturer's protocol. As a positive control, 200  $\mu$ L of 16.5  $\mu$ g/mL BMP-2 solution was added to the inserts and 1 mL medium was added to bottom wells of the transwell plate. At each time point 1 mL medium was collected and changed with fresh medium. The cumulative amount of BMP-2 that passed through the membrane to the bottom of the well after 14 days was quantified. This control was included in order to study the effect of protein sticking to the plate and membrane, as well as its degradation over time. At the end of the experiment (Day 14),  $2.3 \mu\text{g} \pm 0.1 \mu\text{g}$  (mean  $\pm$  SD,  $n = 3$ ) cumulative release was detected from the positive control which was 3.3  $\mu$ g BMP-2 initially added to the inserts of the transwells.

### 2.3.6 Conditions for animal experiment

All animal experiments were performed with prior approval of the ethics committee for laboratory animal use (protocol #EMC 116-15-01). To have a statistically relevant group size, we performed a power analysis with an alpha of 0.05 and power = 80%. Based on similar works performed in an ectopic model using comparable cell-free systems (124-126), we expected a difference in bone formation of approximately 25 mm<sup>3</sup> and an SD of  $\pm 15 \text{ mm}^3$ . Therefore, 34 male Sprague Dawley (SD) rats at 12 weeks old were used in this study to evaluate bone formation. The animals were randomly assigned and housed in pairs in a specific pathogen-free environment and allowed to adapt to the conditions of the animal house for 7 days before starting the study. The animals were maintained at 20-26 °C on a 12 h dark/light cycle with *ad libitum* access to standard rat chow and water. To evaluate the effect of BMP-2 loaded in the different formulations, RCP-MS with a constant concentration of rhBMP-2 (3  $\mu$ g per injection) and incorporated in SLG, SLM or HApN hydrogels were subcutaneously injected (total volume 200  $\mu$ L per injection) in the dorsum of the animals. As controls, SLM+RCP-MS, SLG+RCP-MS and HApN+RCP-MS were implanted without BMP-2 addition.  $n = 6$  replicates were used for each condition and each animal received six randomly assigned injections. All injections were performed using a 19 gauge needle on animals under isoflurane inhalation. At 1, 4 and 10 weeks after implantation, animals were euthanized with CO<sub>2</sub> and the specimens were harvested for further analysis. To reduce the number of animals used in this study, controls were harvested at 1 and 10 weeks after implantation.

### 2.3.7 $\mu$ CT analysis

When animals were euthanized at 4 and 10 weeks following transplantation, retrieved implants were immediately scanned at a resolution of 9  $\mu$ m, using a SkyScan 1172 system (Bruker, Belgium). The following settings were used: X-ray power and tube current were 40 kV and 0.25 mA, respectively. Exposure time was 5.9 s and an average of three pictures was taken at each angle ( $0.9^\circ$ ) to generate final images. These images were further reconstructed by SkyScan NRecon software (Bruker) using a range of 0-0.1 on the histogram scale, 20% beam-hardening correction and ring artefact reduction with a value of 5. For image processing SkyScan CTAnalyser software (Bruker) was used. Threshold levels of 120 (lower) and 255 (higher) were set to extract the amount of mineral volume from the tissue volume (BV/TV).

### 2.3.8 Histology

For histological examination, specimens were fixed in 4% formalin solution for 48 h and decalcified with 10% w/v EDTA for 2-4 weeks. Implants were dehydrated and embedded in paraffin. Sections of 6  $\mu$ m thickness were prepared using a microtome and mounted on subbed glass slides (StarFrost, Knittel Glass, Germany). Three selected cross-sections from each implant, with a minimum distance of 120  $\mu$ m apart were deparaffinized and rinsed with distilled water to be stained with hematoxylin and eosin (H&E). The sections were imaged by NanoZoomer-XR (Hamamatsu, Japan). A square grid (400-800  $\mu$ m) overlay was used to quantify newly formed blood vessels, which were identified based on the presence of erythrocytes within a tubular-like structure. The number of blood vessels was counted within the implants in a blinded fashion by two examiners and averaged.

Ster of differentiation 68 (CD68) marker was used to distinguish cells of the macrophage lineage, inducible nitric oxide synthetase (iNOS) and cluster of differentiation 206 (CD206) markers were used for detection of M1 and M2 macrophage subsets. For detection of CD68, iNOS and CD206 positive cells, sections were deparaffinized and washed. In the case of CD68 and CD206, antigen retrieval was performed using a citrate buffer (10 mM, pH 6.0) at 90  $^\circ$ C for 20 min. For iNOS, 10 mM Tris, pH 9.0, 1 mM EDTA Solution, 0.05% v/v Tween 20 buffer was used. To avoid nonspecific binding, slides were preincubated 30 min with 10% v/v normal goat serum (NGS) (Southern Biotech, USA) in PBS/1%BSA w/v and 2% w/v milk powder to block nonspecific binding followed by 1 h incubation with either primary CD68 antibody (Acris, Germany) diluted to 0.5  $\mu$ g/mL, primary CD206 antibody (Abcam, UK) diluted to 2.5  $\mu$ g/mL or primary iNOS antibody (Abcam) diluted to 2  $\mu$ g/mL. CD68 stained samples were then incubated for 30 min with biotinylated secondary goat anti-mouse antibody diluted 1:100 in PBS + 1% w/v BSA + 5% v/v rat serum (Jackson, PA, USA). For CD206 and iNOS staining, secondary biotin labeled goat antirabbit antibody (Biogenex, UK) diluted 1:50 in PBS+ 1% w/v BSA + 5% v/v rat serum was used. Finally, slides were incubated with label streptavidin-AP (Biogenex) diluted at

1:100, rinsed with 0.2 M Tris-HCl pH 8.5 and stained with substrate. Substrate consisted in 0.1 mg/mL New Fuchsin (Sigma-Aldrich), 0.3 mg/mL naphthol AS-MX phosphate (Sigma-Aldrich), 0.0025% w/v NaNO<sub>2</sub> (Sigma-Aldrich), 3% v/v di-methylformamide (Sigma-Aldrich) and 0.25 mg/mL levamisole (Sigma-Aldrich) dissolved in 0.2 M Tris-HCl (pH 8.5). Slides were counterstained with haematoxylin (Sigma-Aldrich) and analyzed using confocal microscope. Mouse IgG1 antibody (Dako Cytomation, Denmark) and rabbit IgG1 (Dako Cytomation) were used as negative controls.

Type II collagen occurs exclusively in cartilage, therefore, to investigate the presence of cartilaginous tissue within the formulations, collagen II staining was performed on the samples as previously described (127).

After Nanozoomer-XR imaging Hamamatsu Photonics, all the retrieved implants were ranked for CD68, iNOS and CD206-positive cells in terms of both staining intensity and number of cells stained by two observers who scored all stainings and were blinded with regard to treatment. The results obtained by the two observers were averaged and rated on ordinal scale (lowest number = no/minor to highest number = moderate/heavy).

### 2.3.9 Statistical analysis

To investigate whether there were differences in the number of blood vessels and CD68, iNOS and CD206 positive cells between conditions, a Kruskal-Wallis test was applied and Dunn's *post-hoc* was used for analysis.  $\mu$ CT quantitative data and BMP-2 release data were analyzed using one-way analysis of variance and Bonferroni's *post-hoc* multiple comparison test was applied to the obtained results. A value of  $p < 0.05$  was considered to be statistically significant.

Quantitative data are presented as bars, indicating the mean  $\pm$  SD, while qualitative data are presented as box plots, indicating median, and the interquartile distance with the whiskers showing the largest and smallest values.

## 2.4 Results

### 2.4.1 RCP microsphere-alginate *in situ* gelling hydrogels have shear-thinning behavior

Strain-dependent oscillatory rheology of RCP microsphere-alginate hydrogels showed an extremely broad linear viscoelastic region in addition to network rupture at high strains for the alginates containing 8% microspheres (Table 2.1 and Figure S2.3). The SLG alginate with microspheres (SLG + 8% microspheres) broke at 150% strain whereas the formulation containing GDL (which allowed release of Ca<sup>2+</sup> ions to enable the crosslinking of the alginate) (SLG + 8% microspheres + GDL) was not broken at the maximum strain measured, 167% (Table S2.1). This demonstrates that addition of GDL to the formulation, releasing 3.18

$\mu\text{M Ca}^{2+}$  ions (Table 2.1), improved the mechanical properties of the SLG gel as a result of the release of  $\text{Ca}^{2+}$  ions that allowed alginate crosslinking. The viscoelastic region was much smaller for the control consisting of alginate,  $\text{CaCO}_3$  particles (1  $\mu\text{m}$ ) and GDL. This formulation was broken at 40% strain showing the reinforcing effect of the microspheres in the formulation. GDL was not required for the crosslinking of the SLM alginate.

**Table 2.1. Composition of the formulations used for the *in vitro* BMP-2 release study and for the *in vivo* experiment.**

Formulation	Conc. of alginate (%)	Conc. of HApN (%)	RCP-MS with $\text{CaCO}_3$ (mg/mL)	RCP-MS without $\text{CaCO}_3$ (mg/mL)	$\text{CaCO}_3$ (mg/mL)	RCP (mg/mL)	GDL (mg/mL)	Ca solubilized ( $\mu\text{M}$ )	Ca solubilized (%)	Amount of BMP2 ( $\mu\text{g/mL}$ )
SLM with RCP-MS	1.5	-	54	-	27	27	-	-	-	16.1
SLG with RCP-MS	1.5	-	54	-	27	27	5	3.18	0.93	16.1
HApN with RCP-MS	-	10	-	27	-	27	-	-	-	16.1

Interestingly, the optimized formulations of SLM+MS and SLG+MS were thixotropic. When 500% strain was applied, a decrease in both loss and storage moduli was observed and the hydrogel structure was broken showing the shear-thinning effect (Figure 2.1A). When the stress was removed, the hydrogel recovered almost instantaneously indicating that the gel can be formed *in situ* directly after injection *in vivo*. This cycle can be repeated several times without loss of function. Both of the alginates were injectable due to this shear-thinning behavior. The formed hydrogels had storage (elastic) moduli between 1-2 kPa for both alginate gel formulations.

The surface morphologies of the freeze-dried formulations were examined by SEM. Polymer scaffolds for tissue engineering must be highly porous to permit the infiltration of a large number of cells and their differentiation *in situ*. Dry average diameter of RCP-MS was  $\sim 70 \mu\text{m}$  and the formulations studied –alginate SLM, alginate SLG and HApN– formed an interconnected pore network with the RCP-MS homogeneously distributed throughout it (Figure 2.1C). Table 2.1 indicates the composition of the formulations used. The aim was to find the optimal formulation with the minimum of fabrication steps with our desired characteristics that would lead to maximum bone formation *in vivo*.

## 2.4.2 HApN-microsphere formulation have thermoresponsive behavior

HApN hydrogel grafted with PNIPAM has an intrinsic property of thermo-inducible gel formation as shown earlier by D'Este et al. (120). In combination with microspheres the thermoresponsive behavior was retained, which can be seen by the mechanical



characterization of the hydrogel at increasing and decreasing temperatures between 15 °C and 40 °C (Figure 2.1B). In the cooling phase, there was a change from the gel state to the liquid state whereas in the heating phase, liquid to gel transition occurs. Both the storage modulus and loss modulus of the formed gel increased to 5 kPa at 37 °C.

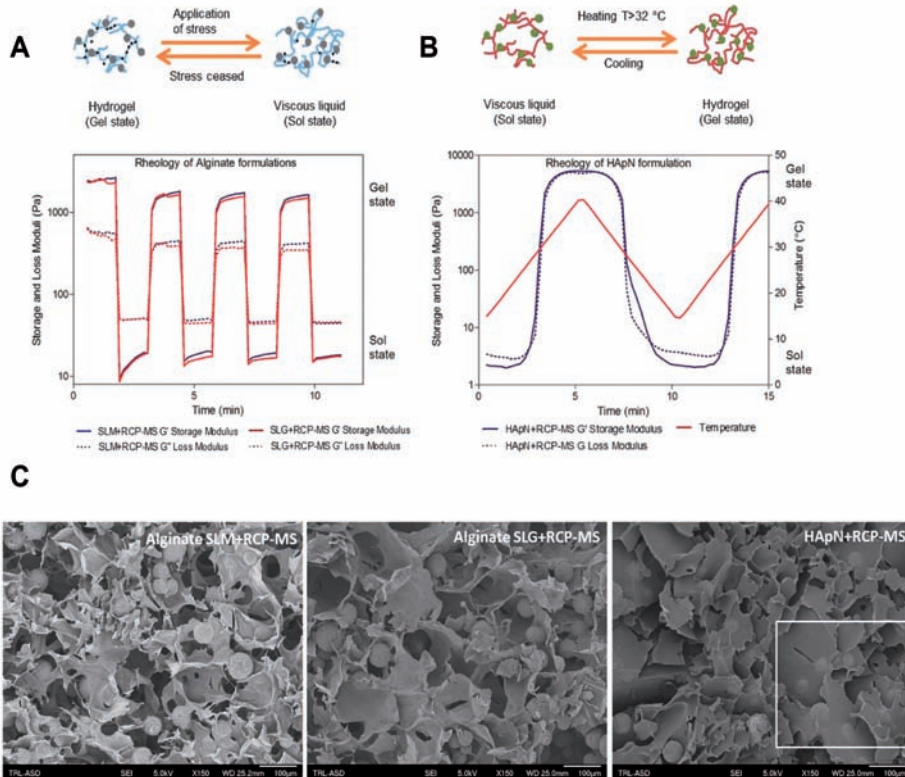


**Figure 2.1. Mechanical properties of the SLM+RCP-MS, SLG+RCP-MS and HApN+RCP-MS formulations.** Schemes illustrate the network of hydrogel with microspheres; gray: RCP-MS with  $\text{CaCO}_3$ , blue: SLM and SLG alginate, black: calcium ions, red: HApN and green: RCP-MS without  $\text{CaCO}_3$ . Thixotropic behavior of the alginate hydrogel formulations containing SLM or SLG alginate and calcium comprising RCP-MS is shown by rheology. GDL was added to the SLG alginate formulation to keep the rheological properties of both types of alginate formulations similar. In both formulations, gel is disrupted under shear stress and hydrogels recuperate when stress is removed within 30 s. B. The thermo-responsiveness of the HApN hydrogel with microspheres is shown by rheology. Gel is formed when suspension is heated to 40 °C and the viscous liquid state forms when the gel is cooled to 15 °C. C. SEM images of the SLM+RCP-MS, SLG+RCP-MS and HApN+RCP-MS formulations (scale bar is 100  $\mu\text{m}$ ). The square grid shows one of the areas of the HApN formulation in which RCP-MS fully embedded in the hydrogel are observed. Arrows indicate RCP-MS.

### 2.4.3 BMP-2 release from HApN-MS hydrogel was lower than alginate-MS hydrogels

Apart from the injectability of the hydrogel, the ability of the hydrogels to provide sustained-BMP-2 release is important for bone formation. We have showed earlier that there is a specific interaction between BMP-2 and RCP (58). Here, the release of BMP-2 from the hydrogels+RCP-MS formulations was studied and compared to hydrogel or RCP-MS only conditions. Both alginate hydrogels with RCP-MS released BMP-2 slower than alginate without RCP-MS, showing the synergistic effect of microspheres and hydrogels to control the release (Figure 2.2A). During the time-course study of two weeks, ~ 10% of BMP-2 ( $202 \pm 42$  ng; mean  $\pm$  SD) was released from SLG+RCP-MS formulation and only ~ 2% ( $46 \pm 23$  ng; mean  $\pm$  SD) was released from SLM+RCP-MS formulation. The numbers indicated that the majority of BMP-2 was retained in the alginate-RCP-MS formulations. These results suggest that a similar slow-degradation of the RCP-MS will also occur *in vivo* as observed by the gradual shrinkage and breakdown of the microspheres over time.

In the HApN formulation, RCP-MS without  $\text{CaCO}_3$  addition were used. Although the RCP-MS without calcium are more porous compared to the ones with calcium carbonate, and therefore, have a larger surface area (Figure S2.1), no differences in BMP-2 release were observed when compared HApN and HApN+RCP-MS. The release from the HApN+MS and from HApN hydrogel only was limited (Figure 2.2B) and the total release was less than 0.2% ( $3.7 \pm 0.4$  ng and  $4.2 \pm 0.2$  ng), a fraction of the 3.3  $\mu\text{g}$  loaded into the gels. To confirm that the unreleased BMP-2 was still inside the hydrogel after 2 weeks, ten times diluted samples were loaded on an SDS-PAGE gel (Figure S2.4). We could detect a band of BMP-2 after 2 weeks of release, which confirmed that HApN hydrogel was preventing BMP-2 release.

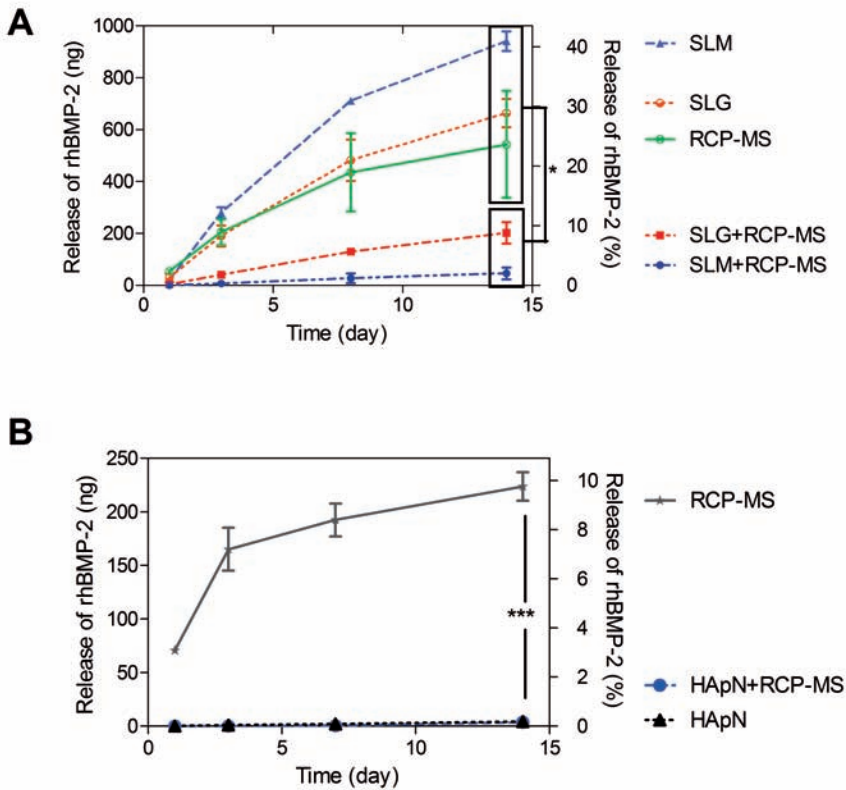


**Figure 2.2.** *In vitro* BMP-2 release from the A) SLM alginate, SLG alginate formulations and collagen-I based recombinant peptide microspheres (RCP-MS) containing  $\text{CaCO}_3$  and B) from hyaluronic acid-pN (HApN) formulations and RCP-MS without  $\text{CaCO}_3$ . The cumulative release of BMP-2 in DMEM with 10% FBS and 1% P/S detected by ELISA is demonstrated over time. BMP-2 release from (A) SLM alginate only (SLM), SLG alginate only (SLG), microspheres containing  $\text{CaCO}_3$  (MS), SLG alginate with microspheres (SLG+MS), SLM alginate with microspheres (SLM+MS); (B) only microspheres without  $\text{CaCO}_3$  (MS), thermoresponsive hyaluronan derivative with microspheres (HApN+MS) and thermoresponsive hyaluronan derivative (HApN) are compared. Statistical difference at 14 days of cumulative release analyzed by one-way ANOVA, \* $p < 0.05$ , \*\*\* $p < 0.001$ .

#### 2.4.4 Injectable BMP-2 loaded hydrogel formulations induced ectopic bone formation

BMP-2 loaded in RCP-MS were injected subcutaneously after encapsulation in the three hydrogel formulations tested; alginate SLM+RCP-MS, alginate SLG+RCP-MS, and thermoresponsive HApN+RCP-MS. Identical formulations without addition of BMP-2 were used as controls. 1 week postinjection, histology revealed noticeable differences in terms of

composite integrity between formulations (Figure 2.3A). In the alginate formulations, both the microspheres and the alginate layer were mostly intact, with some cellular infiltration in the fissures that appeared in the gel. However, in the HApN+RCP-MS formulation, much of the hydrogel had disappeared, many of the microspheres were being degraded, and numerous cells could be observed within the implants (Figure 2.3A). After 4 weeks, bone formation was observed in one third of the alginate harvested formulations (Figure 2.3A).

Bone formation was analyzed by  $\mu$ CT. No mineralization was observed 1 week after implantation. A similar amount of calcified tissue in all three hydrogel formulations tested was observed at 4 weeks postimplantation (Figure 2.3B-C). Interestingly, in the alginate formulations cartilaginous regions were found at that time point, suggesting that endochondral ossification process was occurring near by the RCP+RCP-MS (Figure S2.5). At 10 weeks,  $\mu$ CT confirmed the greatest amount of bone formation when alginate SLG was used as a carrier, showing a more than 3-fold increase compared to the 4 weeks scan (mean  $\pm$  SD, from  $4.4 \pm 5.4 \text{ mm}^3$  mineral volume at 4 weeks to  $22.3 \pm 11 \text{ mm}^3$  at 10 weeks). When alginate SLM+RCP-MS or thermo-responsive HApN+RCP-MS were used, the amount of calcified tissue found within the implants did not change significantly over time (Figure 2.3B). Moreover, the alginate SLG+RCP-MS formulation significantly increased the amount of mineral volume formed at 10 weeks compared to alginate SLM ( $22.3 \pm 11 \text{ mm}^3$  vs.  $4.24 \pm 3 \text{ mm}^3$ ) (Figure 2.3B). As we expected, when alginate formulations were implanted without BMP-2, mineral tissue was barely found (Figure 2.3C). Interestingly, the thermo-responsive HApN+RCP-MS formulation showed calcified tissue on  $\mu$ CT, even without the addition of BMP-2 (Figure 2.3C), but histological analysis did not show bone formation and the formulation structure was almost degraded with or without BMP-2 addition at the end of the experiment (Figure 2.3A).

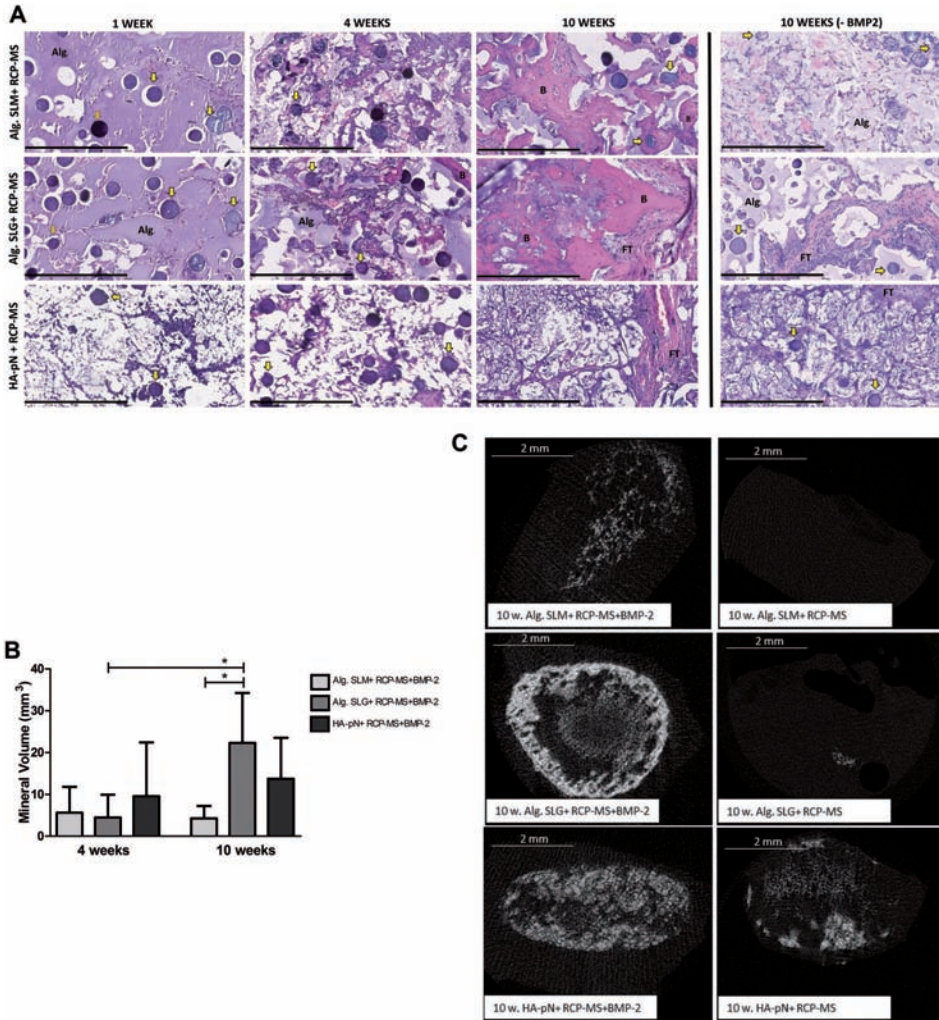


**Figure 2.3. Alginate hydrogel formulations loaded with BMP-2 induced ectopic bone formation.**

A. H&E sections at 1, 4 and 10 weeks after implantation showing the alginate scaffolds (alg), microspheres (indicated by yellow arrows), formed bone (B), and fibrous tissue (FT). Controls (empty gels) are shown at 10 weeks. Images are shown at high magnification (scale bar is 400  $\mu$ m). B. Comparison of the mineral volume obtained in the different formulations with the addition of BMP-2 at 4 and 10 weeks-period. The bars represent the mean  $\pm$  SD (\*  $p < 0.05$ ). C. Reconstructed  $\mu$ CT images 10 weeks after subcutaneous injection of alginate SLM+ RCP-MS, alginate SLM+ RCP-MS and HA+ RCP-MS with and without BMP-2. Alginate SLM (SLM), alginate SLG (SLG), thermoresponsive hyaluronan derivative (HApN), Collagen-I based Recombinant Peptide microspheres (RCP-MS).

### 2.4.5 Inflammatory cell infiltration decreased over time in alginate in comparison to hyaluronan formulations

To investigate the role of inflammation in the bone formation process, we used CD68 as a general marker to identify cells of the macrophage lineage. We observed a significant time dependent decrease in staining in the alginate SLG (median  $\pm$  95% CI,  $39 \pm 8.3$  at 1 week vs.  $7 \pm 7.5$  at 10 weeks,  $p < 0.05$ ) (Figure 2.4A,B). In the alginate SLM+RCP-MS formulation CD68-positive staining was less pronounced than in SLG+RCP-MS at week 1, increased at week 4 and then significantly dropped again at week 10 (mean  $\pm$  95% CI,  $14 \pm 3.9$  at 1 week and  $33.5 \pm 7.3$  vs.  $10 \pm 11$  for 4 and 10 week rank, respectively). In the HApN+RCP-MS formulation, macrophage recruitment was slower than in alginate SLG+RCP-MS formulation and had the highest CD68-positive staining at 10 weeks (median  $\pm$  95% CI, from  $23.5 \pm 6.3$  at week 1 to  $48.5 \pm 5.5$  at the end of the experiment,  $p < 0.01$ ) (Figure 2.4A,B). Furthermore, when we compared the formulations to each other at 1, 4 and 10 weeks postimplantation, the SLG+RCP-MS formulation showed more pronounced infiltration of CD68-positive cells at 1 week than SLM+RCP-MS ( $39 \pm 8.3$  vs.  $14 \pm 3.9$ ,  $p < 0.01$ ) and CD68-positive staining at 10 weeks in the HApN+RCP-MS formulation was significantly higher than in both, alginate SLM+RCP-MS and alginate SLG+RCP-MS ( $10 \pm 11$  for SLM+RCP-MS,  $7 \pm 7.5$  for SLG+RCP-MS vs  $48.5 \pm 5.5$  for HApN+RCP-MS,  $p < 0.05$ ).

To further investigate whether the different formulations promoted the activation of distinct macrophage phenotypes, proinflammatory (M1) and anti-inflammatory (M2) macrophage subsets were identified. To achieve this, iNOS and CD206 markers were used. iNOS, was used as marker for M1 macrophages. The HApN+RCP-MS formulation had significantly more iNOS-positive staining compared to the alginate SLG+RCP-MS formulation at 10 weeks (median  $\pm$  95% CI,  $41.25 \pm 9.6$  vs.  $7 \pm 8.8$ ,  $p < 0.05$ ) (Figure 2.4C).

CD206-positive staining to identify M2 macrophages did not show any difference between formulations at week 1. At 4 weeks, CD206-positive staining was significantly higher in SLM+RCP-MS than in HApN+RCP-MS formulations ( $28.2 \pm 4$  vs.  $10.5 \pm 4.2$ ). At week 10 no significant differences were found between them (Figure 2.4D).



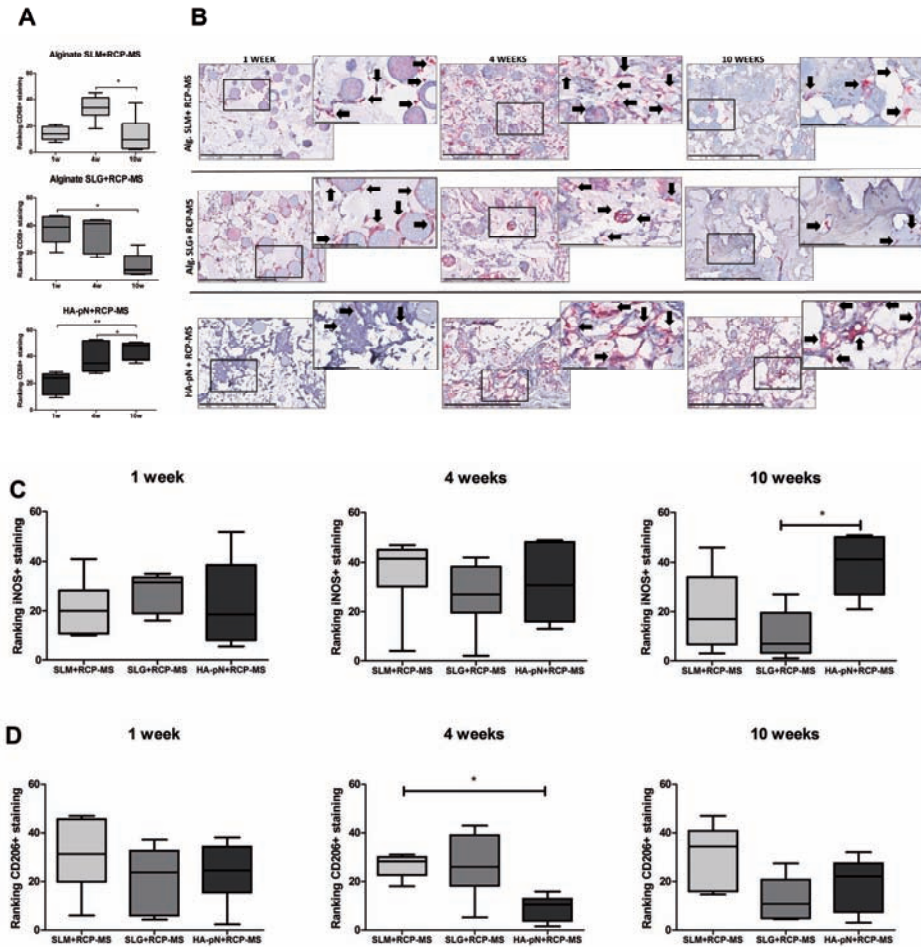


**Figure 2.4. CD68, iNOS and CD206 positive staining differed between hydrogel formulations.**

A. Two blind observers ranked the implants according to the CD68 positive staining found in the formulations at 1, 4 and 10 weeks. B. CD68 staining of a representative sample of each implant formulation at 1 and 10 weeks (scale bar is 400  $\mu$ m). The square grid shows the selected magnified area for each formulation. CD68-positive cells are indicated by black arrows (scale bar is 100  $\mu$ m). C. Ranked implants by two blind observers according to the iNOS positive staining found in the formulations at 1, 4, and 10 weeks. D. Ranked implants by two blind observers according to the CD206 positive staining found in the formulations at 1, 4 and 10 weeks. The line in the middle of the box is plotted at the median. The box extends from the 25th to 75th percentiles and the whiskers are drawn down to the 5th percentile and up to the 95th, (\*  $p < 0.05$ , \*\*  $p < 0.01$ ). Alginate SLM (SLM), alginate SLG (SLG), thermoresponsive hyaluronan derivative (HApN), Collagen-I based Recombinant Peptide microspheres (RCP-MS).

## 2.4.6 Injectable formulations loaded with BMP-2 promoted blood vessel ingrowth

Vascularization is a prerequisite for ossification. In all three formulations blood vessel density increased over time (Figure 2.5A). Interestingly the quantity of blood vessels found within the implants differed markedly between formulations, showing more than 5-fold more vessels in the HApN+RCP-MS formulation –mean  $\pm$  SD;  $395 \pm 82$  counted at 10 weeks– compared to the SLM+RCP-MS –with  $144 \pm 79$  at 10 week ( $p < 0.001$ )– (Figure 2.5A,B). In addition, in SLG+RCP-MS and HApN+RCP-MS the quantity of blood vessels was significantly higher at 10 weeks than at 1 week (mean  $\pm$  SD;  $144 \pm 79$  vs.  $13 \pm 16$  in alginate SLG+RCP-MS, and  $395 \pm 82$  vs.  $38 \pm 27$  in HApN+RCP-MS) (Figure 2.5A). Without BMP-2 no significant increase in the number of blood vessels were observed between 1 and 10 weeks in any of the formulations (data not shown).

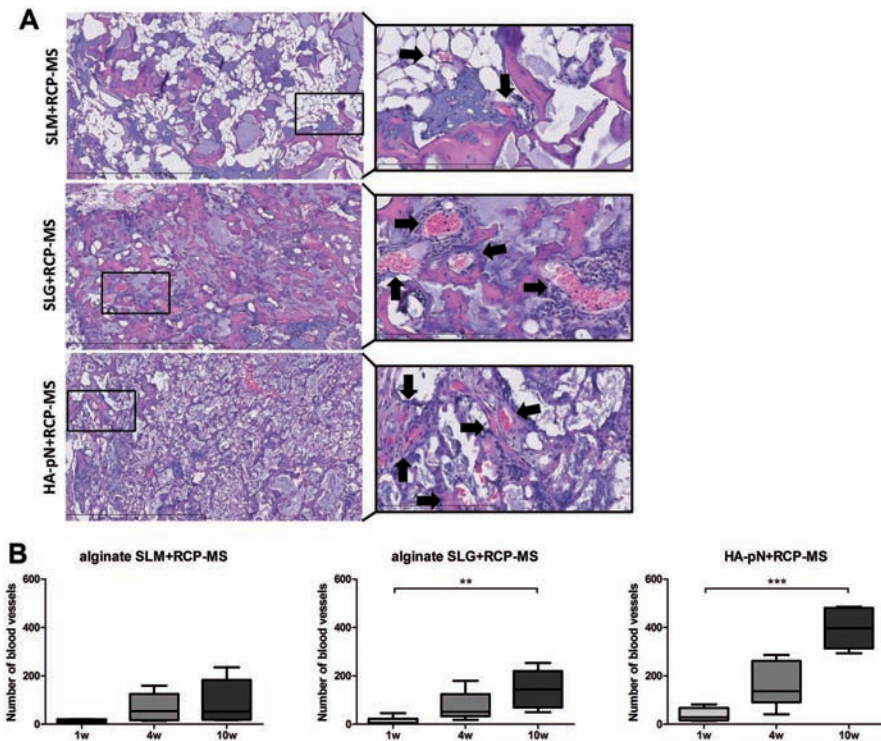




**Figure 2.5. Alginate SLG and hyaluronic acid loaded with BMP-2 significantly promoted blood vessel ingrowth.** A. Representative pictures of each implant formulation at 10 weeks (scale bar is 800  $\mu\text{m}$ ). The square grid shows the selected magnified area for each formulation (scale bar is 200  $\mu\text{m}$ ). B. In each section, blood vessels were counted. The graphs show the absolute number of blood vessels counted per formulation at 1, 4, and 10 weeks. The line in the middle of the box is plotted at the median. The box extends from the 25th to 75th percentiles and the whiskers are drawn down to the 5th percentile and up to the 95th, (\*  $p < 0.05$ , \*\*  $p < 0.01$ , \*\*\*  $p < 0.001$ ). Alginate SLM (SLM), alginate SLG (SLG), thermoresponsive hyaluronan derivative (HApN), Collagen-I based Recombinant Peptide microspheres (RCP-MS).

## 2.5 Discussion

In this study, we have developed three different sustained-release formulations with different physical and chemical properties to be used in bone tissue engineering. We have tested *in situ* gelling HApN formulation with thermo-responsive behavior and two alginate formulations with shear-thinning behavior as potential systems for the induction of *de novo* bone formation. We have found differences in the BMP-2 release pattern when loaded in HApN versus alginate hydrogels. Also, a further decrease in release rate was observed when BMP-2 was absorbed to RCP-MS and then combined with alginate hydrogels. Furthermore, we have shown that the slow-release gel-microsphere system comprised of SLG alginate supported the essential processes needed for bone formation, such as inflammatory cell infiltration, vascularization and osteogenesis *in vivo* and was superior to the SLM alginate and HApN formulations. Through analysis of the phenotype of the infiltrating cells and kinetics of blood vessel invasion we shed some light on the possible reasons for the differences observed between formulations.

Injectable matrices have been the subject of much research in the fields of drug delivery and tissue engineering due to the minimally invasive nature with which they can be delivered (99). We selected alginate and HApN formulations as carriers of RCP-MS for two reasons. First, they are both natural-origin polymers that are commonly used for bone regeneration; second, they can form *in situ* gelling systems. The *in situ* hydrogel forming ability of PNIPAM functionalized HA and alginate has already been shown (120, 128). However, the formulations with microspheres are novel and were developed specifically for this study. One advantage of the system with alginate is that it can form a reversible hydrogel (thixotropic) which has not been observed in other *in situ* gelling alginates (129). This reversible behavior of the gel makes handling much easier since the hydrogel can be prepared in advance and stored prior to application. Another advantage of both types of alginate formulations used in this study was the gelation time, which was so quick that the formed gel stayed in the injection site. In addition, the relatively slow degradation time of the alginates matched the time required for bone formation. The alginates showed some signs of initial degradation on histology by the first week, but after 10 weeks hydrogel was

still present, which kept the microspheres and protein at the site, supported the formation of new bone and delayed the release of BMP-2.

It is still controversial what the ideal BMP-2 release kinetics are to successfully form bone. Some studies have shown BMP2-mediated bone formation was not influenced by the release timing, while others demonstrated that in ectopic sites sustained-release significantly enhanced bone formation compared to burst release (110, 130). BMP-2 is chemoattractant to osteoprogenitor cells (131) and it is generally accepted that the delivery vehicle should maintain BMP-2 concentration within the therapeutic frame for enough time to allow recruitment and differentiation of osteoprogenitor cells. Therefore, the type of hydrogel chosen is important. In our study, the diffusion of BMP-2 seems to be faster in the SLM alginate than in the SLG hydrogel. However, when loaded in the microspheres the opposite happens, being faster the release in the SLG formulation. The slightly acidic environment initially created with GDL, might have solubilized BMP-2 more and led to more release. Previous publications have also shown that using microsphere/hydrogel combinations slows down protein release compared to the use of only hydrogels (64, 132-134). Our results are in agreement with those studies as we have observed 20% more BMP-2 retention when SLG and SLM were combined with RCP-MS. We have previously shown that the RCP-MS can only be degraded by collagenase treatment due to the highly crosslinked network and that when particles are fully degraded, BMP-2 could be released from the RCP-MS (58). Collagenase is crucial for the remodeling of collagenous extracellular matrices, including bone tissues and it is expressed by both osteoblasts and osteoclasts (135-137). These findings suggest that the collagenase expressed by the infiltrating cells might be an important factor for bone formation. In our study, it might have been also relevant for *in vivo* BMP-2 release from the RCP-MS and may have been a determining factor in the differences in bone formation observed between formulations. SLG+RCP-MS lead to more BMP-2 release than SLM+RCP-MS resulting in more bone formation. When HApN was used as a hydrogel, with or without the addition of RCP-MS, most of it was retained and no bone formation was observed. These data suggest a smaller pore size of HApN hydrogel due to higher molecular weight and initial dry content or a strong interaction between thermoresponsive HApN hydrogel and BMP-2 resulting in the retention of the protein. This has been observed previously for HA. In one study, HA-based powder gel composite showed slow release of less than 20% of the total amount of rhBMP-2 (138). Most likely this lack of release prevented the attraction of the necessary cells at the early stages and by the time it had been released the material was too degraded to modulate the release rate or structurally support bone formation. Whether this affinity for BMP-2 is specific to PNIPAM functionalized HA or is a more general phenomenon requires further investigation. It is important to mention that in alginate formulations  $\text{CaCO}_3$  was added to crosslink the hydrogels and therefore, calcium ions could still be present during the experiment. It has been widely demonstrated that the addition of calcium ions enhances the osteogenic capacity of osteoprogenitor cells and

the overall bone formation and, consequently, might have a positive effect in the outcome observed when alginate formulations were used in this study. However, it is unlikely that the significant difference in terms of bone formation between the different slow-release systems tested is only due to the presence of calcium ions, but to their physical properties such as stiffness or degradation rate.

The mechanical properties of the alginates showed that the storage (elastic) moduli are in the range of elastic moduli of endothelial tissue and stromal tissue (139). However, the elastic modulus of HApN with microspheres is higher than that of alginates and comparable to elastic modulus of a smooth muscle (139). These mechanical properties indicate that the gels can retain the microspheres *in situ*, fill a defect and provide initial support during the formation of bone. The mechanical properties of these thixotropic alginate hydrogels (1-2 kPa) are similar to non-*in situ* gelling alginates (140). According to Banerjee et al., gels with very high elastic moduli are undesirable and thixotropic gels with moderate elastic moduli (which were what we used in this study) should be suitable for bone regeneration (141). With regard to HA, 50% crosslinked HA had an elastic modulus of 30 Pa (142), which is far lower than the PNIPAM functionalized hydrogel presented in this study (5 kPa). After bone fracture, following the initial inflammation a callus forms. The mechanical properties of fracture callus have been measured and found to depend on multiple tissue types: the range of the indentation moduli was 0.61-1.27 MPa (median = 0.99 MPa) for granulation tissue, 1.39-4.42 MPa (median = 2.89 MPa) for chondroid tissue and 26.92-1010.00 MPa (median = 132.00 MPa) for woven bone (143). We therefore concluded that an elastic modulus in the range of 1-10 MPa is suitable for supporting the regenerative tissue. Given the mechanical properties of these hydrogels, it could be feasible to apply them directly to repair non-load bearing bone defects. For fractures or defects in the load bearing bones, the application would still require some other kind of mechanical stabilization, be that a traditional cast, internal fixation, or combination with other stronger biomaterials.

HA is a commonly used material for cartilage regeneration. Eglin et al. found that thermoresponsive HApN can be used to support hMSCs for the treatment of degenerated intervertebral disc and therefore HA hydrogels were developed as a bone-cartilage interface (144). Injectable HA has been shown to be successful in a rabbit osteochondral defect model (48). Interestingly, one study suggested that HA might impede bone formation by inhibiting osteoblast differentiation (145). Maus et al. used combinations of commercially available injectable HA with and without 200 µg BMP-2 in a sheep femoral defect. However, none of the conditions resulted in significant bone formation (114). Bakhta et al. used hyaluronan-based hydrogels loaded with 5 µg BMP-2 ectopically and observed significant bone formation within the formulations and a mineral volume of  $4.4 \pm 0.5 \text{ mm}^3$  after 8 weeks (60). However, prior to our study, *in situ* gelling HA had never been used in combination with particles to enhance cell adhesion and to promote bone tissue

formation. We used microspheres rich in RGD motifs as BMP-2 carrier and failed to show bone formation after 10 weeks. Unlike Bakhta et al., who implanted the formulations intramuscularly, which is more conducive to supporting *de novo* bone formation, we injected our formulation subcutaneously and this might account for the discrepancy observed.

How to modulate inflammation has become a hot topic in bone repair in the past decade (146-149). Several groups have studied both the influence of different biomaterials upon macrophage polarization *in vitro* (150-154) and the positive dose-dependent relationship between the dosage of BMP-2 and the inflammatory volume (87, 155-158). Most *in vivo* bone formation studies have investigated the inflammatory response involved by using a single marker to identify monocyte-macrophage-osteoclast cells such as TRAP or have relied on generic histology (e.g. H&E) to assess inflammation (87, 155, 159, 160). In our study, we used CD68, iNOS and CD206 as markers to identify macrophage presence and to indicate their phenotype within our tested formulations. The BMP-2 dose used in this study was low, to prevent potential side-effects associated with higher doses (such as inflammation), to allow us to better investigate the effects of the materials. We observed a late CD68+ cell infiltration in the HApN+RCP-MS formulations, which increased over time. It has been reported that macrophages can specifically recognize HA through receptors such as CD44 or the hyaluronan receptor for endocytosis, HARE (161) and that the HA-CD44 interaction is involved in multiple cellular functions such as inflammation (162). This might explain the high levels of inflammatory cell infiltrate observed at the later time points in the HApN+MS group. In contrast, in alginate formulations, CD68+ staining was lower at 10 weeks than at 1 week, and bone formation was successfully achieved. It is known that alginates from wound dressings interact with wound macrophages (163) and alginate-collagen formulations have been shown to locally integrate with host tissue in an abdominal wall defect model (164). Several studies have shown that the mannuronic acid residues of soluble alginate are cytokine-stimulating to monocytes (165). In our study, at 4 weeks, there was more CD206+ staining in the alginate formulations, especially in the alginate SLM, than in the HApN+MS formulation. These data suggest a possible polarization of the monocytes toward the anti-inflammatory/tissue remodeling M2 phenotype. Moreover, there were significantly more iNOS+ cells in the HApN+RCP-MS formulation than in the alginate formulations at 10 weeks, which is more indicative of a proinflammatory situation. Taken together the results suggest that within alginate formulations there was an initial inflammatory phase that resolved over time, leading to bone formation. In contrast, in the HApN+RCP-MS formulation the presence of proinflammatory cells increased over time and there were with significantly fewer anti-inflammatory CD206 positive cells. This likely also negatively influenced the bone formation process in the HApN+RCP-MS gels.

Vascularization is another critical factor for successful bone formation. It has been demonstrated that HA-based scaffolds promote angiogenesis when used in a wide variety of applications, such as abdominal wall defect repair, brain injury or heart disease models (166-168). Moreover, Cui et al. demonstrated the ability of HA-RGD scaffolds to support angiogenesis in the cortex of the brain (169). Similarly, alginate-based beads loaded with VEGF had been used subcutaneously for bone tissue engineering, promoting angiogenesis (170). Furthermore, a study in which alginate and alginate-RGD hydrogel were injected into the infarct area of rats showed that both increased arteriole density but that the greatest angiogenic response was in the alginate-RGD hydrogel condition (171). Our findings agree with the results obtained in previous studies and we have demonstrated that both thermoresponsive HA and alginate enriched with RGD MS are able to promote vasculature formation ectopically when loaded with BMP-2. It is, however, clear that in this case more does not necessarily mean better: although significantly more vessels were present in the HA implants than in the alginates, this did not lead to the formation of any bony tissue.

## 2.6 Conclusions

*In situ* gelling hydrogels encapsulating BMP-2 loaded RCP-MS represent an injectable slow-release protein delivery system. Alginate formulations effectively promoted bone formation in an ectopic model. While there was successful infiltration of cells into all three formulations, differences between materials were observed in the macrophage phenotype and invasion kinetics. Also, while there was ample vascularization in all three materials there were clear differences in the total number of blood vessels with the higher number present in the HA formulation not increasing the success of *de novo* bone formation. Thus, alginate SLG combined with RCP-MS and loaded with low dose BMP-2 displayed optimal protein release rate, cellular invasion, material degradation rate and vascularization kinetics to support bone formation. This study presents a novel cell-free injectable slow-release system that has potential as a void-filling material for the induction of new bone formation.

# 2.7 Supplemental information

**Table S 2.1** Table showing the strain % at which the structure breaks, as shown by the amplitude sweeping test analyzed by rheology.

Type of structure	Strain % at which the structure breaks
Alginate only	12
Alginate (SLG-20) + 8% RCP-MS	150
Alginate (SLG-20) + 8% RCP-MS + GDL	>167
Alginate + CaCO <sub>3</sub> (1 μm size) + GDL	40

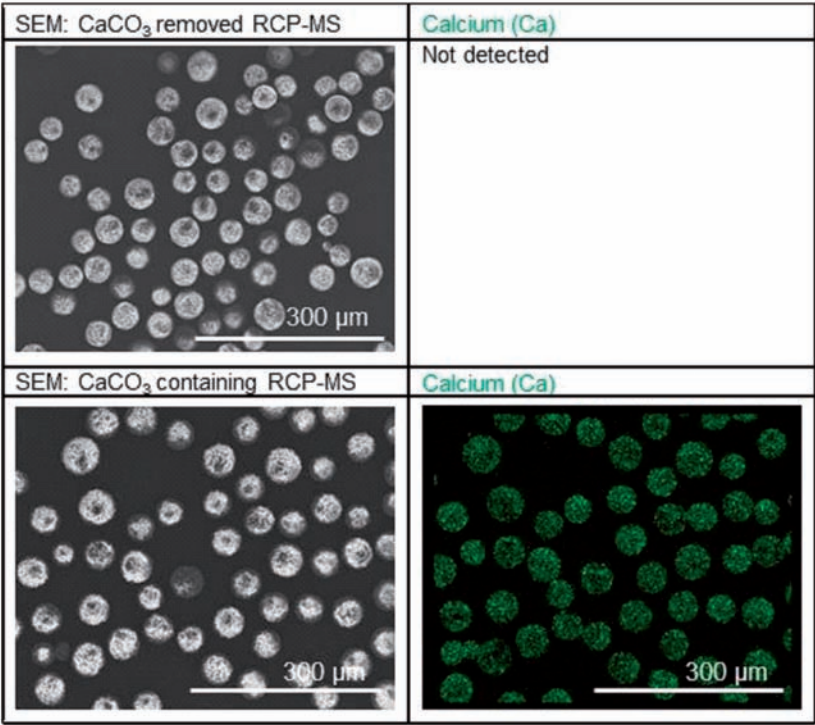


**Figure S2.1.** Scanning electron microscopy (left) and energy-dispersive X-ray spectroscopy (right) mapping of RCP-MS after (upper lane) and before CaCO<sub>3</sub> removal (lower lane).

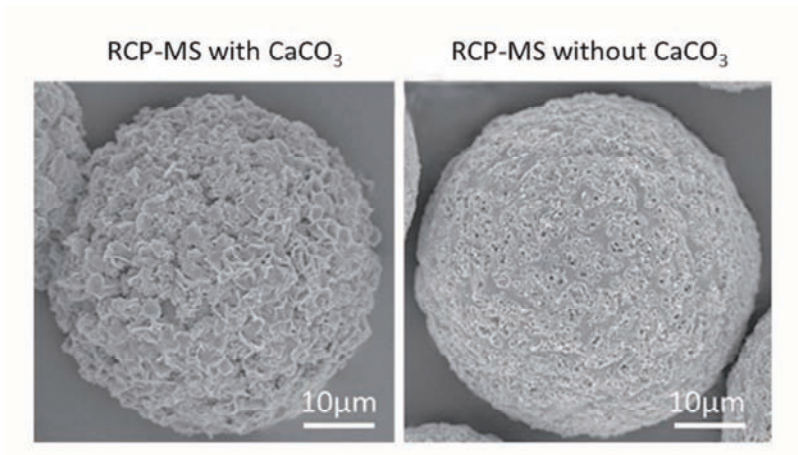


**Figure S2.2.** Morphology of RCP-MS shown by scanning electron microscopy (SEM). The  $\text{CaCO}_3$  crystals are visible on the microspheres on the left as flaky structures.

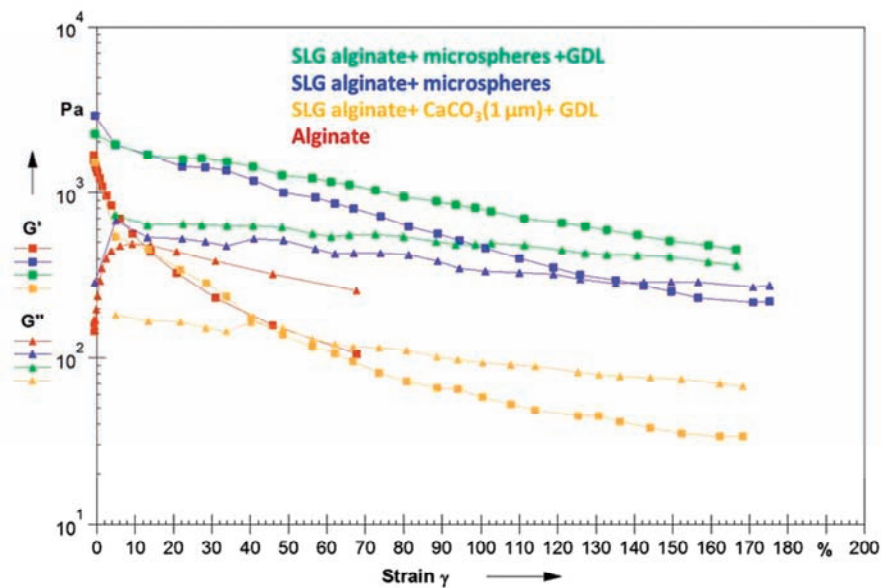


**Figure S2.3.** Strain-dependent oscillatory rheology of in situ gelling alginate hydrogels and of the negative controls consisting of an alginate hydrogel, crosslinked at higher calcium concentration, and an alginate hydrogel containing  $\text{CaCO}_3$  particles.

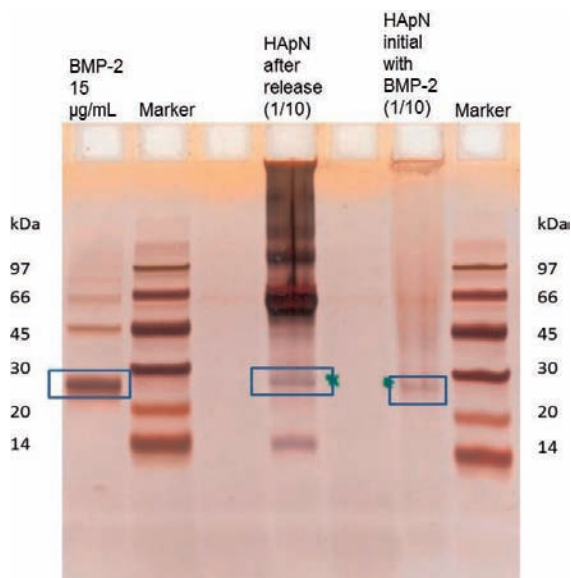


**Figure S2.4. SDS-PAGE of BMP-2 protein.** Bands are shown inside blue rectangles. Lanes from left to right are: control BMP-2 solution at 15 µg/mL; marker; empty lane; HApN hydrogel after release diluted 10 times before loading; empty lane, HApN hydrogel loaded with BMP-2 (before release) diluted 10 times before loading; marker. The density of BMP-2 band after release is more intense than before release. This might be related to the higher interaction between BMP-2 and HApN initially.

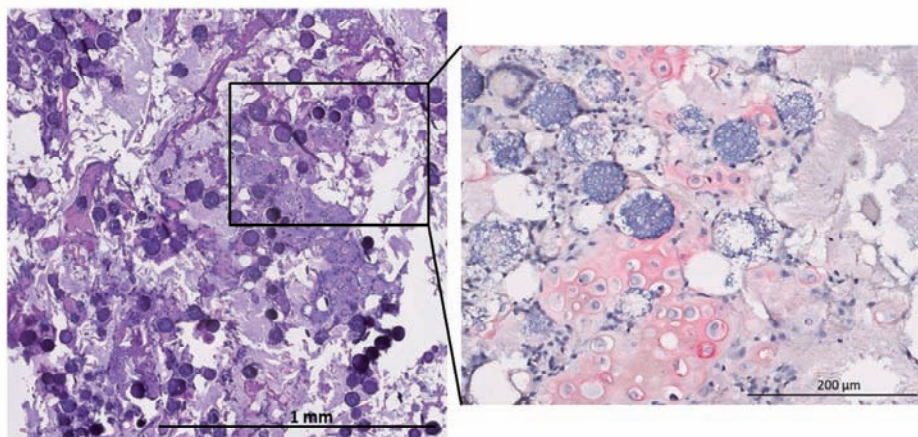


**Figure S2.5. Endochondral ossification was observed within alginate formulations since 4 week-period to the end of the experiment.** Representative picture of alginate SLM+RCP-MS formulation loaded with BMP-2 and stained by H&E at 4 weeks after implantation. The magnification shows collagen II positive cells within the central region of the implant.



## **2.8 Acknowledgments**

The authors would like to thank Dr. Joachim Nickel for his generous gift of BMP-2. The research leading to these results received funding from the European Union Seventh Framework Programme FP7-PEOPLE-2013-ITN under grant agreement n° 607051.



# 3

## Injectable BMP-2 delivery system based on collagen derived microspheres and alginate induced bone formation in a time- and dose-dependent manner

Didem Mumcuoglu<sup>#</sup>, Shorouk Fahmy-Garcia<sup>#</sup>, Yanto Ridwan, Joachim Nickel, Eric Farrell, Sebastiaan G.J.M. Kluijtmans and Gerjo J.V.M van Osch

<sup>#</sup> Authors contributed equally to this work

Eur Cell Mater. 2018 Apr 26;35:242-254. doi: 10.22203/eCM.v035a17.

### 3.1 Abstract

The aim of the current study was to reduce the clinically used supraphysiological dose of bone morphogenetic protein-2 (BMP-2) (usually 1.5 mg/mL), which carries the risk of adverse events, by using a more effective release system. A slow-release system, based on an injectable hydrogel composed of BMP-2-loaded recombinant collagen-based microspheres and alginate, was previously developed. Time- and dose-dependent subcutaneous ectopic bone formation within this system and bone regeneration capacity in a calvarial defect model were investigated. BMP-2 doses of 10 µg, 3 µg and 1 µg per implant (50 µg/mL, 15 µg/mL and 5 µg/mL, respectively) successfully induced ectopic bone formation subcutaneously in rats in a time- and dose-dependent manner, as shown by micro-computed tomography (µCT) and histology. In addition, the spatiotemporal control of BMP-2 retention was shown for 4 weeks *in vivo* by imaging of fluorescently-labelled BMP-2. In the subcritical calvarial defect model, µCT revealed a higher bone volume for the 2 µg of BMP-2 per implant condition (50 µg/mL) as compared to the lower dose used (0.2 µg per implant, 5 µg/mL). Complete defect bridging was obtained with 50 µg/mL BMP-2 after 8 weeks. The BMP-2 concentration of 5 µg/mL was not sufficient to heal a calvarial defect faster than the empty defect or biomaterial control without BMP-2. Overall, this injectable BMP-2 delivery system showed promising results with 50 µg/mL BMP-2 in both the ectopic and calvarial rat defect models, underling the potential of this composite hydrogel for bone regeneration therapies.

### 3.2 Introduction

Autologous bone is widely used in bone grafting surgery. However, its limited availability and the discomfort related to the harvesting procedure have diverted the field to seek for alternative methods involving biomaterials (39). Bone morphogenetic proteins (BMP-2 and BMP-7), being successful in inducing bone formation, are already translated to clinics (101). BMP-2 absorbed on collagen sponge is approved by the United States Food and Drug Administration for spinal fusion, tibial nonunions and oral-maxillofacial reconstructions (172, 173). However, adverse events observed in clinics have limited the use of BMP-2, especially for off-label applications (104, 156, 174, 175). These adverse events, mainly inflammation (87) and swelling (176), are associated with the supraphysiological dose of BMP-2 loaded onto the collagen sponge (88), in combination with the strong burst release. Half of the loaded BMP-2 is released from the collagen sponge in the first two days *in vivo* (103). Possibly these adverse events can be mitigated by using an appropriate release system comprising lower BMP-2 dose (105, 177). Such a system might broaden the potential use of BMP-2 in orthopaedic and maxillofacial surgery applications.

The dose or concentration of BMP-2 is very important for bone formation (178-180). Since no naturally bone-forming cells are present within the intradermal environment, subcutaneous ectopic bone can only be formed by injecting bone-forming cells or an osteoinductive protein, such as BMP-2, that can recruit progenitor cells (181). The concentration or dose of BMP-2 required to induce ectopic bone formation depends on the type of carrier material used. For example, using 5  $\mu\text{g}$  of BMP-2, 32% bone formation is achieved using a 9 mm<sup>3</sup>  $\beta$ -tricalcium phosphate scaffold, whereas hydroxyapatite, with the same amount of BMP-2, only yields 3% bone formation in a rat ectopic model (182). 5  $\mu\text{g}$  of rhBMP-2, implanted with a 6 mm in diameter collagen sponge, are required to induce a small intramuscular bone formation in mice, with a maximum volume of 5 mm<sup>3</sup> (183). 10 mg of silk fibroin particles, loaded with 5  $\mu\text{g}$  of BMP-2, induce the formation of a small volume (2 mm<sup>3</sup>) of ectopic bone after 4 weeks in rats (184). A low dose of BMP-2 (less than 1  $\mu\text{g}$ ), delivered on a collagen sponge or with brushite calcium-phosphate particles, does not form any bone in the palatal submucosa of rats (185), confirming the presence of a threshold dose. This threshold depends on the type of material and application site and is associated with the release kinetics/degradation time of the material and subsequent cellular infiltration rate (178). An *in situ* gelling sustained-BMP-2-release system, which induces ectopic bone formation, is available (186). This hydrogel system is based on BMP-2-loaded microspheres, composed of a recombinant peptide based on the sequence of collagen I (RCP), embedded in a high guluronate-type-alginate. The use of RCP allows for a reproducible production, without risks of disease transmission, which can be associated to purified collagen materials. More importantly, RCP has excellent cell attachment properties (106) and a specific affinity to bind BMP-2 (58), which makes it appealing as a controlled release system. The main advantages of the developed system are its

thixotropic behaviour, resulting in easy handling and injectability, good BMP-2 release profile and good performance *in vivo* in terms of cellular infiltration, degradation and bone formation (186). The aim of the current study was to investigate time- and dose-dependent bone formation using this BMP-2-releasing hydrogel in an ectopic bone formation model and, in addition, to test the bone regeneration capacity of two selected doses of BMP-2 in an orthotopic model. Formulations containing 4 different doses of BMP-2 (10 µg, 3 µg, 1 µg and 0.3 µg per implant; 50 µg/mL, 15 µg/mL, 5 µg/mL and 1.5 µg/mL, respectively) and an empty control were injected subcutaneously into the dorsum of immune-competent rats. Ectopic bone formation was followed over a time course of 10 weeks by micro-computed tomography (µCT), with histology at the endpoint of 10 weeks. To study the spatiotemporal release of BMP-2 *in vivo*, formulations containing 3 different doses of fluorescently-labelled BMP-2 were injected subcutaneously into rats and monitored over a time course of 10 weeks by *in vivo* fluorescence imaging. Finally, two doses of BMP-2 (50 µg/mL and 5 µg/mL) were further investigated in a calvarial defect model. For this purpose, 40 µL of the composite hydrogel formulation, containing 2 µg and 0.2 µg of BMP-2, were injected in 5 mm subcritical calvarial defects in immune competent rats and bone formation was studied by µCT longitudinal imaging for 10 weeks.

### 3.3 Materials and methods

#### 3.3.1 Materials

RCP is a product of Fujifilm, which is commercially available as Cellnest™. RCP is produced by the genetically modified yeast *Pichia pastoris* in a fermentation process previously described (58, 106, 118, 187). RCP is a 571 amino acids protein, having an isoelectric point (pI) of 10.02 and a molecular weight of 51.2 kDa. The recombinant human bone morphogenetic protein-2 (rhBMP-2, amino acids 283 to 396 plus an N-terminal Met-Ala) was expressed in *Escherichia coli*, isolated from inclusion bodies, renatured and purified, as previously described (119). Lyophilized BMP-2 was dissolved in distilled water and the concentration was determined by UV/Vis spectroscopy. Freshly dissolved BMP-2 was used for the experiments. For the fluorescence measurements, rhBMP-2 was fluorescently-labelled using DyLight™ 800 (ThermoFisher Scientific). For the labelling, dissolved BMP-2 solution was adjusted to pH 4.5 by addition of a 2 M sodium acetate solution (pH 4.5). Subsequently, DyLight™ 800 NHS Ester, dissolved in dimethyl sulphoxide (DMSO), was added in a 5-fold molar excess and the mixture was incubated for 4 h at 4 °C while shaking. After incubation, the protein was separated from non-coupled dye by anionic exchange chromatography using a HiTrap® SP HP column (GE Healthcare). Since the protein could not be eluted even at 2 M sodium chloride salt concentration, it was recovered using an aqueous 6 M guanidinium hydrochloride solution. Subsequently, the protein was dialyzed to 1 mM hydrochloric acid and finally to distilled water.

PRONOVA™ SLG20 (sterile alginate, where over 60% of the monomer units are guluronate) was ordered from NovaMatrix (Sandvika, Norway). The properties of the SLG20 alginate are assessed by the producer: viscosity (mPa × s): 20-99; approximate molecular weight (kDa): 75-150; guluronate/mannuronate (G/M) ratio:  $\geq 1.5$ ; endotoxins (EU/g):  $\leq 100$ ; total viable count [colony forming unit (cfu)/g]: sterile (www.novamatrix.biz). Hexamethylene diisocyanate (HMDIC), corn oil, sodium chloride, calcium carbonate ( $\text{CaCO}_3$ ) and glucono delta lactone (GDL) were purchased from Sigma-Aldrich. Ethanol, acetone and hydrochloric acid were purchased from Millipore. The ELISA development kit and reagents for BMP-2 quantification were ordered from Peprotech (Rocky Hill, NJ, USA). Dulbecco's modified Eagle's medium (DMEM), foetal bovine serum (FBS) and penicillin-streptomycin (P/S) were ordered from ThermoFisher Scientific.

### 3.3.2 RCP microsphere preparation

RCP-calcium carbonate composite microspheres were produced by emulsification, as described previously (58). Briefly, a 20% aqueous RCP solution was prepared and mixed with  $\text{CaCO}_3$  fine powder (with a size of  $< 1 \mu\text{m}$ ) in a 1:1 (w/w) ratio. This suspension was emulsified in corn oil at  $50^\circ\text{C}$ , while stirring the emulsion at 800 rpm for 20 min. After cooling down the emulsion, the emulsified microspheres were washed three times with acetone. After overnight drying at  $60^\circ\text{C}$ , microspheres were sieved to  $50\text{--}72 \mu\text{m}$  size using sieves from Retsch GmbH (Haan, Germany). Subsequently, particles were crosslinked by hexamethylene diisocyanate (HMDIC) by mixing and stirring of 1 g of spheres and 1 mL of HMDIC in 100 mL ethanol for 1 d. Non-reacted crosslinker was removed by washing several times with ethanol.  $\text{CaCO}_3$  was left in the particles since  $\text{Ca}^{2+}$  ions are used to crosslink alginate in the final hydrogel formulation. Particles were then  $\gamma$ -sterilized at 25 kG (Synergy Health, Etten Leur, the Netherlands). The release of BMP-2 from RCP microspheres is described by Mumcuoglu et al. (58).

### 3.3.3 Preparation of the RCP microsphere-alginate hydrogel formulations

SLG-20 alginate was dissolved in 0.9% sterile sodium chloride to create a 2% w/v solution. 68 mg of sterile microspheres were incubated with 170  $\mu\text{L}$  of BMP-2- containing solution at  $4^\circ\text{C}$  overnight. Initial BMP-2 concentrations used were 379.4  $\mu\text{g/mL}$ , 113.8  $\mu\text{g/mL}$ , 37.9  $\mu\text{g/mL}$  and 11.4  $\mu\text{g/mL}$ , to yield final BMP-2 concentrations in the hydrogel formulation of 50  $\mu\text{g/mL}$ , 15  $\mu\text{g/mL}$ , 5  $\mu\text{g/mL}$  and 1.5  $\mu\text{g/mL}$ , respectively. Next day, when all BMP-2-containing liquid was absorbed, 1014  $\mu\text{L}$  of the 2% w/v SLG20 solution were added and the swollen microspheres were resuspended. Then, 106  $\mu\text{L}$  of 0.06 M fresh GDL solution were added and mixed immediately. GDL was used to dissolve minute amounts of  $\text{CaCO}_3$ , thereby crosslinking alginate and increasing the mechanical property of the formulation. The formulations were thoroughly mixed, passed through a 19 G needle immediately after

addition of all components and stored overnight at 4 °C to equilibrate. Next day, the prepared formulations were mixed again prior to use.

### **3.3.4 *In vitro* release of BMP-2 from hydrogel formulations**

Hydrogel formulations were prepared as described above, containing either fluorescently-labelled or wild-type BMP-2. Since these experiments had the objective to study only BMP-2 release, the biological activity of these proteins was not tested. 200 µL of each hydrogel were added to each well of a 24-well plate, inserts with a 0.4 µm pore size. 1 mL of DMEM supplemented with 10% FBS and 1% P/S per well was added to the reservoir plate. The plates were incubated at 37 °C under constant agitation at 300 rpm. At each time point, all medium (1 mL) was collected from the reservoir plate and changed with fresh medium (1 mL). Positive controls were 10 µg, 3 µg or 1 µg of wild type or fluorescently-labelled BMP-2 in 1 mL DMEM. At every time point, 100 µL of these positive controls were sampled. The collected release media and control samples were analyzed using the rhBMP-2 ELISA development kit, according to manufacturer's protocol. To calculate the fraction released at each time point, the concentrations detected in the release medium of the hydrogel samples were normalized to the concentrations of the positive controls, to correct for loss by adsorbance to the tube and/or degradation of the protein.

### **3.3.5 Study design and ethics**

All animal experiments were performed with prior approval of the Erasmus Medical Centre ethics committee for laboratory animal use (project number: AVD101002015114 and protocol numbers: EMC 15-114-03 and EMC 15-114-04). 10-week-old male Sprague Dawley (SD) rats (Charles River) were used. The animals were randomly assigned and housed in pairs in specific-pathogen-free conditions and allowed to adapt to the conditions of the animal house for 7 d before implantation. The animals were maintained at 22 ± 5 °C on a 12 h dark/light cycle with access to standard rat chow and water *ad libitum*. 10 weeks after implantation, animals were euthanized with CO<sub>2</sub> and the specimens were harvested for µCT analysis and histology.

### **3.3.6 Subcutaneous injection of *in situ* gelling formulations to study ectopic bone formation**

To evaluate the effect of different doses of BMP-2 on ectopic bone formation, the hydrogel compositions were subcutaneously injected (total volume: 200 µL per injection) into the dorsum of the rats (20 rats in total). Each animal received 4 or 5 randomly assigned injections. All injections were performed on animals under isoflurane inhalation. To study the BMP-2-dose effect on bone formation, 4 different BMP-2 concentrations were used (50, 15, 5 and 1.5 µg/mL), resulting in total doses of 10 µg, 3 µg, 1 µg and 0.3 µg BMP-2 per implant (n = 8 per group), respectively. As a control, alginate with microspheres, but



without BMP-2 was injected ( $n = 6$ ). To investigate the spatiotemporal distribution of BMP-2 in the implanted material *in vivo*, 200  $\mu\text{L}$  of hydrogel containing fluorescently-labelled BMP-2 were injected at different doses: 10  $\mu\text{g}$ , 3  $\mu\text{g}$  and 1  $\mu\text{g}$  ( $n = 6$ ). Longitudinal imaging was performed by  $\mu\text{CT}$  and *in vivo* imaging instruments (IVIS) biweekly until the end of the experiment (10 weeks).

### 3.3.7 Calvarial defect model to study bone regeneration with *in situ* gelling formulations

To evaluate the effect of two hydrogel formulations with a selected dose of BMP-2 on orthotopic bone formation, two defects of 5 mm in diameter were created in the rat calvaria (18 rats in total). Prior to the surgery, animals received intraperitoneal injections of 0.05 mg/kg buprenorphine (Temgesic®; Indivior, Slough, UK) and 5 mL/kg sterile normal saline to account for fluid loss. Surgeries were performed under 2.5% isoflurane anaesthesia. The animal skulls were shaved and disinfected with ethanol swabs. Then, an incision was made through the skin of the calvarium and the periosteum and full-thickness flaps were reflected. The defect was irrigated along the sagittal midline of the skull with 0.1 mL of 1% xylocaine with 1:200,000 epinephrine (AstraZeneca). Under copious sterile saline irrigation, two 5 mm in diameter bone defects were drilled in each animal using a micro trephine drill (Fine Science Tools, Heidelberg, Germany) and any visible debris or bone chips were removed. Then, 40  $\mu\text{L}$  of hydrogel formulation with BMP-2 or, as a control, without BMP-2 were injected into the defect. As sham control, empty defects were used (5 rats, 10 defects). As a biomaterial control, alginate with microspheres were injected into the defects (5 rats, 10 defects). Alginate with microspheres loaded with 50  $\mu\text{g}/\text{mL}$  BMP-2 (3 rats, 3 defects) was used to study healing with a high BMP-2 dose; alginate with microspheres loaded with 5  $\mu\text{g}/\text{mL}$  (5 rats, 10 defects) was used to study healing with a low BMP-2 dose. The animal number of the 50  $\mu\text{g}/\text{mL}$  BMP-2 cohort was kept small because it was expected to induce bone formation, based on the results of a previous ectopic bone formation study shown in Chapter 2 (186). After implantation, the periosteum and the skin above the defects were repositioned and sutured with polylactic acid sutures (Vycril 4.0, Ethicon, Johnson & Johnson, São José dos Campos, Brazil). During the next 3 d, all animals received three postoperative doses of buprenorphine for analgesia every 10 h. Longitudinal imaging was performed biweekly by  $\mu\text{CT}$  until week 10. 10 weeks after implantation, animals were euthanized with  $\text{CO}_2$  and the specimens were harvested for  $\mu\text{CT}$  analysis and histology.

### 3.3.8 $\mu\text{CT}$ imaging

$\mu\text{CT}$  (Quantum FX, PerkinElmer) was used to image animals 1, 2, 4, 6, 8 and 10 weeks after injection and the implants retrieved at week 10. To image the ectopic bone *in vivo*, the following parameters were used: field of view, 73 mm; voltage, 90 kV; current, 160  $\mu\text{A}$ ;

scan time, 120 s; resolution, 148  $\mu\text{m}$ . To image the retrieved ectopic bone field of view of 20 mm, scan time of 120 s and resolution of 40  $\mu\text{m}$  were used. To image the calvarial defects, a 30 mm field of view, scan time of 3 min and resolution of 59  $\mu\text{m}$  were used. The trabecular and cortical bone mineral density (BMD) were determined based on the calibration scanning, using two phantoms with known density (0.25  $\text{g}/\text{cm}^3$  and 0.75  $\text{g}/\text{cm}^3$ ; Bruker  $\mu\text{CT}$ ) measured under identical conditions. For image processing, Analyze software version 11.0 was used (Mayoclinic, Rochester, MN, USA). Threshold levels were set to 0.11  $\text{g}/\text{cm}^3$ , 400 Hounsfield units.

### 3.3.9 Fluorescence imaging *in vivo*

An IVIS Imaging System 200 (PerkinElmer) was used to image fluorescent BMP in the animals immediately after the injection, 3 d and 1, 2, 4, 6, 8 and 10 weeks after injection. The following imaging parameters were used: exposure time, 20 s; excitation, 745 nm; emission, 820 nm and 840 nm. For the image analysis, the region of interest for each implant was selected as a circle with an area of  $3.0 \pm 0.1 \text{ cm}^2$  and the total radiant efficiency  $[(\text{p/s})/(\mu\text{W}/\text{cm}^2)]$  was calculated by the Living Image<sup>®</sup> software (PerkinElmer). A region of interest of  $3 \text{ cm}^2$  was selected since this was the magnitude of the area where the signal was detected directly after injection.

### 3.3.10 Histology

For histological analysis of the subcutaneous ectopic bone formation, specimens were fixed in 4% formalin solution for 48 h and decalcified with 10% ethylenediaminetetraacetic acid (EDTA) for 2-4 weeks. Implants were dehydrated in graded ethanol solution from 70% to 100% and embedded in paraffin. 6  $\mu\text{m}$ -thick sections were prepared using a Leica microtome and mounted on subbed glass slides (ThermoFisher Scientific). Three cross-sections, at least 200  $\mu\text{m}$  apart from each other, were collected from each implant. The sections were deparaffinized and rinsed with distilled water to be stained with haematoxylin and eosin (H&E). For calvaria samples, 10 weeks after implantation, the relevant part of the skull was removed and fixed in neutral buffered 4% formalin solution for 3 d, dehydrated in graded ethanol solution from 70% to 100% and embedded in methyl methacrylate resin. 10  $\mu\text{m}$ -thick sections were generated along the long axis of the cylindrical samples on a saw microtome system (Leica 4 SPI600). Samples were stained with von Kossa and Goldner's trichrome stainings, as previously described (188, 189). The sections were imaged by NanoZoomer-XR (Hamamatsu, Japan).

### 3.3.11 Statistical analysis

The quantitative  $\mu\text{CT}$  data of retrieved ectopic bone were analyzed using one-way analysis of variance (ANOVA) and a Bonferroni *post-hoc* multiple comparison test. *In vivo* calvaria  $\mu\text{CT}$  data were analyzed using two-way analysis of variance (ANOVA) and a Bonferroni

*post-hoc* multiple comparison test. A value of  $p < 0.05$  was considered statistically significant. Linear regression analysis of  $\mu$ CT data was performed by GraphPad, to analyze the time-dependent bone formation

### 3.4 Results

#### 3.4.1 BMP-2 was retained for at least 4 weeks *in vivo*

To monitor the retention of BMP-2 *in vivo*, composite hydrogels (alginate with RCP microspheres), with three different doses of fluorescently-labelled BMP-2, were used. First, it was confirmed *in vitro* that the release of fluorescently-tagged (fluo) BMP-2 from the hydrogels was similar to wild type BMP-2 (Figure 3.1). The difference between the release of the two proteins was less than 10%, showing that labelled protein could be used to study retention of BMP-2 *in vivo*. Then, the fluorescence signal (shown as radiance efficiency) of the 3 doses injected subcutaneously was followed *in vivo* by fluorescence imaging. The fluorescence signal generated by the three different BMP-2 doses decreased until week 4 (Figure 3.2). After 4 weeks, all fluorescence curves levelled off. Interestingly, the fluorescence values did not drop to the background value, indicating the presence of some remaining BMP-2 in the hydrogels. The curves corresponding to the different doses were not significantly different due to high variation among the animals (Figure 3.2).

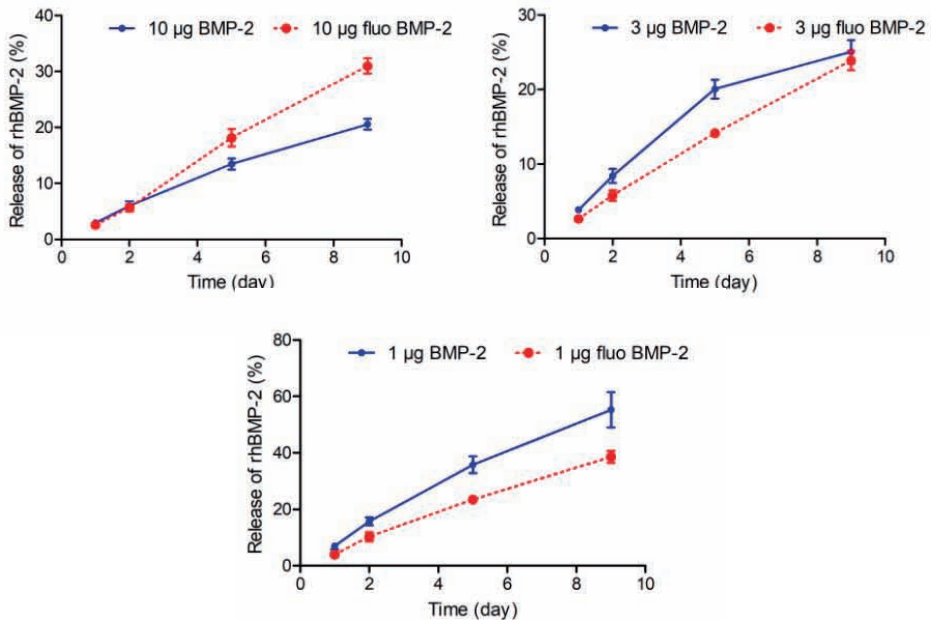


**Figure 3.1.** *In vitro* release of fluorescently-labelled (fluo) and non-labelled BMP-2 from the RCP microspheres with alginate hydrogel, showing no major difference between labelled and non-labelled BMP-2 release *in vitro* in DMEM with 10% FBS and 1% P/S.

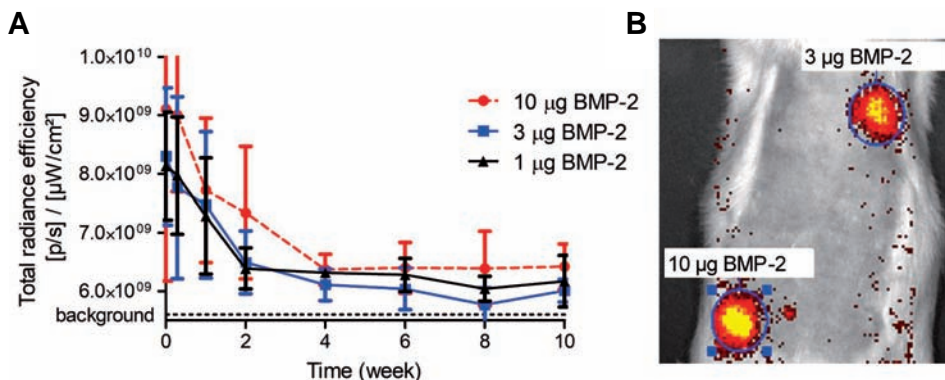


**Figure 3.2.** A. BMP-2 was retained in the RCP microspheres with alginate hydrogels *in vivo* for at least 4 weeks. The total radiance efficiency of the fluorescence signal was shown for three different doses of fluorescent BMP-2 (10 µg, 3 µg and 1 µg) containing RCP microspheres with alginate that were injected subcutaneously in SD rats ( $n = 6$  injections). B. Representative image of *in vivo* fluorescence imaging.

### 3.4.2 Microspheres with alginate hydrogel induced BMP-2 dose-dependent ectopic bone formation

The effect of the BMP-2 dose on subcutaneous ectopic bone formation was investigated over a period of 10 weeks using 4 different BMP-2 doses (representative  $\mu$ CT images are shown in Figure 3.3A). At the 10-week endpoint, the bone volume formation resulted to be dose-dependent (Figure 3.3B). The highest dose of 10 µg (50 µg/mL) induced the largest volume of ectopic bone formation, while the lowest doses of 0.3 µg (1.5 µg/mL) and 0 µg of BMP-2 failed to form bone. The composite hydrogel containing 1 µg of BMP-2 (5 µg/mL) formed just a minute bone volume, indicating that this dose was the threshold of ectopic bone induction in rats for this composite hydrogel. The bone mineral density of the formed bone did not differ significantly (Figure 3.3C): 0.5 g/cm<sup>3</sup> for 3 µg and 10 µg of BMP-2 and 0.35 g/cm<sup>3</sup> for 1 µg of BMP-2. For comparison, tibiae were extracted and imaged using the same instrumental settings. The cortical and trabecular bone of the tibiae had a density between 1.2-2.0 g/cm<sup>3</sup> and 0.15-0.5 g/cm<sup>3</sup>, respectively, showing that ectopic bone formed subcutaneously had a density in the range of trabecular bone.

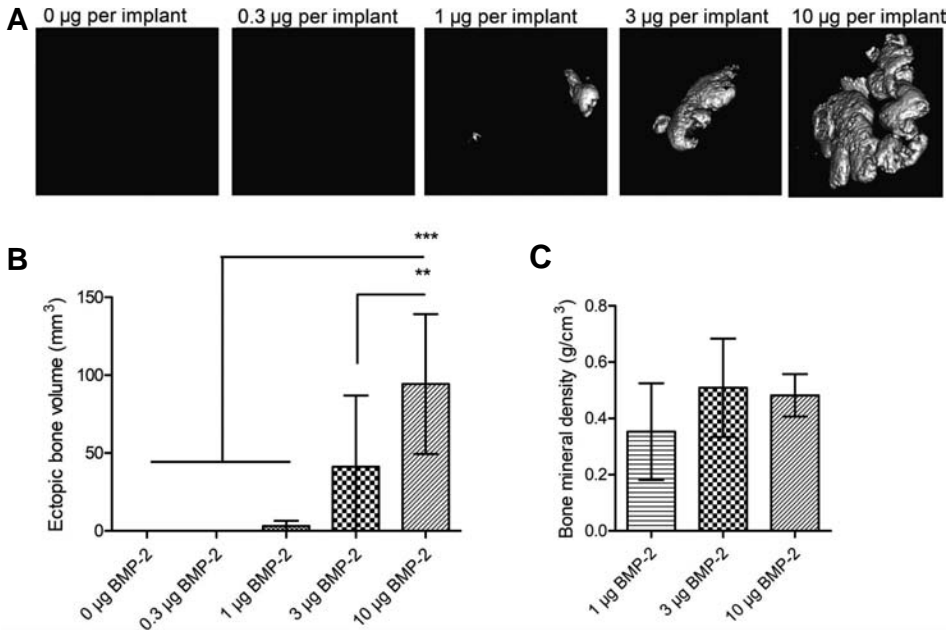


**Figure 3.3. Ectopic bone formation at 10 weeks was BMP-2 dose-dependent.** A. Representative images of  $\mu\text{CT}$  of implants retrieved at 10 weeks. B. Volume of ectopic bone in  $\text{mm}^3$ . C. Bone mineral density after thresholding to  $0.11 \text{ g/cm}^3$ , 400 Hounsfield units. (A, B, C) Five different doses of BMP-2 (10  $\mu\text{g}$ , 3  $\mu\text{g}$ , 1  $\mu\text{g}$ , 0.3  $\mu\text{g}$  and 0  $\mu\text{g}$ ) containing RCP microspheres with alginate (200  $\mu\text{L}$ ) were injected subcutaneously in SD rats ( $n = 8$  injections). Data are shown as mean  $\pm$  SD, one-way ANOVA was performed to compare treatment groups. \*\*  $p < 0.05$ , \*\*\*  $p < 0.001$ .

### 3.4.3 Microspheres with alginate hydrogel containing different doses of BMP-2 showed different kinetics of bone formation

Longitudinal  $\mu\text{CT}$  imaging of rats for 10 weeks revealed a dose-dependent rate of ectopic bone formation (Figure 3.4A,B). The volume of ectopic bone in the 10  $\mu\text{g}$  of BMP-2 group increased linearly between week 1 and week 8, with a rate of  $16.9 \pm 0.8 \text{ mm}^3/\text{week}$  ( $r^2 = 0.99$ ), after which a plateau was reached. A 10-week endpoint was decided based on the longitudinal  $\mu\text{CT}$  imaging data. Ectopic bone volume did not increase between 8 and 10 weeks for the highest dose; therefore, the experiment was ended at 10 weeks. In the 3  $\mu\text{g}$  of BMP-2 group, a two-phase linear trend was observed. Between 2 and 6 weeks, a linear increase in bone volume, with a rate of  $10.2 \pm 0.5 \text{ mm}^3/\text{week}$  ( $r^2 = 0.99$ ), was observed, while a slower linear trend was detected between 6 and 10 weeks, with a rate of  $3.4 \pm 0.4 \text{ mm}^3/\text{week}$  ( $r^2 = 0.99$ ). Although the amount of ectopic bone formed by 1  $\mu\text{g}$  of BMP-2 was very small, with a volume of only  $3.0 \pm 5.5 \text{ mm}^3$  (mean  $\pm$  SD) at week 10, the bone volume linearly increased between 1 week and 10 weeks (rate =  $0.36 \pm 0.1 \text{ mm}^3/\text{week}$ ,  $r^2 = 0.96$ ).

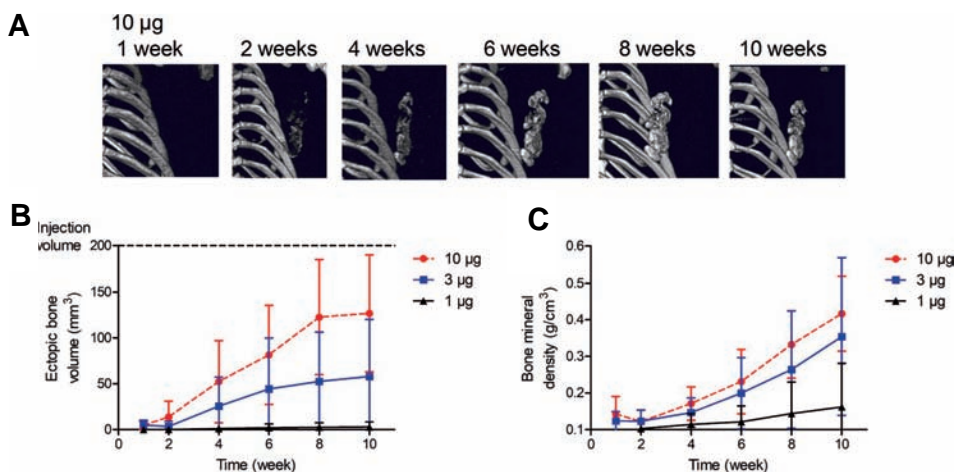


**Figure 3.4. Ectopic bone volume and density increase over the time course of 10 weeks was BMP-2 dose-dependent.** A. Representative  $\mu$ CT images of bone formed by 10  $\mu$ g of BMP-2 administration over 10 weeks. B. Volume of ectopic bone in  $\text{mm}^3$  after thresholding. C. Mineral density of bone in  $\text{g}/\text{cm}^3$  after thresholding. Threshold was set to  $0.035 \text{ g}/\text{cm}^3$  to discriminate mineralized tissue from soft tissue. (A, B, C) Five different doses of BMP-2- (10  $\mu$ g, 3  $\mu$ g, 1  $\mu$ g, 0.3  $\mu$ g and 0  $\mu$ g) containing RCP microspheres with alginate were injected subcutaneously in SD rats ( $n = 8$  injections). Data are shown as mean  $\pm$  SD. Since 0.3  $\mu$ g and 0  $\mu$ g BMP-2 did not form any bone, they are not represented in this figure.

Significant mineralization could be observed after 2 weeks (Figure 3.4C). A linear increase in bone density was seen with 10  $\mu$ g of BMP-2 between 2 and 10 weeks, with a rate of  $0.025 \pm 0.002 \text{ g}/\text{cm}^3$  per week ( $r^2 = 0.98$ ). In contrast to the bone volume, the mineral density did not reach a plateau at 10 weeks, suggesting that mineralization could continue for longer than 10 weeks. Similarly, 3  $\mu$ g of BMP-2 showed a linear increase in bone density between 2 and 10 weeks, with a rate of  $0.019 \pm 0.002 \text{ g}/\text{cm}^3$  ( $r^2 = 0.96$ ). The 1  $\mu$ g-BMP-2-comprising hydrogel clearly mineralized slower than the other two doses, with a rate of only  $0.005 \pm 0.001 \text{ g}/\text{cm}^3$  ( $r^2 = 0.97$ ).

### 3.4.4 Ectopic bone formation was confirmed by histology

The morphology of ectopic bone induced by five different doses of BMP-2 (10  $\mu$ g, 3  $\mu$ g, 1  $\mu$ g, 0.3  $\mu$ g and 0  $\mu$ g) containing hydrogel was evaluated by histology at week 10. Bone tissue could be identified for the 10  $\mu$ g, 3  $\mu$ g and 1  $\mu$ g of BMP-2-comprising hydrogels and no bone was found for the two lowest doses of 0.3  $\mu$ g and 0  $\mu$ g. The largest area of ectopic bone was found in the 10  $\mu$ g samples (Figure 3.5), thereby confirming the  $\mu$ CT data (Figure 3.3). Interestingly, for all BMP-2 doses, remnants of microspheres and gels could be observed, indicating that the implants were not yet fully degraded after 10 weeks. This

result was in line with the long-term retention of BMP-2, as observed by fluorescence imaging. Bone formation was not only observed at the periphery of the hydrogel, but also in some samples within the hydrogel construct. Microspheres were also observed within the hydrogel construct. Some of the microspheres were intact, some were infiltrated with cells. The microspheres which were infiltrated changed the spherical morphology probably as a sign of degradation. Small ossicles were detected around some microspheres. Also, around the implants, a layer of fibrous tissue was observed, which is a typical foreign body response upon implantation (190).

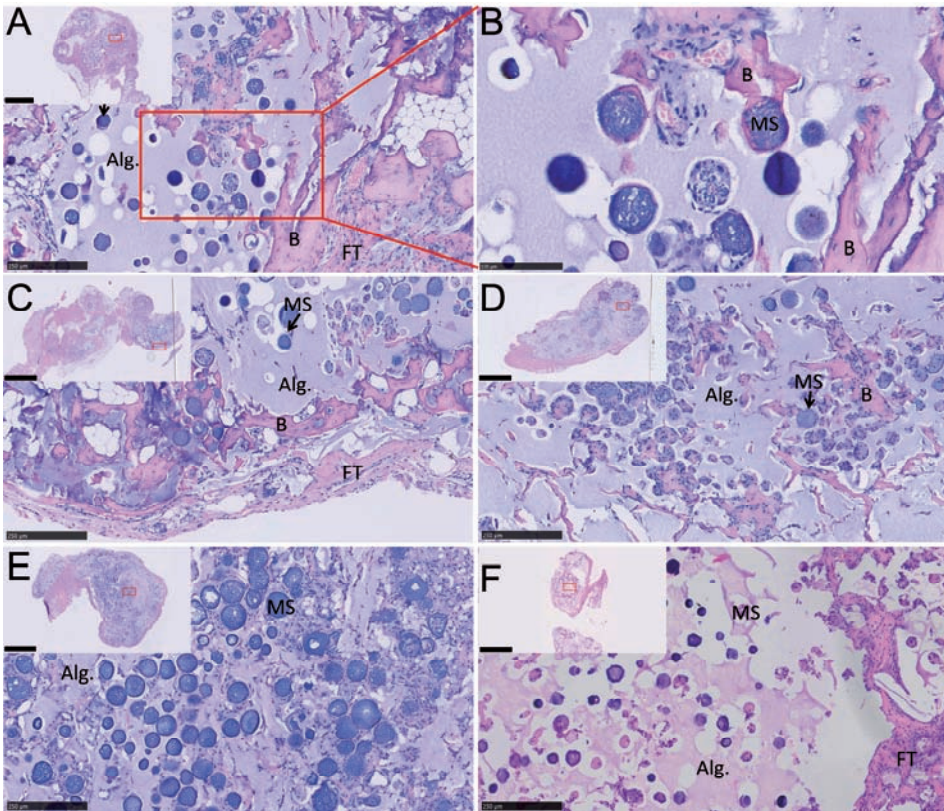


**Figure 3.5. Bone formation was confirmed by histology.** H&E staining for A, 10  $\mu$ g; C, 3  $\mu$ g; D, 1  $\mu$ g, while no bone was observed for E, 0.3  $\mu$ g, and F, 0  $\mu$ g of BMP-2-containing RCP microsphere with alginate gels. B. A closer representation of the 10  $\mu$ g of BMP-2 sample showing bony tissue around microspheres. RCP microspheres (MS), alginate hydrogel (Alg.), bone formation (B) and fibrous tissue (FT) are indicated. Scale bar is 250  $\mu$ m for A, C, D, E, F and 100  $\mu$ m for B. Scale bars of the insert images are 2.5 mm and red boxes indicate the area of high magnification.



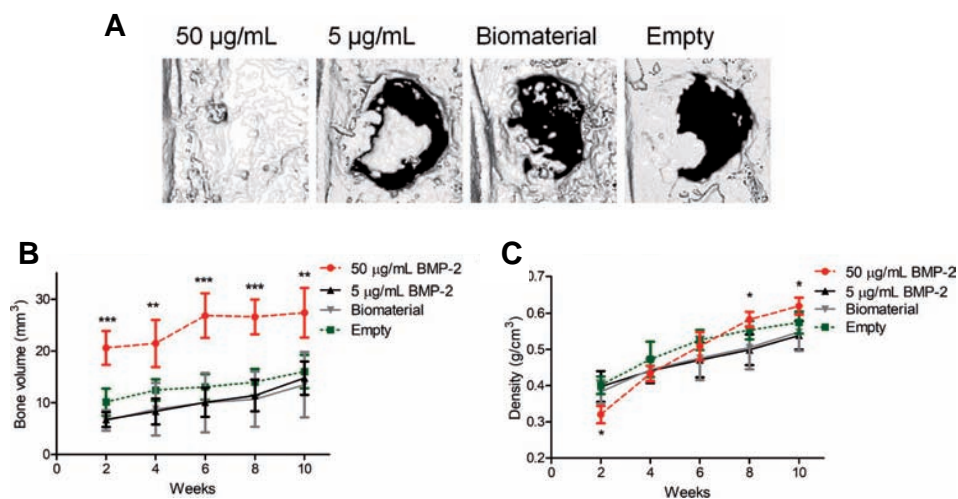


**Figure 3.6.** A. Representative  $\mu$ CT images of calvaria (superior view) at week 10 after surgery and implantation. B. Bone volume showing the regeneration of calvarial defects over 10 weeks. The bone volume of 50  $\mu$ g/mL BMP-2-containing biomaterial was significantly higher at all time points as compared to 5  $\mu$ g/mL BMP-2, biomaterial and empty defect groups (\*\*  $p < 0.01$  or \*\*\*  $p < 0.001$ ). C. Bone density showing the regeneration of calvaria over 10 weeks. Bone density induced by 50  $\mu$ g/mL BMP-2 was lower than that of 5  $\mu$ g/mL BMP-2 group at week 2 (\*  $p < 0.05$ ). At week 8 and 10, density of induced bone tissue was higher in 50  $\mu$ g/mL BMP-2 than 5  $\mu$ g/mL BMP-2 group (\*  $p < 0.05$ ). Treatment groups were empty control ( $n = 10$ ), biomaterial only ( $n = 10$ ), 5  $\mu$ g/mL BMP-2-containing biomaterial ( $n = 10$ ) and 50  $\mu$ g/mL BMP-2-containing biomaterial ( $n = 3$ ). Data are shown as mean  $\pm$  SD, two-way ANOVA was performed to compare treatment groups.

### 3.4.5 Microspheres with alginate hydrogel containing 50 $\mu$ g/mL BMP-2 induced bone formation in a rat calvarial defect model

The regeneration capacity of the composite hydrogels loaded with BMP-2 was tested in a subcritical-sized calvarial defect model. Biomaterial only, 5  $\mu$ g/mL or 50  $\mu$ g/mL BMP-2-loaded biomaterials were injected into a 5 mm calvarial defect and empty defect was used as a control (Figure 3.6A). The bone volume with 50  $\mu$ g/mL BMP-2 was significantly larger than in all other groups (Figure 3.6B), showing the regenerative capacity of this concentration of BMP-2 in the composite hydrogel formulation. The low concentration (5  $\mu$ g/mL) did not form any additional bone as compared to the biomaterial only or empty defect (sham) control. Interestingly, the bone volume of the empty defect was slightly higher at week 2 as compared to the biomaterial only, albeit the difference was not statistically significant. At the end of the experiment, biomaterial and empty defect groups produced similar bone volumes. The bone mineral density gradually increased over time (Figure 3.6C). At week 2, 50  $\mu$ g/mL BMP-2 had a lower density when compared to 5  $\mu$ g/mL



BMP-2. This effect reversed later at week 8 and 10, when 50  $\mu\text{g}/\text{mL}$  BMP-2 induced higher density as compared to 5  $\mu\text{g}/\text{mL}$ -BMP-2-treated group. von Kossa staining and Goldner's trichrome staining on the calvaria confirmed the regeneration of the bone defect (Figure 3.7). Empty defect, biomaterial control or low concentration (5  $\mu\text{g}/\text{mL}$ ) did not bridge the bone defect at week 10. The 50  $\mu\text{g}/\text{mL}$  BMP-2 concentration was effective in bridging the 5 mm calvarial defect.

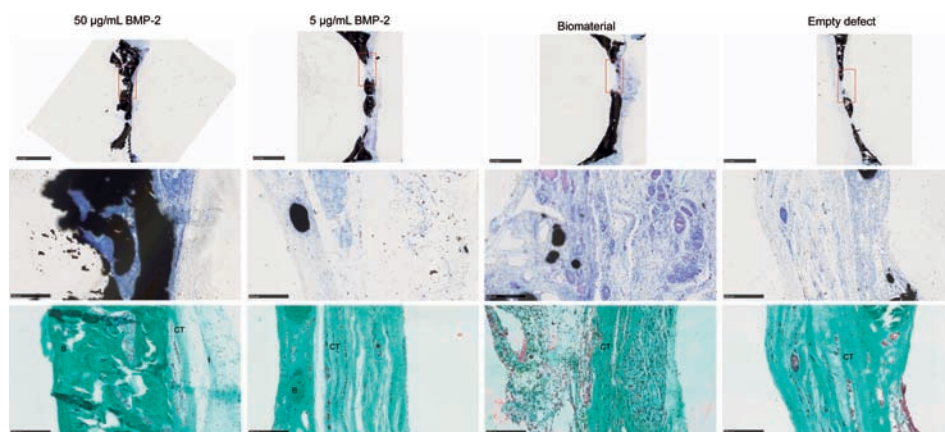


**Figure 3.7.** The first two rows show von Kossa staining, the lower row Goldner's trichrome staining of the calvarial defect samples. From left to right: 50  $\mu\text{g}/\text{mL}$  BMP-2, 5  $\mu\text{g}/\text{mL}$  BMP-2, biomaterial control and empty defect. Bone healing and bridging of the defect was confirmed for the 50  $\mu\text{g}/\text{mL}$  BMP-2 group. Red boxes indicate the area of the defect. Scale bars of the first row are 2.5 mm, second and third row are 250  $\mu\text{m}$ . B: bone; CT: connective tissue.

### 3.5 Discussion

This study aimed at investigating the use of a slow-release system to lower the effective BMP-2 dose, the effect on ectopic bone formation of the BMP-2 dose delivered by an *in situ* gelling hydrogel formulation and the bone repair capacity of two selected doses of BMP-2. The composite hydrogel provided sustained release of BMP-2 for 4 weeks, as shown *in vivo* by fluorescence imaging. Ectopic bone was formed for three different doses of BMP-2 (50, 15 and 5  $\mu\text{g}/\text{mL}$  in a 200  $\mu\text{L}$  implant) in a dose- and time-dependent manner, with the highest BMP-2 dose showing the fastest bone growth and highest bone volume at 10 weeks. The bone-forming dose of 50  $\mu\text{g}/\text{mL}$  (2  $\mu\text{g}$  per implant in a 5 mm defect) was confirmed to be also effective in a subcritical calvarial bone defect model.

The BMP-2 delivery system used was selected based on a previous study where a hydrogel composed of SLG alginate and BMP-2-loaded RCP-microspheres provide superior ectopic bone formation as compared to other hydrogel formulations as shown in Chapter 2 (186).

The advantages of this delivery system are the easy handling (due to its thixotropic behaviour), the sustained-BMP-2-release profile and the presence of cell attachment sites (due to the RCP microspheres). Differently from other injectable hydrogel systems, e.g. the hydrogel developed by Seo et al. (191), the used system contains RCP microspheres that have excellent cell attachment properties (106) and a specific affinity to bind BMP-2 (58).

In the current study, it was shown that *in situ* gelling hydrogel composite with a concentration of 50 µg/mL BMP-2 (2 µg per implant in a 5 mm defect) successfully regenerated bone. In other preclinical studies with BMP-2 carriers, the BMP-2 dose needed to heal a critical sized defect is generally higher; in a rat calvarial model similar to the one used in the current study, complete healing of the defects is achieved with poly(lactic-co-glycolic acid) (PLGA) membranes adsorbed with 5 mg/mL of BMP-2 (192). Young et al. using a 8 mm rat calvarial model and 0.5 µg and 1 µg of BMP-2 per implant delivered with gelatin particles, show an incomplete bone bridging (193). Partial healing of 8 mm rat calvarial defects of approximately 20% and 60% is observed with a composite comprising segmented polyurethane, poly(lactic-co-glycolic acid) and β-tricalcium phosphate loaded with 1.6 µg and 6.5 µg of rhBMP-2, respectively (194). Besides, other BMP-2 carriers induce lower ectopic bone volumes. For example, silk fibroin (2 mm<sup>3</sup>) (184) and collagen sponge (5 mm<sup>3</sup>) (183) form a max of 5 mm<sup>3</sup> of ectopic bone using 5 µg of BMP-2, which is lower than the 41 mm<sup>3</sup> induced with 3 µg (15 µg/mL) of BMP-2, as done in the current ectopic model. In a composite gelatin microsphere, biphasic calcium phosphate hydrogel system, 13 mm<sup>3</sup> of ectopic bone are achieved with 100 µg/mL BMP-2 (110). Considering these earlier studies, the current study showed that the *in situ* gelling formulation of the RCP microspheres with alginate is a promising BMP-2 delivery system that might reduce the required effective dose of BMP-2 and, thus, potentially mitigate the adverse effects of BMP-2.

Besides the required threshold or effective dose of BMP-2, the hydrogel matrix –to which the characteristics of the biomaterial, such as release, integrity, degradation and cell infiltration, should be aligned– also affects the bone formation process. Factors such as speed of bone formation, amount and location of the formed bone are important to consider. The natural fracture healing process requires around 4 weeks in rodents (26), and it can take up to 3-4 months in humans (195). In the used ectopic model, the kinetics of bone formation was shown to be linear for the 10 µg of BMP-2 group, between week 1 and 8, while the main release of BMP-2 was observed in the first 4 weeks, both processes matching the time frame of natural bone healing processes (20). Interestingly, after 4 weeks, a small portion of BMP-2 was retained inside the hydrogel, probably due to the strong interaction between BMP-2 and the RCP microspheres (58). This portion of BMP-2 will only be released upon further degradation of the material and could probably contribute to the bone volume increase after 4 weeks. The main determinant of BMP-2 release *in vivo* is the specific interaction and the degradation of the particles. The RCP

amino acid sequence will most probably be a main contributor to the release profile, although it is not possible to exclude that polarity and ionic strength will also affect the release profile of proteins by changing the interaction with the matrix. With 10  $\mu\text{g}$  of BMP-2, ectopic bone volume reached a plateau at week 8. This suggested that bone formation could be confined to the hydrogel area. Therefore, this hydrogel formulation might eliminate the risk of excessive surrounding soft tissue calcification, which is a major concern in currently used BMP-2-based therapies (88).

The ectopic model results indicated that hydrogels containing 3  $\mu\text{g}$  and 10  $\mu\text{g}$  of BMP-2 were not only forming bone at the periphery of the implants, but in the entire implants. Qualitative analysis of 3D  $\mu\text{CT}$  images revealed that the bone formation started at different locations throughout the implant around week 2. These results corroborated previous findings ((186)), Chapter 2), according to which the hydrogel allows bone-forming cells to infiltrate the gel at early time points.

Interestingly, hydrogels without or with a very low dose of BMP-2 seemed to slightly, though not significantly, impede bone formation in the calvarial defect model at the early time points when compared to the empty control. After 10 weeks, bone formation in defects filled with biomaterial, without or with a low dose of BMP-2, was not different from the empty defect control. It is possible that the empty defect induced higher initial inflammation and faster infiltration of inflammatory cells as compared to the RCP microspheres with alginate and, therefore, the healing process started earlier. The safety of the separate components of this system are verified by Novamatrix and Fujifilm. On their website ([www.novamatrix.biz](http://www.novamatrix.biz)), toxicology studies of alginate are reported. The biocompatibility of RCP is confirmed in a previous study by Parvizi et al. (196). Histological analysis of the samples at week 10 showed infiltrated cells in the defect area for both defects filled with biomaterials and empty control. These cells were mainly macrophages. A hydrogel-dependent cellular response of different hydrogels in ectopic bone formation is already shown (186). For the SLG alginate gel selected for this study, the number of inflammatory cells is initially high and decrease at later time points (186). Alginate is known for poor cell attachment (197, 198). Possibly, alginate slightly delays cell infiltration as compared to natural bone healing environment where there is a fibrin clot hosting the infiltrated cells. These effects could be object of a future study. However, as differences did not reach statistical significance and the endpoint healing for both groups was similar, an inhibitory effect of the hydrogel matrix on the overall bone healing is not expected. Overall, the benefit of having a slow-release system outweighs this minor effect, since the BMP condition healed much better than the control.

### **3.6 Conclusions**

The injectable slow BMP-2 release delivery system resulted in a time- and dose-dependent bone formation in an ectopic and orthotopic model. This delivery system, composed of alginate and RCP microspheres, provided sustained release of BMP-2, favoured cell attachment and induced bone formation at a relatively low dose of BMP-2, making it promising for bone regeneration therapies.

### **3.7 Acknowledgments**

The authors thank Vincent Paes and Charlotte Gerkes for their technical assistance during the performance of the calvarial surgeries. This work was supported by the use of imaging equipment provided by the Applied Molecular Imaging Erasmus MC facility. The research leading to these results has received funding from the People Programme (Marie Curie Actions) of the European Union's Seventh Framework Programme FP7-2007-2013/ under REA grant agreement number 607051.

# 4

## Nell-1, HMGB1, and CCN2 enhance migration and vasculogenesis, but not osteogenic differentiation compared to BMP-2

Shorouk Fahmy-Garcia, Marjolein van Driel, Janneke Witte-Bouma, Heike Walles,  
Johannes P.T.M. van Leeuwen, Gerjo J.V.M van Osch, and Eric Farrell

Tissue Eng Part A. 2018 Feb;24(3-4):207-218. doi: 10.1089/ten.TEA.2016.0537.

## 4.1 Abstract

Currently, autografts still represent the gold standard treatment for the repair of large bone defects. However, these are associated with donor-site morbidity and increased pain, cost, and recovery time. The ideal therapy would use biomaterials combined with bone growth factors to induce and instruct bone defect repair without the need to harvest patient tissue. In this line, bone morphogenetic proteins (BMPs) have been the most extensively used agents for clinical bone repair, but at supraphysiological doses that are not without risk. Because of the need to eliminate the risks of BMP-2 use *in vivo*, we assessed the ability of three putative osteogenic factors, nel-like molecule type 1 (Nell-1), high mobility group box 1 (HMGB1), and CCN2, to enhance the essential processes for bone defect repair *in vitro* and compared them to BMP-2. Although it has been reported that Nell-1, HMGB1, and CCN2 play a role in bone formation, less is known about the contribution of these proteins to the different events involved, such as cell migration, osteogenesis, and vasculogenesis. In this study, we investigated the effects of different doses of Nell-1, HMGB, CCN2, and BMP-2 on these three processes as a model for the recruitment and differentiation of resident cells in the *in vivo* bone defect repair situation, using cells of human origin. Our data demonstrated that Nell-1, HMGB1, and CCN2 significantly induced mesenchymal stem cell migration (from 1.58-fold increase compared to control), but BMP-2 did not. Interestingly, only BMP-2 increased osteogenesis in marrow stromal cells, whereas it inhibited osteogenesis in preosteoblasts. Moreover, the four proteins studied promoted significantly endothelial cell migration, reaching a maximum of 2.4-fold increase compared to control, and induced formation of tube-like structures. Nell-1, HMGB1, and CCN2 had these effects at relatively low doses compared to BMP-2. This work indicates that Nell-1, HMGB1, and CCN2 might enhance bone defect healing via the recruitment of endogenous cells and induction of vascularization and act via different processes than BMP-2.

## 4.2 Introduction

Currently, bone grafting is used to replace missing bone and to repair bone fractures, with 2.2 million transplantations per year (199). Autografts represent the gold standard due to their histocompatibility and capacity to become vascularized and fully integrated with the surrounding bone. Although autografts have an excellent success rate, the harvesting of autologous bone is associated with an 8.6% rate of major and 20.6% minor complications (200). Therefore, different approaches are being taken to overcome these limitations. The ideal regenerative medicine approach would involve an off-the-shelf product that can recruit a patient's own cells and stimulate them to differentiate into mature osteoblasts while at the same time inducing tissue vascularization. One such approach is growth factor-based therapy. This involves the use of molecules that are essential for tissue formation combined with biomaterials (201).

Bone morphogenetic protein-2 (BMP-2) and BMP-7 are the most studied bone-forming proteins. Moreover, currently BMP-2 is the only BMP approved as a bone graft substitute (86). However, despite the therapeutic potential of BMP-2 in bone repair, large doses (up to 40 mg) are needed to produce a significant osteogenic effect (202), and this can result in undesired ectopic bone formation, soft tissue swelling, bone resorption, and tumor growth enhancement through angiogenesis stimulation (87, 203, 204).

Accordingly, alternative proteins are being assessed for their osteogenic induction capacity. Three of such proteins are nel-like molecule type 1 (Nell-1), connective tissue growth factor (CCN2), and high mobility group box 1 (HMGB1). Bone regeneration is a complex process that involves a series of well-orchestrated biological events. At the cellular level, migration, proliferation, angiogenesis, osteogenic differentiation, and subsequent mineralization are essential processes to enable bone formation and repair to occur (205). To optimize *in vivo* bone defect repair using biologicals, more knowledge of the effect of these factors on the different processes is necessary.

Nell-1 is a secretory protein and its overexpression induces altered bone formation and it is considered an essential factor for human craniosynostosis (206). It has been shown to promote bone formation on mice *in vivo* (207, 208), and in a comparison study, Nell1-based bone grafts were comparable to BMP2-based grafts in rat spinal fusion (209). Recent studies performed on osteoporotic mice and sheep have shown that Nell-1 could potentially be used as a therapy for osteoporotic bone loss (210, 211). Furthermore, Nell-1 has been shown to increase osteogenic differentiation *in vitro* (212). However, whether Nell-1 is able to recruit osteoprogenitor cells is not known yet. Moreover, several genes affected by Nell-1 appear to promote angiogenesis at early stages of bone regeneration (213) but whether it is able to promote endothelial cell (EC) recruitment and differentiation is still unknown.

CCN2 has been used mostly in rats and has been shown to promote bone and cartilage regeneration (214, 215). It is one of the six CCN matricellular proteins characterized by their conserved modular structure (216) and interacts with integrins, enhancing cellular processes such as adhesion, extracellular matrix (ECM) synthesis, cytoskeleton reorganization, and survival (217-219). *In vitro* studies have shown that overexpressing cells with CCN2 promote mesenchymal cell proliferation, migration, and aggregation (220, 221). In addition, it has been shown that CCN2 expression was increased in mesenchymal stem cells (MSCs) and osteoblasts during formation of new bone, suggesting its role in bone development (216), but its effect when added to either human osteoprogenitor cells or osteoblasts has not been investigated yet. Furthermore, CCN2 is a necessary mediator for the production of vascular basement membranes (222), however, its effect on angiogenesis remains unclear (223-226).

HMGB1, unlike Nell-1 and CCN2, has never been used as growth factor-based therapy, but knowledge about the potency of this factor in the different processes involved in bone repair makes it an attractive candidate. HMGB1 is a chromatin protein mainly known due to its role as an alarmin (227, 228). Consequently, many studies showed that HMGB1 is a potent proinflammatory cytokine secreted by monocytes and macrophages able to regulate migration of mesangioblasts, smooth muscle cells, or myoblasts among others (229-232). Recently, it has been shown that HMGB1 has an osteo-modulatory action (233), being chemotactic to MSCs (234) as well as osteoblasts and osteoclasts during endochondral ossification (227, 235). Although HMGB1 is known to be able to upregulate osteogenic markers when added to MSC culture *in vitro* (236), its direct effect on osteoprogenitor and preosteoblast mineralization has not been studied. In addition, various studies have identified it as a putative proangiogenic factor and its overexpression is related with an increased ability to develop blood vessels (230, 237, 238).

Nell-1, HMGB1, and CCN2 are indicated to play a role in bone formation. However, their effect on major cell types and specific processes involved in bone formation is barely studied, and they were never directly compared. The main goal of this study is to compare side by side Nell-1, HMGB1, and CCN2 to BMP-2 and assess whether they are able to induce cell migration, osteogenic differentiation, and neovascularization, indispensable processes needed for bone formation. This was performed using cells from human origin: two types of osteoprogenitors (human MSCs and fetal osteoblasts) and human umbilical vein endothelial cells (HUVECs).

## **4.3 Materials and methods**

### **4.3.1 Cell culture**

Human MSCs were obtained from leftover material from iliac crest biopsies of four donors (age 9-12 years; three males and one female) undergoing cleft palate reconstruction



surgery (Erasmus MC Ethics Committee number MEC-2014-106) with implicit consent. Cells were seeded at a density of 50,000 cells/cm<sup>2</sup> in  $\alpha$ -MEM (Gibco, BRL), supplemented with 10% fetal calf serum (FCS), 1 ng/mL fibroblast growth factor (FGF2), 25  $\mu$ g/mL ascorbic acid-2-phosphate, 1.5  $\mu$ g/mL fungizone, and 50  $\mu$ g/mL gentamicin. After 24 h, nonadherent cells were washed out and adherent cells were expanded in the abovementioned medium. The medium was renewed twice per week until MSCs neared confluency. Then, cells were used for migration or osteogenic differentiation assays. Simian virus-immortalized human fetal osteoblast (SV-HFO) cells (239) were expanded and cultured as previously described (240).

HUVECs (Lonza) were cultured at a density of 5,000 cells/cm<sup>2</sup> in endothelial growth medium (EGM-2 with SingleQuots; Lonza). Medium was renewed every 2-3 days. When cells neared confluency, they were used for migration or tube formation assays.

#### 4.3.2 Migration assay

MSC and HUVEC migration was assessed using modified Boyden chambers (polyethylene terephthalate cell culture inserts, pore size: 8  $\mu$ m in diameter, Millipore-Merck). Briefly, to analyze MSC migration,  $\alpha$ -MEM containing Nell-1 (0.07-3.5 nM [10-500 ng/mL, R&D Systems), CCN2 (0.89-8.9 nM [10-100 ng/mL; Abnova), HMGB1 (0.4-4 nM [10-100 ng/mL; R&D Systems), and BMP-2 (0.38-38 nM [10-1000 ng/mL; kindly provided by Dr. Joachim Nickel, Fraunhofer IGB) was added to the lower chamber of a 24-well plate. Platelet-derived growth factor-AB (PDGF-AB) (20 ng/mL) or 10% FCS was used as positive controls.  $6 \times 10^3$  MSCs suspended in a volume of 200  $\mu$ l  $\alpha$ -MEM were added into the upper chamber. The plates were incubated at 37 °C for 17 h. To test the chemotactic effect of Nell-1 (10-500 ng/mL), CCN2 (10-100 ng/mL), HMGB1 (10-100 ng/mL), and BMP-2 (10-1000 ng/mL) on HUVECs, the endothelial cell basal medium (EBM-2, Lonza) containing Nell-1, CCN2, HMGB1, or BMP-2 was added in the lower chamber. EGM-2 was used as positive control.  $5 \times 10^4$  HUVECs were added into the upper chamber. The plates were incubated at 37 °C for 10 h. In both cases, the membrane was then washed and the cells remaining on the upper surface of the chambers were mechanically removed with a cotton swab. Those that had migrated to the lower surface were fixed with 4% formalin, stained with 4',6-diamidino-2-phenylindole (DAPI) (100 ng/mL) in the dark for 5 min, and imaged using fluorescence microscopy (Zeiss Axiovert 200 M Fluorescence Imaging) in five random fields for each membrane and counted using ImageJ software.

#### 4.3.3 Osteogenic differentiation

Osteogenic differentiation assays were performed on MSCs and SV-HFOs. 3,000 cells/cm<sup>2</sup> (MSCs) or 9,000 cells/cm<sup>2</sup> (SV-HFOs) were seeded with  $\alpha$ -MEM in a 12-well plate. For MSCs, after 24 h, the medium was replaced with the complete osteogenic medium: DMEM high glucose (Gibco) with 10% FCS, 1.5  $\mu$ g/mL fungizone, 50  $\mu$ g/mL gentamicin, 1

ng/mL FGF2, 25 µg/mL ascorbic acid-2-phosphate, 10 mM β-glycerophosphate, and 0.1 µM dexamethasone. For SV-HFOs, the osteogenic differentiation medium consisted of phenol red-free α-MEM (Gibco), pH 7.5, supplemented with 20 mM HEPES (Sigma), streptavidin/penicillin, 1.8 mM CaCl<sub>2</sub>·2H<sub>2</sub>O (Sigma), 2% heat-inactivated charcoal-treated FCS, 0.1 µM dexamethasone, and 10 mM β-glycerophosphate. During each medium refreshment, medium was supplemented with proteins of interest: Nell-1 (10-500 ng/mL), CCN2 (10-100 ng/mL), HMGB1 (10-100 ng/mL), and BMP-2 (10-1000 ng/mL). Osteogenic differentiation was carried out until onset of mineralization, monitored by measuring calcium concentration in the culture supernatant. Cells were scraped from the culture dish in phosphate-buffered saline (PBS)/0.1% Triton X-100. Cell lysates were sonicated on ice before analysis.

#### **4.3.4 DNA and protein measurements**

For DNA measurement, cell lysates were incubated for 30 min at 37 °C with 100 µL heparin (8 IU/mL in PBS) and 50 µL RNase A (50 µg/mL in PBS) solution. Ethidium bromide solution (25 µg/mL) was added and DNA content was measured on the Wallac 1420 Victor2 (PerkinElmer Life and Analytical Science) plate reader using an excitation filter of 340 nm and emission filter of 590 nm. For standards, calf thymus DNA (Sigma) was used. Protein was measured in cell lysates with BCA protein assay (Pierce™ BCA protein assay; Thermo Scientific) according to the manufacturer's instructions.

#### **4.3.5 Alkaline phosphatase activity**

Alkaline phosphatase (ALP) activity was performed as described previously (241) by determining the release of paranitrophenol from paranitrophenyl phosphate (pNPP) in cell lysates. pNPP (20 mM) was added to each sample at 37 °C. After exactly 10 min, the reaction was stopped by adding 0.06 M NaOH. Absorption was measured on the Wallac 1420 Victor2 plate reader at 405 nm. For standards, ALP (10 U/mL) from bovine kidney (Sigma) was used.

#### **4.3.6 Mineralization**

To quantify the calcium content, cell lysates were incubated 48 h in 0.24 M HCl at 4 °C. For analysis of calcium concentration in the culture medium, supernatant was collected from day 9 onward. In both cases, the calcium content was colorimetrically determined after addition of 1 M ethanolamine buffer (pH 10.6), 19.8 mM 8-hydroxyquinoline, and 0.35 mM O-cresolphthalein complexone, at 595 nm on the Wallac 1420 Victor2.

For von Kossa staining, cell cultures were fixed for 15 min in 4% formaldehyde, stained by 5% silver nitrate solution (Sigma; 85228) for 30 min under a 60 W light, and imaged using an inverted microscope (Olympus CKX41).

#### 4.3.7 HUVEC tube formation assay

Growth factor-reduced Matrigel (Corning) was added to a 96-well plate and incubated at 37 °C for 1 h. HUVECs were resuspended in EBM-2 supplemented with Nell-1, CCN2, HMGB1, or BMP-2. EGM-2 complete medium was used as positive and EBM-2 as negative control. Fifteen thousand cells were seeded on top of the Matrigel, incubated at 37 °C, and imaged after 4, 6, and 24 h using an inverted microscope. Three independent experiments in triplicate were performed. The results were analyzed using ImageJ software.

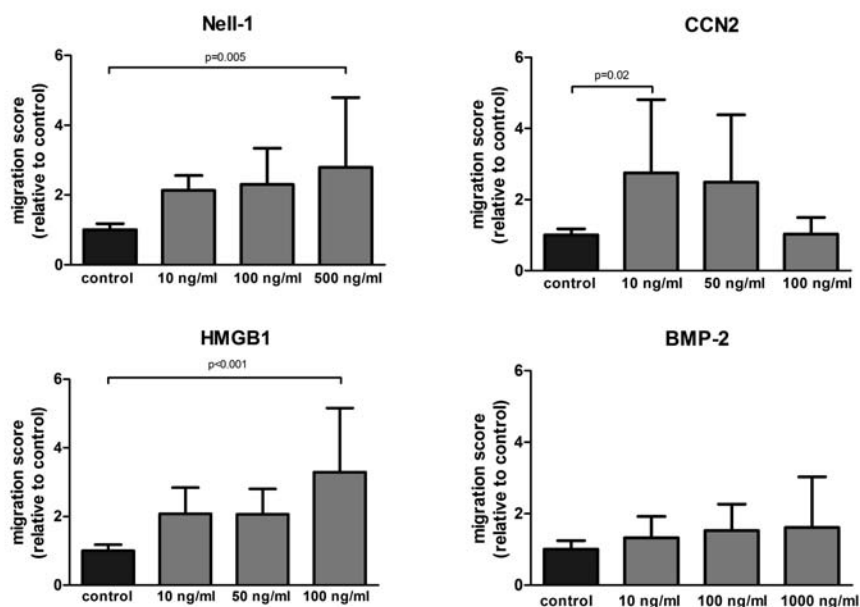
#### 4.3.8 Statistical analysis

Data were analyzed with IBM Statistics 21 (SPSS). A linear mixed model was applied; the different conditions (different doses of the proteins studied) were considered a fixed parameter and the donors (experiments) as a random factor. A descriptive analysis was performed to assess the normal distribution of the data. When multiple comparisons were analyzed, the Bonferroni test was performed.  $p < 0.05$  was considered statistically significant.

### 4.4 Results

#### 4.4.1 Nell-1, CCN2, and HMGB1 stimulated MSC migration, whereas BMP-2 did not

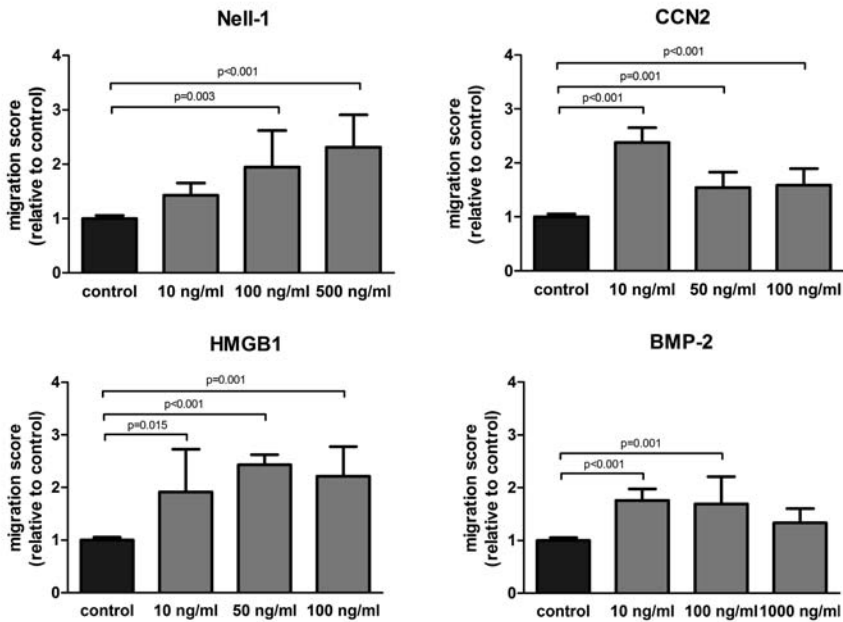
To determine whether the proteins could recruit progenitor cells to the site of injury, we assessed their effects on migration of MSCs. The positive control PDGF-AB was chemoattractant showing a 4.6-fold increase compared to negative control (data not shown). Nell-1, CCN2, HMGB1, but not BMP-2, were capable of inducing MSC migration (Figure 4.1). Nell-1 increased migration 2-, 2.3-, and 2.79-fold compared to control in a dose-dependent manner, although only statistically significant ( $p < 0.05$ ) with the highest dose. CCN2 significantly increased migration at the lowest and medium dose (2.75- and 2.48-fold, respectively), while the highest dose had no effect compared to control. In contrast, HMGB1 was chemotactic at the highest dose tested, 100 ng/mL, with more than 5-fold increase compared to control. Although there was a trend toward a stimulation of migration of BMP-2 on MSCs (1.3-1.6-fold increase), this effect was not significant.



**Figure 4.1. *Nell-1*, *CCN2*, and *HMGB1* stimulated MSC migration.** Average migration of MSCs exposed to several doses of each factor relative to the negative control ( $n = 4$  donors in duplicate). The bars represent the mean  $\pm$  SD.

#### 4.4.2 *Nell-1*, *CCN2*, *HMGB1*, and *BMP-2* proteins stimulated EC migration

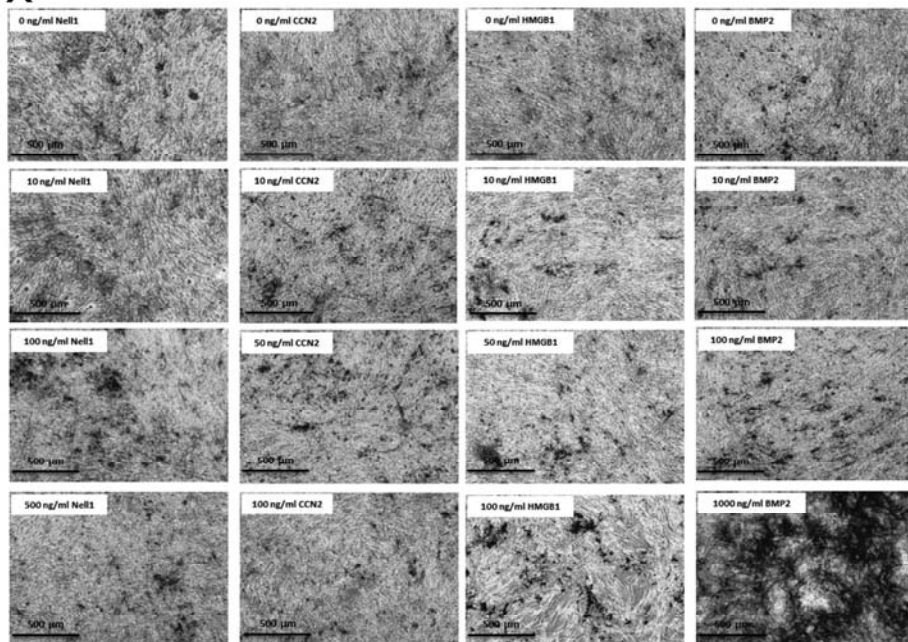
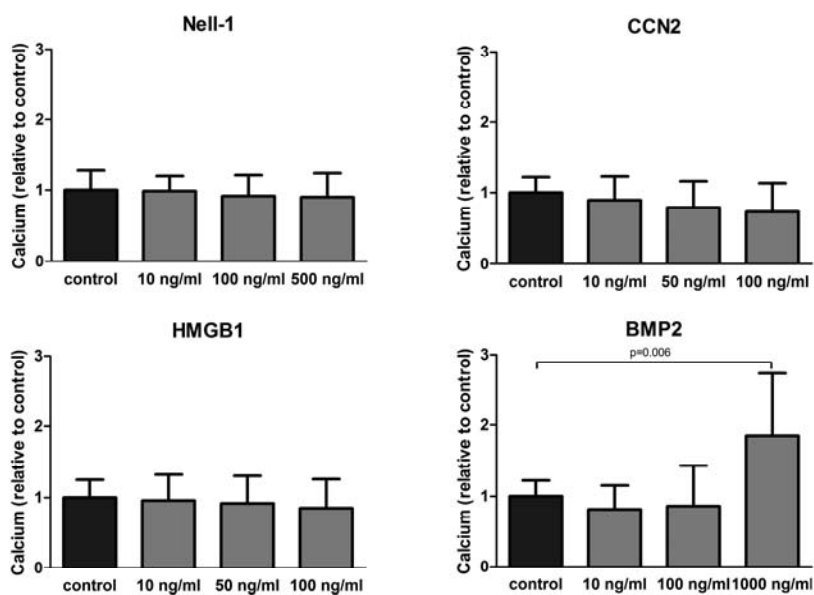
We explored the role of *Nell-1*, *CCN2*, *HMGB1*, and *BMP-2* on HUVEC recruitment. The positive control (EGM-2 complete medium) showed a 3.2-fold increase in migration compared to negative control (EBM-2). Interestingly, similar to MSCs, *Nell-1* and *CCN2* stimulated HUVECs to migrate. Specifically, *Nell-1* increased migration in a dose-dependent manner, showing more than 2-fold increase with the highest dose, while *CCN2* had a greater effect at the lowest dose (more than 2-fold increase compared to control) (Figure 4.2). Although *HMGB1* showed less pronounced effect on HUVEC than MSC migration, it had a significant effect on migration in all the tested doses, showing a 2-fold increase compared to the control. It is noteworthy that, in contrast to the other three proteins that had similar effects on both cell types with regard to dose, *BMP-2* showed different effects, demonstrating a significantly higher EC migration at the lowest and medium dose supplied with more than 1.5-fold increase compared to control (Figure 4.2).



**Figure 4.2. Nell-1, CCN2, HMGB1, and BMP-2 stimulated EC migration.** Average migration of HUVECs exposed to several doses of each factor relative to the negative control ( $n = 3$  independent experiments in duplicate). The bars represent the mean  $\pm$  SD.

#### 4.4.3 BMP-2 enhanced MSC osteogenic differentiation; Nell-1, CCN2, and HMGB1 had no effect

Osteogenic differentiation of MSCs was assessed by calcium deposition. Supplementation with Nell-1, CCN2 or HMGB1 did not cause any increase or decrease in mineralization. However, when BMP-2 was added, we observed a dose-dependent stimulatory effect, with a significant increase in nodule formation at the highest dose provided (Figure 4.3A). The results were corroborated quantitatively by measuring the calcium content in the cell lysates, showing that addition of BMP-2 at the highest dose provided (1000 ng/mL) had an almost 2-fold increase in mineralization compared to the standard osteogenic differentiation media (Figure 4.3B).

**A****B**

**Figure 4.3. Effect of Nell-1, CCN2, HMGB1, and BMP-2 on the MSC mineralization.** Human MSCs were induced to mineralize in the absence or continuous presence of Nell-1, CCN2, HMGB1, or BMP-2. A. Von Kossa staining of nodule formation at the onset of mineralization. Pictures were taken at 4× magnification. B. Quantification of calcium deposition (nmol/cm<sup>2</sup>) in the ECM at the onset of mineralization relative to control (osteogenic differentiation medium). n = 3 donors in triplicate. The bars represent the mean ± SD.

#### 4.4.4 BMP-2 inhibited preosteoblast differentiation and mineralization; Nell-1, CCN2, and HMGB1 had no effect

The addition of Nell-1, CCN2, and HMGB1 did not increase mineralization or ALP activity at either of the time points studied (Figure 4.4A). Interestingly, and in contrast to the effect observed with MSCs, the addition of BMP-2 to the preosteoblast culture had a direct inhibitory effect on differentiation and mineralization. The decrease in ALP activity became significant at day 16. In addition, a reduction in the ECM calcium content at the lowest dose provided was detected (Figure 4.4A,B). However, when the highest dose was provided (1 µg/mL), the inhibitory effect was no longer observed and the mineralization reached control levels.

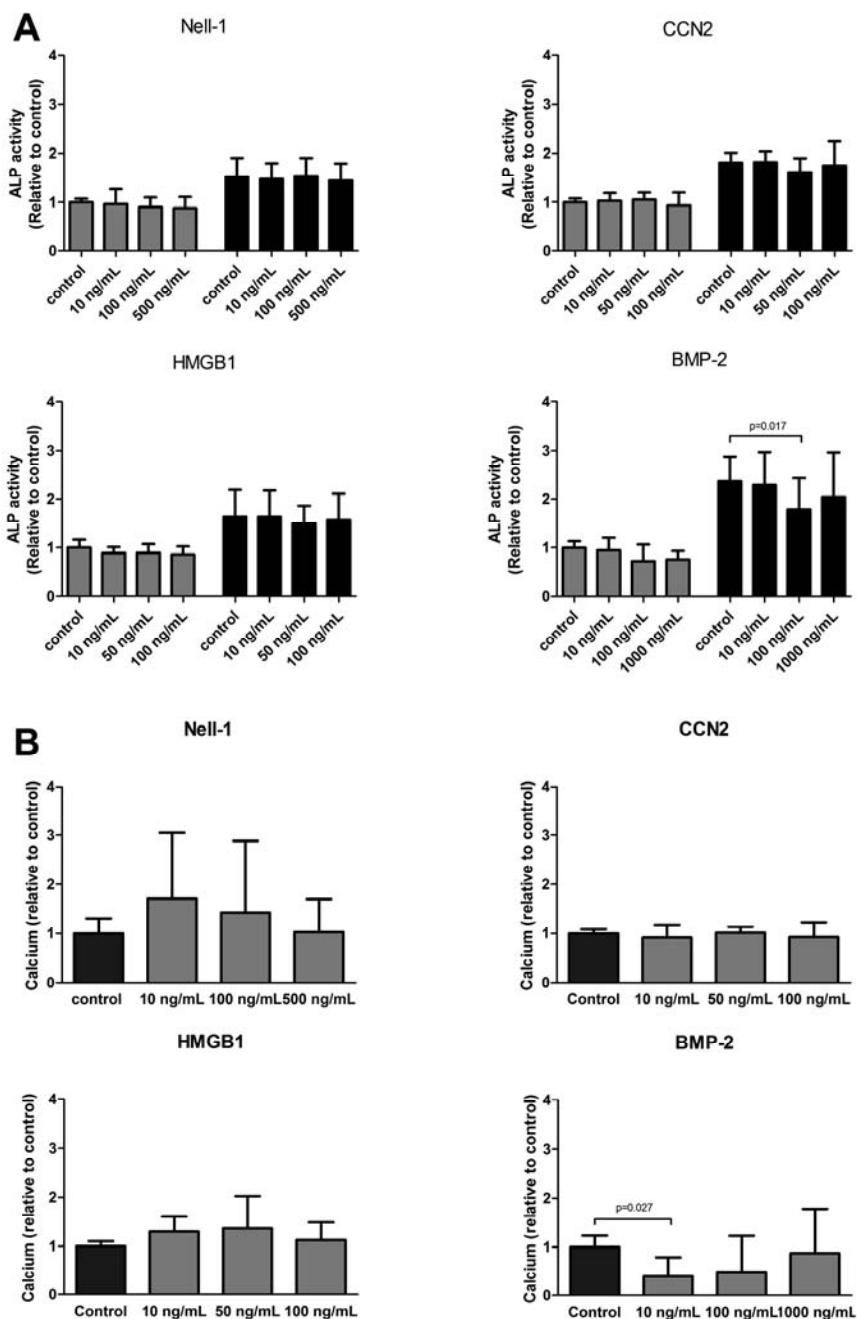




**Figure 4.4. Effect of Nell-1, CCN2, HMGB1, and BMP-2 on the osteoblast differentiation measured by ALP activity and mineralization.** A. ALP activity ( $\text{mU}/\text{cm}^2$ ) during SV-HFO culture in osteogenic differentiation medium (control) and after continuous addition of the tested proteins at day 9 (gray bars) and 16 (black bars) of culture. Results are shown relative to day 9 control. B. Quantification of calcium deposition ( $\text{nmol}/\text{cm}^2$ ) in the ECM at day 16. Values are expressed as fold change compared to osteogenic medium without additional proteins. Results are shown relative to control in both graphs ( $n = 3$  experiments performed in triplicate). The bars show the mean  $\pm$  SD. ALP, alkaline phosphatase.

#### 4.4.5 Nell-1, CCN2, HMGB1, and BMP-2 stimulated neovascularization

We have determined the capability of the factors to promote formation of tubular-like structures by ECs *in vitro*. There was a significant improvement in tube formation at the medium dose of Nell-1 added (100 ng/mL). Furthermore, CCN2 and HMGB1 were able to enhance tube formation at the lowest doses supplied. BMP-2 also enhanced tube formation in a dose-dependent manner, resulting in a significant effect on tube formation when the highest dose was added (Figure 4.5).

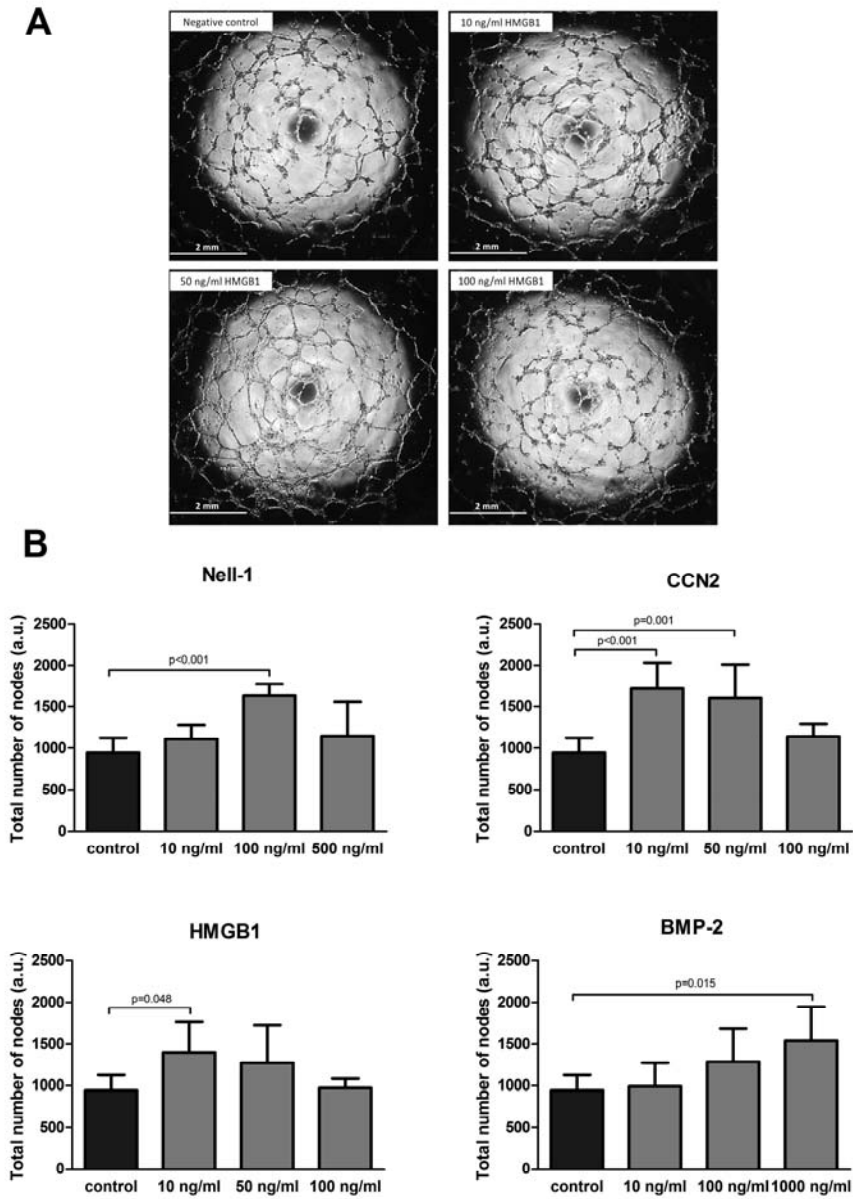


**Figure 4.5. Effect of Nell-1 CCN2, HMGB1, and BMP-2 HUVEC on tube formation on Matrigel.**  
*A. Representative picture of tube-like structures formed by HUVEC after 6 h of treatment with vehicle control, 10 ng/mL HMGB1, 50 ng/mL HMGB1, and 100 ng/mL HMGB1. Pictures were taken with 1.5× magnification. B. Quantification of tube formation, and total number of nodes analyzed. The bars show the mean ± SD.*

## 4.5 Discussion

We directly compared four proteins that are acknowledged for their apparent ability to stimulate osteogenesis *in vitro* or *in vivo* (216, 227, 242, 243). This is the first study to directly compare these proteins for their ability to induce recruitment, osteogenic differentiation, and neovascularization using human cells. Our results demonstrate the ability of Nell-1, CCN2, and HMGB1 to attract both MSCs and ECs even at low doses compared to BMP-2. Since new blood vessel formation is crucial for bone development, we assessed neovascularization in an *in vitro* model, demonstrating that all four tested proteins were able to stimulate formation of tube-like structures. Interestingly, in contrast to BMP-2, Nell-1, CCN2, and HMGB1 did not significantly increase the osteogenic differentiation capacity of MSCs above that induced by dexamethasone. Also of note, we observed that BMP-2 negatively impacted preosteoblast mineralization, whereas the others had no effect.

### 4.5.1 Effects on cell migration

It is generally thought that BMPs are mediators of osteoprogenitor cell recruitment. However, it had been published that BMP-2 had no effect in the recruitment of MSCs, neither in the cultured MSCs nor in the marrow ablation tissues (244). In our study, we did not see any increase in MSC migration by BMP-2 either. The BMP-2 chemotactic effect seems to vary between EC subtypes; studies performed with ECs showed that BMP-2 was not able to stimulate human aortic EC migration (203), but it stimulated HUVEC migration (245). Our data confirmed that BMP-2 is able to stimulate migration of HUVEC when doses between 10 and 100 ng/mL are supplied.

Where BMP-2 had no effect on MSC migration and less than doubled the migration of HUVEC, we observed up to a 3-fold increase in MSC and HUVEC migration when HMGB1, CCN2, or Nell-1 was added to the culture. HMGB1, as a signal of tissue damage, is known to be capable of inducing migration in many different cell types, including inflammatory cells (232, 246, 247). Fewer articles exist investigating the effects of HMGB1 on osteogenic cells, but those that do indicate it to be important in cell recruitment. Meng et al. demonstrated that HMGB1 promotes MSC migration up to 2.5-fold compared to control (234). Our results confirm these findings, showing that HMGB1 has a highly significant chemotactic effect on MSCs above doses of 50 ng/mL. To date, there is very little reported about HMGB1's chemotaxis on primary ECs. Low doses of HMGB1 are able to promote endothelial progenitor cell migration using transwells coated with fibronectin or fibrinogen (248). Bauer et al. have performed a wound healing migration assay and have shown that 1 µg/mL of HMGB1 is able to induce migration of HUVEC (249). We show that HMGB1 is highly chemoattractant to HUVECs, and even a hundred times lower concentration than 1 µg/mL is sufficient to induce more than a 2-fold increase compared to control. In addition, from 10 to 100 ng/mL, we observed a similar chemoattractant effect, suggesting a low dose is sufficient to stimulate EC migration. CCN2 has been shown

to promote migration of human MSCs and human dermal microvascular ECs when transfected with pCCN2 (220, 221). Nonetheless, the effect of the addition of the protein CCN2 to MSCs or ECs had not been studied before. We demonstrated that the addition of low dose (10 ng/mL = 0.89 nM) of CCN2 to the media is sufficient to obtain a significant migratory response from MSCs and HUVECs, reaching more than a 4-fold increase compared to the control. The fact that CCN2 showed an inverse dose response is potentially interesting for endogenous cell recruitment through slow-release systems.

Nell-1 has been shown to inhibit renal carcinoma cell migration and adhesion (250). However, we did not find published data about the effect of Nell-1 on MSC and EC migration. We demonstrated in this study its ability to promote migration of both cell types. In fact, it was able to promote EC migration at lower doses than BMP-2 (BMP-2, 100 ng/mL = 3.8 nM; Nell-1, 100 ng/mL = 0.7 nM) and MSC migration when BMP-2 did not.

#### **4.5.2 Effects on osteogenesis**

BMP-2 is the best known osteogenic factor. Next to the capacity to induce bone formation *in vivo*, the capacity of BMP-2 to induce osteogenic differentiation of MSCs *in vitro* has already been tested (251, 252). Our data confirm this as we observed an almost 2-fold increase when 1 µg/mL of BMP-2 was added to the culture. However, little is known about its effect on osteoblasts. In this study, we observed an inhibition of mineralization when BMP-2 was added to osteoblast cultures in a concentration range of 10–100 ng/mL. Interestingly, we did not observe that inhibitory effect when the highest dose was added (1 µg/mL). This could be due to the fact that SV-HFOs express activin (253) which may interfere with BMP-2 or simply because BMP-2 is not an essential stimulus when the cells are already committed to the osteogenic pathway. Many studies indicated HMGB1's role in the induction of endochondral ossification *in vivo* and that it may act as a bone resorption signal (227). However, HMGB1 has not been used as a therapeutic agent for bone regeneration and whether it has any effect on either osteoprogenitor or osteoblast differentiation and mineralization is barely studied. We did not observe any effect on osteogenic differentiation when HMGB1 was added to the MSC or preosteoblast culture media. Although it has been shown that CCN2 expression is increased in MSCs and osteoblasts during bone formation (216), the effect of the addition of the protein CCN2 to MSCs or to osteoblasts had not been examined previously. Our study demonstrates that while it promotes migration of osteoprogenitor cells, CCN2 is not able to increase osteogenesis in contrast to a published study by Safadi et al. (254), who used rat primary osteoblasts and showed an increase on calcium deposition when 100 ng/mL of CCN2 was added to the culture beginning at day 11. We cannot exclude that the differences in experimental setup, including addition of dexamethasone and single dosing of CCN2, might explain the results.

With regard to Nell-1, most of the osteogenic differentiation studies have been performed with either human osteosarcoma cell lines or murine osteoblast-like cells (255-257). These studies have shown that, when transfected with Nell-1, these cells increase late osteogenic differentiation markers and ECM mineralization. Recently, Pang et al. have identified a functional transcript of Nell-1 able to induce osteogenic differentiation of a murine MSC line (258). However, no information on human MSCs or osteoblasts was available. We observed an osteogenic trend when Nell-1 was added at low doses to preosteoblasts, although with high variability between cultures. Even then, comparison on a molar basis suggests that Nell-1 could have an osteogenic inducing effect even at low doses, in contrast to BMP-2 that exhibited the reverse effect. Although we did not observe a significant effect of Nell-1 on osteogenic differentiation, a synergistic effect of Nell-1 and BMP-2 has been shown on osteogenesis *in vitro* (259). Moreover, Nell-1 can suppress BMP2-induced inflammation and enhance BMP2-induced bone formation *in vivo* (260-262). Therefore, Nell-1 is a potentially interesting candidate to be used alone or with BMP-2. Nell-1 and BMP-2 might stimulate different stages of osteogenic differentiation; where Nell-1 stimulates osteoprogenitor cell migration and could enhance preosteoblast differentiation, BMP-2 might promote differentiation of skeletal stem cells.

### 4.5.3 Effects on vascularization

BMP-2 had been shown to stimulate angiogenesis in developing tumors (203, 263). In bone tissue engineering, however, BMP-2 is frequently used in combination with angiogenic factors as vascular endothelial growth factor (VEGF) or angiopoietin 1 (94, 264, 265), suggesting that BMP-2 does not optimally induce vascularization. In this study, we demonstrated the ability of BMP-2 to induce the formation of tube-like structures at a dose of 1 µg/mL, a relatively much higher dose than required for CCN2, HMGB1, or Nell-1. HMGB1 is known to have diverse roles in angiogenesis during disease and tissue repair (238) and it has been suggested to induce angiogenesis through a VEGF-dependent mechanism (266). HMGB1 was shown to induce tube formation by microvascular ECs at doses ranging from 0.1 to 1 µg/mL (267, 268). In this study, we show that much lower doses of HMGB1 are sufficient to recruit ECs and to promote tube formation. CCN2 has been shown to act as a proangiogenic factor, coordinating vasculature formation during skeletal development (217, 269) and also as an antiangiogenic agent inhibiting VEGF-induced angiogenesis (225), suggesting that CCN2 regulates angiogenesis through direct and indirect mechanisms (270). We show that CCN2 has proangiogenic properties when it is added directly to ECs, even at much lower doses than those required for BMP-2 to induce a similar effect. Therefore, CCN2 might also be an interesting factor to be combined in future studies with a powerful osteoinductive growth factor, due to its chemotactic and angiogenic features. Although some studies have shown that Nell-1 induces VEGF expression in human pericytes and perivascular stem cells (208, 271), to our knowledge, there are no previous publications investigating the effects of Nell-1 on vascularization of

ECs. We demonstrate that the addition of Nell-1 positively affects EC migration within a tight dose range, producing a significant increase at 100 ng/mL, a larger dose than needed with either HMGB1 or CCN2, but still 10 times lower than that needed with BMP-2.

## 4.6 Conclusions

To accelerate and optimize bone remodeling, using more than one type of growth factor involved in bone formation could be preferable to reduce possible side effects due to high doses used when single-factor therapies are applied. In addition, several studies have shown that not only the dose but also the timing of release of the proteins from the carrier used for bone formation greatly modifies the outcome (90). Based on the promising properties of Nell-1, HMGB1, CCN2, and BMP-2 with regard to their promotion of bone formation-related processes, *in vivo* analyses using dual release systems should be performed to assess their potency for bone defect repair.

## 4.7 Acknowledgments

The authors thank Dr. Joachim Nickel for his generous gift of BMP-2. The research leading to these results has received funding from the European Union Seventh Framework Programme FP7-PEOPLE-2013-ITN under grant agreement no. 607051.

# 5

## Follistatin effects in migration, vascularization and osteogenesis *in vitro* and bone repair *in vivo*

Shorouk Fahmy-Garcia, Eric Farrell, Janneke Witte-Bouma, Iris Robbesom-van den Berge, Melva Suarez, Didem Mumcuoglu, Heike Walles, Sebastiaan G.J.M. Kluijtmans, Bram C.J. van der Eerden, Gerjo J.V.M. van Osch, Johannes P.T.M. van Leeuwen, Marjolein van Driel

## 5.1 Abstract

The use of biomaterials and signaling molecules to induce bone formation is a promising approach in the field of bone tissue engineering. Follistatin (FST) is a glycoprotein able to bind irreversibly to activin A, a protein that has been reported to inhibit bone formation. We investigated the effect of FST in critical processes for bone repair, such as cell recruitment, osteogenesis and vascularization, and ultimately its use for bone tissue engineering. *In vitro*, FST promoted mesenchymal stem cell (MSC) and endothelial cell (EC) migration as well as essential steps in the formation and expansion of the vasculature such as EC tube-formation and sprouting. FST did not enhance osteogenic differentiation of MSCs, but increased committed osteoblast mineralization. *In vivo*, FST was loaded in an *in situ* gelling formulation made by alginate and recombinant collagen-based peptide microspheres and implanted in a rat calvarial defect model. Two FST variants (FST288 and FST315) with major differences in their affinity to cell-surface proteoglycans, which may influence their effect upon *in vivo* bone repair, were tested. *In vitro*, most of the loaded FST315 was released over 4 weeks, contrary to FST288, which was mostly retained in the biomaterial. However, none of the FST variants improved *in vivo* bone healing compared to control. These results demonstrate that FST enhances crucial processes needed for bone repair. Further studies need to investigate the optimal FST carrier for bone regeneration.



## 5.2 Introduction

Biomaterial scaffolds functionalized to stimulate endogenous repair mechanisms incorporating bone-forming factors offer a potential alternative to bone-grafts. Furthermore, injectable systems are a promising option since they can potentially deliver growth factors in a less invasive manner and conform to complex shapes, which is especially important within the craniofacial complex (99). Therefore, choosing the right material and growth factor(s) is critical to induce the key events needed for bone formation. In previous work (Chapter 2), we have developed an *in situ* gelling formulation made by alginate and Recombinant Collagen-based Peptide (RCP) microspheres (MS) that were able to considerably slow down the release of bone morphogenetic protein-2 (BMP-2) and support bone formation (272). However, despite the therapeutic potential of BMP-2 in bone repair, it is not free of complications such as ectopic bone formation, respiratory failure, inflammation, pseudarthrosis and cancer (104).

The transforming growth factor beta (TGF- $\beta$ ) family comprises more than 30 signaling proteins that are essential developmental factors stimulating diverse cellular differentiation and growth responses (273). Among them, bone morphogenetic proteins (BMPs) and the activin/inhibin subfamily members such as BMP-2 or activins have been shown to be fundamental in the regulation of bone organogenesis (274, 275). Particularly, activin A is one of the most abundant TGF- $\beta$  family member proteins found in bone (276). Consequently, bone contains high concentrations of BMPs and activins as well as their antagonists such as noggin or follistatin (FST), which block signaling and are essential regulators of endogenous bone repair. Their importance is such that Matzuk et al. demonstrated that FST-deficient mice were growth-retarded and among others showed skeletal defects, dying within hours of birth (277). The effect of FST on bone repair and the major target it antagonizes, activin A, is not clear. It has been previously reported that activin A stimulates osteoclast formation (278, 279), and that the administration of soluble activin receptors enhances bone formation and bone mineral density in both mice and monkeys (276, 280, 281).

In bone, FST is mainly expressed by osteoblasts, but also to a lesser extent by osteocytes in both developing mouse mandible and in the callus of repairing bone (282). Its role in osteogenic differentiation is controversial, both a positive and a negative effect upon osteoblasts during osteogenic differentiation have been reported (283, 284). *In vivo*, several studies have used FST-overexpressing mice to assess its effect upon muscle healing and bone morphology, concluding that FST improved muscle healing after injury, but its overexpression leads to a decreased quality of the skeleton (285, 286). Kawao et al. have demonstrated that in response to hypergravity, FST acts as a circulating molecule regulating muscle and bone metabolism and the interaction between them (287). Taken together, these data suggest that FST administration, as the major antagonist of activin A, is

involved in bone formation and may have a significant therapeutic potential to trigger bone regeneration.

The role of FST in some of the other essential processes needed for bone repair such as cell recruitment or vascularization is suggested but remains unclear. FST has been associated with angiogenin, a key protein implicated in activation of endothelial cells and stimulation of new blood vessel growth (288). Nonetheless, whether FST promotes angiogenesis is uncertain. Some studies have shown that FST induces tumor-associated angiogenesis (289, 290), but FST was also found to inhibit it (291).

FST is a structurally complex monomeric glycoprotein widely distributed throughout adult tissues (292). The FST gene consists of six exons with an alternative splicing site that generates two major forms and, after further proteolysis and glycosylation, results in two different variants of the protein. FST288, which consists of 288 amino acids and FST315, which consists of 315 amino acids (293). The FST315 variant includes an acidic C-terminal tail domain encoded by exon 6, whereas the FST288 protein ends after exon 5 due to a stop codon inserted as a result of alternative splicing. Importantly, although both FST variants contain a heparin-binding sequence, which affords an ability to bind to cell surface proteoglycans on many cells, the C-terminal domain in FST315 seems to neutralize the basic residues of the heparin binding sequence (294). Thus, FST315 can only bind to proteoglycans after binding to activin, which causes a conformational change that exposes the heparin-binding motif (295). Therefore, in general FST315 exhibits weak cell-surface binding capability and is considered the circulating form of the protein, while FST288 is the tissue-bound variant due to its ability to bind to heparan-sulfate proteoglycans (292, 296). The structural differences between both FST variants may have an impact on their properties and ultimately their regulatory role. In fact, several groups have studied the pharmacokinetic/pharmacodynamic (PK/PD) relationships and their effect in muscle regeneration (297, 298) but unfortunately, most of the published studies did not specify which FST variant was used (283, 284, 286, 287, 299).

No receptor for FST has been found but it is known to bind almost irreversibly to activin A, neutralizing its function (300, 301). Both variants of FST inhibit activin A function, although it has been shown that the affinity of FST288 for activin A is higher than that of FST315 (302). Also, FST is able to interact with other members of the TGF- $\beta$  superfamily neutralizing or regulating their functions such as activin B, myostatin and BMPs. With 10-fold lower affinity than for activin A, FST can also bind to BMP-4, 6 and 7 (303-305). As bone metabolism is regulated mostly by BMPs and activin A, FST seems to play a pivotal role in bone physiology.

This study has been performed to investigate the use of FST for bone tissue engineering. *In vitro*, we have investigated whether FST is able to attract osteoprogenitor and endothelial cells from human origin and promote their differentiation. We then assessed the effect of

FST in bone regeneration in a rat calvarial defect model and loaded two different doses of both variants of FST –FST315 and FST288– in our previously developed controlled-delivery system of RCP encapsulated in an injectable alginate hydrogel (272).

## 5.3 Materials and methods

### 5.3.1 Cell culture

Human MSCs were obtained from leftover material from iliac crest biopsies of four juvenile donors (age 9-12 years) undergoing cleft palate reconstruction surgery with implicit consent (Erasmus MC medical ethical committee number MEC-2014-106) and expanded as previously described (131). Then, cells at passage 4 were used either for migration or osteogenic differentiation assays.

Primary microvascular endothelial cells (MVECs) were isolated from the foreskin of three juvenile donors (age 9 mos-4 yrs) as previously described (306) after their guardians had provided full informed consent (University of Wurzburg ethical board vote 182/10). Then, cells were cultured as monolayers in endothelial cell growth medium MV (ECGM; PromoCell). Cells were passaged at 70-80% confluence and were used between passages 3 and 5 for sprouting assays.

Human umbilical vein endothelial cells (HUVECs) (Lonza, Walkersville, MD, USA) were cultured at a density of 5,000 cells/cm<sup>2</sup> in endothelial growth medium (EGM-2 with SingleQuots (Lonza)). Nonadherent cells were removed by replacing the medium after 2-3 days. When cells neared confluency they were used between passages 9 and 12 either for migration or tube formation assays.

Calvarial-derived Simian Virus-immortalized Human Fetal Osteoblast (SV-HFO) cells (239) were expanded and cultured as published previously (307). Briefly, cells were seeded in phenol-red free  $\alpha$ -Minimal Essential Medium ( $\alpha$ -MEM Gibco, BRL, Paisley, UK), pH 7.5, supplemented with 20 mM HEPES (Sigma, St. Louis, MI), penicillin/streptomycin, 1.8 mM CaCl<sub>2</sub>·2H<sub>2</sub>O (Sigma) and 2% heat-inactivated charcoal-treated fetal calf serum (FCS). All cell cultures were performed in 5% CO<sub>2</sub> at 37 °C in a humidified atmosphere.

### 5.3.2 Migration assay

The effect of FST upon MSC and HUVEC migration was assessed using modified Boyden chambers (polyethylene terephthalate cell culture inserts, pore size: 8  $\mu$ m in diameter, Millipore-Merck, NL). The human recombinant FST variants used in this study were made via CHO-S cell expression using the FST's native leader sequences, followed by affinity protein chromatography using Hi-trap heparin (GE Healthcare Life Science), and desalted to a 50 mM KPO<sub>4</sub> buffer (165 mM sucrose, 0.01% Tween-20, pH 7.4). SDS-PAGE showed a protein purity higher than 95%.

To analyze MSC migration,  $\alpha$ -MEM (Gibco) containing FST315 (0.8-5 nM (28-175 ng/mL)) was added to the lower chamber of a 24-well plate. The doses selected were based in a previous publication, in which 100 and 500 ng/mL of FST were used, showing that these range of doses was able to enhance osteoblast osteogenic differentiation (284), and in previous non-published studies carried out in our department in which lower FST doses were tested.  $\alpha$ -MEM containing PDGF-AB (20 ng/mL) was used as positive control. The controls used to investigate MSC migration were also used as controls in another publication (131).  $6 \times 10^3$  MSCs suspended in a volume of 200  $\mu$ L  $\alpha$ -MEM were added to the upper chamber. Cell migration was followed at 5% CO<sub>2</sub> and 37 °C in a humidified atmosphere for 17 h.

To test HUVEC migration, endothelial cell basal medium (EBM-2, Lonza) containing FST was added to the lower chamber.  $5 \times 10^4$  HUVECs were added into the upper chamber of the transwells and incubated at 5% CO<sub>2</sub> and 37 °C in a humidified atmosphere for 10 h. EGM-2 medium was used as positive control. The membrane was then washed and the cells were fixed with 4% formalin and stained with 4',6-diamidino-2-phenylindole (DAPI) (100 ng/mL) in the dark for 5 min. Cells remaining on the upper surface of the membrane were mechanically removed with a cotton swab and those which had migrated to the lower surface were imaged using fluorescence microscopy (Zeiss Axiovert 200M Fluorescence Imaging, Sliedrecht, NL) in five random fields for each membrane and counted using ImageJ software.

### **5.3.3 HUVEC Tube formation assay**

Growth factor-reduced matrigel (Corning, USA) was added to a 96-wells plate and incubated at 37 °C for 1 hour. HUVECs were trypsinized and resuspended in EBM medium supplemented with FST315 2-fold concentrated to achieve 28 ng/mL, 70 ng/mL and 175 ng/mL as final concentrations. EGM-2 complete medium was used as positive control and EBM-2 medium as negative control. 15,000 cells were seeded on top of the matrigel and incubated at 37 °C in the presence of 5% CO<sub>2</sub> in a humidified atmosphere. Tube formation was imaged after 4, 6 and 24 hours of incubation. The results were analyzed using ImageJ software.

### **5.3.4 3D-culture spheroid assay**

To generate the spheroids, 250,000 MVECS were suspended in 40 mL of Vasculife® complete medium (Lifeline, Germany) with 10 mL of methyl cellulose (Methocel™ (Dow, USA)), seeded in nonadherent round-bottom 96-well plates (100  $\mu$ L/well) and incubated overnight at 37 °C and 5% CO<sub>2</sub> in a humidified atmosphere. The following day spheroids (500 cells approx. per spheroid) were harvested, transferred to a 50 mL tube and centrifuged (3 min, 500 g). Supernatant was removed and the pellet was covered with 5 mL of Methocel™. Immediately prior to use, collagen preparation was made by 3.3 mL

pepsin-extracted type I collagen (Rat tail collagen High Concentration, Type I, BD Biosciences, USA) solubilized in 1.7 mL 0.1% acetic acid and 0.5 mL Medium 199 (10x) (Sigma). 0.5 mL of NaOH 0.2 N was used to reach a neutral pH. Collagen preparation was mixed with the spheroid-containing methocel solution and seeded in 24-well plates (1 mL/well). Plates were placed into an incubator to let the collagen gel polymerize for 30 min. Then, collagen gels were overlaid with 200  $\mu$ L medium containing FST315 10-fold concentrated to achieve a final concentration of 28 ng/mL. VEGF at 27.5 ng/mL was used as positive control and basal medium as negative control. After 24 h of culture, cell invasion was visualized using a ZEISS Axiovert 25 microscope at 10x magnification.

### 5.3.5 Osteogenic differentiation

Osteogenic differentiation assays were performed on MSCs and SV-HFOs. 3,000 cells/cm<sup>2</sup> (MSCs) or 9,000 cells/cm<sup>2</sup> (SV-HFOs) were seeded in  $\alpha$ -MEM in 12-well plates. For MSCs, the medium was replaced after 24 h with complete osteogenic medium; DMEM High Glucose (Gibco) with 10% FCS, 1.5  $\mu$ g/mL fungizone, 50  $\mu$ g/mL gentamicin, 25  $\mu$ g/mL ascorbic acid-2-phosphate, 10 mM  $\beta$ -glycerophosphate and 0.1  $\mu$ M dexamethasone. For SV-HFOs, medium was replaced after 48 h with osteogenic differentiation medium consisting of phenol-red free  $\alpha$ -MEM (Gibco) supplemented with 20 mM HEPES (Sigma, MO, USA), streptomycin/penicillin, 1.8 mM CaCl<sub>2</sub>·2H<sub>2</sub>O (Sigma), 2% heat-inactivated charcoal-treated FCS, 0.1  $\mu$ M dexamethasone and 10 mM  $\beta$ -glycerophosphate. To both cultures FST315 (28 ng/mL, 70 ng/mL and 175 ng/mL) was added during each medium refreshment. The experiment was carried out until onset of mineralization, monitored by measuring calcium concentration in the culture supernatant. For biochemical analyses, medium was collected and cells were scraped from the culture dish in PBS containing 0.1% Triton X-100. Supernatants were stored at -80 °C. Cell lysates were thawed and sonicated on ice in a sonifier cell disruptor (Soniprep 150, MSE, London, UK) or in a water-bath sonifier (Ultrasonic Cleaner CD-4800, Norville, UK) before analysis.

### Alkaline phosphatase (ALP) activity and protein measurement

ALP activity was performed as described previously (241). Briefly, it was assayed by determining the release of paranitrophenol from paranitrophenylphosphate (pNPP) in the SV-HFO cell lysates as previously described (131). Absorption was measured on the Wallac 1420 Victor2 plate reader at 405 nm. For standards, ALP (10 U/mL) from bovine kidney (Sigma) was used.

Protein was measured in cell lysates using the BCA protein assay (Pierce™ BCA Protein assay, Thermo Scientific, Rockford, IL) according to manufacturer's instructions.

### Mineralization

To quantify the calcium content, cell lysates were incubated for 48 h in 0.24 M HCl at 4 °C. For analysis of calcium concentration in the culture medium, supernatant was collected and measured directly from day 9 onwards. In both cases, calcium content was colorimetrically determined after addition of 1 M ethanolamine buffer (pH 10.6), 19.8 mM 8-hydroxyquinoline and 0.35 mM O-cresolphthalein complexone, at 595 nm on the Wallac 1420 Victor2. Besides, to assess that calcium deposition was, in fact, observed due to the osteogenic differentiation of the cultured cells and not just due to a mere calcium precipitation, MSCs and SVHFOs were also cultured in osteogenic medium but in the absence of dexamethasone. The results showed that, without the addition of dexamethasone, calcium deposition was not detectable (Figure S5.1).

For von Kossa staining, cell cultures were fixed for 15 minutes in 4% formaldehyde. After fixation, cells were washed five times with distilled water. Subsequently, calcium was stained by 5% (w/v) silver nitrate solution (Sigma, 85228) for 30 minutes under a 60 W light. Next, the culture plate was rinsed with distilled water and dehydrated with ascending concentrations of ethanol (70%, 96% and 100%). Subsequently, ethanol was removed, and cell culture plates were air-dried and imaged using inverted microscope (Olympus CKX41, Zoeterwoude, NL).

### Quantification of FST and activin A

Quantification of both human FST and human activin was measured using the follistatin DuoSet ELISA kit and the activin A DuoSet ELISA kit (R&D Systems). Briefly, 48-72 h after replacement, conditioned medium was collected until onset of mineralization and stored at -80 °C. The ELISAs were performed according to the manufacturer's protocol.

### 5.3.6 Preparation of the hydrogel formulation for protein release and *in vivo* studies

RCP-MS with an average size of 50 µm were produced by emulsification using calcium carbonate (CaCO<sub>3</sub>) as described previously (58). Pronova SLG20 (sterile alginate where over 60% of the monomer units are guluronate) was ordered from Novamatrix (Sandvika, Norway) and was dissolved in 0.9% sterile sodium chloride to create 2% w/v solution.

34 mg of calcium containing microspheres were incubated overnight at 4 °C with FST315, FST288 or BMP-2. The recombinant human BMP-2 (rhBMP-2, amino acids 283 to 396 plus an N-terminal Met-Ala) was expressed in *Escherichia coli*, isolated from inclusion bodies, renatured and purified, as previously described (119), and it was kindly provided by Dr. Joachim Nickel (Fraunhofer IGB, Germany). For release assays, 85 µL of FST288 or FST315 at a concentration of 112.5 µg/mL was added to the MS to achieve a final concentration of 1.48 µg in the final formulation. For *in vivo* studies, FST288 and FST315 at 152 µg/mL and 15.2

$\mu\text{g/mL}$  were added overnight to the MS to achieve a concentration of 20 and 2  $\mu\text{g/mL}$ . 85  $\mu\text{L}$  of 380  $\mu\text{g/mL}$  BMP-2 were added to the MS, resulting in a concentration of 50  $\mu\text{g/mL}$  within the final formulation. After overnight incubation, on top of swollen particles, 507  $\mu\text{L}$  of SLG was added. Then, the mixture was supplemented with 53  $\mu\text{L}$  of 0.06 M fresh glucono delta lactone (GDL) solution (Sigma). GDL was used to dissolve the  $\text{CaCO}_3$  so that alginate could be crosslinked and increase the mechanical property of the formulation. The prepared formulation was incubated overnight at 4 °C to equilibrate. Next day, the formulation was mixed again prior to *in vitro* and *in vivo* studies.

### Release of FST315 and FST288 from the hydrogel formulation

The formulations were prepared as described above; 100  $\mu\text{L}$  from the hydrogel with 1.48  $\mu\text{g}$  of either one of the both variants of FST was added to each well of 24-well plate inserts with 0.4  $\mu\text{m}$  pore size. 1 mL DMEM with 10% FBS and 1% Penicillin/Streptomycin per well was added to reservoir plate. The plates were incubated at 37 °C under constant agitation at 300 rpm. At each time point the medium was collected and replaced with fresh medium. The collected release media was analyzed by duoset FST ELISA kit (R&D) according to manufacturer's protocol. As positive control, 100  $\mu\text{L}$  of 1.48  $\mu\text{g/mL}$  FST288 and FST315 solution were added to the inserts without hydrogel constructs and 1 mL medium was added to bottom wells of the transwell plate. At each time point 1 mL medium was collected and changed with fresh medium.

### 5.3.7 *In vivo* study

All animal experiments were performed with prior approval of the ethics committee for laboratory animal use (protocol #EMC 116-15-04).

26 Sprague Dawley (SD) male rats (Envigo, NL) at 12 weeks old were used in this study to evaluate bone formation. The animals were randomly assigned and housed in pairs in a specific pathogen-free environment and allowed to adapt to the conditions of the animal house for 7 days before starting the study. The animals were maintained at 20-26 °C on a 12 h dark/light cycle with *ad libitum* access to standard rat chow and water. To evaluate the effect of FST288, FST315 and BMP-2, the proteins were loaded in the alginate formulation. 40  $\mu\text{L}$  of the protein loaded-composite was injected in the defect. Two different concentrations of FST315 and FST288 were loaded in the defects, 800 ng ( $n = 9$  defects) and 80 ng ( $n = 9$  defects). BMP-2 was used as positive control and the concentration loaded per defect was 2  $\mu\text{g}$  ( $n = 3$  defects). As negative control, biomaterials without FST were implanted ( $n = 10$  defects). Each animal received two implants in bilateral defects. Animals were euthanized with  $\text{CO}_2$  and the specimens were harvested for further analysis 10 weeks after implantation. The biomaterial only control used in this experiment was also used as control in Chapter 3 (272) to reduce the number of experimental animals.

### **Surgical procedure and fluorochrome labelling**

The rat calvarial defect was performed as previously described (308). After general anesthesia using 2.5% isoflurane, the animals received intraperitoneal injections of 0.05 mg/kg of buprenorphine (Temgesic®, Indivior, UK) for perioperative analgesia and 5 mL/kg sterile normal saline to account for fluid losses. The animal skulls were shaved and disinfected with ethanol swabs. Then, an incision was made through the skin of the calvarium and periosteum, and full-thickness flaps were reflected. The defect was irrigated with 0.1 mL of 1% xylocaine with 1:200,000 epinephrine (AstraZeneca, NL) along the sagittal midline of the skull. Under copious sterile saline irrigation, two 5 mm-diameter bone defects were prepared with a trephine bur (Fine Science Tools, Germany) in each animal and any debris or bone chips were removed. The defects were treated with the biomaterial loaded with FST, BMP-2 or the biomaterial alone as described above. Then the periosteum and the skin over it were repositioned and sutured with polylactic acid sutures (Vycril 4.0, Ethicon, Johnson Prod., São José dos Campos, Brazil). All animals received three postoperative doses of buprenorphine for analgesia every 10 h during the next days. 4 weeks postoperative, rats were subcutaneously injected with 25 mg/kg of Calcein (Sigma) in a 2% sodium bicarbonate solution. Fluorochrome label was analyzed using a light/fluorescence microscope with a filter block (Zeiss Axiovert 200M Fluorescence Imaging, Slidrecht, NL).

### **μCT analysis**

Quantum FX μCT (Perkin Elmer, Waltham, MA, USA) was used to image animals biweekly until the end of the experiment. To image the bone formation *in vivo* the following parameters were used; Field of view: 30 mm, Voltage: 90 kV, Current: 160 μA, Scan Time: 3 min. To image the implants after retrieval, a field of view of 20 mm and a scan time of 4.5 min were used. Mineral volume and bone mineral density (BMD) were measured on basis of calibration scanning, using two phantoms with known density (0.25 g/cm<sup>3</sup> and 0.75 g/cm<sup>3</sup>; Bruker μCT) under identical conditions. For image processing, analysis software was used (Mayoclinic, Rochester, MN, USA), threshold levels were set to 0.12 g/cm<sup>3</sup>.

### **Histological evaluation**

10 weeks after implantation, the relevant part of the skull was removed and fixed in neutral buffered 4% formalin solution for 3 days, dehydrated in graded ethanol solution from 70% to 100%, and finally embedded in methyl methacrylate resin. Sections of 10 μm were generated along the long axis of the cylindrical samples on a saw Microtome system (Leica 4 SP1600, Germany). Samples were stained with von Kossa and Goldner's trichrome as previously described (131, 189).



### 5.3.8 Statistical analysis

Data were analyzed with IBM Statistics 21 (SPSS) and GraphPad software (GraphPad, San Diego, USA). Migration, osteogenesis and angiogenesis were analyzed using a linear mixed model; the different conditions (different doses of the proteins studied) were considered a fixed parameter and the donors (experiments) as a random factor. *Ex vivo* data were also analyzed using a linear mixed model. Data are presented indicating the mean  $\pm$  SD and a value of  $p < 0.05$  was considered to be statistically significant.

FST release data were analyzed using a Student's T-test, while *in vivo*  $\mu$ CT data were analyzed using two-way analysis of variance. If the overall differences were significant, differences between groups were analyzed by Bonferroni *post-hoc* test. Data are presented indicating the mean  $\pm$  SEM.

## 5.4 Results

### 5.4.1 FST attracts both MSC and HUVEC cells *in vitro*

To determine if FST could recruit osteoprogenitor cells and ECs to the site of injury, we assessed its ability to attract MSCs and HUVECs. FST significantly stimulated MSC migration compared to plain medium control at all doses tested; 1.68-fold, 1.857-fold and 1.581-fold increase, respectively ( $p = 0.009$ ,  $p = 0.001$ ,  $p = 0.002$ ) (Figure 5.1A). Migration of HUVECs towards FST-containing medium was less pronounced but reached significance at the medium dose (1.28-fold increase of migration compared to control,  $p = 0.036$ ) (Figure 5.1B).

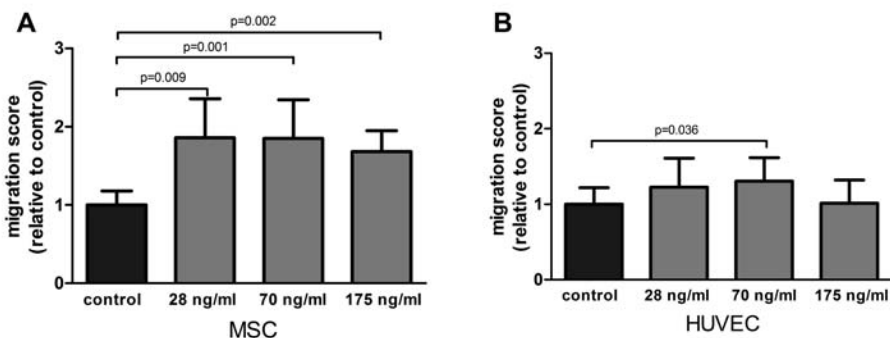


**Figure 5.1. Effect of FST upon MSC and HUVEC in a migration assay.** A. Average migration of MSCs exposed to several doses of FST315 relative to the negative control ( $n = 4$  donors in duplicate). B. Average migration of HUVECs exposed to several doses of FST315 relative to the negative control ( $n = 3$  independent experiments in duplicate). The bars represent the mean  $\pm$  SD.

### 5.4.2 FST promotes neovascularization and angiogenesis *in vitro*

Formation and expansion of the vasculature within the newly formed tissue are the crucial steps in neovascularization, and therefore, in bone repair. Several *in vitro* assays were performed to mimic the different steps of the vascularization process. To determine the capability of FST to promote vasculogenesis *in vitro*, HUVECs were seeded on matrigel coated plates in the absence or presence of FST. FST significantly triggered the formation of tube-like structures in an inverse dose-dependent manner, showing 1.6-fold increase when the lowest dose was supplied compared to the basal medium ( $p = 0.014$ ) (Figure 5.2A). As positive control, EC were also treated with EGM-2 complete medium. EGM-2 medium stimulated formation of tube-like structures 1.7 times more than the basal medium (data not shown).

To assess whether 28 ng/mL of FST is also able to induce sprouting angiogenesis, spheroid-sprouting assays were done using MVECs. The spheroid serves as starting point for the growth of capillary-like sprouts. FST stimulated the formation of endothelial cell sprouts from the spheroids, showing more than 2-fold increase in the number of sprouts compared to control (Figure 5.2B) and with a similar potency to VEGF (data not shown). In summary, these data indicate that FST is able to stimulate the distinct mechanisms involved in the formation of the vascular network.

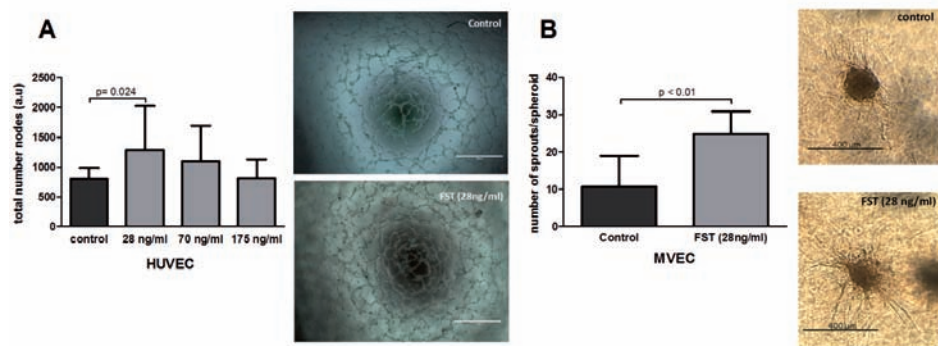


**Figure 5.2. Effect of FST on neovascularization.** A. Effect of FST315 on vasculogenesis. Total number of nodes was quantified ( $n = 3$  experiments in triplicate). Next to the graph, representative pictures of tube-like structures are shown after 6 h incubation in the presence and absence of FST (scale bar: 1000  $\mu$ m). B. Effect of FST315 on angiogenesis. MVEC spheroids were embedded in collagen and incubated for 24 h. The total number of sprouts per spheroid w/o the addition of FST at 28 ng/mL dose are plotted in the graph ( $n = 10$  individual spheroids per experimental group). Next to the graph, representative pictures of cell spheroids in the presence and absence of FST are shown after 24 h incubation (scale bar: 400  $\mu$ m). The bars show the mean  $\pm$  SD.

### 5.4.3 FST does not stimulate MSC osteogenic mineralization, but stimulates committed osteoblast mineralization

The osteogenic properties of FST were studied in MSCs stimulated towards the osteoblastic lineage as well as in fetal calvarial-derived committed preosteoblasts (SV-HFO). The addition of FST did not affect mineralization of MSCs, as shown by quantitative measurement of calcium deposition and von Kossa mineral staining (Figure 5.3A). Interestingly, adding FST to the preosteoblast culture had a direct positive effect on the mineralization process at any of the tested doses, showing a minimum of 2-fold increase compared to the control (osteogenic differentiation medium)( Figure 5.3B).

Additional experiments also indicated a positive effect of FST on committed osteoblast differentiation, as shown via activity of the enzyme alkaline phosphatase. Alkaline phosphatase (ALP) is expressed during osteoblastic differentiation and plays a key role in bone mineralization (309). When the lowest dose of FST was applied to the pre-osteoblast culture, a small but significant increase in ALP activity was observed before mineralization started (day 9). At day 16, FST enhanced ALP activity in all concentrations tested (Figure 5.3B).

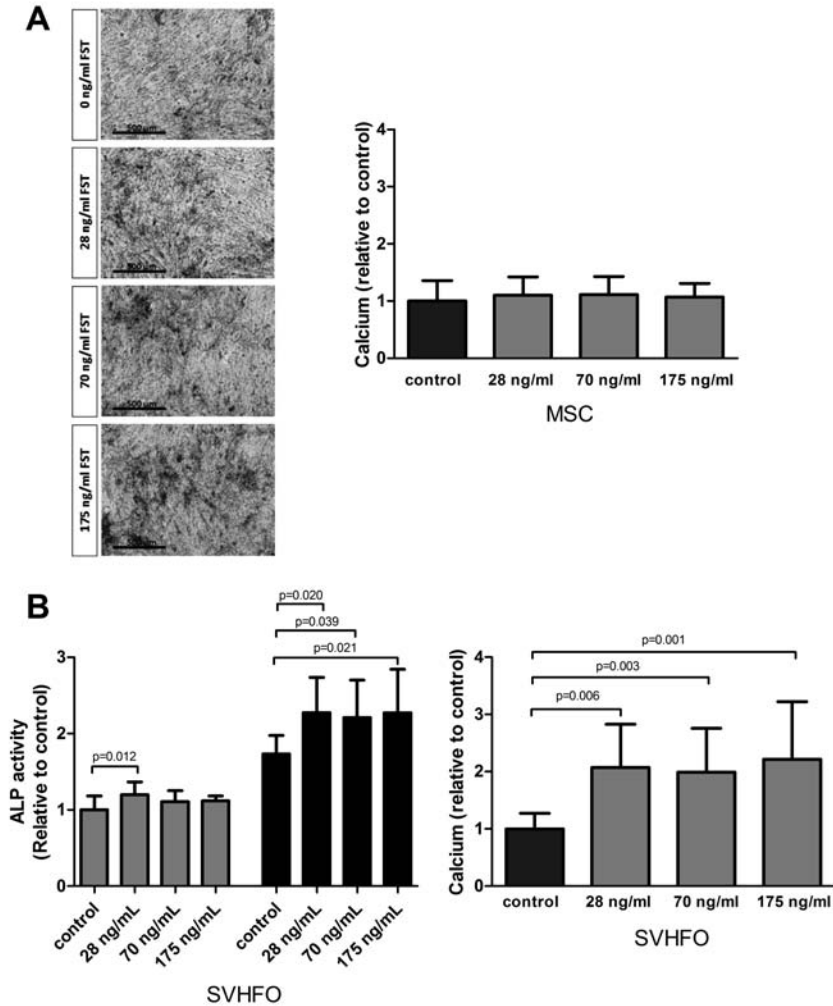


**Figure 5.3. Effect of FST on osteogenic differentiation.** Human MSCs and osteoblasts were induced to mineralize in the absence or continuous presence of FST315. **A.** Quantification of calcium deposition ( $\text{nmol}/\text{cm}^2$ ) in the MSC extracellular matrix at the onset of mineralization relative to control (osteogenic differentiation medium) ( $n = 4$  donors performed in triplicate). Donor dependently, mineralization started between 18-22 days of culture. Representative pictures of the Von Kossa staining at the onset of mineralization (scale bar:  $500 \mu\text{m}$ ). **B.** Left graph: alkaline phosphatase (ALP) activity ( $\text{mU}/\text{cm}^2$ ) during SV-HFO culture with and without continuous FST treatment at day 9 (grey bars) and 16 (black bars) of culture. Results are shown relative to day 9 control. Right graph: Quantification of calcium deposition ( $\text{nmol}/\text{cm}^2$ ) in the SV-HFO extracellular matrix at day 16 relative to control ( $n = 3$  experiments performed in triplicate). The bars show the mean  $\pm$  SD.

#### 5.4.4 FST production changes during osteogenic differentiation

To regulate cellular processes, such as extracellular matrix mineralization, two FST molecules encircle activin, neutralizing its receptor binding sites (310). We measured the levels of FST and activin produced during the different phases of osteogenic differentiation in MSC and SV-HFO cultures by ELISA. FST was produced in high quantities by MSCs at the onset of mineralization (day 16) and its release significantly decreased during full mineralization (Figure 5.4A). Activin production levels did not significantly differ during MSC culture, but remained low (at least 15 times lower than the FST levels at the same time points) (Figure 5.4B). Unlike MSCs, SV-HFOs are already osteogenic-committed cells and therefore, mineralization occurs earlier than in MSCs. In SV-HFOs, the production of FST decreased from day 9 onwards during osteogenic differentiation (Figure 5.4C), a similar pattern to what was observed in MSCs, though earlier in culture. Activin levels were undetectable in SV-HFO cultures

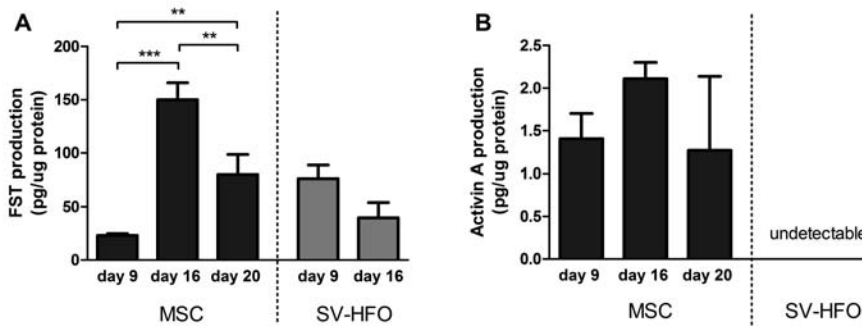


**Figure 5.4. Production of FST and activin A by MSCs and osteoblasts.** FST (graph A) and activin A (graph B) levels were measured in supernatant of MSC and SV-HFO that were induced to mineralize until onset of mineralization. Production was corrected for cell lysate protein content. The bars show the mean  $\pm$  SD. \*\* $p < 0.01$  and \*\*\* $p < 0.001$ .

#### 5.4.5 FST288 release is lower than FST315 release from the alginate-MS hydrogel

It is generally believed that controlled-release systems are optimal for bone formation as they offer spatiotemporal control to mimic the native healing cascades. The previously developed alginate-MS hydrogel was shown to provide sustained protein release (272) (Chapter 2). We first evaluated the release profile of FST288 and FST315 from this formulation. After 4 weeks, the cumulative amount of FST315 and FST288 found in the medium was quantified. To correct for the effect of protein sticking to the plate and membrane, as well as its degradation over time, 1.48  $\mu\text{g/mL}$  of FST288 and FST315 were

added to the upper part of the transwells without the hydrogel formulation. For FST288  $671.60 \pm 220.6$  ng (mean  $\pm$  SEM) and for FST315  $688.5 \pm 78.2$  ng (mean  $\pm$  SEM) were detected, meaning that both FST variants have a similar degradation rate. There are important differences between both FST variants; unlike FST288, FST315 has a C-terminal tail containing several acidic residues, which decrease its heparin affinity. Most likely this difference might affect the release profile of the FST variants. In fact, when the release of both FST variants from the alginate-MS formulation was studied over four weeks, significant differences were observed between the release of FST315 and FST288.  $555 \pm 58$  ng of FST315 was released from the formulation, while only  $169.4 \pm 6.8$  ng of FST288 was released during the same period. Therefore, the amount of FST315 exuded to the medium was three times more than the amount of FST288 ( $p < 0.001$ ) (Figure 5.5). The numbers indicated that the majority of FST315 was released from the hydrogel formulation, contrary to FST288, which was mostly retained in it.

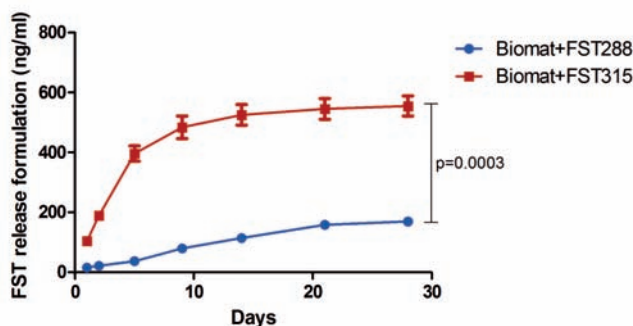


**Figure 5.5. *In vitro* release of FST288 compared to FST315.** The cumulative release of FST288 and FST315 from the alginate-MS formulation in DMEM with 1% P/S detected by ELISA is demonstrated over four weeks. Data are presented indicating the mean  $\pm$  SEM. Statistical difference at 28 days of cumulative release analyzed by Student's T-test,  $p < 0.001$ .

#### 5.4.6 FST315 and FST288 do not improve bone healing in calvarial defects, but show a more homogeneous bone formation than controls

Given the promising effects of FST on migration, osteogenesis and vascularization *in vitro*, we decided to investigate whether FST is able to promote bone repair and if there are differences between FST315 and FST288 to induce bone formation. To do so, both FST variants loaded in alginate-MS hydrogel were injected into 5 mm calvarial defects. *In vivo* longitudinal  $\mu$ CT-scans were performed biweekly to monitor the mineralized bone volume (BV) within the defects, and normalized to the BV observed in healthy SD male rats of the same age. At week 2, the positive control with BMP-2 loaded biomaterial exhibited the same amount of bone volume as the healthy animals, which translated into full defect

healing at the end of the experiment (Figure S5.1). Implantation of the biomaterial alone led to 66% bone volume compared to healthy animals at the end of the experiment (Figure 5.6A,B).

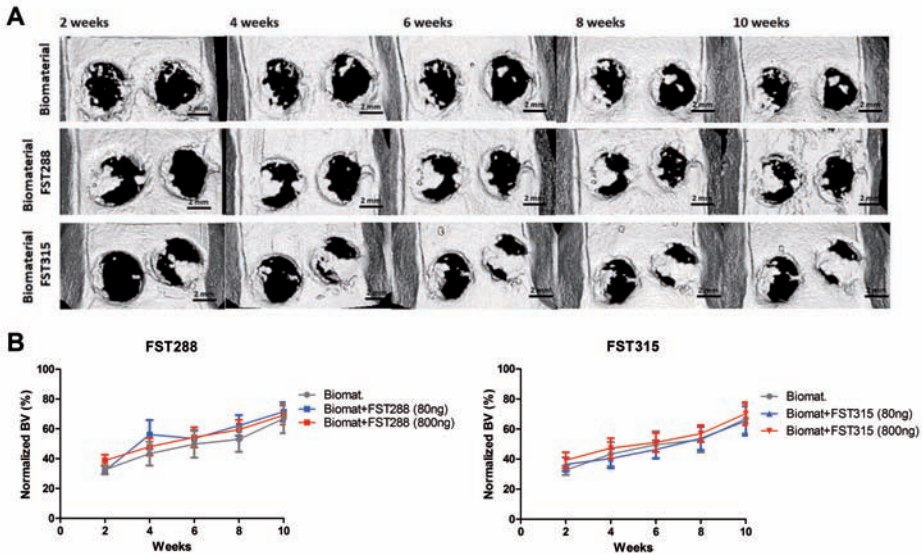


**Figure 5.6. In vivo  $\mu$ CT analysis of rat skulls implanted with FST288 and FST315 over time.** A. Representative in vivo  $\mu$ CT images of the skulls at 2, 4, 6, 8 and 10 weeks after implantation (scale bar: 2 mm) of either biomaterial alone or loaded with FST288 or FST315. In the representative  $\mu$ CT images of both FST variants the right defect was loaded with 800 ng of FST and the left defect was loaded with 80 ng of FST. B. Graphical representations of in vivo  $\mu$ CT analysis. Bone volume was normalized to animals without surgical intervention. The effect of the formulation loaded with FST288 (left graph) and FST315 (right graph) was compared to the effect of the use of the biomaterial alone as control group.

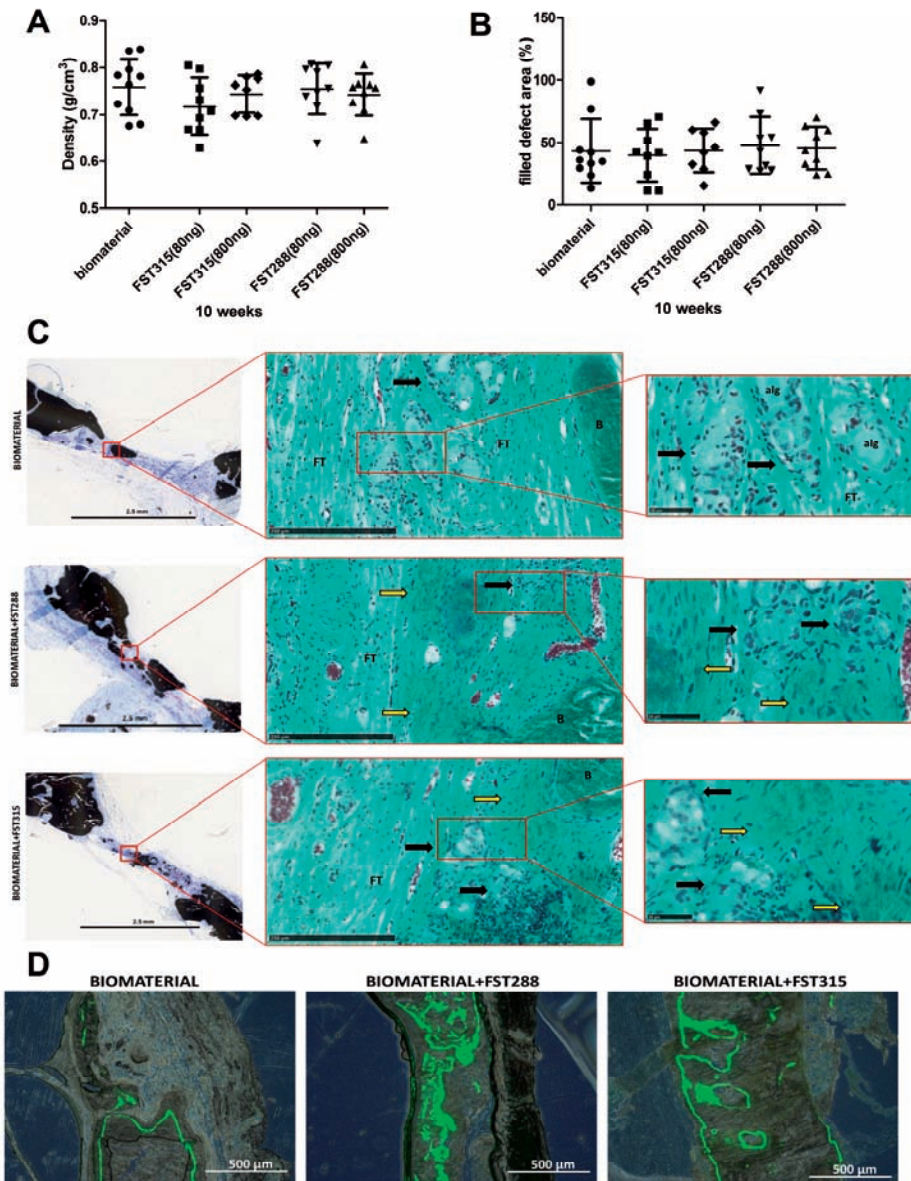
No major differences between FST-treated animals and the ones treated with only the biomaterial were observed during 10-weeks follow up. At week 2, 30% of the bone volume observed in healthy animals was already achieved in all the tested conditions. During the time course of the experiment, mild differences in terms of BV were observed between the FST variants. However, at week 10 the overall BV observed was similar in all conditions, varying between 65-71% of the defect area (Figure 5.6A,B).

The retrieved implants were also scanned *ex vivo*, which allows longer scan times and finer resolution. Bone mineral density of the formed bone did not differ significantly between conditions (Figure 5.7A) and was comparable to the density found in the calvaria of healthy animals ( $0.77 \pm 0.03 \text{ g/cm}^3$ , mean  $\pm$  SD,  $n = 4$  animals). The bone coverage of the defect

oscillated between 40-47% of the total defect area (Figure 5.7B), which is slightly lower than the coverage found in the *in vivo* longitudinal  $\mu$ CT-scans at 10 weeks. This difference is due to motion artifacts and the settings used in longitudinal  $\mu$ CT-scans on live animals. Either way,  $\mu$ CT-scans showed that bone formation not only occurred around the edge of the defect, but also in the central area. Interestingly, more areas with mineralization were observed in the FST conditions, but overall mineral density did not differ from the controls (Figure 5.7C). On histology, circular regions were observed in all the conditions. These regions have a similar size to the microspheres used ( $\sim 50 \mu\text{m}$ ) and in the FST conditions were surrounded by immature ECM, while in the controls were mostly surrounded by fibrous tissue (Figure 5.7C). This is more evident when analyzing the mineralization pattern by measuring calcein fluorochrome incorporation. In the controls, the label was mostly present on the outer periphery of the formed bone and hardly any signal was found in the inner side at 4 weeks. In the FST-treated samples the label was found in both periphery and inward area, indicating a broader and more homogeneous mineralization progression (Figure 5.7D). Besides, in the control samples alginate was still visible, whereas in the FST-treated samples this was undetectable (Figure 5.7C, Figure S5.2). Histological analysis also showed blood vessels ingrowth in all the conditions tested (Figure 5.7C, Figure S5.2).

**Figure 5.7. Newly formed bone tissue at 10 weeks of healing.** A. Bone density observed by *ex vivo*  $\mu$ CT analysis in the different conditions after implant harvesting. B. Percentage of defect filling by newly formed mineralized tissue analyzed by *ex vivo*  $\mu$ CT. Mean is indicated as the line plotted in the middle of the graphs  $\pm$  SD. C. Representative pictures of rat skulls implanted with the biomaterial w/o the addition of the FST variants at 10 weeks. Histological analysis includes von Kossa and Goldner's trichrome staining. Von Kossa staining was used to distinguish mineralized tissue (black) (scale bar: 2.5 mm), while Goldner's trichrome staining was used to determine bone histomorphometry. The square grid delimitates the selected magnified area for each image that is shown with Goldner's trichrome staining (scale bars are 250  $\mu\text{m}$  and 50  $\mu\text{m}$ , respectively), showing erythrocytes (red/purple), nuclei (blue/ grey), alginate remains (alg), formed bone (B) and fibrous tissue (FT). Immature ECM is indicated by yellow arrows and regions where the microspheres have been likely degraded are indicated by black arrows. D. Representative fluorescence images of the central region of the explants showing calcein fluorochrome incorporation in the newly formed bone tissue at 10 weeks postimplantation (scale bar: 500  $\mu\text{m}$ ) with or without the addition of the FST variants. Fluorescence images are combined with bright-field images of the same area.





## 5.5 Discussion

This study investigated the use of FST for bone repair. We have found that FST was able to recruit and differentiate ECs, promote cell sprouting and the formation of tube-like structures *in vitro*. Furthermore, FST was also able to recruit osteoprogenitor cells and to enhance committed osteoblast differentiation and mineralization *in vitro*. However, when FST was loaded in our previously developed slow-release formulation ((272), Chapter 2) and implanted in a calvarial defect model, bone repair was not improved in 10 weeks' time.

FST is known to be upregulated by migrating ECs (311); however, the chemokinetic effect of FST upon ECs was not studied yet. Our results have shown that FST is able to stimulate HUVEC migration when exogenously added to the culture. Furthermore, to assess its effect upon ECs differentiation, we have used two different *in vitro* models –3D spheroid-sprouting assays and tube-formation assays– to investigate both angiogenesis and vasculogenesis as two of the pivotal processes of the vasculature formation. Interestingly, the formation of tube-like structures seemed to be inversely dose-dependent and FST was able to significantly promote both processes when 28 ng/mL (0.8 nM) was added to the culture in the absence of VEGF or any other co-stimulatory factor. *In vitro* studies have shown that both FST and activin are distinctly expressed during the different phases of angiogenesis by bovine aortic ECs (BAECs) and MVECs (311, 312). A few studies investigated the effect of activin (25-50 ng/mL) inducing vasculogenesis upon BAECs and sinusoidal ECs (SECs), showing a positive effect when combined with VEGF but contradictory results when used alone to enhance tubulogenesis (313, 314). Krneta et al. explored the effect of FST and activin in a sprouting angiogenesis assay, showing that FST at 120 ng/mL was able to promote EC sprouting almost at the same level as FGF, while activin addition at 50 ng/mL did not enhance sprouting more than basal control (290). The combination of FGF and activin significantly decreased sprouting (290). *In vivo*, a few papers have shown that FST improved a neovascularization when used on skeletal muscle injury in mice (286) and promoted angiogenesis in the rabbit cornea, especially when combined with FGF (289). It would be interesting to further study this synergistic effect on bone repair. Although we did not specifically study the vascularization processes in our *in vivo* bone defect model, we have found blood vessels ingrowth in all the treated samples, suggesting that FST does not interfere with the natural cascade of events needed for the formation of the vasculature and consequently, it does not have an anti-vasculogenic effect.

Whether FST could attract MSCs and induce bone formation was not studied before. In our *in vitro* study we have demonstrated that FST is able to recruit MSCs. Minor differences were observed between doses, meaning that probably a low dose of FST is enough to promote a chemotactic response upon MSCs. We also investigated the effect of FST upon MSCs and osteoblasts under osteogenic conditions. It is known that FST is highly expressed in developing bone tissues, mainly in osteoblasts (282); however, the effect of

FST on osteoblast mineralization was unclear due to conflicting results observed when supplied to mouse and human osteoblast cultures (283, 284). In our *in vitro* study, FST further enhanced osteogenic differentiation in committed osteoblasts and not in MSCs.

The stimuli involved in MSC's differentiation to osteoblastic cells may differ from those needed to convert preosteoblasts into mature osteoblasts. For example, it is well-known that TGF- $\beta$ -Smad signalling is crucial in the early phases of osteogenic differentiation, however, it inhibits osteoblast maturation and mineralization (315). Consequently, different signal inputs are needed at different stages of the osteoblast differentiation pathway. Our findings suggest that FST's osteogenic effect might be sensitive to which differentiation stage the osteoprogenitor cells are. Previous studies have shown that once FST is synthesized, it remains in the extracellular matrix, exerting an antifibrotic effect (316, 317). Indeed, based on previous studies in which have been shown that activin A suppresses osteoblast mineralization by changing the ECM composition and maturity (284, 318), and in our results, we might conclude that FST is not an osteogenic factor *per se*, but a factor that enhances the mineralization process through its involvement changing the ECM composition while it remains in it. We must remember that FST can only exert its function indirectly, by binding to other molecules and neutralizing their function. Its main antagonist is activin, but FST can also bind to BMPs, with much lower affinity (305). Abe et al. demonstrated in their study that administration of FST to rat mandibular osteoblasts did not cause significant changes in bone nodule number. BMP-2 facilitated the secretion of FST and this increase in FST interfered with BMP-2 action decreasing bone nodule formation (283). Eijken et al. showed in their study that, while FST prevented activin from binding to its receptor, it had no effect on basal or BMP2-induced signalling in human osteoblasts (SV-HFO) (284). Besides, there are several studies that investigated the effect of the addition of activin to osteogenic differentiation of human NHOst cells, showing that its addition strongly inhibited the mineralization process (276, 284). As no receptor has been found for FST, it is widely assumed that FST exerts its regulatory function via antagonizing other proteins with a pivotal role in bone physiology. FST is able to bind almost irreversibly to activin, and with lower affinity to other members of the TGF- $\beta$  family such as bone morphogenetic proteins. In our *in vitro* experiments, both MSCs and SVHFOs secreted high levels of FST but much lower levels of activin under osteogenic conditions. In fact, the secretion of FST was at least 15-fold higher than the secretion of activin at the same time-points. This amount of FST is much greater than the 2:1 molar ratio needed to neutralize all the activin produced by the cells. The addition of FST to the culture media enhanced mineralization of SVHFOs, but not of MSCs. These findings suggest that FST, even when it is found in a much higher concentration than activin, has a positive effect on osteoblast mineralization but does not affect MSC mineralization. FST can antagonize BMP functions as well as those of the activins, and in view of the sharing of type II receptors between activins and BMPs, further studies should investigate the secretion of these proteins at the different phases of MSC's osteogenic differentiation and the interplay between them.

To investigate the ability of FST to promote bone repair in an orthotopic model, FST was loaded within an *in situ* gelling alginate-based delivery system and implanted in a rat calvarial defect model. We hypothesized that FST, based on previous *in vivo* studies and on our *in vitro* results, may have a positive effect on bone formation. We have used two different FST variants (FST288 and FST315) to assess whether their structural variations – which modulate their properties such as the ability to bind to the cell surface–, could lead to differences between variants in terms of bone repair. In fact, *in vitro* release from the biomaterial showed that during 4 weeks, only 25% of FST288 was released to the medium compared to 80% of FST315.

Two different doses of FST288 and FST315 were loaded within the biomaterial to elucidate if there is a limiting concentration of FST that leads to bone repair enhancement and whether FST excess prevents bone repair. FST doses used (800 ng and 80 ng per implant) were based on both our *in vitro* studies and the literature. Serum levels of FST are found in the ng range in mice (319), and our results show that the lowest dose of FST used in the *in vitro* experiments (28 ng/mL) improved crucial processes involved in bone formation such as cell migration, osteogenesis and neovascularization. However, none of the variants improved bone formation compared to the biomaterial in 10 weeks' time. Besides, during the degradation of the biomaterial the protein is released and the differences in FST concentrations of the separate defects may become minor.

Timing of secretion of FST during bone repair seems crucial. When a demineralized matrix was subcutaneously implanted in rats, FST was highly expressed during the initial stages of osteogenesis but decreased along with differentiation (320). Injections of FST in the implants 10 days after implantation resulted in lower calcium content in the implants suggesting that the endochondral ossification process was retarded or inhibited (320). Nagamine et al. showed that neither FST nor activin were expressed in osteogenic cells at the periosteum or at the cortical bone in the intact femurs of the rat (321). Interestingly, in a fractured-femur FST was highly expressed during the first stages of bone healing in osteogenic cells, as well as in the ECM of the periosteum and proliferating chondrocytes, while activin A was almost undetectable in those regions. Furthermore, Activin A was detected especially around osteoclast-like cells on the surface of the newly-formed trabecular bone (321), which is in line with previous publications (282). Altogether indicates that the expression of FST during different phases of both intramembranous and endochondral ossification is important. However, the role of FST in bone repair has been investigated either using ectopic models or long bone fracture models (320, 321) in which the mechanisms of bone formation differ considerably from the events taking place in the development of the flat bones of the skull. It is difficult to compare *in vitro* and *in vivo* studies, but our *in vitro* experiments have shown that FST effects do not respond to a classical dose-response curve; MSC migration and mineralization may need different FST doses that may not fit with FST release timing and dosage from the biomaterial chosen in

this study. In fact, when the alginate formulation was implanted alone, residual alginate was still visible 10 weeks postimplantation, whereas in the FST-treated samples this phenomenon was not detected. In FST-treated samples mineralization occurred both on the outer and inner area of the defect, contrary to what was observed in the controls, where calcein was mostly incorporated on the outer periphery of the defect. An alginate-based formulation was used as FST carrier to achieve FST's slow release, but FST appears to be an early player in bone formation. As we have previously mentioned, our data and the literature suggest that FST exerts its function through the ECM, enhancing its mineralization. The slow-release alginate-based system may not be optimal for bone repair when loaded with FST and might influence the FST effect upon ECM mineralization due to a suboptimal FST release timing.

Alginate has been widely used for bone tissue engineering due to its biocompatibility, easy handling and degradation properties (66). We have previously used RCP encapsulated in an injectable alginate hydrogel ectopically, and the formulation releasing BMP-2 effectively promoted bone formation ((186), Chapter 2). However, when used in bone defect repair, alginate seemed to not only delay the protein release, but also cell and cytokine infiltration within the defects (272). Activin A has been identified as a pivotal molecule during the initial inflammatory response (295), which can be also provoked by surgical stress. Interestingly, FST increased in the circulation several hours after activin A and it is believed that the increase observed in FST levels was partly responsible for the clearance of activin A from the bloodstream (295). In our study, alginate, due to its chemostatic effect, could have prevented or delayed the cascade of events needed for bone repair such as the influx of inflammatory cells and growth factors, or the clearance of activin A from the injury site. Bleeding could also have affected the physical-chemical properties of the biomaterial. Certainly, it would be interesting to assess whether FST addition shows a positive effect in a bone defect when used in a different type of delivery system with a faster release. The affinity to bind cell surface receptors dictates the main biological action of FST. FST315 is considered to act more in an endocrine fashion whereas FST288 does it in an autocrine manner. In fact, FST315 has been used systemically as a therapeutic agent to treat skeletal muscle diseases; however, it exhibits rapid clearance kinetics. Consequently, newly engineered FST315 variants with improved pharmacokinetic properties have been developed, showing promising results in the treatment of several musculoskeletal injury models (297, 298). In our study we aimed to enhance *in situ* bone formation and in the view of our release studies and the greater affinity for cell surface proteoglycans of FST288, the use of this FST variant in a rapid release system is intriguing, and could prompt the assessment of new strategies in bone defect repair.

## 5.6 Conclusions

To our knowledge, this is the first study that instead of focusing in osteogenic differentiation to investigate FST possible role in bone formation, assesses the effect of FST upon chemotaxis and vasculogenesis as well due to their essential role in bone formation, and directly evaluates its possible influence in an orthotopic bone defect such as calvarial defect. FST plays an important role in bone metabolism, mostly acting as activin controller but also regulating the function of other members of the TGF- $\beta$  family (296, 320). However, FST action spans so many different processes that its effect in particular cellular events involved in bone formation was unclear. In summary, this study has shown that FST is able to stimulate cell recruitment, vasculogenesis and osteogenesis; vital processes for a successful bone regeneration. Using the calvarial defect model we could not show a clear improvement in bone repair with FST –which can be due to several causes such as poor bone-forming capacity, underdosage and suboptimal release kinetics among others–, though we observed a more homogeneous mineralization. There is still a lack of knowledge about the role of FST in the acute phase reaction and the effect of its administration in the early phases of bone repair. Therefore, to move on further using growth factor-based therapies, mechanistic approaches should be taken in consideration to investigate how and in which extent FST, as well as its interaction with other proteins, such as activins and BMPs, regulates key processes in bone metabolism and repair. Besides, the optimal release kinetics of FST must be investigated *in vivo* to successfully translate its use into bone tissue engineering based therapies.

## 5.7 Supplemental information

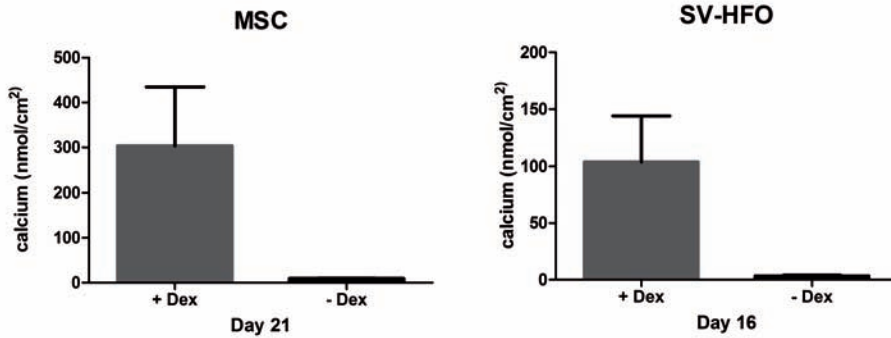


**Figure S5.1. Calcium deposition in MSC and SV-HFO culture in the presence and absence of dexamethasone.** Human MSCs and osteoblasts were induced to mineralize using medium consisting in DMEM High Glucose with 10% FCS, 1.5  $\mu\text{g/mL}$  fungizone, 50  $\mu\text{g/mL}$  gentamicin, 25  $\mu\text{g/mL}$  ascorbic acid-2-phosphate, and 10 mM  $\beta$ -glycerophosphate in the absence or continuous presence of dexamethasone. Quantification of calcium deposition ( $\text{nmol/cm}^2$ ) in the MSC and SV-HFO extracellular matrix at day 21 and day 16 showed that calcium deposits were only detected in the presence of dexamethasone ( $n=1$  donor performed in triplicate). The bars show the mean  $\pm$  SD.

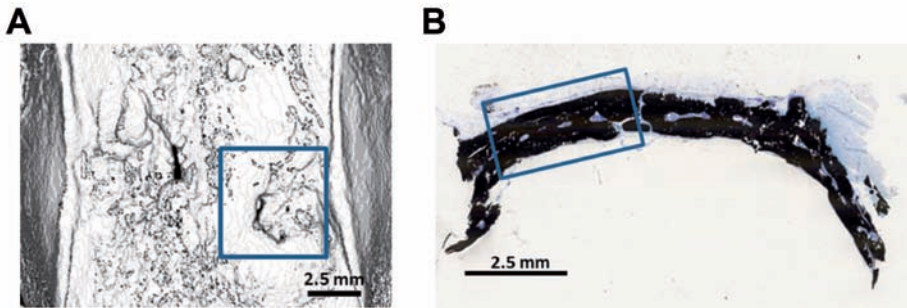


**Figure S5.2. Bone regeneration in calvarial defects with 2  $\mu\text{g}$  of BMP-2 loaded in the formulation.** A.  $\mu\text{CT}$  analysis indicated healed defects, bridged by mineralized bone tissue. B. Representative histological section stained with von Kossa. The square indicates the approximate area of the defect. Scale bars: 2.5 mm.

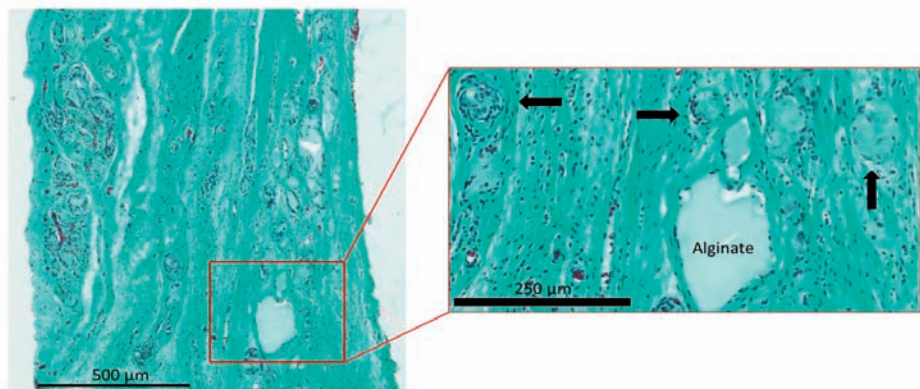


**Figure S5.3.** Residual alginate was found in the bone defects 10 weeks postimplantation in the control-treated samples. Samples were stained with Goldner's trichrome (scale bars: 500  $\mu\text{m}$ ). The square grid delimitates a magnified area (scale bar: 250  $\mu\text{m}$ ) in which areas with alginate are found. The black arrows indicate regions where the microspheres might have been degraded and cell-infiltration has occurred.

## 5.8 Acknowledgments

The authors would like to thank Dr. Joachim Nickel for his generous gift of BMP-2 and Yanto Ridwan, who provided expertise that greatly assisted this study. We would also like to show our gratitude to Nicole Kops and Marijke Schreuders-Koedam for sharing their pearls of wisdom with us during the histological analysis and to Miguel Rodrigues, for his invaluable help with the vascularization assays.



# 6

General discussion and conclusions



## 6.1 Discussion

The human skeleton is an interesting organ with a remarkable ability to regenerate itself after injury. However, in cases where significant bone loss has occurred the conditions for spontaneous bone healing are not ideal. Therefore, the use of bone grafts is required to stimulate bone-healing (30). During the 1940s, bone grafting became an essential procedure. Back then, bone grafting was focused mainly in withstanding the mechanical loading applied by the patient while maintaining inertness (40). Currently, bone grafts are considered a dynamic substitute. The main goal of bone tissue engineering (TE) is to induce the essential cellular processes needed for successful bone repair by delivering bone-progenitor cells and/or bone-forming factors in the injury site. However, many risks and regulatory limitations are raised from the use of cells in TE, encouraging the use of cell-free systems as off-the-shelf alternative (75). Growth factors are pivotal components for bone repair and remodeling. Therefore, their use to exploit the tissue's healing potential is considered a promising therapeutic tool. Several factors involved in bone repair have been broadly investigated. Among them, bone morphogenetic proteins (BMPs), platelet-derived growth factor (PDGF), fibroblast growth factor (FGF), vascular endothelial growth factor (VEGF), and transforming growth factor- $\beta$  (TGF- $\beta$ ) are probably some of the most well studied growth factors (77, 322, 323). However, many parameters are decisive in the use of growth-factor therapy for bone repair; the dose, function and delivery kinetics of the growth factor(s) used or the mechanical stability, porosity and rate of degradation of the implanted scaffold are some of them (324, 325). The optimization and screening of all of the actors involved in an ideal tissue-engineered product (which is, at least, an expensive time-consuming process) is one of the main reasons why most of the studies do not translate to clinically relevant devices. To move from lab bench to clinic bedside in the treatment of bone defects using growth-factor therapies, it is necessary to assess the effect of promising bone-factors in bone repair through basic and preclinical research and to investigate their use when combined with the other TE intersecting components.

### 6.1.1 Protein alternatives for bone tissue engineering: Are we looking for a needle in a haystack?

The most used growth factors in bone TE are the BMPs. Among them, BMP-2 and BMP-7 are the strongest osteoinductive proteins, which prompted in the commercialization of BMP-2 and the Food and Drug Administration (FDA) approval of BMP-7 under a Humanitarian Device Exemption (326). However, BMP-7 market approval did not succeed, and currently only BMP-2 is commercialized for certain bone repair procedures when loaded in an absorbable collagen sponge (86). Nevertheless, the clinical applications of BMP-2 as off-label drug, and the complications related to the supraphysiological doses of the protein delivered locally –exceeding on average one million times the physiological

protein amount— made the use of BMP-2 controversial (327). Therefore, the search of alternative growth factors which also induce the signaling cascades needed for repair seems inevitable.

In this thesis, we aimed to elucidate the role of a series of proteins such as Nell-1, HMGB1, CCN2 and FST on some of the key processes needed for bone formation (**Chapter 4** and **Chapter 5**). Most of the studies performed *in vitro* to evaluate potential putative bone-forming factors focus mainly in their effect in osteogenic differentiation (328-331), which is not the only crucial process needed to eventually improve overall bone formation. Vascularization and the recruitment of progenitor cells to the injured site are also indispensable events in bone repair (20, 332). Accordingly, we have evaluated *in vitro* the role of Nell-1, HMGB1, CCN2 and FST in chemotaxis, vasculogenesis and osteogenic differentiation using primary human endothelial cells (ECs), human primary mesenchymal stem cells (MSCs) and fetal calvarial-derived committed preosteoblasts (SV-HFOs).

We have chosen Nell-1, HMGB1, CCN2 and FST based on the literature since they are known to have a role in overall bone formation (211, 217, 227, 296). However, information about their effect upon some of the specific processes needed for bone repair was lacking, which might be a limiting factor for their translation into future clinical applications. For example, nothing was reported on the chemokinetic effect of Nell-1 or FST on MSCs and endothelial cells. On the other hand, although HMGB1 has been classified as a bone-active cytokine (227), it has been never used as a therapeutic agent in bone TE, and therefore its effect on osteogenic differentiation and mineralization has been barely studied. In fact, the effect of exogenous administration of HMGB1 in tissue regeneration was not investigated until very recently (333). Finally, CCN2 overexpression was already known to enhance MSC osteogenic differentiation (221); however, investigating the addition of the protein directly to the osteoprogenitor cell culture, might be relevant to approach cell-free systems in bone TE. We have compared these four proteins directly to BMP-2, demonstrating that Nell-1, CCN2, HMGB1 and FST significantly induced MSC migration while BMP-2 did not. In addition, all the proteins tested were able to induce human EC migration and vasculogenic differentiation at lower doses than BMP-2 when compared on a molar basis. Indeed, when combined, Nell-1 has shown to inhibit BMP-2-induced inflammation to treat a rat bone femoral defect (260).

Seeking for growth factors that promote both angiogenesis and osteogenesis has gained interest. PDGF is one of these factors (334, 335) and its use has been translated to the clinics under FDA premarket approval (336). In this study, BMP-2 and FST were the only tested factors capable to also enhance osteogenic differentiation. BMP-2 increased the early production of the calcified matrix in MSCs as shown previously by several studies (251, 252), while inhibited it upon committed preosteoblasts (**Chapter 4**). On the contrary, FST had no effect in MSC osteogenic differentiation but further enhanced committed osteoblast differentiation and mineralization. FST was, therefore, the most promising of the

proteins investigated in this thesis in terms of enhancement of bone-related processes and we have further studied its effect in bone regeneration using rat calvarial defect model (**Chapter 5**). Nonetheless, when FST was loaded within an *in situ* gelling slow-release alginate formulation previously tested for BMP-2 bone formation (**Chapter 2** and **Chapter 3**), bone repair was not improved, though a more homogeneous mineralization was observed, which highlights the need of tailoring the release kinetics of the protein to assure its efficacy *in vivo*.

After the successes and pitfalls of BMPs usage it has been also demonstrated that there is no Philosopher's Stone for bone repair and that the combination of factors could be what mimics better the natural cascade of events needed for bone formation. In fact, the lack of functional vascular supply in tissue engineered construct is currently a major hurdle in bone TE (324, 337) and several approaches have been undertaken to coordinate the sequential cascade of events needed for bone formation. One of them is the delivery of more than one factor in the bone defect. This is usually performed by using dual delivery systems which are often based on the delivery of BMP-2 and another factor with significant chemotactic and/or angiogenic effect such as VEGF or SDF-1, among others (90, 265, 338, 339). In this line, Nell-1, CCN2, HMGB1 and FST have proved to enhance bone-related processes and might be of special interest when considering reducing the side effects observed in single-factor therapies.

### 6.1.2 *In situ* gelling hydrogels are the smart future, but are we there yet?

A growing number of hydrogels are being developed worldwide to repair bone defects. This is due to their minimally invasive administration procedures and their ability to fill irregular areas (340). Stimuli-sensitive hydrogels, which undergo gelation *in situ* in response to external stimuli such as temperature, pH, electrolytes, visible light (VL) or magnetic field are gaining interest because of their injectability and improved mechanical properties (341-344).

In this thesis, recombinant collagen peptide microspheres (RCP-MS) enriched with RGD sequences were loaded with BMP-2 and embedded in three different injectable hydrogels. Two different types of *in situ* gelling formulations were used, i.e. thixotropic alginate formulations, and a thermoresponsive hyaluronan derivative (HApN) hydrogel. All of the used formulations presented a reversible behavior, making the handling of the hydrogels much easier since they can be prepared and stored prior to usage. Thus, the gelation time of the formulations is quick enough (< 5 minutes) to keep the formed gel in place after injection and for the length of the carried studies. HApN hydrogel did not sustain ectopic bone formation; however, hyaluronan-based constructs were highly vascularized at the end of the study (**Chapter 2**). ECs have been successfully cultured on hyaluronic acid coated polymers and sprouting angiogenesis has been spatially guided in collagen gels modified with hyaluronic acid (345, 346). Thus, hyaluronic acid-based

hydrogels have been used previously as pre-vascularized scaffolds in regenerative medicine (347). Gellan gum-HA spongy-like hydrogels have induced neovascularization in a rat ischemic model (348) and *in situ* gelling HA-based hydrogel enhanced postmyocardial infarction vascularization. However, the gelation time of the hydrogel was 15 min approximately (168), what may exceed the optimal time to treat some specific areas such as the craniofacial complex in which bone defects might not be well-confined and leakage of the ungelled liquid in the surrounding tissue should be avoid. The formation of a functional vasculature is one of the limiting factors for the success of tissue-engineered constructs. The use of this *in situ* gelling thermoresponsive hyaluronan-based system with embedded rich RGD collagen microspheres presented in this thesis might be interesting for restoring soft tissues milieu with in-growing vasculature.

Alginate *in situ* gelling formulation successfully induced bone formation ectopically and in a calvarial bone defect model (**Chapters 2 and 3**). A major drawback of hydrogels usage is their lack of mechanical robustness –hydrogels elastic moduli ranges from ~ kPa to MPa, whereas the moduli of native bone ranges between 7-30 GPa for cortical bone and 0.05-5 GPa for cancellous bone (349)–. The mechanical properties of the thixotropic alginate hydrogels presented in this thesis are also in the kPa range and therefore are not able to withstand the mechanical loading of load-bearing bones defects (350). However, there are many situations in which their use is beneficial, especially acting as bone fillers in areas where the use of pre-fabricated materials would be inappropriate or treating non-load bearing bones, such as skull, forehead, orbital cavity, and zygoma among others. The use of *in situ* gelling hydrogels is also an interesting approach for bone augmentation in cases such as periodontitis, a common oral disease and one of the major causes of bone loss in orthodontics (351).

To improve their mechanical competence, hydrogels are being complexed with ceramic-based materials such as hydroxyapatite or calcium phosphates to enhance their mechanical properties and osteoconductivity while preserving their elasticity. A recent study conducted by Thorpe et al. (352) investigated the use of a thermally triggered injectable hydrogel loaded with hydroxyapatite nanoparticles, showing that the use of the formulation alone was enough to provide adequate mechanical support for continued animal activity following a femur defect. However, when translating it to large critically sized bone defects it is likely to be mechanically insufficient, mostly in early repair stages (352). Besides, different kinds of resorbable and non-resorbable injectable materials have been tested in load-bearing sites such as *in situ* hardening calcium phosphate-based cements or Cortoss®, a commercialized resin-based synthetic material (353, 354). Nonetheless, calcium phosphate-based cements usually lack 3D-porous structures, lose mechanical properties upon degradation and their brittle nature often make them suboptimal for load-bearing applications (355, 356). Cortoss®, for example, loses strength with time and lack of vascular invasion (357-359). In sum, there is an increasing interest for

developing hybrid scaffolds that combine the strength of the ceramic-based materials, and the biocompatibility and biodegradability of hydrogels. This opens the door to new directions for future studies, moving the field closer to develop functional load-bearing injectable materials.

### 6.1.3 Do we need slow delivery of bone growth factors in bone repair?

The fact that supraphysiological dosages of growth factors are needed to produce a significant healing effect in bone repair is one of the major challenges that need to be overcome in the growth factor-based therapies field to translate preclinical studies into clinical trials. It is generally accepted that one of the main causes is the insufficient spatiotemporal control of the currently used delivery systems, which could be solved with the application of controlled-release systems. In fact, several studies using BMP-2 soaked in a collagen sponge –same two components as the ones used in the commercially available INFUSE® Bone Graft Kit– demonstrated that 50 to 80% of the protein was released within the first days *in vivo* (89, 103). In this thesis, HMDIC crosslinked RCP-MS with a diameter range of 50-75  $\mu\text{m}$  were selected as BMP-2 carriers since only 15% of the protein was released during the first day and 30% during the first two weeks (58). The release of BMP-2 was further reduced more than 2-fold when loaded in high guluronate (SLG) alginate and more than 5-fold when loaded in both thermoresponsive hyaluronic acid and high mannuronate (SLM) alginate formulations. Alginate SLG formulation was, as shown in **Chapter 2**, the most optimal promoting ectopic bone formation when loaded with BMP-2. Threshold dose and BMP2's release kinetics from the alginate SLG formulation was further studied in an ectopic bone model in **Chapter 3**. Alginate SLG formulation presented absence of burst release and a prolonged retention of BMP-2. Protein signal was detected up to 4 weeks and the slow release of the protein resulted in a significant amount of bone volume at the end of the study. This carrier formulation loaded with BMP-2 led to a dose- and time-dependent ectopic bone formation. Previously, the role of BMP-2 in ectopic bone formation was reported using different biomaterials such as silk fibroin (184), collagen sponge (183) and biphasic calcium phosphate hydrogel systems (110); however, lower ectopic bone volumes were obtained in these studies, although larger doses of BMP-2 were used. BMP-2 binds to RCP with high affinity (58), and therefore, the use of alginate hydrogel with embedded RCP-MS brings a significant reduction in the necessary dose of BMP-2 to significantly promote ectopic bone formation compared to earlier studies.

Alginate-based biomaterials have been used for a wide range of regenerative medicine applications (360), and in our study the suitability of the SLG formulation for growth factor-based therapies and bone repair was further tested by implanting it in a rat calvarial defect either alone or loaded with BMP-2 (**Chapter 3**). Although the formulation alone and the empty control exhibited similar amount of bone volume at the endpoint, the formulation

seemed to impede bone healing at the early time points when compared to the empty defects (**Chapter 3**). The inflammatory phase is a critical period in fracture healing. During this phase, different types of cells are recruited and a vast array of inflammatory cytokines are released to initiate repair responses following injury (361). The alginate could have acted as a physical barrier; delaying the healing process until BMP-2 started to be released and RGD enriched RCP-MS were reachable for cell-adhesion and further cell infiltration. Nonetheless, BMP-2 loaded formulation could overcome this impediment and exhibited the same amount of bone volume as the healthy animals just two weeks after implantation, which translated into full defect healing at the end of the experiment.

It is extremely difficult to establish a correlation from animals to humans due to different bone healing mechanisms. As previously discussed, in our ectopic bone model study, bone formation was achieved using one hundred times less protein amount than the lowest BMP-2 concentration used with INFUSE® Bone Graft Kit (362). However, when used in a calvarial defect model, the effective dose was roughly twenty times less than the currently dose used with INFUSE® Bone Graft Kit. Recently, Moser et al. reported an experiment in which different dosages of BMP-2 were loaded in both slow and rapid release systems ectopically and within bone defects. They concluded that slow delivery of BMP-2 was effective in sites with non-osteogenic activity (130). In another study, long and short term delivery of BMP-2 were compared, demonstrating that releasing the protein over 4 weeks resulted in significantly higher ectopic bone formation than releasing it within the first 3 days (363). Our results are in accordance with these findings. Bone-forming cells are not present in the subcutaneous environment. Since alginate SLG formulation combined with low BMP-2 dose resulted in a sustained protein release, it matched the release timing needed for ectopic bone formation. However, when used in an orthotopic defect in which osteogenic activity is found, the need not only of sustained release but also of a burst release might be accentuated and essential to further reduce the effective protein dosage. In that scenario, the use of a combination of strategies to allow different protein release kinetics is desirable. This could be achieved, for instance, by covalently conjugating growth factors to hydrogels. Recently, linking TGF- $\beta$  to an injectable chitosan-based hydrogel resulted in stable protein release even when tested in cells and serum-containing environment (364). Using a combination between physical adsorption-based and conjugation-based delivery techniques to ensure both burst release and continuous treatment is intriguing, and might help to overcome some of the challenges that growth-factor based therapies face.

FST is known to be an essential regulatory protein in bone metabolism and showed promising results promoting bone-related processes in our *in vitro* studies. Therefore, in parallel to the previous study, FST potency for bone defect repair was assessed in a rat calvarial bone defect model and SLG formulation was also used as protein carrier (**Chapter 5**). In a previous study Funaba et al. implanted DBM subcutaneously in rats to investigate



FST involvement in osteochondral ossification (320). Their results showed that FST was highly expressed by osteoblasts in their proliferating state, whereas it was not longer expressed in non-proliferating cells. The administration of FST at days 9 and 10 postimplantation decreased calcium content suggesting that FST plays a role in bone modeling in a stage-specific manner. So far, FST has never been used as a growth factor-based bone TE strategy. Our data indicated that bone repair was not improved in 10 weeks' time when FST was loaded in the alginate SLG formulation. In our study, we have used a slow delivery system to release FST over time. However, FST may be an early player in bone formation, having a role in the vasculature formation and indirectly triggering ECM mineralization. It could even be that FST burst release is necessary to trigger bone formation and that its continuous release might inhibit the following events needed for bone modeling. If that was the case, the use of an alginate-based slow-release system might be an unsuitable carrier to evaluate FST performance since it would not fit with the pharmacokinetics of the protein.

The ideal pharmacokinetics for growth factor delivery in bone repair is often based on what has been generally accepted as the optimal BMP-2 pharmacokinetics, which includes both burst and sustained release. Nonetheless, the release profile of the protein should not be only determined by the rate of degradation, crosslinking extent or porous size of the carrier, but also by the impact of the target site on the local release kinetics and the role(s) that the protein plays in various processes involved in bone repair. Different factors need different release kinetics. Therefore, as it has been previously suggested (91, 365), individualizing growth factor release kinetics that respond specifically to a particular situation may help to overcome the limitations that growth factor therapies face when improving skeletal repair.

#### 6.1.4 The art of making bones. Do we use the proper preclinical tools?

Many tissue-engineered products fail to make it to the clinics due to the inconsistencies observed between the *in vitro* and the *in vivo* preclinical studies. To reduce and eventually replace animal testing, a vast amount of effort is being put into the development of sophisticated *in vitro* models capable of mimicking the complexity of the cellular processes that take part in bone turnover (366-369). So far, *in vitro* studies are not able to recreate the *in vivo* milieu, but they are very useful to assess in a more direct, simple and detailed way the effect of specific agents while controlling most of the parameters when compared to *in vivo* studies. Therefore, by using *in vitro* studies we were able to investigate the intrinsic response of different cell types to several doses of Nell-1, CCN2, HMGB1, and FST. To assess the effect of those factors upon different biological processes, primary cells and an osteoblastic cell line were used (Chapter 4 and Chapter 5). SV-HFO is a well-characterized preosteoblast cell line in which human fetal osteoblasts are immortalized by simian virus 40 (SV40) (239). The SV-HFO cell line is considered a suitable model for

studying the stimulating effect of bone-forming factors and the metabolism of human bone cells (370-373); however, SV40-induced immortalization is usually accompanied by karyotypic instability (374) and that is also the case in SV-HFO cells (239). Cell lines offer an unlimited supply, are more reproducible and are usually less complicated to culture, but the obtained data might be less reflective of the *in vivo* environment than the data obtained when using primary cells. However, since cell lines are genetically manipulated, their genotype and phenotype is likely to suffer alterations over time, which might have an impact on their primary functions or response to exogenous stimulation (375). To make their use more reliable, some strategies are being developed to expand the utility of cell lines such as the establishment of immortalized cell lines with chromosomal consistency (376). In our study, FST addition significantly increased the differentiation and mineralization of a calvarial-derived osteoblastic cell line. However, it did not improve calvarial bone repair *in vivo*. This can be due to several causes, such as intrinsic differences between the effect of FST on an osteogenic-committed cell line in a 2D culture and its effect in the *in vivo* situation, where numerous processes and cell types are simultaneously involved.

*In vivo* animal studies provide a closer approximation to the clinical scenario and are generally used to further investigate bone TE strategies once their biological activity and toxicity among other parameters have been screened *in vitro* (377). Therefore, *in vivo* studies are considered in many cases the clinical trials' anteroom. In this thesis, the bone-forming capacity of three *in situ* gelling formulations loaded with BMP-2 was firstly assessed subcutaneously in rats due to its technical simplicity, relatively low estimated animal discomfort and reduction of the number of treated specimens (**Chapter 2**). The selected formulation was subsequently investigated in a rat calvarial defect. It is an standardized non-load bearing orthotopic defect to evaluate bone regeneration, and it is especially adequate when studying the use of tissue-engineered constructs to repair craniofacial bone defects (378). Calvarial defect models do not need external fixation and are relatively easy to standardize and evaluate. They have been also widely used to investigate an extensive range of BMP2-based products (264, 379-383). Nonetheless, it is important to mention that calvarial bones are formed via intramembranous ossification and therefore, this model could be less accurate when investigating strategies for endochondral bone regeneration (308). It has been postulated that "A human is not just 80 kilograms of rat" (384). Indeed, their skeleton present a more primitive bone structure, with open growth plates, limited trabecular content and a lack of cortical bone Haversian canals (385). Therefore, preclinical testing is also frequently performed in large skeletally mature animals such as horses, dogs, goats or sheep, and less often on non-human primates, who are considered the most suitable model for human bone (386). Certainly, the use of large animals –especially non-human primates– arise cultural and ethical questions as well as exponentially increases research costs. Nonetheless, larger does not mean closer to human scenario. For instance, rhesus monkeys were used to predict the

optimal concentration of BMP-2 to treat spine fusion in humans, however, proportionally lower doses are needed in rhesus monkeys than in humans, indicating that rhesus monkeys could be more responsive to BMP-2 administration than humans (387). This highlights the fact that there is not an ideal animal model and that both the choice of bone defects and animal species should rely on a compelling rationale. In this thesis, the use of a rat calvarial defect model allowed us to evaluate not only the biocompatibility of the selected formulation but its capability to trigger bone repair w/o BMP-2. Its closest clinical translation would be addressed to the treatment of flat bones. Per contra, to assess its performance in long bones and/or load-bearing locations, other bone defect models would be selected such as femoral bone defects.

## 6.2 Conclusions and future perspectives

In conclusion, we have tested an *in situ* gelling cell-free product to be used as BMP-2 slow-release system for bone TE applications. This injectable material resulted in time- and dose-dependent bone formation both ectopically and orthotopically. Using this RCP-MS alginate-based controlled-release system for the induction of new bone formation may provide the beneficial properties of both a protein carrier and a support scaffold when applied as a void-filler. It would also be interesting to further study the performance of this newly developed biomaterial in load-bearing locations like the femur, the tibia or the mandible. There, to ensure mechanical stability, it would be combined with fixation techniques, such as fusion cages, plates and screws or used in composite devices in combination with stiffer materials such as calcium phosphates, fiber meshes or 3D printed polymers (388-392). It has been shown that mechanical strain has an effect on BMP signalling and, consequently, on endogenous BMP production and osteoblast differentiation (393, 394). Besides, in a non-human primate study in which BMP-2-loaded collagen was used to treat spinal arthrodesis, tissue compression squeezed the protein out of the sponge preventing bone induction (395). Thus, both BMP-2 production and release may vary under mechanical strain and should be taken in consideration when investigating the effect of this *in situ* gelling system upon load-bearing bones regeneration. Consequently, to more closely mimic the clinical scenario, it would be interesting to investigate the effect of this *in situ* gelling system on a large defect, which are difficult to treat and are often found after trauma or tumors surgical treatments in the clinics. Therefore, the next step could be testing the system in segmental bone defects with and without fixation (for example, to treat long-bone tibia segmental defects or segmental bone defects in the maxilla). To do so, it would be plausible to use an animal specie more similar to humans in terms of bone physiology, such as dogs, sheep or goats.

Recruitment and differentiation of progenitor cells that form skeletal and vascular tissues are crucial processes during bone healing (26, 332, 396). We have studied the ability of four different proteins to enhance bone-formation related processes and we have

demonstrated that Nell-1, HMGB1, CCN2, and FST are able to attract both osteoprogenitor cells and ECs. In addition, all of the proteins tested were able to stimulate vascularization *in vitro*. It should be noted that the proteins tested were able to induce and/or enhance some of the key events that take place in bone formation when 2D cell cultures were used. To be able to translate these results to a setting closer to clinical translation and improve our understanding upon whether these proteins would promote similar responses *in vivo* and why, some considerations should be taken. 3D cultures are closer to the *in vivo* situation since they offer the possibility to set up more complex biological settings and could be used to study, for instance, the interaction of different types of cells, such as activated-macrophages, endothelial cells and osteoprogenitor cells under protein-stimulation. Besides, the actions of Nell-1, HMGB1, CCN2, FST and BMP-2 span so many processes that mechanistic studies are needed to clarify the biological activity of this proteins within bone healing context. In that way, carriers can be tailored-made to improve their release timing and overall, to optimize their use for bone TE applications.

# 7

Summary



Bone defects are generally treated with bone grafts, which are used as a filler and scaffold to facilitate wound healing and promote bone formation. The current gold standard is the use of autologous bone grafts, however, there are many disadvantages associated with their usage such as limited supply and the generation of an additional surgical site, resulting in added operative time and donor-site morbidity (36). Moreover, the limited moulding properties of autologous bone grafts make their use difficult in morphologically complex structures such as the craniofacial skeleton. Injectable biomaterials offer great promise in tissue repair applications, especially for the treatment of irregular bone defects. Currently developed cell-free biomaterials aim to deliver biomolecules such as growth factors (GFs) to a tissue defect in a manner that provides an adequate environment for cell survival, proliferation, and differentiation, triggering the required biological events for full bone repair. GFs are signalling polypeptides indispensable for the maintenance of tissue homeostasis, wound healing and tissue regeneration (397). However, their use in clinical applications is limited due to their short effective half-life and low stability (398). Besides, regulating the spatiotemporal delivery of the proteins of interest is challenging and currently used delivery systems experience insufficient local retention. As a consequence large doses of the protein are needed to produce a biological effect (91). Bone morphogenetic protein-2 (BMP-2) is widely used to treat bone defects due to its powerful osteoinductive nature and has been used in a large number of carriers. However, because of the supraphysiological doses of the protein needed, it is related to many adverse effects in clinics (105). This thesis aimed to identify and evaluate the therapeutic potential of novel injectable slow-release biomaterials in order to reduce the dose of BMP-2 needed for a successful bone repair, and to investigate alternative promising proteins for their osteogenic induction capacity.

Among injectable biomaterials, *in situ* gelling hydrogels provide a 3D architecture, an appropriate microenvironment for the recruitment and differentiation of the cells involved in bone repair (47). Thus, *in situ* gelling hydrogels are easier to keep in place while preventing leakage, what makes their use appealing to repair non-confined bone defects. In **Chapter 2**, the use of three *in situ* gelling release systems for bone induction is reported. In search of an optimal *in situ* gelling slow-release system Collagen-I based Recombinant Peptide Microspheres (RCP-MS) were embedded in three different hydrogels and used as BMP-2 carrier. RCP-MS have previously shown a small burst release succeeded by sustained release of BMP-2 *in vitro* (58), demonstrating their potential as growth factor delivery vehicles. Consequently, 3.3  $\mu\text{g}$  (16.5  $\mu\text{g}/\text{mL}$ ) of BMP-2 were loaded in RCP-MS and dispersed in two types of alginate –high mannuronate (SLM) and high guluronate (SLG)– and one type of thermoresponsive hyaluronic acid. Both types of alginate displayed a shear stress thixotropic behavior and sustained release of BMP-2, while the thermoresponsive hyaluronic formed a gel structure at 32 °C or above and retained most of the BMP-2. Alginate and hyaluronic acid formulations were injected subcutaneously in rats, showing significant differences in the outcome. Vascularization occurred within all the

formulations, but bone formation was only observed in the alginate formulations. Moreover, inflammation decreased over time in both alginate formulations, but increased in the hyaluronic acid. From the alginate formulations, alginate SLG combined with RCP-MS and loaded with low dose BMP-2 displayed the greatest amount of bone formation at the end of the study. Therefore, alginate SLG combined with RCP-MS was selected as the best choice and was used as *in situ* gelling formulation in further studies presented in this thesis.

To reduce the clinically used supraphysiological dose of BMP-2, it is necessary to know the *in vivo* release profile of BMP-2 from the alginate SLG formulation. With this aim, time- and dose-dependent subcutaneous ectopic bone formation using 4 different doses of BMP-2 – 10 µg (50 µg/mL), 3 µg (15 µg/mL), 1 µg (5 µg/mL) and 0.3 µg (1.5 µg/mL)– was assessed in **Chapter 3**. Ectopically, the density of bone formed by 50 µg/mL and 15 µg/mL was similar, although the bone volume formed was time- and dose-dependent. The highest bone volume was observed when the highest dose (10 µg, 50 µg/mL) was used and no bone formation was detected when the lowest dose was used (0.3 µg, 1.5 µg/mL). In addition, the fluorescence signal generated by fluorescently labelled BMP-2 confirmed that the protein was still detectable within the formulation for at least four weeks *in vivo*, matching the time frame of natural bone healing process (20). To test the bone regeneration capacity of BMP-2 in a bone defect when loaded in alginate SLG+RCP-MS, two doses of BMP-2 –200 ng (50 µg/mL) and 20 ng (5 µg/mL)– were investigated in a 5 mm rat calvarial defect model. The 50 µg/mL BMP-2 loaded biomaterial showed full defect healing at the end of the experiment. However, the implantation of 5 µg/mL BMP-2 or the biomaterial alone did not significantly induce more bone formation than the empty control. The results indicate a threshold dose for effective BMP-2 use, which should be higher than 5 µg/mL BMP-2 –ranging between 15-50 µg/mL– to induce bone formation both ectopically and orthotopically when used in combination with alginate SLG+RCP-MS.

Because of the need to eliminate the risks of BMP-2 use *in vivo*, the ability of four putative osteogenic factors –Nell-like molecule type 1 (Nell-1), high mobility group box 1 (HMGB1), connective tissue growth factor (CTGF, also called CCN2) (in **Chapter 4**) and follistatin (FST) (in **Chapter 5**)– to enhance the essential processes needed for bone repair was assessed. Bone regeneration is a complex process that involves a series of well-orchestrated biological events. At the cellular level, migration, proliferation, angiogenesis, osteogenic differentiation and subsequent mineralization are crucial processes to enable bone formation and repair to occur. It is therefore likely that an off-the-shelf product for bone defect repair will not succeed if those key processes are unbalanced or inhibited. Therefore, we evaluated whether Nell-1, CCN2, HMGB1 and FST enhance migration, vascularization and osteogenic differentiation, comparing them to BMP-2. These studies demonstrated that Nell-1, CCN2, HMGB1 and FST significantly induced human mesenchymal stem cell (MSC) migration but BMP-2 did not. All the proteins studied



induced human endothelial cell (EC) migration and vasculogenic differentiation. BMP-2 enhanced MSC osteogenic differentiation but inhibited the production of the calcified matrix upon committed osteoblasts, whereas FST increased differentiation and subsequent mineralization of committed osteoblasts. *In vitro* screening indicated the potential of FST to be used as both pro-vasculogenic and pro-osteogenic factor. Overall, these results have shown that Nell-1, HMGB1, CCN2 and FST promoted bone formation related processes that might accelerate and optimize bone remodeling. Consequently, the study shed some light to the possibility of the use of Nell-1, HMGB1, CCN2 and FST to reduce the possible side effects observed when single factor therapies are applied.

Since FST was the most promising protein investigated in this thesis in terms of enhancement of bone-related processes *in vitro*, in **Chapter 5** two FST variants –FST288 and FST315– were investigated. FST288 and FST315 present major differences in their affinity to cell-surface proteoglycans, which may influence their effect upon *in vivo* bone repair and their release from the formulation. In fact, the *in vitro* release profile of FST288 and FST315 from alginate SLG RCP-MS showed that most of the loaded FST315 was released over 4 weeks, contrary to FST288, which was mostly retained in the formulation. Both FST variants were loaded in the alginate SLG formulation and implanted in a rat calvarial defect. Although a broader and more homogeneous mineralization occurred in the FST-treated samples compared to the biomaterial treated samples, bone repair was not significantly improved in 10 weeks' time. In this study, the RCP-MS alginate-based formulation was used as FST carrier to achieve FST's slow release, but FST might be an early player in bone formation. Besides, when used in bone defect repair, alginate may not only delay the protein release, but also the cell and cytokine infiltration within the defects. In conclusion, the slow/late release alginate-based system may not be optimal for bone repair when loaded with FST and might influence the FST effect upon extracellular matrix (ECM) mineralization due to a suboptimal FST release timing.

In conclusion, we have proven the therapeutic potential of an *in situ* gelling system based on RCP-MS and alginate loaded with a reduced-BMP2 dose for bone repair. The application of this system is suitable for the treatment of non-load bearing bone defects and therefore, its use within the craniofacial complex might be especially interesting. Further studies should be performed to assess its efficacy in the appropriate animal models to investigate its possible translation to the clinics. Besides, we have investigated *in vitro* the effect of Nell-1, HMGB1, CCN2 and FST on some of the key processes needed for bone formation, showing that their use might be promising to further reduce the side effects observed in single-factor therapies. Therefore, *in vivo* analyses using dual release systems should be performed to assess their potency for bone defect repair. For FST, however, we demonstrated that its use does not promote bone repair in an orthotopic defect when loaded in RCP-MS and alginate, which can be due to several causes such as poor bone-forming capacity, underdosage and suboptimal release kinetics among others. To move on

further using growth factor-based therapies, mechanistic approaches should be taken in consideration to investigate how and in which extent the factor of interest regulates key processes in bone repair. Besides, the optimal release kinetics of the factor(s) must be investigated *in vivo* to successfully translate its use into bone tissue engineering based therapies.

# 8

## References



1. Romer AS. *The "ancient history" of bone*. Ann N Y Acad Sci. 1963; 109, 168-176.
2. Bengtson S, Zhao Y. *Predatorial borings in late precambrian mineralized exoskeletons*. Science. 1992; 257, 367-369.
3. Wagner DO, Aspenberg P. *Where did bone come from?* Acta Orthop. 2011; 82, 393-398.
4. Halstead LB. *Calcified tissues in the earliest vertebrates*. Calcif Tissue Res. 1969; 3, 107-124.
5. Omelon S, Georgiou J, Henneman ZJ, et al. *Control of vertebrate skeletal mineralization by polyphosphates*. PLoS One. 2009; 4, e5634.
6. Grabowski P. *Physiology of Bone*. Endocr Dev. 2015; 28, 33-55.
7. Buck DW, Dumanian GA. *Bone biology and physiology: Part I. The fundamentals*. Plast Reconstr Surg. 2012; 129, 1314-1320.
8. Clarke B. *Normal bone anatomy and physiology*. Clin J Am Soc Nephrol. 2008; 3 Suppl 3, S131-139.
9. Barnosky AD, Lowe L. *Mammal anatomy: An illustrated guide*. New York: Marshall Cavendish; 2010.
10. Long F, Ornitz DM. *Development of the endochondral skeleton*. Cold Spring Harb Perspect Biol. 2013; 5, a008334.
11. Percival CJ, Richtsmeier JT. *Angiogenesis and intramembranous osteogenesis*. Dev Dyn. 2013; 242, 909-922.
12. Berendsen AD, Olsen BR. *Bone development*. Bone. 2015; 80, 14-18.
13. Florencio-Silva R, Sasso GR, Sasso-Cerri E, et al. *Biology of Bone Tissue: Structure, Function, and Factors That Influence Bone Cells*. Biomed Res Int. 2015; 2015, 421746.
14. Capulli M, Paone R, Rucci N. *Osteoblast and osteocyte: Games without frontiers*. Arch Biochem Biophys. 2014; 561, 3-12.
15. Rutkovskiy A, Stenslokken KO, Vaage IJ. *Osteoblast Differentiation at a Glance*. Med Sci Monit Basic Res. 2016; 22, 95-106.
16. Miller SC, de Saint-Georges L, Bowman BM, et al. *Bone lining cells: structure and function*. Scanning Microsc. 1989; 3, 953-960; discussion 960-951.
17. Dierkes C, Kreisel M, Schulz A, et al. *Catabolic properties of microdissected human endosteal bone lining cells*. Calcif Tissue Int. 2009; 84, 146-155.
18. Wein MN. *Bone Lining Cells: Normal Physiology and Role in Response to Anabolic Osteoporosis Treatments*. Curr Mol Biol Rep. 2017; 3, 79-84.
19. Buck DW, Dumanian GA. *Bone biology and physiology: Part II. Clinical correlates*. Plast Reconstr Surg. 2012; 129, 950e-956e.
20. Marsell R, Einhorn TA. *The biology of fracture healing*. Injury. 2011; 42, 551-555.
21. Loi F, Cordova LA, Pajarinen J, et al. *Inflammation, fracture and bone repair*. Bone. 2016; 86, 119-130.
22. Giannoudis PV, Hak D, Sanders D, et al. *Inflammation, Bone Healing, and Anti-Inflammatory Drugs: An Update*. J Orthop Trauma. 2015; 29 Suppl 12, S6-9.
23. Saran U, Gemini Piperni S, Chatterjee S. *Role of angiogenesis in bone repair*. Arch Biochem Biophys. 2014.
24. Mountziaris PM, Mikos AG. *Modulation of the inflammatory response for enhanced bone tissue regeneration*. Tissue Eng, Part B. 2008; 14, 179-186.
25. Hadjidakis DJ, Androulakis II. *Bone remodeling*. Ann N Y Acad Sci. 2006; 1092, 385-396.
26. Einhorn TA, Gerstenfeld LC. *Fracture healing: mechanisms and interventions*. Nat Rev Rheumatol. 2015; 11, 45-54.
27. Campana V, Milano G, Pagano E, et al. *Bone substitutes in orthopaedic surgery: from basic science to clinical practice*. J Mater Sci Mater Med. 2014; 25, 2445-2461.
28. Guerado E, Caso E. *Challenges of bone tissue engineering in orthopaedic patients*. World J Orthop. 2017; 8, 87-98.

29. Older J. *Bone Implant Grafting*. London: Springer-Verlag London; 1992.
30. Roberts TT, Rosenbaum AJ. *Bone grafts, bone substitutes and orthobiologics: the bridge between basic science and clinical advancements in fracture healing*. Organogenesis. 2012; 8, 114-124.
31. Elsalanty ME, Genecov DG. *Bone grafts in craniofacial surgery*. Craniomaxillofac Trauma Reconstr. 2009; 2, 125-134.
32. Di Matteo B, Tarabella V, Filardo G, et al. *An orthopaedic conquest: the first inter-human tissue transplantation*. Knee Surg Sports Traumatol Arthrosc. 2014; 22, 2585-2590.
33. Meeder PJ, Eggers C. *The history of autogenous bone grafting*. Injury. 1994; 25 Suppl 1, A2-3.
34. Younger EM, Chapman MW. *Morbidity at bone graft donor sites*. J Orthop Trauma. 1989; 3, 192-195.
35. Ahlmann E, Patzakakis M, Roidis N, et al. *Comparison of anterior and posterior iliac crest bone grafts in terms of harvest-site morbidity and functional outcomes*. J Bone Joint Surg Am. 2002; 84-A, 716-720.
36. Rogers GF, Greene AK. *Autogenous bone graft: basic science and clinical implications*. J Craniofac Surg. 2012; 23, 323-327.
37. Delloye C, Cornu O, Druetz V, et al. *Bone allografts: What they can offer and what they cannot*. J Bone Joint Surg Br. 2007; 89, 574-579.
38. Pryor LS, Gage E, Langevin CJ, et al. *Review of bone substitutes*. Craniomaxillofac Trauma Reconstr. 2009; 2, 151-160.
39. Polo-Corrales L, Latorre-Estevales M, Ramirez-Vick JE. *Scaffold design for bone regeneration*. J Nanosci Nanotechnol. 2014; 14, 15-56.
40. Sutherland D. BM. *Grafts and Bone Graft Substitutes*: Humana Press; 2005.
41. Gruskin E, Doll BA, Futrell FW, et al. *Demineralized bone matrix in bone repair: history and use*. Adv Drug Deliv Rev. 2012; 64, 1063-1077.
42. Huebsch N, Mooney DJ. *Inspiration and application in the evolution of biomaterials*. Nature. 2009; 462, 426-432.
43. Navarro M, Michiardi A, Castano O, et al. *Biomaterials in orthopaedics*. J R Soc Interface. 2008; 5, 1137-1158.
44. Rambhia KJ, Ma PX. *Controlled drug release for tissue engineering*. J Control Release. 2015; 219, 119-128.
45. Bai X, Gao M, Syed S, et al. *Bioactive hydrogels for bone regeneration*. Bioact Mater. 2018; 3, 401-417.
46. Kretlow JD, Klouda L, Mikos AG. *Injectable matrices and scaffolds for drug delivery in tissue engineering*. Adv Drug Deliv Rev. 2007; 59, 263-273.
47. Liu M, Zeng X, Ma C, et al. *Injectable hydrogels for cartilage and bone tissue engineering*. Bone Res. 2017; 5, 17014.
48. D'Este M, Sprecher CM, Milz S, et al. *Evaluation of an injectable thermoresponsive hyaluronan hydrogel in a rabbit osteochondral defect model*. J Biomed Mater Res A. 2016; 104, 1469-1478.
49. Bellini D, Cencetti C, Meraner J, et al. *An in situ gelling system for bone regeneration of osteochondral defects*. Eur Polym J. 2015; 72, 642-650.
50. Rey-Rico A, Silva M, Couceiro J, et al. *Osteogenic Efficiency of in Situ Gelling Poloxamine Systems with and without Bone Morphogenetic Protein-2*. Eur Cells Mater. 2011; 21, 317-340.
51. Levengood SL, Zhang M. *Chitosan-based scaffolds for bone tissue engineering*. J Mater Chem B. 2014; 2, 3161-3184.
52. Moreira CD, Carvalho SM, Mansur HS, et al. *Thermogelling chitosan-collagen-bioactive glass nanoparticle hybrids as potential injectable systems for tissue engineering*. Mater Sci Eng C Mater Biol Appl. 2016; 58, 1207-1216.

53. Kim S, Tsao H, Kang Y, et al. *In vitro evaluation of an injectable chitosan gel for sustained local delivery of BMP-2 for osteoblastic differentiation*. J Biomed Mater Res B Appl Biomater. 2011; 99, 380-390.
54. Huang Z, Tian J, Yu B, et al. *A bone-like nano-hydroxyapatite/collagen loaded injectable scaffold*. Biomed Mater. 2009; 4, 055005.
55. Sargeant TD, Desai AP, Banerjee S, et al. *An in situ forming collagen-PEG hydrogel for tissue regeneration*. Acta Biomater. 2012; 8, 124-132.
56. Nguyen BB, Moriarty RA, Kamalitinov T, et al. *Collagen Hydrogel Scaffold Promotes Mesenchymal Stem Cell and Endothelial Cell Coculture for Bone Tissue Engineering*. J Biomed Mater Res A. 2017.
57. Kuo KC, Lin RZ, Tien HW, et al. *Bioengineering vascularized tissue constructs using an injectable cell-laden enzymatically crosslinked collagen hydrogel derived from dermal extracellular matrix*. Acta Biomater. 2015; 27, 151-166.
58. Mumcuoglu D, de Miguel L, Jekhmane S, et al. *Collagen I derived recombinant protein microspheres as novel delivery vehicles for bone morphogenetic protein-2*. Mater Sci Eng C Mater Biol Appl. 2018; 84, 271-280.
59. Martinez-Sanz E, Ossipov DA, Hilborn J, et al. *Bone reservoir: Injectable hyaluronic acid hydrogel for minimal invasive bone augmentation*. J Control Release. 2011; 152, 232-240.
60. Bhakta G, Lim ZX, Rai B, et al. *The influence of collagen and hyaluronan matrices on the delivery and bioactivity of bone morphogenetic protein-2 and ectopic bone formation*. Acta Biomater. 2013; 9, 9098-9106.
61. Yang HS, La WG, Bhang SH, et al. *Heparin-conjugated fibrin as an injectable system for sustained delivery of bone morphogenetic protein-2*. Tissue Eng, Part A. 2010; 16, 1225-1233.
62. Li Y, Meng H, Liu Y, et al. *Fibrin gel as an injectable biodegradable scaffold and cell carrier for tissue engineering*. Sci World J. 2015; 2015, 685690.
63. Ahmed TA, Dare EV, Hincke M. *Fibrin: a versatile scaffold for tissue engineering applications*. Tissue Eng, Part B. 2008; 14, 199-215.
64. Yan J, Miao Y, Tan H, et al. *Injectable alginate/hydroxyapatite gel scaffold combined with gelatin microspheres for drug delivery and bone tissue engineering*. Mater Sci Eng C Mater Biol Appl. 2016; 63, 274-284.
65. Bhat A, Hoch AJ, Decaris ML, et al. *Alginate hydrogels containing cell-interactive beads for bone formation*. FASEB J. 2013; 27, 4844-4852.
66. Venkatesan J, Bhatnagar I, Manivasagan P, et al. *Alginate composites for bone tissue engineering: a review*. Int J Biol Macromol. 2015; 72, 269-281.
67. He X, Dziak R, Mao K, et al. *Integration of a novel injectable nano calcium sulfate/alginate scaffold and BMP2 gene-modified mesenchymal stem cells for bone regeneration*. Tissue Eng, Part A. 2013; 19, 508-518.
68. Liang Y, Kiick KL. *Heparin-functionalized polymeric biomaterials in tissue engineering and drug delivery applications*. Acta Biomater. 2014; 10, 1588-1600.
69. Lee J, Choi WI, Tae G, et al. *Enhanced regeneration of the ligament-bone interface using a poly(L-lactide-co-epsilon-caprolactone) scaffold with local delivery of cells/BMP-2 using a heparin-based hydrogel*. Acta Biomater. 2011; 7, 244-257.
70. Fathi A, Mithieux SM, Wei H, et al. *Elastin based cell-laden injectable hydrogels with tunable gelation, mechanical and biodegradation properties*. Biomaterials. 2014; 35, 5425-5435.
71. Ozsvar J, Mithieux SM, Wang R, et al. *Elastin-based biomaterials and mesenchymal stem cells*. Biomater Sci. 2015; 3, 800-809.
72. Annabi N, Mithieux SM, Weiss AS, et al. *Cross-linked open-pore elastic hydrogels based on tropoelastin, elastin and high pressure CO<sub>2</sub>*. Biomaterials. 2010; 31, 1655-1665.

73. Calori GM, Mazza E, Colombo M, et al. *The use of bone-graft substitutes in large bone defects: any specific needs?* Injury. 2011; 42 Suppl 2, S56-63.
74. Langer R, Vacanti JP. *Tissue engineering*. Science. 1993; 260, 920-926.
75. Fisher JN, Peretti GM, Scotti C. *Stem Cells for Bone Regeneration: From Cell-Based Therapies to Decellularised Engineered Extracellular Matrices*. Stem Cells Int. 2016; 2016, 9352598.
76. Tasso R, Ulivi V, Reverberi D, et al. *In vivo implanted bone marrow-derived mesenchymal stem cells trigger a cascade of cellular events leading to the formation of an ectopic bone regenerative niche*. Stem Cells Dev. 2013; 22, 3178-3191.
77. Devescovi V, Leonardi E, Ciapetti G, et al. *Growth factors in bone repair*. Chir Organi Mov. 2008; 92, 161-168.
78. Urist MR. *Bone: formation by autoinduction*. Science. 1965; 150, 893-899.
79. Muthukumaran N, Ma S, Reddi AH. *Dose-dependence of and threshold for optimal bone induction by collagenous bone matrix and osteogenin-enriched fraction*. Coll Relat Res. 1988; 8, 433-441.
80. Wozney JM, Rosen V, Celeste AJ, et al. *Novel regulators of bone formation: molecular clones and activities*. Science. 1988; 242, 1528-1534.
81. Chen D, Zhao M, Mundy GR. *Bone morphogenetic proteins*. Growth Factors. 2004; 22, 233-241.
82. Burkus JK, Gornet MF, Dickman CA, et al. *Anterior lumbar interbody fusion using rhBMP-2 with tapered interbody cages*. J Spinal Disord Tech. 2002; 15, 337-349.
83. Epstein NE. *Pros, cons, and costs of INFUSE in spinal surgery*. Surg Neurol Int. 2011; 2, 10.
84. Long D, Watts C. *Off-label use of drugs and devices: role of medical professionals in the establishment of parameters for their use*. Neurosurgery. 2013; 72, 1014-1020; discussion 1120.
85. Poeran J, Opperer M, Rasul R, et al. *Change in Off-Label Use of Bone Morphogenetic Protein in Spine Surgery and Associations with Adverse Outcome*. Global Spine J. 2016; 6, 650-659.
86. Hustedt JW, Blizzard DJ. *The controversy surrounding bone morphogenetic proteins in the spine: a review of current research*. Yale J Biol Med. 2014; 87, 549-561.
87. Zara JN, Siu RK, Zhang X, et al. *High doses of bone morphogenetic protein 2 induce structurally abnormal bone and inflammation in vivo*. Tissue Eng, Part A. 2011; 17, 1389-1399.
88. James AW, LaChaud G, Shen J, et al. *A Review of the Clinical Side Effects of Bone Morphogenetic Protein-2*. Tissue Eng, Part B. 2016; 22, 284-297.
89. Geiger M, Li RH, Friess W. *Collagen sponges for bone regeneration with rhBMP-2*. Adv Drug Deliv Rev. 2003; 55, 1613-1629.
90. Kim YH, Tabata Y. *Dual-controlled release system of drugs for bone regeneration*. Adv Drug Deliv Rev. 2015.
91. Vo TN, Kasper FK, Mikos AG. *Strategies for controlled delivery of growth factors and cells for bone regeneration*. Adv Drug Deliv Rev. 2012; 64, 1292-1309.
92. Luvizuto ER, Tangl S, Dobsak T, et al. *Effect of recombinant PDGF-BB on bone formation in the presence of beta-tricalcium phosphate and bovine bone mineral matrix: a pilot study in rat calvarial defects*. BMC Oral Health. 2016; 16, 52.
93. Kaigler D, Wang Z, Horger K, et al. *VEGF scaffolds enhance angiogenesis and bone regeneration in irradiated osseous defects*. J Bone Miner Res. 2006; 21, 735-744.
94. Kempen DH, Lu L, Heijink A, et al. *Effect of local sequential VEGF and BMP-2 delivery on ectopic and orthotopic bone regeneration*. Biomaterials. 2009; 30, 2816-2825.



95. Bayer EA, Gottardi R, Fedorchak MV, et al. *The scope and sequence of growth factor delivery for vascularized bone tissue regeneration*. J Control Release. 2015; 219, 129-140.
96. Ogilvie CM, Lu C, Marcucio R, et al. *Vascular endothelial growth factor improves bone repair in a murine nonunion model*. Iowa Orthop J. 2012; 32, 90-94.
97. Farokhi M, Mottaghtalab F, Shokrgozar MA, et al. *Importance of dual delivery systems for bone tissue engineering*. J Control Release. 2016; 225, 152-169.
98. Van Vlierberghe S, Dubruel P, Schacht E. *Biopolymer-based hydrogels as scaffolds for tissue engineering applications: a review*. Biomacromolecules. 2011; 12, 1387-1408.
99. Kretlow JD, Young S, Klouda L, et al. *Injectable biomaterials for regenerating complex craniofacial tissues*. Adv Mater. 2009; 21, 3368-3393.
100. Amini AA, Nair LS. *Injectable hydrogels for bone and cartilage repair*. Biomed Mater. 2012; 7, 024105.
101. McKay WF, Peckham SM, Badura JM. *A comprehensive clinical review of recombinant human bone morphogenetic protein-2 (INFUSE Bone Graft)*. Int Orthop. 2007; 31, 729-734.
102. Valentin-Opran A, Wozney J, Csimma C, et al. *Clinical evaluation of recombinant human bone morphogenetic protein-2*. Clin Orthop Relat Res. 2002, 110-120.
103. Li RH, Wozney JM. *Delivering on the promise of bone morphogenetic proteins*. Trends Biotechnol. 2001; 19, 255-265.
104. Poon B, Kha T, Tran S, et al. *Bone morphogenetic protein-2 and bone therapy: successes and pitfalls*. J Pharm Pharmacol. 2016; 68, 139-147.
105. Agrawal V, Sinha M. *A review on carrier systems for bone morphogenetic protein-2*. J Biomed Mater Res B Appl Biomater. 2016.
106. Parvizi M, Plantinga JA, van Speuwel-Goossens CA, et al. *Development of recombinant collagen-peptide-based vehicles for delivery of adipose-derived stromal cells*. J Biomed Mater Res A. 2016; 104, 503-516.
107. Ramirez-Rodriguez GB, Montesi M, Panseri S, et al. (\*) *Biomimetic Recombinant Collagen-Based Scaffold Mimicking Native Bone Enhances Mesenchymal Stem Cell Interaction and Differentiation*. Tissue Eng Part A. 2017; 23, 1423-1435.
108. Bjornoy SH, Mandaric S, Bassett DC, et al. *Gelling kinetics and in situ mineralization of alginate hydrogels: A correlative spatiotemporal characterization toolbox*. Acta Biomater. 2016; 44, 243-253.
109. Zhang J, Wang Q, Wang A. *In situ generation of sodium alginate/hydroxyapatite nanocomposite beads as drug-controlled release matrices*. Acta Biomater. 2010; 6, 445-454.
110. Poldervaart MT, Wang H, van der Stok J, et al. *Sustained release of BMP-2 in bioprinted alginate for osteogenicity in mice and rats*. PLoS One. 2013; 8, e72610.
111. Sun J, Tan H. *Alginate-based biomaterials for regenerative medicine applications*. Materials. 2013; 6, 1285-1309.
112. Tam SK, Dusseault J, Bilodeau S, et al. *Factors influencing alginate gel biocompatibility*. J Biomed Mater Res A. 2011; 98, 40-52.
113. Zhao N, Wang X, Qin L, et al. *Effect of hyaluronic acid in bone formation and its applications in dentistry*. J Biomed Mater Res A. 2016; 104, 1560-1569.
114. Maus U, Andereya S, Gravius S, et al. *Lack of effect on bone healing of injectable BMP-2 augmented hyaluronic acid*. Arch Orthop Trauma Surg. 2008; 128, 1461-1466.
115. Kisiel M, Martino MM, Ventura M, et al. *Improving the osteogenic potential of BMP-2 with hyaluronic acid hydrogel modified with integrin-specific fibronectin fragment*. Biomaterials. 2013; 34, 704-712.

116. Bhakta G, Rai B, Lim ZX, et al. *Hyaluronic acid-based hydrogels functionalized with heparin that support controlled release of bioactive BMP-2*. Biomaterials. 2012; 33, 6113-6122.
117. Kim J, Kim IS, Cho TH, et al. *Bone regeneration using hyaluronic acid-based hydrogel with bone morphogenic protein-2 and human mesenchymal stem cells*. Biomaterials. 2007; 28, 1830-1837.
118. De Boer AL, Van Urk H, Bouwstra JB, et al. *RGD containing recombinant gelatin*. Google Patents; 2012.
119. Kirsch T, Nickel J, Sebald W. *Isolation of recombinant BMP receptor 1A ectodomain and its 2:1 complex with BMP-2*. FEBS Lett. 2000; 468, 215-219.
120. D'Este M, Alini M, Eglin D. *Single step synthesis and characterization of thermoresponsive hyaluronan hydrogels*. Carbohydr Polym. 2012; 90, 1378-1385.
121. Cardoso DA, van den Beucken JJ, Both LL, et al. *Gelation and biocompatibility of injectable alginate-calcium phosphate gels for bone regeneration*. J Biomed Mater Res A. 2014; 102, 808-817.
122. Kuo CK, Ma PX. *Ionically crosslinked alginate hydrogels as scaffolds for tissue engineering: part 1. Structure, gelation rate and mechanical properties*. Biomaterials. 2001; 22, 511-521.
123. Schmitt A, Rodel P, Anamur C, et al. *Calcium alginate gels as stem cell matrix-making paracrine stem cell activity available for enhanced healing after surgery*. PLoS One. 2015; 10, e0118937.
124. Hulsart-Billstrom G, Hu Q, Bergman K, et al. *Calcium phosphates compounds in conjunction with hydrogel as carrier for BMP-2: a study on ectopic bone formation in rats*. Acta Biomater. 2011; 7, 3042-3049.
125. Luca L, Rougemont AL, Walpoth BH, et al. *The effects of carrier nature and pH on rhBMP-2-induced ectopic bone formation*. J Control Release. 2010; 147, 38-44.
126. Kisiel M, Ventura M, Oommen OP, et al. *Critical assessment of rhBMP-2 mediated bone induction: an in vitro and in vivo evaluation*. J Control Release. 2012; 162, 646-653.
127. Utomo L, Pleumeekers MM, Nimeskern L, et al. *Preparation and characterization of a decellularized cartilage scaffold for ear cartilage reconstruction*. Biomed Mater. 2015; 10, 015010.
128. Van Tomme SR, Storm G, Hennink WE. *In situ gelling hydrogels for pharmaceutical and biomedical applications*. Int J Pharm. 2008; 355, 1-18.
129. Hori Y, Winans AM, Irvine DJ. *Modular injectable matrices based on alginate solution/microsphere mixtures that gel in situ and co-deliver immunomodulatory factors*. Acta Biomater. 2009; 5, 969-982.
130. Moser N, Lohse N, Golstein J, et al. *Do we need retarded delivery of bone growth factors in facial bone repair? An experimental study in rats*. Eur Cell Mater. 2017; 34, 162-179.
131. Fahmy-Garcia S, van Driel M, Witte-Buoma J, et al. *Nell-1, HMGB1 and CCN2 enhance migration and vasculogenesis, but not osteogenic differentiation compared to BMP2*. Tissue Eng. Part A. 2018; 24, 207-218.
132. Chen FM, Zhao YM, Sun HH, et al. *Novel glycidyl methacrylated dextran (Dex-GMA)/gelatin hydrogel scaffolds containing microspheres loaded with bone morphogenetic proteins: formulation and characteristics*. J Control Release. 2007; 118, 65-77.
133. Kempen DH, Lu L, Hefferan TE, et al. *Retention of in vitro and in vivo BMP-2 bioactivities in sustained delivery vehicles for bone tissue engineering*. Biomaterials. 2008; 29, 3245-3252.
134. Lee J, Lee KY. *Injectable microsphere/hydrogel combination systems for localized protein delivery*. Macromol Biosci. 2009; 9, 671-676.

135. Bord S, Horner A, Hembry RM, et al. *Production of collagenase by human osteoblasts and osteoclasts in vivo*. Bone. 1996; 19, 35-40.
136. Partridge NC, Walling HW, Bloch SR, et al. *The regulation and regulatory role of collagenase in bone*. Crit Rev Eukaryot Gene Expr. 1996; 6, 15-27.
137. Chiusaroli R, Maier A, Knight MC, et al. *Collagenase cleavage of type I collagen is essential for both basal and parathyroid hormone (PTH)/PTH-related peptide receptor-induced osteoclast activation and has differential effects on discrete bone compartments*. Endocrinology. 2003; 144, 4106-4116.
138. Lee JH, Kim J, Baek HR, et al. *Fabrication of an rhBMP-2 loaded porous beta-TCP microsphere-hyaluronic acid-based powder gel composite and evaluation of implant osseointegration*. J Mater Sci Mater Med. 2014; 25, 2141-2151.
139. Cox TR, Erler JT. *Remodeling and homeostasis of the extracellular matrix: implications for fibrotic diseases and cancer*. Dis Model Mech. 2011; 4, 165-178.
140. West ER, Xu M, Woodruff TK, et al. *Physical properties of alginate hydrogels and their effects on in vitro follicle development*. Biomaterials. 2007; 28, 4439-4448.
141. Banerjee A, Arha M, Choudhary S, et al. *The influence of hydrogel modulus on the proliferation and differentiation of encapsulated neural stem cells*. Biomaterials. 2009; 30, 4695-4699.
142. Barbucci R, Lamponi S, Borzacchiello A, et al. *Hyaluronic acid hydrogel in the treatment of osteoarthritis*. Biomaterials. 2002; 23, 4503-4513.
143. Leong PL, Morgan EF. *Measurement of fracture callus material properties via nanoindentation*. Acta Biomater. 2008; 4, 1569-1575.
144. Donnelly H, Smith CA, Sweeten PE, et al. *Bone and cartilage differentiation of a single stem cell population driven by material interface*. J Tissue Eng. 2017; 8, 2041731417705615.
145. Kaneko K, Higuchi C, Kunugiza Y, et al. *Hyaluronan inhibits BMP-induced osteoblast differentiation*. FEBS Lett. 2015; 589, 447-454.
146. Mountziaris PM, Spicer PP, Kasper FK, et al. *Harnessing and modulating inflammation in strategies for bone regeneration*. Tissue Eng, Part B. 2011; 17, 393-402.
147. Subramanian S, Mitchell A, Yu WL, et al. *Salicylic Acid-Based Polymers for Guided Bone Regeneration Using Bone Morphogenetic Protein-2*. Tissue Eng, Part A. 2015; 21, 2013-2024.
148. Yuasa M, Yamada T, Taniyama T, et al. *Dexamethasone enhances osteogenic differentiation of bone marrow- and muscle-derived stromal cells and augments ectopic bone formation induced by bone morphogenetic protein-2*. PLoS One. 2015; 10, e0116462.
149. Maciel J, Oliveira MI, Colton E, et al. *Adsorbed fibrinogen enhances production of bone- and angiogenic-related factors by monocytes/macrophages*. Tissue Eng, Part A. 2014; 20, 250-263.
150. Grotenhuis N, De Witte SF, van Osch GJ, et al. *Biomaterials Influence Macrophage-Mesenchymal Stem Cell Interaction In Vitro*. Tissue Eng, Part A. 2016; 22, 1098-1107.
151. Chen Z, Wu C, Gu W, et al. *Osteogenic differentiation of bone marrow MSCs by beta-tricalcium phosphate stimulating macrophages via BMP2 signalling pathway*. Biomaterials. 2014; 35, 1507-1518.
152. Grotenhuis N, Bayon Y, Lange JF, et al. *A culture model to analyze the acute biomaterial-dependent reaction of human primary macrophages*. Biochem Biophys Res Commun. 2013; 433, 115-120.
153. He H, Zhang S, Tighe S, et al. *Immobilized heavy chain-hyaluronic acid polarizes lipopolysaccharide-activated macrophages toward M2 phenotype*. J Biol Chem. 2013; 288, 25792-25803.

154. Lin CC, Metters AT, Anseth KS. *Functional PEG-peptide hydrogels to modulate local inflammation induced by the pro-inflammatory cytokine TNFalpha*. *Biomaterials*. 2009; 30, 4907-4914.
155. Lee KB, Taghavi CE, Song KJ, et al. *Inflammatory characteristics of rhBMP-2 in vitro and in an in vivo rodent model*. *Spine (Phila Pa 1976)*. 2011; 36, E149-154.
156. Shields LB, Raque GH, Glassman SD, et al. *Adverse effects associated with high-dose recombinant human bone morphogenetic protein-2 use in anterior cervical spine fusion*. *Spine (Phila Pa 1976)*. 2006; 31, 542-547.
157. Tannoury CA, An HS. *Complications with the use of bone morphogenetic protein 2 (BMP-2) in spine surgery*. *Spine J*. 2014; 14, 552-559.
158. Carragee EJ, Hurwitz EL, Weiner BK. *A critical review of recombinant human bone morphogenetic protein-2 trials in spinal surgery: emerging safety concerns and lessons learned*. *Spine J*. 2011; 11, 471-491.
159. Xu L, Huang S, Hou Y, et al. *Sox11-modified mesenchymal stem cells (MSCs) accelerate bone fracture healing: Sox11 regulates differentiation and migration of MSCs*. *FASEB J*. 2014.
160. Zhang XC, Zhang ZY, Shen G, et al. *Enhanced osteogenic activity and anti-inflammatory properties of Lenti-BMP-2-loaded TiO<sub>2</sub> nanotube layers fabricated by lyophilization following trehalose addition*. *Int J Nanomed*. 2016; 11.
161. Fernandes Stefanello T, Szarpak-Jankowska A, Appaix F, et al. *Thermoresponsive hyaluronic acid nanogels as hydrophobic drug carrier to macrophages*. *Acta Biomater*. 2014; 10, 4750-4758.
162. Chen WY, Abatangelo G. *Functions of hyaluronan in wound repair*. *Wound Repair Regen*. 1999; 7, 79-89.
163. Thomas A, Harding KG, Moore K. *Alginates from wound dressings activate human macrophages to secrete tumour necrosis factor-alpha*. *Biomaterials*. 2000; 21, 1797-1802.
164. Ayala P, Caves J, Dai E, et al. *Engineered composite fascia for stem cell therapy in tissue repair applications*. *Acta Biomater*. 2015; 26, 1-12.
165. Otterlei M, Ostgaard K, Skjak-Braek G, et al. *Induction of cytokine production from human monocytes stimulated with alginate*. *J Immunother (1991)*. 1991; 10, 286-291.
166. Hemshekhar M, Thushara RM, Chandranayaka S, et al. *Emerging roles of hyaluronic acid bioscaffolds in tissue engineering and regenerative medicine*. *Int J Biol Macromol*. 2016; 86, 917-928.
167. Deng Y, Ren J, Chen G, et al. *Injectable in situ cross-linking chitosan-hyaluronic acid based hydrogels for abdominal tissue regeneration*. *Sci Rep*. 2017; 7, 2699.
168. Abdalla S, Makhoul G, Duong M, et al. *Hyaluronic acid-based hydrogel induces neovascularization and improves cardiac function in a rat model of myocardial infarction*. *Interact Cardiovasc Thorac Surg*. 2013; 17, 767-772.
169. Cui FZ, Tian WM, Hou SP, et al. *Hyaluronic acid hydrogel immobilized with RGD peptides for brain tissue engineering*. *J Mater Sci Mater Med*. 2006; 17, 1393-1401.
170. Agarwal T, Kabiraj P, Narayana GH, et al. *Alginate Bead Based Hexagonal Close Packed 3D Implant for Bone Tissue Engineering*. *ACS Appl Mater Interfaces*. 2016; 8, 32132-32145.
171. Yu J, Gu Y, Du KT, et al. *The effect of injected RGD modified alginate on angiogenesis and left ventricular function in a chronic rat infarct model*. *Biomaterials*. 2009; 30, 751-756.
172. Burkus JK, Transfeldt EE, Kitchel SH, et al. *Clinical and radiographic outcomes of anterior lumbar interbody fusion using recombinant human bone morphogenetic protein-2*. *Spine (Phila Pa 1976)*. 2002; 27, 2396-2408.
173. Rengachary SS. *Bone morphogenetic proteins: basic concepts*. *Neurosurg Focus*. 2002; 13, e2.

174. Epstein NE. *Complications due to the use of BMP/INFUSE in spine surgery: The evidence continues to mount.* Surg Neurol Int. 2013; 4, S343-352.
175. Woo EJ. *Adverse events reported after the use of recombinant human bone morphogenetic protein 2.* J Oral Maxillofac Surg. 2012; 70, 765-767.
176. Perri B, Cooper M, Laurysen C, et al. *Adverse swelling associated with use of rh-BMP-2 in anterior cervical discectomy and fusion: a case study.* Spine J. 2007; 7, 235-239.
177. Mumcuoglu D, Siverino C, Tabisz B, et al. *How to use BMP-2 for clinical applications? A review on pros and cons of existing delivery strategies.* J Transl Sci. 2017; 3.
178. Bessa PC, Casal M, Reis RL. *Bone morphogenetic proteins in tissue engineering: the road from laboratory to clinic, part II (BMP delivery).* J Tissue Eng Regen Med. 2008; 2, 81-96.
179. Choi JW, Jeong WS, Yang SJ, et al. *Appropriate and Effective Dosage of BMP-2 for the Ideal Regeneration of Calvarial Bone Defects in Beagles.* Plast Reconstr Surg. 2016; 138, 64e-72e.
180. Yamaji K, Kawanami M, Matsumoto A, et al. *Effects of dose of recombinant human BMP-2 on bone formation at palatal sites in young and old rats.* Dent Mater J. 2007; 26, 481-486.
181. Scott MA, Levi B, Askarinam A, et al. *Brief review of models of ectopic bone formation.* Stem Cells Dev. 2012; 21, 655-667.
182. Tazaki J, Murata M, Akazawa T, et al. *BMP-2 release and dose-response studies in hydroxyapatite and beta-tricalcium phosphate.* Biomed Mater Eng. 2009; 19, 141-146.
183. Kim IS, Lee EN, Cho TH, et al. *Promising efficacy of Escherichia coli recombinant human bone morphogenetic protein-2 in collagen sponge for ectopic and orthotopic bone formation and comparison with mammalian cell recombinant human bone morphogenetic protein-2.* Tissue Eng, Part A. 2011; 17, 337-348.
184. Bessa PC, Balmayor ER, Hartinger J, et al. *Silk fibroin microparticles as carriers for delivery of human recombinant bone morphogenetic protein-2: in vitro and in vivo bioactivity.* Tissue Eng Part C Methods. 2010; 16, 937-945.
185. Martinez-Sanz E, Alkhraisat MH, Paradas I, et al. *Osteoinduction in the palatal submucosa by injecting BMP-2 on 2 different carriers.* J Craniofac Surg. 2012; 23, 594-598.
186. Fahmy-Garcia S, Mumcuoglu D, de Miguel L, et al. *Novel In Situ Gelling Hydrogels Loaded with Recombinant Collagen Peptide Microspheres as a Slow-Release System Induce Ectopic Bone Formation.* Adv Healthc Mater. 2018; 7, e1800507.
187. Tuin A, Kluijtmans SG, Bouwstra JB, et al. *Recombinant Gelatin Microspheres: Novel Formulations for Tissue Repair?* Tissue Eng, Part A. 2010; 16, 1811-1821.
188. van der Eerden BC, Oei L, Roschger P, et al. *TRPV4 deficiency causes sexual dimorphism in bone metabolism and osteoporotic fracture risk.* Bone. 2013; 57, 443-454.
189. Gruber HE. *Adaptations of Goldner's Masson trichrome stain for the study of undecalcified plastic embedded bone.* Biotech Histochem. 1992; 67, 30-34.
190. Morais JM, Papadimitrakopoulos F, Burgess DJ. *Biomaterials/tissue interactions: possible solutions to overcome foreign body response.* AAPS J. 2010; 12, 188-196.
191. Seo BB, Koh JT, Song SC. *Tuning physical properties and BMP-2 release rates of injectable hydrogel systems for an optimal bone regeneration effect.* Biomaterials. 2017; 122, 91-104.
192. Ono M, Sonoyama W, Nema K, et al. *Regeneration of calvarial defects with Escherichia coli -derived rhBMP-2 adsorbed in PLGA membrane.* Cells Tissues Organs. 2013; 198, 367-376.

193. Young S, Patel ZS, Kretlow JD, et al. *Dose effect of dual delivery of vascular endothelial growth factor and bone morphogenetic protein-2 on bone regeneration in a rat critical-size defect model*. Tissue Eng Part A. 2009; 15, 2347-2362.
194. Rodriguez-Evora M, Delgado A, Reyes R, et al. *Osteogenic effect of local, long versus short term BMP-2 delivery from a novel SPU-PLGA-betaTCP concentric system in a critical size defect in rats*. Eur J Pharm Sci. 2013; 49, 873-884.
195. Garcia P, Histing T, Holstein JH, et al. *Rodent animal models of delayed bone healing and non-union formation: a comprehensive review*. Eur Cell Mater. 2013; 26, 1-12; discussion 12-14.
196. Parvizi M. *Cardiovascular tissue engineering and regeneration based on adipose tissue-derived stem/stromal cells*: University of Groningen; 2016.
197. Rowley JA, Madlambayan G, Mooney DJ. *Alginate hydrogels as synthetic extracellular matrix materials*. Biomaterials. 1999; 20, 45-53.
198. Sarker B, Singh R, Silva R, et al. *Evaluation of fibroblasts adhesion and proliferation on alginate-gelatin crosslinked hydrogel*. PLoS One. 2014; 9, e107952.
199. Giannoudis PV, Dinopoulos H, Tsiridis E. *Bone substitutes: an update*. Injury. 2005; 36 Suppl 3, S20-27.
200. Finkemeier CG. *Bone-grafting and bone-graft substitutes*. J Bone Joint Surg Am. 2002; 84-A, 454-464.
201. Brydone AS, Meek D, Maclaine S. *Bone grafting, orthopaedic biomaterials, and the clinical need for bone engineering*. Proc Inst Mech Eng H. 2010; 224, 1329-1343.
202. Carreira AC, Lojudice FH, Halcsik E, et al. *Bone morphogenetic proteins: facts, challenges, and future perspectives*. J Dent Res. 2014; 93, 335-345.
203. Langenfeld EM, Langenfeld J. *Bone morphogenetic protein-2 stimulates angiogenesis in developing tumors*. Mol Cancer Res. 2004; 2, 141-149.
204. Carragee EJ, Chu G, Rohatgi R, et al. *Cancer risk after use of recombinant bone morphogenetic protein-2 for spinal arthrodesis*. J Bone Joint Surg Am. 2013; 95, 1537-1545.
205. Blonder J, Xiao Z, Veenstra TD. *Proteomic profiling of differentiating osteoblasts*. Expert Rev Proteomics. 2006; 3, 483-496.
206. Ting K, Vastardis H, Mulliken JB, et al. *Human NELL-1 expressed in unilateral coronal synostosis*. J Bone Miner Res. 1999; 14, 80-89.
207. Aghaloo T, Cowan CM, Chou YF, et al. *Nell-1-induced bone regeneration in calvarial defects*. Am J Pathol. 2006; 169, 903-915.
208. Zhang X, Peault B, Chen W, et al. *The Nell-1 growth factor stimulates bone formation by purified human perivascular cells*. Tissue Eng, Part A. 2011; 17, 2497-2509.
209. Yuan W, James AW, Asatrian G, et al. *NELL-1 based demineralized bone graft promotes rat spine fusion as compared to commercially available BMP-2 product*. J Orthop Sci. 2013; 18, 646-657.
210. James AW, Chiang M, Asatrian G, et al. *Vertebral Implantation of NELL-1 Enhances Bone Formation in an Osteoporotic Sheep Model*. Tissue Eng, Part A. 2016; 22, 840-849.
211. James AW, Shen J, Zhang X, et al. *NELL-1 in the treatment of osteoporotic bone loss*. Nat Commun. 2015; 6, 7362.
212. Cowan CM, Zhang X, James AW, et al. *NELL-1 increases pre-osteoblast mineralization using both phosphate transporter Pit1 and Pit2*. Biochem Biophys Res Commun. 2012; 422, 351-357.
213. Turner NJ, Londono R, Dearth CL, et al. *Human NELL1 protein augments constructive tissue remodeling with biologic scaffolds*. Cells Tissues Organs. 2013; 198, 249-265.

214. Kikuchi T, Kubota S, Asaumi K, et al. *Promotion of bone regeneration by CCN2 incorporated into gelatin hydrogel*. Tissue Eng. Part A. 2008; 14, 1089-1098.
215. Abd El Kader T, Kubota S, Nishida T, et al. *The regenerative effects of CCN2 independent modules on chondrocytes in vitro and osteoarthritis models in vivo*. Bone. 2014; 59, 180-188.
216. Arnott JA, Lambi AG, Mundy C, et al. *The role of connective tissue growth factor (CTGF/CCN2) in skeletogenesis*. Crit Rev Eukaryot Gene Expr. 2011; 21, 43-69.
217. Ivkovic S, Yoon BS, Popoff SN, et al. *Connective tissue growth factor coordinates chondrogenesis and angiogenesis during skeletal development*. Development. 2003; 130, 2779-2791.
218. Hendesi H, Barbe MF, Safadi FF, et al. *Integrin mediated adhesion of osteoblasts to connective tissue growth factor (CTGF/CCN2) induces cytoskeleton reorganization and cell differentiation*. PLoS One. 2015; 10, e015325.
219. Kubota S, Takigawa M. *The role of CCN2 in cartilage and bone development*. J Cell Commun Signal. 2011; 5, 209-217.
220. Markiewicz M, Nakerakanti SS, Kapanadze B, et al. *Connective tissue growth factor (CTGF/CCN2) mediates angiogenic effect of SIP in human dermal microvascular endothelial cells*. Microcirculation. 2011; 18, 1-11.
221. Wang JJ, Ye F, Cheng LJ, et al. *Osteogenic differentiation of mesenchymal stem cells promoted by overexpression of connective tissue growth factor*. J Zhejiang Univ Sci B. 2009; 10, 355-367.
222. Hall-Glenn F, De Young RA, Huang BL, et al. *CCN2/connective tissue growth factor is essential for pericyte adhesion and endothelial basement membrane formation during angiogenesis*. PLoS One. 2012; 7, e30562.
223. Takigawa M. *CCN2: a master regulator of the genesis of bone and cartilage*. J Cell Commun Signal. 2013; 7, 191-201.
224. Lau LF, Lam SC. *The CCN family of angiogenic regulators: the integrin connection*. Exp Cell Res. 1999; 248, 44-57.
225. Inoki I, Shiomi T, Hashimoto G, et al. *Connective tissue growth factor binds vascular endothelial growth factor (VEGF) and inhibits VEGF-induced angiogenesis*. FASEB J. 2002; 16, 219-221.
226. Hashimoto G, Inoki I, Fujii Y, et al. *Matrix metalloproteinases cleave connective tissue growth factor and reactivate angiogenic activity of vascular endothelial growth factor 165*. J Biol Chem. 2002; 277, 36288-36295.
227. Yang J, Shah R, Robling AG, et al. *HMGB1 is a bone-active cytokine*. J Cell Physiol. 2008; 214, 730-739.
228. Harris HE, Andersson U, Pisetsky DS. *HMGB1: a multifunctional alarmin driving autoimmune and inflammatory disease*. Nat Rev Rheumatol. 2012; 8, 195-202.
229. Andersson U, Wang H, Palmblad K, et al. *High mobility group 1 protein (HMG-1) stimulates proinflammatory cytokine synthesis in human monocytes*. J Exp Med. 2000; 192, 565-570.
230. Palumbo R, Sampaolesi M, De Marchis F, et al. *Extracellular HMGB1, a signal of tissue damage, induces mesoangioblast migration and proliferation*. J Cell Biol. 2004; 164, 441-449.
231. Riuzzi F, Sorci G, Donato R. *The amphoterin (HMGB1)/receptor for advanced glycation end products (RAGE) pair modulates myoblast proliferation, apoptosis, adhesiveness, migration, and invasiveness. Functional inactivation of RAGE in L6 myoblasts results in tumor formation in vivo*. J Biol Chem. 2006; 281, 8242-8253.
232. Rouhiainen A, Kuja-Panula J, Wilkman E, et al. *Regulation of monocyte migration by amphoterin (HMGB1)*. Blood. 2004; 104, 1174-1182.

233. Martinotti S, Patrone M, Manfredi M, et al. *HMGB1 Osteo-Modulatory Action on Osteosarcoma SaOS-2 Cell Line: An Integrated Study From Biochemical and -Omics Approaches*. J Cell Biochem. 2016; 117, 2559-2569.
234. Meng E, Guo Z, Wang H, et al. *High mobility group box 1 protein inhibits the proliferation of human mesenchymal stem cells and promotes their migration and differentiation along osteoblastic pathway*. Stem Cells Dev. 2008; 17, 805-813.
235. Li M, Li F, Xu J, et al. *rhHMGB1 drives osteoblast migration in a TLR2/TLR4- and NF-kappaB-dependent manner*. Biosci Rep. 2016.
236. Feng L, Xue D, Chen E, et al. *HMGB1 promotes the secretion of multiple cytokines and potentiates the osteogenic differentiation of mesenchymal stem cells through the Ras/MAPK signaling pathway*. Exp Ther Med. 2016; 12, 3941-3947.
237. Yu Y, Xie M, Kang R, et al. *HMGB1 is a therapeutic target for leukemia*. Am J Blood Res. 2012; 2, 36-43.
238. Yang S, Xu L, Yang T, et al. *High-mobility group box-1 and its role in angiogenesis*. J Leukoc Biol. 2014; 95, 563-574.
239. Chiba H, Sawada N, Ono T, et al. *Establishment and characterization of a simian virus 40-immortalized osteoblastic cell line from normal human bone*. Jpn J Cancer Res. 1993; 84, 290-297.
240. van Driel M, Koedam M, Buurman CJ, et al. *Evidence that both 1alpha,25-dihydroxyvitamin D3 and 24-hydroxylated D3 enhance human osteoblast differentiation and mineralization*. J Cell Biochem. 2006; 99, 922-935.
241. Lowry OH, Roberts NR, Wu ML, et al. *The quantitative histochemistry of brain. II. Enzyme measurements*. J Biol Chem. 1954; 207, 19-37.
242. Zhang X, Zara J, Siu RK, et al. *The role of NELL-1, a growth factor associated with craniosynostosis, in promoting bone regeneration*. J Dent Res. 2010; 89, 865-878.
243. Gugala Z, Davis AR, Fouletier-Dilling CM, et al. *Adenovirus BMP2-induced osteogenesis in combination with collagen carriers*. Biomaterials. 2007; 28, 4469-4479.
244. Bais MV, Wigner N, Young M, et al. *BMP2 is essential for post natal osteogenesis but not for recruitment of osteogenic stem cells*. Bone. 2009; 45, 254-266.
245. Finkenzeller G, Hager S, Stark GB. *Effects of bone morphogenetic protein 2 on human umbilical vein endothelial cells*. Microvasc Res. 2012; 84, 81-85.
246. Scaffidi P, Misteli T, Bianchi ME. *Release of chromatin protein HMGB1 by necrotic cells triggers inflammation*. Nature. 2002; 418, 191-195.
247. Yang H, Antoine DJ, Andersson U, et al. *The many faces of HMGB1: molecular structure-functional activity in inflammation, apoptosis, and chemotaxis*. J Leukoc Biol. 2013; 93, 865-873.
248. Chavakis E, Hain A, Vinci M, et al. *High-mobility group box 1 activates integrin-dependent homing of endothelial progenitor cells*. Circ Res. 2007; 100, 204-212.
249. Bauer EM, Shapiro R, Billiar TR, et al. *High mobility group Box 1 inhibits human pulmonary artery endothelial cell migration via a Toll-like receptor 4- and interferon response factor 3-dependent mechanism(s)*. J Biol Chem. 2013; 288, 1365-1373.
250. Nakamura R, Oyama T, Tajiri R, et al. *Expression and regulatory effects on cancer cell behavior of NELL1 and NELL2 in human renal cell carcinoma*. Cancer Sci. 2015; 106, 656-664.
251. Rickard DJ, Sullivan TA, Shenker BJ, et al. *Induction of rapid osteoblast differentiation in rat bone marrow stromal cell cultures by dexamethasone and BMP-2*. Dev Biol. 1994; 161, 218-228.
252. Edgar CM, Chakravarthy V, Barnes G, et al. *Autogenous regulation of a network of bone morphogenetic proteins (BMPs) mediates the osteogenic differentiation in murine marrow stromal cells*. Bone. 2007; 40, 1389-1398.



253. Woeckel VJ, van der Eerden BC, Schreuders-Koedam M, et al. *1alpha,25-dihydroxyvitamin D3 stimulates activin A production to fine-tune osteoblast-induced mineralization*. J Cell Physiol. 2013; 228, 2167-2174.
254. Safadi FF, Xu J, Smock SL, et al. *Expression of connective tissue growth factor in bone: its role in osteoblast proliferation and differentiation in vitro and bone formation in vivo*. J Cell Physiol. 2003; 196, 51-62.
255. Zhang X, Kuroda S, Carpenter D, et al. *Craniosynostosis in transgenic mice overexpressing Nell-1*. J Clin Invest. 2002; 110, 861-870.
256. Bokui N, Otani T, Igarashi K, et al. *Involvement of MAPK signaling molecules and Runx2 in the NELL1-induced osteoblastic differentiation*. FEBS Lett. 2008; 582, 365-371.
257. Zou X, Shen J, Chen F, et al. *NELL-1 binds to APR3 affecting human osteoblast proliferation and differentiation*. FEBS Lett. 2011; 585, 2410-2418.
258. Pang S, Shen J, Liu Y, et al. *Proliferation and Osteogenic Differentiation of Mesenchymal Stem Cells Induced by a Short Isoform of NELL-1*. Stem Cells. 2015; 33, 904-915.
259. Cowan CM, Jiang X, Hsu T, et al. *Synergistic effects of Nell-1 and BMP-2 on the osteogenic differentiation of myoblasts*. J Bone Miner Res. 2007; 22, 918-930.
260. Shen J, James AW, Zara JN, et al. *BMP2-induced inflammation can be suppressed by the osteoinductive growth factor NELL-1*. Tissue Eng, Part A. 2013; 19, 2390-2401.
261. Shen J, James AW, Zhang X, et al. *Novel Wnt Regulator NEL-Like Molecule-1 Antagonizes Adipogenesis and Augments Osteogenesis Induced by Bone Morphogenetic Protein 2*. Am J Pathol. 2016; 186, 419-434.
262. Zhu S, Song D, Jiang X, et al. *Combined effects of recombinant human BMP-2 and Nell-1 on bone regeneration in rapid distraction osteogenesis of rabbit tibia*. Injury. 2011; 42, 1467-1473.
263. Raida M, Clement JH, Leek RD, et al. *Bone morphogenetic protein 2 (BMP-2) and induction of tumor angiogenesis*. J Cancer Res Clin Oncol. 2005; 131, 741-750.
264. Choi H, Jeong BC, Hur SW, et al. *The Angiopoietin-1 Variant COMP-Ang1 Enhances BMP2-Induced Bone Regeneration with Recruiting Pericytes in Critical Sized Calvarial Defects*. PLoS One. 2015; 10, e0140502.
265. Patel ZS, Young S, Tabata Y, et al. *Dual delivery of an angiogenic and an osteogenic growth factor for bone regeneration in a critical size defect model*. Bone. 2008; 43, 931-940.
266. Biscetti F, Straface G, De Cristofaro R, et al. *High-mobility group box-1 protein promotes angiogenesis after peripheral ischemia in diabetic mice through a VEGF-dependent mechanism*. Diabetes. 2010; 59, 1496-1505.
267. Kim HY, Park SY, Lee SW, et al. *Inhibition of HMGB1-induced angiogenesis by cilostazol via SIRT1 activation in synovial fibroblasts from rheumatoid arthritis*. PLoS One. 2014; 9, e104743.
268. Sachdev U, Cui X, Hong G, et al. *High mobility group box 1 promotes endothelial cell angiogenic behavior in vitro and improves muscle perfusion in vivo in response to ischemic injury*. J Vasc Surg. 2012; 55, 180-191.
269. Shimo T, Nakanishi T, Nishida T, et al. *Connective tissue growth factor induces the proliferation, migration, and tube formation of vascular endothelial cells in vitro, and angiogenesis in vivo*. J Biochem. 1999; 126, 137-145.
270. Brigstock DR. *Regulation of angiogenesis and endothelial cell function by connective tissue growth factor (CTGF) and cysteine-rich 61 (CYR61)*. Angiogenesis. 2002; 5, 153-165.
271. Askarinam A, James AW, Zara JN, et al. *Human perivascular stem cells show enhanced osteogenesis and vasculogenesis with Nel-like molecule 1 protein*. Tissue Eng, Part A. 2013; 19, 1386-1397.

272. Mumcuoglu D, Fahmy-Garcia S, Ridwan Y, et al. *Injectable BMP-2 delivery system based on collagen-derived microspheres and alginate induced bone formation in a time- and dose-dependent manner*. Eur Cell Mater. 2018; 35, 242-254.
273. Hinck AP, Huang T. *TGF-beta antagonists: same knot, but different hold*. Structure. 2013; 21, 1269-1270.
274. Rahman MS, Akhtar N, Jamil HM, et al. *TGF-beta/BMP signaling and other molecular events: regulation of osteoblastogenesis and bone formation*. Bone Res. 2015; 3, 15005.
275. Abe Y, Minegishi T, Leung PC. *Activin receptor signaling*. Growth Factors. 2004; 22, 105-110.
276. Pearsall RS, Canalis E, Cornwall-Brady M, et al. *A soluble activin type IIA receptor induces bone formation and improves skeletal integrity*. Proc Natl Acad Sci U S A. 2008; 105, 7082-7087.
277. Matzuk MM, Lu N, Vogel H, et al. *Multiple defects and perinatal death in mice deficient in follistatin*. Nature. 1995; 374, 360-363.
278. Sakai R, Eto Y, Ohtsuka M, et al. *Activin enhances osteoclast-like cell formation in vitro*. Biochem Biophys Res Commun. 1993; 195, 39-46.
279. Koseki T, Gao Y, Okahashi N, et al. *Role of TGF-beta family in osteoclastogenesis induced by RANKL*. Cell Signal. 2002; 14, 31-36.
280. Fajardo RJ, Manoharan RK, Pearsall RS, et al. *Treatment with a soluble receptor for activin improves bone mass and structure in the axial and appendicular skeleton of female cynomolgus macaques (Macaca fascicularis)*. Bone. 2010; 46, 64-71.
281. Bialek P, Parkington J, Li X, et al. *A myostatin and activin decoy receptor enhances bone formation in mice*. Bone. 2014; 60, 162-171.
282. Inoue S, Nomura S, Hosoi T, et al. *Localization of follistatin, an activin-binding protein, in bone tissues*. Calcif Tissue Int. 1994; 55, 395-397.
283. Abe Y, Abe T, Aida Y, et al. *Follistatin restricts bone morphogenetic protein (BMP)-2 action on the differentiation of osteoblasts in fetal rat mandibular cells*. J Bone Miner Res. 2004; 19, 1302-1307.
284. Eijken M, Swagemakers S, Koedam M, et al. *The activin A-follistatin system: potent regulator of human extracellular matrix mineralization*. FASEB J. 2007; 21, 2949-2960.
285. Gajos-Michniewicz A, Pawlowska E, Ochedalski T, et al. *The influence of follistatin on mechanical properties of bone tissue in growing mice with overexpression of follistatin*. J Bone Miner Metab. 2012; 30, 426-433.
286. Zhu J, Li Y, Lu A, et al. *Follistatin improves skeletal muscle healing after injury and disease through an interaction with muscle regeneration, angiogenesis, and fibrosis*. Am J Pathol. 2011; 179, 915-930.
287. Kawao N, Morita H, Obata K, et al. *Role of follistatin in muscle and bone alterations induced by gravity change in mice*. J Cell Physiol. 2017.
288. Gao X, Hu H, Zhu J, et al. *Identification and characterization of follistatin as a novel angiogenin-binding protein*. FEBS Lett. 2007; 581, 5505-5510.
289. Kozian DH, Ziche M, Augustin HG. *The activin-binding protein follistatin regulates autocrine endothelial cell activity and induces angiogenesis*. Lab Invest. 1997; 76, 267-276.
290. Krneta J, Kroll J, Alves F, et al. *Dissociation of angiogenesis and tumorigenesis in follistatin- and activin-expressing tumors*. Cancer Res. 2006; 66, 5686-5695.
291. Ogino H, Yano S, Kakiuchi S, et al. *Follistatin suppresses the production of experimental multiple-organ metastasis by small cell lung cancer cells in natural killer cell-depleted SCID mice*. Clin Cancer Res. 2008; 14, 660-667.
292. Patel K. *Follistatin*. Int J Biochem Cell Biol. 1998; 30, 1087-1093.

293. Phillips DJ, de Kretser DM. *Follistatin: a multifunctional regulatory protein*. Front Neuroendocrinol. 1998; 19, 287-322.
294. Schneyer AL, Wang Q, Sidis Y, et al. *Differential distribution of follistatin isoforms: application of a new FS315-specific immunoassay*. J Clin Endocrinol Metab. 2004; 89, 5067-5075.
295. Hedger MP, Winnall WR, Phillips DJ, et al. *The regulation and functions of activin and follistatin in inflammation and immunity*. Vitam Horm. 2011; 85, 255-297.
296. Gajos-Michniewicz A, Piastowska AW, Russell JA, et al. *Follistatin as a potent regulator of bone metabolism*. Biomarkers. 2010; 15, 563-574.
297. Datta-Mannan A, Yaden B, Krishnan V, et al. *An engineered human follistatin variant: insights into the pharmacokinetic and pharmacodynamic relationships of a novel molecule with broad therapeutic potential*. J Pharmacol Exp Ther. 2013; 344, 616-623.
298. Yaden BC, Croy JE, Wang Y, et al. *Follistatin: a novel therapeutic for the improvement of muscle regeneration*. J Pharmacol Exp Ther. 2014; 349, 355-371.
299. Bowser M, Herberg S, Arounleut P, et al. *Effects of the activin A-myostatin-follistatin system on aging bone and muscle progenitor cells*. Exp Gerontol. 2013; 48, 290-297.
300. Sidis Y, Schneyer AL, Sluss PM, et al. *Follistatin: essential role for the N-terminal domain in activin binding and neutralization*. J Biol Chem. 2001; 276, 17718-17726.
301. Schneyer A, Schoen A, Quigg A, et al. *Differential binding and neutralization of activins A and B by follistatin and follistatin like-3 (FSTL-3/FSRP/FLRG)*. Endocrinology. 2003; 144, 1671-1674.
302. Hashimoto O, Kawasaki N, Tsuchida K, et al. *Difference between follistatin isoforms in the inhibition of activin signalling: activin neutralizing activity of follistatin isoforms is dependent on their affinity for activin*. Cell Signal. 2000; 12, 565-571.
303. Cash JN, Angerman EB, Keutmann HT, et al. *Characterization of follistatin-type domains and their contribution to myostatin and activin A antagonism*. Mol Endocrinol. 2012; 26, 1167-1178.
304. Sidis Y, Mukherjee A, Keutmann H, et al. *Biological activity of follistatin isoforms and follistatin-like-3 is dependent on differential cell surface binding and specificity for activin, myostatin, and bone morphogenetic proteins*. Endocrinology. 2006; 147, 3586-3597.
305. Glistler C, Kemp CF, Knight PG. *Bone morphogenetic protein (BMP) ligands and receptors in bovine ovarian follicle cells: actions of BMP-4, -6 and -7 on granulosa cells and differential modulation of Smad-1 phosphorylation by follistatin*. Reproduction. 2004; 127, 239-254.
306. Kleinhans C, Barz J, Wurster S, et al. *Ammonia plasma treatment of polystyrene surfaces enhances proliferation of primary human mesenchymal stem cells and human endothelial cells*. Biotechnol J. 2013; 8, 327-337.
307. Eijken M, Koedam M, van Driel M, et al. *The essential role of glucocorticoids for proper human osteoblast differentiation and matrix mineralization*. Mol Cell Endocrinol. 2006; 248, 87-93.
308. Spicer PP, Kretlow JD, Young S, et al. *Evaluation of bone regeneration using the rat critical size calvarial defect*. Nat Protoc. 2012; 7, 1918-1929.
309. Wennberg C, Hessle L, Lundberg P, et al. *Functional characterization of osteoblasts and osteoclasts from alkaline phosphatase knockout mice*. J Bone Miner Res. 2000; 15, 1879-1888.
310. Thompson TB, Lerch TF, Cook RW, et al. *The structure of the follistatin:activin complex reveals antagonism of both type I and type II receptor binding*. Dev Cell. 2005; 9, 535-543.
311. Kozian DH, Augustin HG. *Rapid identification of differentially expressed endothelial cell genes by RNA display*. Biochem Biophys Res Commun. 1995; 209, 1068-1075.

- 312. Glienke J, Schmitt AO, Pilarsky C, et al. *Differential gene expression by endothelial cells in distinct angiogenic states*. Eur J Biochem. 2000; 267, 2820-2830.
- 313. Maeshima K, Maeshima A, Hayashi Y, et al. *Crucial role of activin a in tubulogenesis of endothelial cells induced by vascular endothelial growth factor*. Endocrinology. 2004; 145, 3739-3745.
- 314. Endo D, Kogure K, Hasegawa Y, et al. *Activin A augments vascular endothelial growth factor activity in promoting branching tubulogenesis in hepatic sinusoidal endothelial cells*. J Hepatol. 2004; 40, 399-404.
- 315. Wu M, Chen G, Li YP. *TGF-beta and BMP signaling in osteoblast, skeletal development, and bone formation, homeostasis and disease*. Bone Res. 2016; 4, 16009.
- 316. Maeshima A, Mishima K, Yamashita S, et al. *Follistatin, an activin antagonist, ameliorates renal interstitial fibrosis in a rat model of unilateral ureteral obstruction*. Biomed Res Int. 2014; 2014, 376191.
- 317. Nakamura T, Sugino K, Titani K, et al. *Follistatin, an activin-binding protein, associates with heparan sulfate chains of proteoglycans on follicular granulosa cells*. J Biol Chem. 1991; 266, 19432-19437.
- 318. Alves RD, Eijken M, Bezstarosti K, et al. *Activin A suppresses osteoblast mineralization capacity by altering extracellular matrix (ECM) composition and impairing matrix vesicle (MV) production*. Mol Cell Proteomics. 2013; 12, 2890-2900.
- 319. Barakat B, O'Connor AE, Gold E, et al. *Inhibin, activin, follistatin and FSH serum levels and testicular production are highly modulated during the first spermatogenic wave in mice*. Reproduction. 2008; 136, 345-359.
- 320. Funaba M, Ogawa K, Murata T, et al. *Follistatin and activin in bone: expression and localization during endochondral bone development*. Endocrinology. 1996; 137, 4250-4259.
- 321. Nagamine T, Imamura T, Ishidou Y, et al. *Immunohistochemical detection of activin A, follistatin, and activin receptors during fracture healing in the rat*. J Orthop Res. 1998; 16, 314-321.
- 322. Linkhart TA, Mohan S, Baylink DJ. *Growth factors for bone growth and repair: IGF, TGF beta and BMP*. Bone. 1996; 19, 1S-12S.
- 323. Lieberman JR, Daluiski A, Einhorn TA. *The role of growth factors in the repair of bone. Biology and clinical applications*. J Bone Joint Surg Am. 2002; 84-A, 1032-1044.
- 324. Bai Y, Yin G, Huang Z, et al. *Localized delivery of growth factors for angiogenesis and bone formation in tissue engineering*. Int Immunopharmacol. 2013; 16, 214-223.
- 325. Bueno EM, Glowacki J. *Cell-free and cell-based approaches for bone regeneration*. Nat Rev Rheumatol. 2009; 5, 685-697.
- 326. Axelrad TW, Einhorn TA. *Bone morphogenetic proteins in orthopaedic surgery*. Cytokine Growth Factor Rev. 2009; 20, 481-488.
- 327. El Bialy I, Jiskoot W, Reza Nejadnik M. *Formulation, Delivery and Stability of Bone Morphogenetic Proteins for Effective Bone Regeneration*. Pharm Res. 2017; 34, 1152-1170.
- 328. Luong LN, Ramaswamy J, Kohn DH. *Effects of osteogenic growth factors on bone marrow stromal cell differentiation in a mineral-based delivery system*. Biomaterials. 2012; 33, 283-294.
- 329. Del Angel-Mosqueda C, Gutierrez-Puente Y, Lopez-Lozano AP, et al. *Epidermal growth factor enhances osteogenic differentiation of dental pulp stem cells in vitro*. Head Face Med. 2015; 11, 29.

330. Burdick JA, Mason MN, Hinman AD, et al. *Delivery of osteoinductive growth factors from degradable PEG hydrogels influences osteoblast differentiation and mineralization*. J Control Release. 2002; 83, 53-63.
331. Chen CY, Tseng KY, Lai YL, et al. *Overexpression of Insulin-Like Growth Factor 1 Enhanced the Osteogenic Capability of Aging Bone Marrow Mesenchymal Stem Cells*. Theranostics. 2017; 7, 1598-1611.
332. Saran U, Gemini Piperni S, Chatterjee S. *Role of angiogenesis in bone repair*. Arch Biochem Biophys. 2014; 561, 109-117.
333. Lee G, Espirito Santo AI, Zwingenberger S, et al. *Fully reduced HMGB1 accelerates the regeneration of multiple tissues by transitioning stem cells to GAlert*. Proc Natl Acad Sci U S A. 2018; 115, E4463-E4472.
334. Uutela M, Wirzenius M, Paavonen K, et al. *PDGF-D induces macrophage recruitment, increased interstitial pressure, and blood vessel maturation during angiogenesis*. Blood. 2004; 104, 3198-3204.
335. Hollinger JO, Onikepe AO, MacKrell J, et al. *Accelerated fracture healing in the geriatric, osteoporotic rat with recombinant human platelet-derived growth factor-BB and an injectable beta-tricalcium phosphate/collagen matrix*. J Orthop Res. 2008; 26, 83-90.
336. FDA. *Notification premarket approval Augment® Bone Graft*. 2015.
337. Koike N, Fukumura D, Gralla O, et al. *Tissue engineering: creation of long-lasting blood vessels*. Nature. 2004; 428, 138-139.
338. Park SY, Kim KH, Shin SY, et al. *Dual delivery of rhPDGF-BB and bone marrow mesenchymal stromal cells expressing the BMP2 gene enhance bone formation in a critical-sized defect model*. Tissue Eng, Part A. 2013; 19, 2495-2505.
339. Lee CH, Jin MU, Jung HM, et al. *Effect of dual treatment with SDF-1 and BMP-2 on ectopic and orthotopic bone formation*. PLoS One. 2015; 10, e0120051.
340. Bergman K, Engstrand T, Hilborn J, et al. *Injectable cell-free template for bone-tissue formation*. J Biomed Mater Res A. 2009; 91, 1111-1118.
341. Nguyen MK, Lee DS. *Injectable biodegradable hydrogels*. Macromol Biosci. 2010; 10, 563-579.
342. Almeida H, Amaral MH, Lobao P, et al. *In situ gelling systems: a strategy to improve the bioavailability of ophthalmic pharmaceutical formulations*. Drug Discov Today. 2014; 19, 400-412.
343. Hu J, Hou Y, Park H, et al. *Visible light crosslinkable chitosan hydrogels for tissue engineering*. Acta Biomater. 2012; 8, 1730-1738.
344. Zhao W, Odelius K, Edlund U, et al. *In Situ Synthesis of Magnetic Field-Responsive Hemicellulose Hydrogels for Drug Delivery*. Biomacromolecules. 2015; 16, 2522-2528.
345. Baier Leach J, Bivens KA, Patrick CW, Jr., et al. *Photocrosslinked hyaluronic acid hydrogels: natural, biodegradable tissue engineering scaffolds*. Biotechnol Bioeng. 2003; 82, 578-589.
346. Borselli C, Oliviero O, Battista S, et al. *Induction of directional sprouting angiogenesis by matrix gradients*. J Biomed Mater Res A. 2007; 80, 297-305.
347. Rath SN, Arkudas A, Lam CX, et al. *Development of a pre-vascularized 3D scaffold-hydrogel composite graft using an arterio-venous loop for tissue engineering applications*. J Biomater Appl. 2012; 27, 277-289.
348. Silva LP, Pirraco RP, Santos TC, et al. *Neovascularization Induced by the Hyaluronic Acid-Based Spongy-Like Hydrogels Degradation Products*. ACS Appl Mater Interfaces. 2016; 8, 33464-33474.
349. Henkel J, Woodruff MA, Epari DR, et al. *Bone Regeneration Based on Tissue Engineering Conceptions - A 21st Century Perspective*. Bone Res. 2013; 1, 216-248.

- 350. Gibbs DM, Black CR, Dawson JI, et al. *A review of hydrogel use in fracture healing and bone regeneration*. J Tissue Eng Regen Med. 2016; 10, 187-198.
- 351. Frencken JE, Sharma P, Stenhouse L, et al. *Global epidemiology of dental caries and severe periodontitis - a comprehensive review*. J Clin Periodontol. 2017; 44 Suppl 18, S94-S105.
- 352. Thorpe AA, Freeman C, Farthing P, et al. *In vivo safety and efficacy testing of a thermally triggered injectable hydrogel scaffold for bone regeneration and augmentation in a rat model*. Oncotarget. 2018; 9, 18277-18295.
- 353. Kumar P, Vinitha B, Fathima G. *Bone grafts in dentistry*. J Pharm Bioallied Sci. 2013; 5, S125-127.
- 354. Tarsuslugil SM, O'Hara RM, Dunne NJ, et al. *Development of calcium phosphate cement for the augmentation of traumatically fractured porcine specimens using vertebroplasty*. J Biomech. 2013; 46, 711-715.
- 355. Laurencin C, Khan Y, El-Amin SF. *Bone graft substitutes*. Expert Rev Med Devices. 2006; 3, 49-57.
- 356. Blattter TR, Jestaedt L, Weckbach A. *Suitability of a calcium phosphate cement in osteoporotic vertebral body fracture augmentation: a controlled, randomized, clinical trial of balloon kyphoplasty comparing calcium phosphate versus polymethylmethacrylate*. Spine (Phila Pa 1976). 2009; 34, 108-114.
- 357. Boyd D, Towler MR, Wren A, et al. *Comparison of an experimental bone cement with surgical Simplex P, Spineplex and Cortoss*. J Mater Sci Mater Med. 2008; 19, 1745-1752.
- 358. Luo S, Zhu W, Liu F, et al. *Preparation of a Bis-GMA-Free Dental Resin System with Synthesized Fluorinated Dimethacrylate Monomers*. Int J Mol Sci. 2016; 17.
- 359. Sanus GZ, Tanriverdi T, Ulu MO, et al. *Use of Cortoss as an alternative material in calvarial defects: the first clinical results in cranioplasty*. J Craniofac Surg. 2008; 19, 88-95.
- 360. Sun J, Tan H. *Alginate-Based Biomaterials for Regenerative Medicine Applications*. Materials (Basel). 2013; 6, 1285-1309.
- 361. Pape HC, Marcucio R, Humphrey C, et al. *Trauma-induced inflammation and fracture healing*. J Orthop Trauma. 2010; 24, 522-525.
- 362. FDA. *INFUSE® Bone Graft. Important Medical Information*. 2004.
- 363. Jeon O, Song SJ, Yang HS, et al. *Long-term delivery enhances in vivo osteogenic efficacy of bone morphogenetic protein-2 compared to short-term delivery*. Biochem Biophys Res Commun. 2008; 369, 774-780.
- 364. Choi B, Kim S, Fan J, et al. *Covalently conjugated transforming growth factor-beta1 in modular chitosan hydrogels for the effective treatment of articular cartilage defects*. Biomater Sci. 2015; 3, 742-752.
- 365. Luginbuehl V, Meinel L, Merkle HP, et al. *Localized delivery of growth factors for bone repair*. Eur J Pharm Biopharm. 2004; 58, 197-208.
- 366. Bouet G, Marchat D, Cruel M, et al. *In vitro three-dimensional bone tissue models: from cells to controlled and dynamic environment*. Tissue Eng, Part B. 2015; 21, 133-156.
- 367. Papadimitropoulos A, Scherberich A, Guven S, et al. *A 3D in vitro bone organ model using human progenitor cells*. Eur Cell Mater. 2011; 21, 445-458; discussion 458.
- 368. Kohli N, Ho S, Brown SJ, et al. *Bone remodelling in vitro: Where are we headed?: -A review on the current understanding of physiological bone remodelling and inflammation and the strategies for testing biomaterials in vitro*. Bone. 2018; 110, 38-46.

369. Peroglio M, Gaspar D, Zeugolis DI, et al. *Relevance of bioreactors and whole tissue cultures for the translation of new therapies to humans*. J Orthop Res. 2018; 36, 10-21.
370. Iba K, Sawada N, Chiba H, et al. *Transforming growth factor-beta 1 downregulates dexamethasone-induced tetranectin gene expression during the in vitro mineralization of the human osteoblastic cell line SV-HFO*. FEBS Lett. 1995; 373, 1-4.
371. van Driel M, Koedam M, Buurman CJ, et al. *Evidence for auto/paracrine actions of vitamin D in bone: 1 $\alpha$ -hydroxylase expression and activity in human bone cells*. FASEB J. 2006; 20, 2417-2419.
372. Morhayim J, van de Peppel J, Demmers JA, et al. *Proteomic signatures of extracellular vesicles secreted by nonmineralizing and mineralizing human osteoblasts and stimulation of tumor cell growth*. FASEB J. 2015; 29, 274-285.
373. Drabek K, van de Peppel J, Eijken M, et al. *GPM6B regulates osteoblast function and induction of mineralization by controlling cytoskeleton and matrix vesicle release*. J Bone Miner Res. 2011; 26, 2045-2051.
374. Tooouli CD, Huschtscha LI, Neumann AA, et al. *Comparison of human mammary epithelial cells immortalized by simian virus 40 T-Antigen or by the telomerase catalytic subunit*. Oncogene. 2002; 21, 128-139.
375. Kaur G, Dufour JM. *Cell lines: Valuable tools or useless artifacts*. Spermatogenesis. 2012; 2, 1-5.
376. Maeda T, Tashiro H, Katabuchi H, et al. *Establishment of an immortalised human ovarian surface epithelial cell line without chromosomal instability*. Br J Cancer. 2005; 93, 116-123.
377. Li Y, Chen SK, Li L, et al. *Bone defect animal models for testing efficacy of bone substitute biomaterials*. J Orthop Translat. 2015; 3, 95-104.
378. Gomes PS, Fernandes MH. *Rodent models in bone-related research: the relevance of calvarial defects in the assessment of bone regeneration strategies*. Lab Anim. 2011; 45, 14-24.
379. Pelaez M, Susin C, Lee J, et al. *Effect of rhBMP-2 dose on bone formation/maturation in a rat critical-size calvarial defect model*. J Clin Periodontol. 2014; 41, 827-836.
380. Rahman CV, Ben-David D, Dhillon A, et al. *Controlled release of BMP-2 from a sintered polymer scaffold enhances bone repair in a mouse calvarial defect model*. J Tissue Eng Regen Med. 2014; 8, 59-66.
381. Fan J, Im CS, Cui ZK, et al. *Delivery of Phenamil Enhances BMP-2-Induced Osteogenic Differentiation of Adipose-Derived Stem Cells and Bone Formation in Calvarial Defects*. Tissue Eng, Part A. 2015; 21, 2053-2065.
382. Choi JM, Jeong WS, Park EJ, et al. *The Efficacy of Cyclic Injection of Bone Morphogenetic Protein-2 in Large-Scale Calvarial Bone Defects*. J Craniofac Surg. 2016.
383. Ben-David D, Srouji S, Shapira-Schweitzer K, et al. *Low dose BMP-2 treatment for bone repair using a PEGylated fibrinogen hydrogel matrix*. Biomaterials. 2013; 34, 2902-2910.
384. Wiesmayer P. *Skin on a chip – Research without animal experiments*. Innovation Origins. 2018.
385. Holstein JH, Garcia P, Histing T, et al. *Advances in the establishment of defined mouse models for the study of fracture healing and bone regeneration*. J Orthop Trauma. 2009; 23, S31-38.
386. Pearce AI, Richards RG, Milz S, et al. *Animal models for implant biomaterial research in bone: a review*. Eur Cell Mater. 2007; 13, 1-10.

- 387. Barnes B, Boden SD, Louis-Ugbo J, et al. *Lower dose of rhBMP-2 achieves spine fusion when combined with an osteoconductive bulking agent in non-human primates.* Spine (Phila Pa 1976). 2005; 30, 1127-1133.
- 388. Lin S, Cao C, Wang Q, et al. *Design of stiff, tough and stretchy hydrogel composites via nanoscale hybrid crosslinking and macroscale fiber reinforcement.* Soft Matter. 2014; 10, 7519-7527.
- 389. Mancini IAD, Vindas Bolanos RA, Brommer H, et al. *Fixation of Hydrogel Constructs for Cartilage Repair in the Equine Model: A Challenging Issue.* Tissue Eng, Part C. 2017; 23, 804-814.
- 390. D'Este M, Eglin D. *Hydrogels in calcium phosphate moldable and injectable bone substitutes: Sticky excipients or advanced 3-D carriers?* Acta Biomater. 2013; 9, 5421-5430.
- 391. Short AR, Koralla D, Deshmukh A, et al. *Hydrogels That Allow and Facilitate Bone Repair, Remodeling, and Regeneration.* J Mater Chem B Mater Biol Med. 2015; 3, 7818-7830.
- 392. Ma S, Scaraggi M, Wang D, et al. *Nanoporous Substrate-Infiltrated Hydrogels: a Bioinspired Regenerable Surface for High Load Bearing and Tunable Friction.* Adv Funct Mater. 2015; 25, 7366-7374.
- 393. Wang L, Zhang X, Guo Y, et al. *Involvement of BMPs/Smad signaling pathway in mechanical response in osteoblasts.* Cell Physiol Biochem. 2010; 26, 1093-1102.
- 394. Kopf J, Petersen A, Duda GN, et al. *BMP2 and mechanical loading cooperatively regulate immediate early signalling events in the BMP pathway.* BMC Biol. 2012; 10, 37.
- 395. Martin GJ, Jr., Boden SD, Marone MA, et al. *Posterolateral intertransverse process spinal arthrodesis with rhBMP-2 in a nonhuman primate: important lessons learned regarding dose, carrier, and safety.* J Spinal Disord. 1999; 12, 179-186.
- 396. Bohm AM, Dirckx N, Maes C. *Recruitment of osteogenic cells to bone formation sites during development and fracture repair.* Z Rheumatol. 2016; 75, 316-321.
- 397. Mina M. *Stem Cell Biology and Tissue Engineering in Dental Sciences.* Boston: Academic Press; 2015. p. 85-97.
- 398. Wang Z, Wang Z, Lu W, et al. *Novel biomaterial strategies for controlled growth factor delivery for biomedical applications.* Npg Asia Materials. 2017; 9, e435.





## Appendices

Nederlandse Samenvatting

List of publications

Acknowledgements

PhD portfolio

Curriculum Vitae



## Nederlandse samenvatting

Grote botdefecten worden gewoonlijk behandeld met transplantaten om het defect op te vullen en wondgenezing en botvorming te stimuleren. De huidige gouden standaard is het gebruik van patiënteigen botweefsel. Nadelen hiervan zijn dat er een beperkte hoeveelheid bot beschikbaar is in het lichaam van de patiënt en dat er een extra ingreep nodig is om bot te verkrijgen. Dit laatste leidt tot een langere operatietijd en het kan problemen geven, zoals pijn, op de plaats waar bottransplantaat wordt weggehaald. Bovendien is het bij complexe botstructuren, zoals in het hoofd-halsgebied, lastig om het patiënteigen bottransplantaat de correcte vorm te geven.

Injecteerbare biomaterialen zouden hiervoor een oplossing kunnen bieden. Recent zijn er systemen ontwikkeld die als doel hebben biologisch actieve eiwitten, zoals groeifactoren, naar de plaats van het botdefect te brengen. Groeifactoren zijn eiwitten die onmisbaar zijn voor wondgenezing en weefselherstel. Het klinische gebruik wordt echter beperkt door hun korte halfwaardetijd en instabiliteit. Daarnaast is het een uitdaging de groeifactoren op de gewenste plek te houden. Daarom is een hoge dosis van groeifactoren nodig. Bone morphogenetic protein-2 (BMP-2) is een veelgebruikte groeifactor om botdefecten te behandelen. Vanwege de hoge benodigde dosis is er een hoog risico op bijwerkingen. Om de benodigde dosis BMP-2 te kunnen verlagen, onderzochten we voor dit proefschrift de therapeutische potentie van nieuwe injecteerbare langzame afgiftesystemen. Ook identificeerden we andere veelbelovende eiwitten die botherstel kunnen stimuleren.

Hydrogelen zijn biomaterialen die na injectie in het lichaam een vaste gel vormen en kunnen zorgen voor een geschikte micro-omgeving voor het aantrekken en differentiëren van cellen die betrokken zijn bij botherstel. In **hoofdstuk 2** werden verschillende hydrogelen onderzocht die gebruikt zouden kunnen worden als eiwit-afgiftesysteem voor botherstel. We gebruikten microbolletjes gemaakt van peptiden die op collageen type I gebaseerd zijn (RCP-MS). Uit eerdere laboratorium experimenten was bekend dat de RCP-MS microbolletjes eerst een korte piekafgifte laten zien, gevolgd door het langdurig langzaam vrijkomen van BMP-2. In de RCP-MS werd 3.3 µg (16.5 µg/mL) BMP-2 geladen en gemengd met drie verschillende hydrogelen: twee typen alginaat, hoog mannuronaat (SLM) en hoog guluronaat (SLG), en hyaluronzuur. Beide typen alginaat hadden een thixotropisch gedrag, wat betekent dat ze een gelvorm hebben, maar door de hoge schuifkrachten tijdens injecteren tijdelijk vloeibaar worden. Beide alginaat systemen lieten de BMP-2 langzaam vrijkomen. Het hyaluronzuur was thermo-responsief. Dat wil zeggen dat het vloeibaar is bij kamertemperatuur en een gel vormt in het lichaam. Deze gel liet weinig afgifte zien in de laboratoriumtesten. De systemen van RCP-MS met alginaat of hyaluronzuur werden geïnjecteerd onder de huid van ratten. Bloedvatvorming werd aangetroffen bij alle systemen, maar botvorming werd alleen gezien met alginaat. Bovendien nam de ontsteking af in de loop van de tijd bij beide alginaten, maar bleef sterk

aanwezig bij hyaluronzuur. Alginaat SLG gemengd met RCP-MS en een lage dosis BMP-2 vormde het meeste bot. Op grond hiervan werd deze combinatie gekozen voor de vervolgstudies die beschreven zijn in dit proefschrift.

Om de dosis BMP-2 te kunnen verlagen, is het nodig om te weten wat het afgifteprofiel van BMP-2 uit alginaat SLG is. Daarom onderzochten we in **hoofdstuk 3** hoe de botvorming na injectie van het systeem onder de huid, verliep in de tijd. We vergeleken vier doses BMP-2: 10 µg (50 µg/mL), 3 µg (15 µg/mL), 1 µg (5 µg/mL) en 0,3 µg (1,5 µg/mL). De dichtheid van het gevormde bot was bij 50 µg/mL en 15 µg/mL gelijk, terwijl het volume van het gevormde bot afhankelijk was van tijd en dosis. Het grootste botvolume werd gezien met de hoogste dosis (10 µg, 50 µg/mL). Met de laagste dosis (0,3 µg, 1,5 µg/mL) werd helemaal geen botvorming waargenomen. Door het BMP-2 fluorescent te labelen constateren dat BMP-2 na vier weken nog detecteerbaar was, wat overeenkomt met het tijdsbestek van natuurlijke botgenezing. Om het vermogen te onderzoeken van het alginaat SLG+RCP-MS met BMP-2 om een botdefect te herstellen, testten we twee doses BMP-2 in een 5 mm botdefect in het schedeldak van ratten: 200 ng (50 µg/mL) en 20 ng (5 µg/mL). Het systeem met 50 µg/mL BMP-2 liet volledig herstel zien aan het einde van het experiment. Het systeem met 5 µg/mL BMP-2 of zonder BMP-2 herstelde vergelijkbaar met de controle die niet behandeld was. Deze resultaten wijzen op een effectieve dosis voor botvorming die hoger is dan 5 µg/mL BMP-2 (tussen 15-50 µg/mL) wanneer BMP-2 wordt gebruikt in combinatie met alginaat SLG+RCP-MS.

Om de risico's op bijwerkingen van BMP-2 te kunnen verminderen, werden vier alternatieve eiwitten geëvalueerd: Nell-like molecule type 1 (Nell-1), high mobility group box 1 (HMGB1), connective tissue growth factor (CTGF of CCN2) (in **hoofdstuk 4**) en follistatine (FST) (in **hoofdstuk 5**). Bij botherstel is een serie van goed georganiseerde biologische processen betrokken: celmigratie in het defect, celdeling, vorming van bloedvaten, celdifferentiatie naar botvormende cel en daaropvolgend, verkalking van de matrix. Daarom zal een product voor het herstel van botdefecten niet slagen wanneer één van deze centrale processen geremd wordt of als de processen niet in evenwicht zijn. Om die reden hebben we onderzocht of Nell-1, CCN2, HMGB1 en FST celmigratie, bloedvatvorming en differentiatie naar botcel kunnen verhogen. Nell-1, CCN2, HMGB1 en FST stimuleerden de migratie van mesenchymale stamcellen (MSCs), terwijl BMP-2 dat niet deed. Alle onderzochte eiwitten stimuleerden de migratie van endotheelcellen en de bloedvatvorming. BMP-2 verhoogde de differentiatie van MSCs naar botcellen, maar remde de verkalking van de matrix, terwijl FST zowel de differentiatie van de cellen als de verkalking van de matrix verhoogde. Deze screening liet de potentie van FST zien om te worden gebruikt als eiwit om bloedvat- en botvorming te stimuleren. De resultaten lieten zien dat Nell-1, HMGB1, CCN2 en FST, sommige processen bevorderen die botherstel zouden kunnen versnellen. Deze eiwitten zouden mogelijk als combinaties gebruikt

kunnen worden, om bijwerkingen te verminderen wanneer deze eiwitten afzonderlijk worden gebruikt.

Aangezien FST het meest veelbelovende eiwit was voor stimuleren van botvorming-gerelateerde processen in de laboratorium experimenten, hebben we twee varianten van FST, FST288 en FST315, onderzocht (in **hoofdstuk 5**). FST288 en FST315 verschillen in hun affiniteit voor cel-oppervlakte proteoglycanen, wat invloed kan hebben op botherstel in het lichaam en de afgiftesnelheid uit de hydrogelen. Het afgifteprofiel van FST288 en FST315 vanuit alginaat SLG+RCP-MS liet zien dat het meeste van de FST315 werd afgegeven over een periode van vier weken, in tegenstelling tot FST288 dat in het biomateriaal bleef. Beide FST varianten werden vervolgens geladen in het alginaat SLG+RCP-MS systeem en geïnjecteerd in een botdefect in het schedeldak van ratten. In de FST behandelde defecten was botherstel niet significant verbeterd, hoewel de verkalking meer homogeen was. In deze studie werd alginaat RCP-MS gebruikt als FST-drager om langzame afgifte van FST te bewerkstelligen, maar FST is waarschijnlijk met name van belang bij de vroege processen in botvorming. Daarnaast vertraagde alginaat niet alleen het vrijkomen van eiwitten, maar ook de ingroei van cellen in het botdefect. Het langzame afgiftesysteem gebaseerd op alginaat is niet optimaal voor botherstel wanneer het geladen is met FST omdat de timing van afgifte wellicht niet optimaal is.

Concluderend hebben we de potentie bewezen van een eiwit-afgiftesysteem voor botherstel. Dit systeem, gebaseerd op RCP-MS en alginaat geladen met een lage dosis BMP-2, vormt in het lichaam een gel en is geschikt voor de behandeling van defecten in niet-belaste botten en daarom interessant voor het gebruik in het hoofd-halsgebied. Verder onderzoek moet de doeltreffendheid uitwijzen in een groter diemodel om vervolgens de vertaling naar de kliniek te kunnen maken. Daarnaast hebben we de effecten van Nell-1, HMGB1, CCN2 en FST onderzocht op een aantal cruciale processen voor botvorming. Hiermee laten we zien dat het gebruik hiervan veelbelovend is om bijwerkingen, zoals gezien in enkelvoudige therapieën, te verminderen. Verdere studies, inclusief dierexperimenten, met tweevoudige afgiftesystemen voor herstel van botdefecten zouden moeten worden uitgevoerd. Voor FST hebben we laten zien dat het gebruik in het alginaat+RCP-MS systeem het herstel van een botdefect niet verbetert. Dit kan verschillende oorzaken hebben, zoals slechte botvormende capaciteit, te lage dosering en een suboptimaal afgifteprofiel. Om groeifactor-gebaseerde therapieën verder te ontwikkelen, moeten we beter onderzoeken in welke mate de gekozen groeifactor de processen regelt die nodig zijn voor botherstel. Daarnaast moet het optimale afgifteprofiel van de groeifactor(en) na injectie worden onderzocht om het gebruik ervan succesvol te kunnen vertalen naar therapieën voor het herstel van botdefecten.



## List of publications

**Fahmy-Garcia S<sup>#</sup>**, Mumcuoglu D<sup>#</sup>, de Miguel L, Dieleman V, Witte-Bouma J, van der Eerden BCJ, van Driel M, Eglin D, Verhaar JAN, Kluijtmans SGJM, van Osch GJVM, Farrell E. *Novel in situ gelling hydrogels loaded with recombinant collagen peptide microspheres as a slow-release system induce ectopic bone formation*. Adv Healthc Mater. 2018. 7(21):e1800507

Mumcuoglu D<sup>#</sup>, **Fahmy-Garcia S<sup>#</sup>**, Ridwan Y, Nicke J, Farrell E, Kluijtmans SG, van Osch GJ. *Injectable BMP-2 delivery system based on collagen-derived microspheres and alginate induced bone formation in a time- and dose-dependent manner*. Eur Cell Mater. 2018. 26;35:242-254

**Fahmy-Garcia S**, van Driel M, Witte-Bouma J, Walles H, van Leeuwen JPTM, van Osch GJVM, Farrell E. *Nell-1, HMGB1, and CCN2 enhance migration and vasculogenesis, but not osteogenic differentiation compared to BMP2*. Tissue Eng Part A. 2018. 24(3-4):207-218

**Fahmy-Garcia S**, Farrell E\*, Witte-Bouma J, Robbesom-van den Berge I, Suarez M, Mumcuoglu D, Walles H, Kluijtmans SGJM, van der Eerden BCJ, van Osch GJVM, van Leeuwen JPTM, van Driel M. *Follistatin effects in migration, vascularization and osteogenesis in vitro and bone repair in vivo*. Front. Bioeng. Biotechnol. 2019. 10.3389/fbioe.2019.00038

Fernandes Patrício TM, Mumcuoglu D, Montesi M, Panseri S, Witte-Bouma J, **Fahmy-Garcia S**, Tampieri A, Farrell E\*, Sprio S. *Hybrid magnetic microspheres proposed as a sustained carrier of rhBMP-2*. Manuscript in preparation.





## Acknowledgements

Some romantic scientist said to me that at your PhD defense no one knows more than you about the topic you are defending. No one in the world. And this is a pretty huge planet. I am certain that during this period I met some of the brightest people I will ever meet, and that is overwhelming. In fact, I needed to move to a city that lives below sea level and carry out a PhD to realize that I actually like what I have studied in college. The culprits were, in the first place, my promotor and co-promotor. Thank you for this adventure. **Prof. dr. Gerjo van Osch**, I never imagined that this journey would be that amazing, and you are one of the guiltiest. When I started working in your lab, I seriously thought that I was going to get fired in less than two months, and here we are! **Gerjo**, I do not only admire you, but I think you made me grow both professionally and personally. **Prof. dr. Johannes van Leeuwen**, it has been a pleasure to have you as a mentor. **Hans**, leaving aside how scared I was of your directness and your height the first time we met (then I realized that those features were intrinsic to the Dutch population), I believe that you significantly improved my scientific thinking. Your curiosity and comments during our meetings always gave rise to new doubts and approaches, which –I hope– has been reflected in how this thesis started and ended. **Dr. Eric Farrell**, what can I say that you don't know already? You have been my closest supervisor (there are less than three meters from my desk to yours). Thank you for being always there to guide me and answer all my questions; you know, it was never the last one. **Eric**, after more than 4 years, many meetings and some after-work *boudewijns*, I do not only consider you my promotor, but also a friend. To **Dr. Marjolein van Driel**, because talking with you about life and science made every cappuccino that we shared worth it. **Marjolein**, thanks for your advice, sweetness and optimism.

**Sandra**, if it was not for you, I might be still filling in the form 1. Thanks for taking care of all of those important things that I would not even think about.

To you, lab-technicians, who are always in the trench. Without your expertise I would probably be still in the lab. **Wendy**, I love to talk with you, even more when it is about life and our dreamed trips. Thank you **Nicole** for always troubleshooting everything in a particularly wonderful smiley manner! and **Janneke**, you are one of the most patient and calm people I know, essential features to help out an impatient PhD student. **Iris**, I still remember the beginning of my PhD when culturing SVHFOs and MSCs over and over with you was my daily routine. During those first months, plenty of indecision and insecurities, it was really nice to work beside you. Sorry for making you cut smelly MMA at the end of this –please, don't hate me–. **Marijke**, you have a gift to solve things quickly and easily. Thanks for using it with me every time I asked. **Yanto**, I think it is impossible to count the number of hours we've spent together in the animal facility. Thanks for all your help in that basement!

**Kavitha, Roberto** and **Bram**, I will always appreciate talking with you about science, life and northern lights! **Yvonne** and **Jeroen**, I am grateful for your advice during my whole time in the lab. **Niamh**, discovering you as my partner in crime is one of the greatest things that happened to me in this new “post doc life”. **Andrea**, the red seat chair near your desk has my name engraved on it because of the many times I get to talk to you; firstly about work, then about practically anything. I wrote these acknowledgements before annoying you with paronymph thingys, so sorry beforehand about what is going to come.

To all my PhD-colleagues, carrying out this thesis without you wouldn't have been the same. To the old ones, **Jess, Wu, Maarten, Mairead**, and to the new ones, **Chantal, Virginia, Enrique, Mauricio, Joelle** and **Tim. Yannick**, my cat met you before I did, but sharing an office made that easy to solve. Thanks for always trying to help out. I am grateful to you all for being part of the beginning and the end of my PhD. **Marta**, thanks for all the time that we have spent together downstairs, on the fifth floor and everywhere else. See you in Stockholm! **Serdar**, it has been nice to know that you were covering my back in case I was running low on sugars, always offering sweets from your magic drawer. **Johannes**, it was good to almost-share a desk with you –now I have stolen yours–. Thank God you were my roommate in TERMIS! I could not have handled any morning hyperactivity. **Mathijs**, I mostly remember you behind a western blot! It is a shame that I probably won't see you boogieing at conferences while making fun of me. **Callie** and **Caioimhe**, I really enjoyed sharing not only the office with you but our lives with all the good and the bad. Without you, I wouldn't know what a mimosa is. **Callie**, thank you so much for forcing me to use crutches and coming over to cheer me up –especially when I could not go anywhere–. Your friendship is one of those good things that came out of this PhD. To **Sohrab**, we have not only shared (past tense, I must emphasize) the same haircut, but so many memories while stealing your Nespresso cups –sadly I have my own now–. You are my favourite fake brother, and I do miss having you around in the lab. **Panithi**, every moment with you is hilarious! I keep learning from you. You are so genuine that having you as a friend is a real gift. **Lizette**, I still remember a random day, in which I was tremendously stressed and without realizing, I found myself dialing your phone number. From then till now my paranimph lady. By the way, thanks for accepting the offer; it is an honour taking in account your tight agenda.

Thank you to all the Bioinspire members with who I had the possibility of going through many nice places in Europe while learning more and more about you and our common program. Especially to **Dr. Sebastiaan Kluijtmans, Dr. Joachim Nickel** and **Prof. Dr. Heike Walles**; your critical-thinking and contribution were very important for me to succeed in my part of the project. Thank you for hosting me in your institutions. **Laura**, who I started many experiments with and shared many lab-hours. You helped to make my starting point a nice one. **Didem**, we have worked side-by-side for a large part of the project, and I want to thank you for your support. **Claudia**, thanks for hosting me, for not

only being a collaborator but a true friend, and most importantly: for cooking me pistachio pasta. **Melva** and **Miguel**, your help during my secondment in Würzburg was crucial. Thanks for sharing laughs and advice.

Uno necesita tener siempre un pueblo al que ir, y a 33 minutos en tren de Rotterdam, está Leiden. Es allí donde me he sentido más cerca de casa gracias a a las innumerables paellas y fiestas organizadas por **Juan, Victorio, Guillem, Elena, Erjen, Mónica, Albert, Nadia, David, y Lia**.

A **Bernardo**, por ser más que un compañero de piso. En contra de lo que sucede en la mayoría de casas compartidas, nosotros teníamos siempre la nevera llena. A **Rosa y Oscar**. Os conocí nada más llegar y ya no me he separado ni un poquito de ninguno de vosotros – ni pienso hacerlo–. A **Bea, Laura, Lucía, Jorge, Isa, Marina y Dani**. Aunque ya no viváis aquí, siempre seréis mi Rotterdam. A **Mónica, Coral, Juanma, Hama, Jorien, Josh, Niall y Nathalie**; por compartir el frío y la rutina.

A mis princesas: **Susana, Laura, Elena, Elisa, Lara, Iris, María Jesús, Cristina, Azahara, Rosa, Beatriz, Isabel y Arantxa**. Los 1826 km que nos separan no son ni serán nada. Nos queremos y discutimos como lo hacen las familias. Y vosotras sois parte de la mía desde hace más de dos décadas. Gracias **Moisés, Estela, Alba, Giovanni, Irene, Rocío, María y Teresa**, por ser las personas a las que escapar durante esta tesis, y a **Iván, Alberto, Ceci y Pedro**, por ser la Valencia a la que una siempre quiere volver.

A mi abuela, porque aunque no pudo formar parte de esto, siempre resuena y resuena.

Alguien dijo que el amor se hereda como un abrigo sin botones, y yo lo heredé por cuatro. **Madyan, Hagar, Aiaat y Yihad**, os quiero tanto que salpica.

A mi **padre**. Por luchar siempre mientras yo le daba de comer a los patos. Gracias baba por quererme diferente. Y a **Farida**, porque como tú siempre decías, pariste a tres, pero siempre has querido a cinco.

Fuiste tu **madre**, la que criándonos no tuvo tiempo ni de mirarse al espejo. Eres la mujer más valiente que conozco. La que trabaja doble para poder venir a cuidarme. A la que admiro y la que le debo mucho más que un doctorado.

A **Jordi**. Porque sin ti, ¿qué?

Sin ti, nada. Haces que contigo yo solo quiera dibujarme mapas. Eres mi trozo favorito de futuro. La única verbena en la que una se atreve a bailar. Te quiero.



## PhD portfolio

### Personal details

**Name PhD Student:** Shorouk Fahmy Garcia

**Erasmus MC department(s):** Departments of Orthopaedics and Internal Medicine

**PhD period:** March 2014 – December 2017

**Research School:** Postgraduate School Molecular Medicine

**Promotors:** Prof. Gerjo J.V.M. van Osch, PhD and Prof. Johannes P.T.M. van Leeuwen, PhD

**Co-Promotor:** Eric Farrell, PhD and Marjolein van Driel, PhD

### PhD Training

Courses and Workshops		Workload (ECTS)
2014	Research Integrity (EMC)	0.3
2014	Photoshop and Illustrator Workshop (Molmed)	0.3
2014	FELASA Course on Laboratory Animal Science (LUMC), Leiden	4
2014	Intellectual Property Course (Fujifilm), Tilburg	2
2015	Biomedical English Writing Course (Molmed)	2
2015	Basic Introduction Course on SPSS (Molmed)	1
2015	Introduction in GraphPad Prism (Molmed)	0.3
2015	PhD Day (EMC)	0.3
2016	Time Management Workshop	0.2
2016	Biomedical English Writing and Communication Course (Molmed)	3
2016	PhD Day (EMC)	
2017	Monocytes: origins, destinations, functions and diagnostic targets	0.2
2017	SCORE-Day	0.3
2014-2017	Bio-Inspire Training program (biannually)	1

### (Inter)national Conferences

2014	New Frontiers in Regenerative Medicine, Nijmegen	1
2015	19 <sup>th</sup> Molecular Medicine Day, Rotterdam. Poster Presentation	0.5
2015	4 <sup>th</sup> Strategies in Tissue Engineering, Wurzburg. Podium Presentation	1

		<b>Workload (ECTS)</b>
2015	4 <sup>th</sup> Joint meeting of ECTS & IBM, Rotterdam, Rotterdam. Poster Presentation	1
2015	24 <sup>th</sup> annual NBTE meeting, Lunteren. Podium Presentation	1
2016	20 <sup>th</sup> Molecular Medicine Day, Rotterdam. Poster Presentation	0.5
2016	eCM: Stem cells, Bone Fixation, Repair & Regeneration, Davos. Podium Presentation	1
2016	TERMIS-EU Conference, Uppsala. Poster Presentation	1
2016	25 <sup>th</sup> annual NBTE meeting, Lunteren. Poster Presentation	1

#### **Bio-Inspire and Department(s) presentations and meetings**

2014-2017	Bio-Inspire EU project consortium meetings (biannually), Europe	2
2014-2017	Research meetings depts of Internal Medicine and Orthopaedics (weekly)	2
2014-2017	Meetings depts of Orthopaedics and Oral Maxillofacial Surgery (weekly)	2
2014-2017	Meet-the-Professor meeting (biannually)	0.5
2015-2017	Orthopaedic Science Day (annually)	0.5
2014-2017	Journal Club (monthly)	1

#### **Student Supervision**

2016	Partial supervision Bachelor Thesis Veerle Dieleman (Avans Hogeschool Breda)	5
------	--	---

#### **Miscellaneous**

2014-2017	Visiting PhD student at Fujifilm Company, Tilburg	2
2015	Visiting PhD student at Fraunhofer Institute, Wurzburg (6 weeks)	5
2016	Organization Lab day Internal Medicine	0.5
2017	Organization Lab day Orthopaedics, ENT, Oral Maxillofacial Surgery	0.5

#### **Awards and Grants**

2016	Erasmus Trustfonds conference travel grant	
2016	First Prize Poster Presentation. TERMIS-EU Conference, Uppsala	

43.9

## Curriculum Vitae

Shorouk Fahmy-Garcia (شروق فهمي) was born on 30<sup>th</sup> of January 1987 in Valencia (Spain). She is the first of five siblings. Shorouk studied at Campanar High School in Valencia, in the same neighbourhood where she lived, which was very useful in balancing the academic and social life of a teenager. By then, her parents and teachers messed up her life by convincing her to follow a scientific career, leading Shorouk to embark on a series of adventures. In 2005, she was admitted to a combined bachelor and master degree programme –*licenciatura*, equivalent to Master of Science– in Biotechnology that was carried out at the Polytechnic University of Valencia (UPV). During her studies, she went on an Erasmus scholarship to Prague, and carried out her studies at both Czech University of Life Sciences and the University of Chemistry and Technology. In 2010 she started her master's thesis at the Cytogenetic, Biological Markers and Molecular Biology Laboratory in the Haematology Department of the Hospital La Fe (Valencia), under the supervision of Dr. José Vicente Cervera and Prof. Dr. Ramón Serrano. The main focus of the thesis was to assess the impact of the aberrant methylation of two antagonist Wnt signalling pathway genes in the development of Myelodysplastic Syndromes. As she always wanted to pursue a fine arts degree, she decided to enrol in 2011 at the BSc. Fine Arts (UPV) while doing an internship at the Laboratory of Integrative systems Biology, Institute of Molecular and Cellular Biology of Plants, Valencia (supervisor: Dr. Mario Fares). The main goal of the internship was to study how molecular chaperones contribute to emerge functions in nature. 2012 was a memorable year in which she defended her master's thesis, ended her internship and was awarded with an EU fellowship to continue her studies in the Middle East. She enrolled in an MRes in Biomedical Sciences and moved to Cairo, where she joined Ain Shams University under the coordination of Prof. Dr. Mohamed Hazem. Maybe it was not the best political moment in the country but it was an extraordinary experience. She returned at the end of 2013 to Valencia and defended her master's thesis on epigenetic processes that affect the progression from Myelodysplastic Syndromes to Acute Myeloid Leukaemia (supervisor: Dr. Amparo Gimeno). At the beginning of 2014 she moved to Rotterdam to start her PhD project at two departments: Orthopaedics and Internal Medicine under the supervision of Prof. Dr. Gerjo van Osch, Prof. Dr. Hans van Leeuwen, Dr. Eric Farrell and Dr. Marjolein van Driel. Her PhD project was part of a Marie Curie ITN called Bio-Inspire and it involved, among others, Fujifilm Manufacturing and Universitätsklinikum Würzburg, in which she carried out part of her studies. During 2018 she decided to travel for a few months with Jordi, her partner in crime, around South America and Southeast Asia. Shorouk is currently working at Erasmus MC as a postdoctoral researcher in both the Departments of Orthopaedics and Oral and Maxillofacial Surgery. She lives with Jordi and an evil cat. Shorouk enjoys cinema, theatre and good food. When she is not thinking about work, she is usually thinking about where to go with Google Maps open. In fact, it's exactly what she did after finishing writing this curriculum vitae.







